AN EXPERIMENTAL INVESTIGATION OF THE EFFECT OF BAFFLES ON TRANSIENT NATURAL CONVECTION OF A CONFINED FLUID

A THESIS

Presented to

The Faculty of the Graduate Division

by

Reginald Brown Pollard

In Partial Fulfillment

of the Requirements for the Degree

Doctor of Philosophy

in the School of Mechanical Engineering

Georgia Institute of Technology

July, 1974

AN EXPERIMENTAL INVESTIGATION OF THE EFFECT OF BAFFLES

ON TRANSIENT NATURAL CONVECTION OF A CONFINED FLUID

Approved:

W. O. Carlson, Chairman

S. P. Kezios

C. W. Gorton

Date approved by Chairman: 7/10/74

ACKNOWLEDGMENTS

The author is deeply indebted to many people who made this work possible. First of all, he would like to thank Dr. W. O. Carlson, his advisor, who gave generously of his time, patience, and encouragement, not only during all phases of this investigation, but throughout the entire duration of his graduate work at this institution. He would like to thank Dr. T. W. Jackson for his discussions and comments on the investigation. He would like to thank Dr. C. W. Gorton and Dr. S. P. Kezios for their service on the reading committee. Also, the author is appreciative of the assistance received from the following individuals Dr. J. W. Tatom, Mr. Edward Schneider, and Mr. Vance Meek.

The author would like to express his gratitude to the National Science Foundation for the grant GK-135 that made this investigation possible.

Finally, the author would like to acknowledge his debt to his wife, Joan, and to his parents, Mr. and Mrs. Sam Pollard, and his wife's parents, Mr. and Mrs. E. R. Cato. The attainment of his educational goals would not have been possible without their encouragement and support.

TABLE OF CONTENTS

TABLE OF CONTENTS (Concluded)

LIST OF TABLES

LIST OF ILLUSTRATIONS

LIST OF ILLUSTRATIONS (Continued)

LIST OF ILLUSTRATIONS (Continued)

LIST OF ILLUSTRATIONS (Continued)

LIST OF ILLUSTRATIONS (Concluded)

SUMMARY

An experimental investigation of transient free convection phenomena was considered in a vertical, closed container where the fluid was heated with a constant heat flux on the bottom and sides without a change of phase. Water was used as the test fluid in the tank which was approximately two feet wide, two feet in breadth, and ten feet deep. The water was heated on two parallel sides and at the bottom by electrical resistance elements. The other two parallel sides of the tank were made of glass to allow for both visual and photographic observation of the fluid motion.

Bulk and wall temperature measurements were made in the container with and without baffles for various heat flux ratios, aspect ratios, baffle to tank width ratios, and baffle inclination. The tests covered a range of modified Grashof numbers from 7.5×10^8 to 4.6×10^{15}. Measured bulk temperature profiles indicate that baffles are more effective during early stages of heating for all aspect ratios. Horizontal baffles were found to be generally more effective than baffles inclined up or down.

An extensive photographic analysis, using neutral density particles and a Schlieren system, of the flow around the various baffle configurations indicates that baffles are effective in promoting a more uniform bulk mixing process. The photographs also reveal that reattachment of the boundary layer flow does not occur for many of the baffles tested. Previous investigations had concluded that reattachment would occur for all baffles and hence their effectiveness would be reduced.

An empirical correlation equation for baffle effectiveness was developed. It was found that the effectiveness was dependent primarily on the heat flux ratio, aspect ratio, baffle to tank width ratio, and the number of baffles present. The effectiveness was found to be only weakly dependent on the baffle angle of inclination to the walls. The correlation equation developed will predict baffle effectiveness within ± 20 percent.

Bulk and wall temperature measurements without baffles present indicate local heat transfer coefficients which are slightly higher than predicted by theory for a vertical surface in an infinite medium. Further, the temperature distribution along a vertical surface with turbulent flow is shown to fit an equation similar to that for laminar flow but with an exponent of 1/7.

NOMENCLATURE

Latin Symbol	Definition	Units
a	radial position	ft
A	constant in Eq. (4.6), page 119	dimensionless
b	exponent in Eq. (4.6), page 119	dimensionless
B	baffle width	ft
Bi	Biot number = hx/k_w	dimensionless
c	specific heat capacity	Btu/lbm°F
C	constant in Eq. (5.15), page 141	dimensionless
E	baffle effectiveness	dimensionless
Fo	Fourier number = $\alpha\tau/y^2$	dimensionless
g	acceleration of gravity	ft/sec^2
Gr	Grashof number = $g\beta\theta x^3/\nu^2$	dimensionless
Gr^*	modified Grashof number = $g\beta qx^4/k\nu^2$	dimensionless
h	film coefficient	$Btu/ft^2hr°F$
J_1	constant defined by Eq. (A-6), p. 151	dimensionless
J_2	constant defined by Eq. (A-7), p. 151	dimensionless
k	thermal conductivity	Btu/ft hr°F
L	container height	ft
m	exponent in Eq. (4.6), page 119	dimensionless
n	exponent in Eq. (4.6), page 119	dimensionless
N	number of baffles	dimensionless
Nu	Nusselt number = hx/k	dimensionless

NOMENCLATURE (Continued)

Latin Symbol	Definition	Units
o	exponent in Eq. (4.6), page 119	dimensionless
p	exponent in Eq. (4.6), page 119	dimensionless
Pr	Prandtl number = ν/α	dimensionless
q	heat flux	$Btu/ft^2 sec$
r	radius	ft
Ra	Rayleigh number = Gr·Pr	dimensionless
t	fluid thickness	ft
T	temperature	°F
$\overline{T}$	average temperature	°F
u	boundary layer velocity	ft/sec
U	characteristic boundary layer velocity	ft/sec
W	container width	ft
x	distance along container height	ft
y	distance normal to container wall	ft
Greek Symbol		
α	thermal diffusivity	ft^2/sec
β	coefficient of volume expansion	1/°F
δ	boundary layer thickness	ft
ν	kinematic viscosity	ft^2/sec
ρ	density	lbm/ft^3
τ	time	sec
θ	temperature difference	°F

NOMENCLATURE (Concluded)

Subscripts	Definition
Av	average value
b	bottom
B	bulk liquid
fp	flat plate
i	initial
L	based on length
max	maximum
N	no baffles
p	heating plates
r	radial position
s	side
T	total
w	wall
x	local height
∞	ambient

CHAPTER I

INTRODUCTION

Historical Background

In the field of heat transfer the amount of literature to be found on the subject of free or natural convection is enormous. However, the majority of this information pertains to either steady state or transient free convection over surfaces in fluids of infinite extent. When free convection within a closed container is considered, it is found that the number of investigations is relatively small because intensive interest in this area of free convection has only developed within the past 10 to 15 years.

The rapidly expanding missile, chemical, and nuclear industries have been faced with many problems involving closed-container free convection. For example, propellants in large rocket tanks are quite sensitive to heat transfer to the fluid from the container walls through the free convection mechanism. Also, the cooling of nuclear reactors and high temperature gas turbine blades are other areas in which problems of closed-container free convection exist.

Lately, many attempts to understand and predict transient free convection phenomena in closed containers have been made. Although these efforts have been delayed by a lack of knowledge of the turbulent free convection heat transfer mechanism within a container, the results of many investigations (1-5)* help in predicting these phenomena. Interest in

*Numbers in parentheses indicate reference cited.

this area, which came to be called thermal stratification, grew from problems experienced when large volumes of fluids are subject to heat transfer from the surroundings. In such situations the energy absorbed by the fluid from the container walls is concentrated in the upper portion of the fluid thus producing severe temperature gradients. However, under some circumstances, a uniform energy distribution throughout the fluid is desirable.

Although many tests and much analytical analysis have been performed to predict when and under what conditions stratification will occur, very little attention has been directed toward methods of stratification reduction. That is, methods to disperse the energy throughout the bulk fluid. There are basically two methods to reduce stratification in a particular situation, these are: (1) the use of mechanical devices (e.g. pumps) to mix the fluid and (2) a change in container geometry, so that the bulk fluid will be mixed. It should be kept in mind here that, although a temperature gradient may exist along the container walls and in the boundary layer, this does not infer that such a gradient must exist in the bulk fluid.

At present, two types of changes in container design for reducing stratification have been considered; these are: (1) the addition of baffles on the vertical walls of the container and (2) a change in bottom shape. The latter was not investigated during this study.

Neff (6) performed one of the first experimental studies on stratification reduction techniques using both cryogenic and non-cryogenic fluids. Three different bottom shapes and the addition of baffles on the vertical

walls were investigated. The baffle configurations employed were: (a) horizontal, (b) inclined upward, and (c) inclined downward.

The effectiveness of baffles in reducing stratification in Neff's one-foot diameter non-cryogenic tank appeared at first to be small. The results of these tests showed that: (a) perforated baffles were partially effective in reducing stratification, (b) baffles inclined downward were more effective than baffles which were horizontal or inclined upward, and (c) multiple baffles were more effective than single baffles in reducing stratification. In the report, no analytical or calculated values of the effectiveness of the various baffle designs were presented. Although Neff noted no consistent stratification reduction trend developed from the non-cryogenic test data, certain baffle configurations and wall heating rates appeared promising; thus, further tests of the baffles inclined downward were conducted in a cryogenic fluid. In the non-cryogenic flow visualization tests Neff also noted that the flow in the central portion of the tank remained in a downward direction, although the flow around the baffle edges was upward.

In most tests the baffles inclined downward were effective until the volume below the baffles became filled with the wall-heated fluid at which time their effectiveness decreased. Other factors which were found to increase baffle effectiveness were: (a) large baffles (baffles that extend into the bulk volume a large distance), (b) low wall heating rates, and (c) greater baffle pitch angle from the horizontal.

Vliet and Brogan (7) and Vliet (8) made studies on the effect of baffles on natural convection and stratification. Vliet defined a term

called baffle effectiveness:

$$E = \frac{M_{TN} - M_T}{M_{TN} - \frac{\bar{T}L^2}{2}} \tag{1.1}$$

where $\bar{T}$ is the average fluid temperature and M_T is the temperature moment about the bottom of the vessel

$$M_T = \int_o^L (T-T_i)\, x dx \tag{1.2}$$

where T is the fluid temperature; T_i the initial uniform temperature; x the axial height; and L the tank total height. The subscript "N" refers to the no baffle case. Equation (1.1) was derived by comparison of the dimensionless temperature moment with baffles to the dimensionless temperature moment without baffles. Details of the derivation of Equation (1.1) are given in Appendix E. As noted by Vliet and Brogan (7), the baffle effectiveness parameter has the following significance:

(1) When zero, the baffle is completely ineffective. That is, the same temperature profiles are obtained as without baffles.

(2) When equal to one, the baffle results in a uniform temperature or a complete thermal equilibrium condition (100 percent effective).

(3) If asymptotic temperature shapes are approached either with or without baffles, the parameter also approaches an asymptotic value.

Values of the effectiveness varied from 0.6 down to 0.05 in Vliet's small tank. The higher values for effectiveness were for the largest baffles located in a staggered position along the two heated walls. It should

also be noted that only two different side heat fluxes were investigated. No bottom heat was used in the tests.

In reference (8) it was noted that, in tests without baffles, the stratification process is initiated with a rather large surface flow from each of the heated side walls, which meets in the vessel center line and forms a downward moving warm plume. A model of this process is illustrated in Figure 1, and has been previously described by many investigators. Tatom (5) used such a model to obtain an analytical model for the stratification process. Vliet noted that, when baffles were added to the walls under the same conditions as no baffles, the initial effect was to cause energy to be transferred into the lower portion, or unstratified, regions of the fluid. Later, the effect of the baffles decreased as the stratification progressed into the lower regions of the vessel. The only baffles tested by Vliet were horizontal and, like Neff (6), he found that increasing the number of baffles generally increases the effectiveness.

Some of the earliest work performed on baffles was done by Griffith and Davis (9). They performed several experiments on free convection from a heated, constant temperature plate in various positions. However, their baffle tests were performed when the plate was in a vertical position. Both horizontal and concave downward baffles were tested for qualitative results. It was found that, by adding a baffle at the bottom of the plate (similar to a bottom in a tank), the cooling of the plate was reduced by 4.0 percent. Also, it was found by Griffith and Davis that the introduction of baffles above the bottom of the heated vertical plate increased the cooling of the plate. It was noted that the reason for this

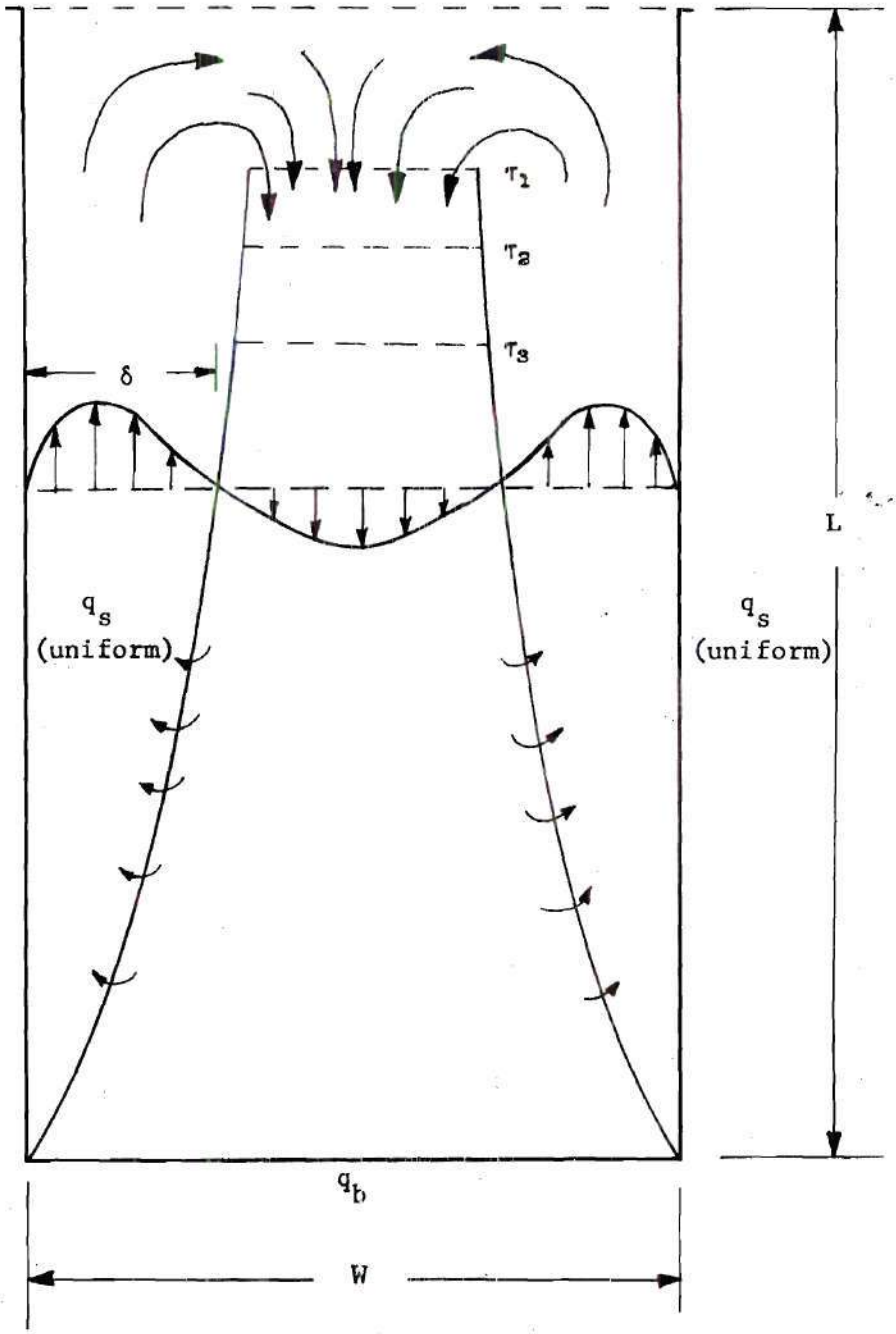

Figure 1. Stratification Model

effect was that the baffles allowed colder fluid to come in contact with the plate. That is, without baffles the fluid in contact with the plate near the top has been previously heated by the lower portion of the plate. Griffith and Davis also performed some experiments on the effect of conical baffles. These tests were performed on a cylindrical heated surface. A comparison was made on the heat loss (a) from the bare cylinder, (b) with a horizontal baffle at the top of the cylinder, and (c) with a downward conical baffle at the top. It was found that the heat transferred from the plate for a given temperature difference was in the ratio of 13.8 : 8.3 : 6.7 for the freely exposed surface, the horizontal baffle, and the conical baffle, respectively.

The experimental investigation conducted by Griffith and Davis was perhaps the first work to be done in the area of turbulent heat transfer coefficients for free convection from vertical plates. The results of this work along with some of the later investigations such as those by Eckert and Jackson (10,11), Fujii (12), Tritton (13), and Bayley (14) constitute the sources of information for heat transfer coefficients used in solving many problems involving confined fluids. Upon surveying the existing literature, one finds little information regarding the values of heat transfer coefficients for completely confined fluids or measurements of wall temperatures. Also, the addition of baffles on the vertical walls of the tank will affect the heat transfer from the walls and hence should change the wall temperature distribution. The baffle should have a similar effect as adding a vortex generator in forced convection heat transfer in tubes.

The work of Lighthill (15) and Martin (16) on free convection in an open thermosyphon are the only two investigations found that approach a truly confined fluid which is only being heated. In both cases, however, the hot fluid flowing up the heated walls is subjected to a cooling section which continues to supply cool fluid to the heated container. Also, their investigations were for the case of steady-state and constant wall temperatures. The results of Lighthill's analytical investigation are seen in many of the analytical models of stratification. However, his most important results lie in his description of the various flow regimes possible in a heated cylinder. As noted in reference (15), there exists the possibility of six different flow regimes depending on the values of the modified Grashof number, Gr_a, and the aspect ratio, L/a.

It was found by Lighthill that turbulence decreases the heat transfer from the walls when the tube is completely filled with the turbulent boundary layer. Otherwise, the turbulent boundary layer increases the transfer of heat as in the case of flow over a flat plate. Also, the Grashof number at which the heat transfer becomes most effective increases sharply with increasing aspect ratio.

Martin's experimental study of free convection in an open thermosyphon verified much of Lighthill's analytical results. However, in the fully mixed turbulent regime, Martin found considerable difference between the estimated and experimental heat transfer rates. Also, he found that this regime was more stable and persisted, whereas, Lighthill had noted that it was unstable and would be replaced by a stable boundary layer flow for high Rayleigh numbers. Martin obtained the following relation for the

the heat transfer from long tubes during laminar flow,

$$Nu_r = 0.44\left(Ra_r \cdot \frac{r}{L}\right)^{0.23} \tag{1.3}$$

For turbulent free-convection heat transfer, he found

$$Nu_r = 0.1 \cdot Ra_r^{\frac{1}{3}} \quad \text{for } (200 > Pr > 6.0) \tag{1.4}$$

In the above equations, the subscript r denotes the tube radius. It should be noted that the exponents in the above equations are characteristic of the respective regimes. Also, in the turbulent regime, the heat transfer results are independent of the aspect ratio as noted from Equation (1.4).

Eckert and Jackson (11) performed an analytical investigation on heat transfer in coolant passages as related to turbines. Their problem was quite similar to the one under investigation except, as in the investigations of (15) and (16), the hot fluid flowing up the heated walls exchanges its heat with a large reservoir. They employed the von Kármán integral analysis and found that the effect of three different velocity profiles on the boundary layer thickness was small. Their relation for the heat transfer coefficient compares favorably with that of Jakob (17).

Jakob (17), by correlating the data of several investigators on bilogarithmic axes, developed the empirical equation;

$$Nu' = \frac{k_{c-v}}{k} = C[Gr_t \cdot Pr]^n \left(\frac{L}{t}\right)^{-\frac{1}{9}} \tag{1.5}$$

for Gr_t from 2×10^4 to 2.1×10^5, C is 0.20, and $n = \frac{1}{4}$; thus for a given L/t, $h \propto t^{\frac{1}{4}}$. For Gr_t from 2.1×10^5 to 1.1×10^7, C is 0.071 and $n = \frac{1}{3}$ but for a given L/t, h is independent of t.

McAdams (18) noted that, for an (L/t) of 17.5, Eq. (1.5) for an enclosure is the same as the equation for turbulent free convection over a vertical plate for $Gr \cdot Pr$ from 10^9 to 10^{12}:

$$Nu_L = 0.13[Gr_L \cdot Pr]^{\frac{1}{3}}. \tag{1.6}$$

In the above equations, t indicates the fluid thickness and L its height. Neff (6) used McAdams' results to illustrate the relative magnitude of the heat transfer coefficients within an enclosure to those for a flat plate in an infinite medium. Jakob's equation suggests that

$$Nu' \leqq Nu_{fp} \quad \text{when } L/t < 17.5 \tag{1.7}$$

and

$$Nu' \geqq Nu_{fp} \quad \text{when } L/t > 17.5. \tag{1.8}$$

Here, Nu' is defined in terms of the temperature difference between the two walls of the enclosure.

By comparing the theoretical and experimental relations for free convection over vertical flat plates in an infinite medium with those of enclosures, an indication of the heat transfer rates obtainable for a completely confined fluid is possible. Neff (6) compared the results of Lighthill (15), Martin (16), and McAdams (18) to those of Eckert and

Jackson (10). The results deduced from the trends of the Nusselt number correlations indicate that

$$Nu_{fp} \geqq Nu_{enclosure}. \tag{1.9}$$

Assuming, as Hartnett and Welsh (19), that equivalent heat transfer rates result with constant wall heat flux or constant wall temperature, the Nusselt number may be expressed as;

$$Nu_L = \frac{hL}{k} = \frac{(q/A)_c L}{k\theta} . \tag{1.10}$$

For identical fluids, equal heating rates and lengths for an enclosure and a flat plate,

$$h_{fp} \geqq h_{enclosure} \tag{1.11}$$

which implies that

$$\theta_{fp} \leqq \theta_{enclosure}. \tag{1.12}$$

The fact that an equal or greater driving potential is required for an enclosure, as noted by Neff, results from the interfering flow and stratification that occurs in confined fluids.

The experimental investigation of Hartnett and Welsh (19) verified the data of Martin (16). They also noted that the difference between the cases of a uniform wall temperature and uniform heat flux for free convection within a closed container is negligible. That is, the same value

for Nusselt number is approximately obtained for equal values of the product Gr·Pr for the two cases. Their apparatus was designed such that both laminar and turbulent flow could be investigated.

For a confined fluid which is not exchanging heat with a cooling reservoir (e.g., as in a thermosyphon), both the bulk and wall temperature are changing with time. Thus, the use of heat transfer results obtained from tests conducted in an infinite medium with steady state conditions prevailing is questioned when applied to a confined fluid. Kolar (20) conducted an analytical and experimental investigation of the thermal boundary layer of a confined fluid and found that, after an initial starting transient, the process could be considered as a quasi-steady condition. He found that the temperature profiles within certain regions of the laminar boundary layer exhibited the property of similarity and could be predicted fairly well by the infinite medium results. Kolar used the results of Gebhart and Adams (21) in defining a time parameter after which the process could be considered quasi-static.

Siegel (22) previously derived expressions for the time required for a vertical flat plate in laminar flow to reach steady-state after undergoing a step change in surface temperature or a step change in uniform heat flux. Siegel's results for the time to reach steady-state are functions of the Rayleigh and Prandtl number and the length or position along the plate. The time to reach steady-state is decreased for increasing values of g, β, q, or θ_w. In most cases this time is relatively small when compared to the overall process. His time parameter for the case of uniform heat flux is somewhat similar to that derived by Kolar.

Cheesewright (23), in a recent experimental investigation of the steady state turbulent boundary on a vertical flat plate, verified the temperature profiles in the turbulent boundary layer measured by Griffith and Davis. Also, he noted that the heat transfer coefficient from the plate agreed with that of Eckert and Jackson (10) for $Gr > 2 \times 10^{10}$, while for $8 \times 10^{9} < Gr < 2 \times 10^{10}$ the results agreed best with those of Bayley (14). Further, the theoretical velocity and temperature profiles used in many analyses were found not to be in agreement with the experimental data.

Present Investigation

The present investigation was undertaken to provide additional and extended information on the effect of baffles on thermal stratification in containers. Also, to present heat transfer results for transient natural convection from the vertical side walls of large containers where the turbulent flow regime is predominant. The effects on the bulk and wall temperature profiles were studied by varying the modified Grashof number, Gr_x^*, the ratio of bottom to side heat flux, q_b/q_s, the aspect ratio, L/W, the baffle to tank width ratio, B/W, and the number of baffles. The test fluid used throughout all the tests was water, because of its availability and its physical properties are well known. In order to better interpret the results from the wall and bulk temperature measurements, a photographic study of the flow for many of the baffle designs was also made.

In the first portion of this chapter, a brief summary of the work performed in the above or related areas was presented. It should be noted

that, although some work has been performed in the area of baffles in tanks, most of this work is qualitative in nature. Only the effect of baffles in relatively small tanks was investigated and in most cases laminar flow existed along the vertical walls. In larger tanks, such as the one used in this investigation, turbulent flow will exist over a major portion of the container side walls even when baffles are added.

Heat transfer results for the vertical walls of a container, such as the one used in this study, could not be found in the open literature. The results from many of the analytical models used in predicting when and with what severity thermal stratification will occur depend on accurate knowledge of the heat transfer from the vertical walls of the container. Most analytical models of stratification at present incorporate the results, either analytical or experimental, obtained from investigations on vertical plates in an infinite medium. However, the boundary conditions governing the two different models are different; thus one should not expect the heat transfer results to be the same. The heat transfer coefficients on the vertical walls are calculated by two different methods, the first assumes the process is quasi-steady while the second is variable in time. In turn, these values are compared with results obtained from analytical models for vertical plates in infinite fluids. The heat transfer coefficients on the bottom of the container are not considered, since this portion of the container has been thoroughly examined by many investigators. For example, see references (24) and (25).

In Chapter II a brief description of the apparatus used in obtaining the experimental results is described. The thermal boundary condition

on the bottom and side walls is constant heat flux. Also, the test procedure and methods of obtaining the experimental data are described in Chapter II. Chapters III and IV present the experimental results and illustrate the effect the various baffle designs have on the overall bulk temperature profiles. The results of wall temperature measurements and film coefficients for the vertical walls with and without baffles are presented in Chapter V.

CHAPTER II

EXPERIMENTAL PROGRAM

Test Apparatus

The apparatus used in conducting the experiments is shown in Figures 2, 3, and 4. The test tank constructed by Tatom (5) was designed so that visual and photographic observation of the fluid motion could be made. The addition of the control panel, for the present investigation, gave the added advantages of quick operation and ease in gathering data. The control panel was constructed for the installation of the different switches, valves, and gages. Figure 4 presents a view of the panel and associated instruments. Complete operation of the test facility was possible from the control panel except during draining of the tank. As presented in Figure 2, the total test system is composed of:

1. test tank and baffles
2. control panel and instrumentation
3. photographic system
4. power supply
5. fill, drain, and filtration system.

Each of these major systems is discussed in the following sections.

Test Tank and Baffles

The test tank used throughout all of the tests is described in detail in reference (5). However, for completeness, a brief description will be given. The tank is constructed of aluminum, plate glass and

Legend.
A - Light Source
B - Thermocouple Junction Box
C - Camera and Tripos
D - Tape Recorder
E - Potentiometer
F - Ampere Meter
G - Side Voltmeter
H - Bottom Voltmeter

Figure 2. Experimental Apparatus

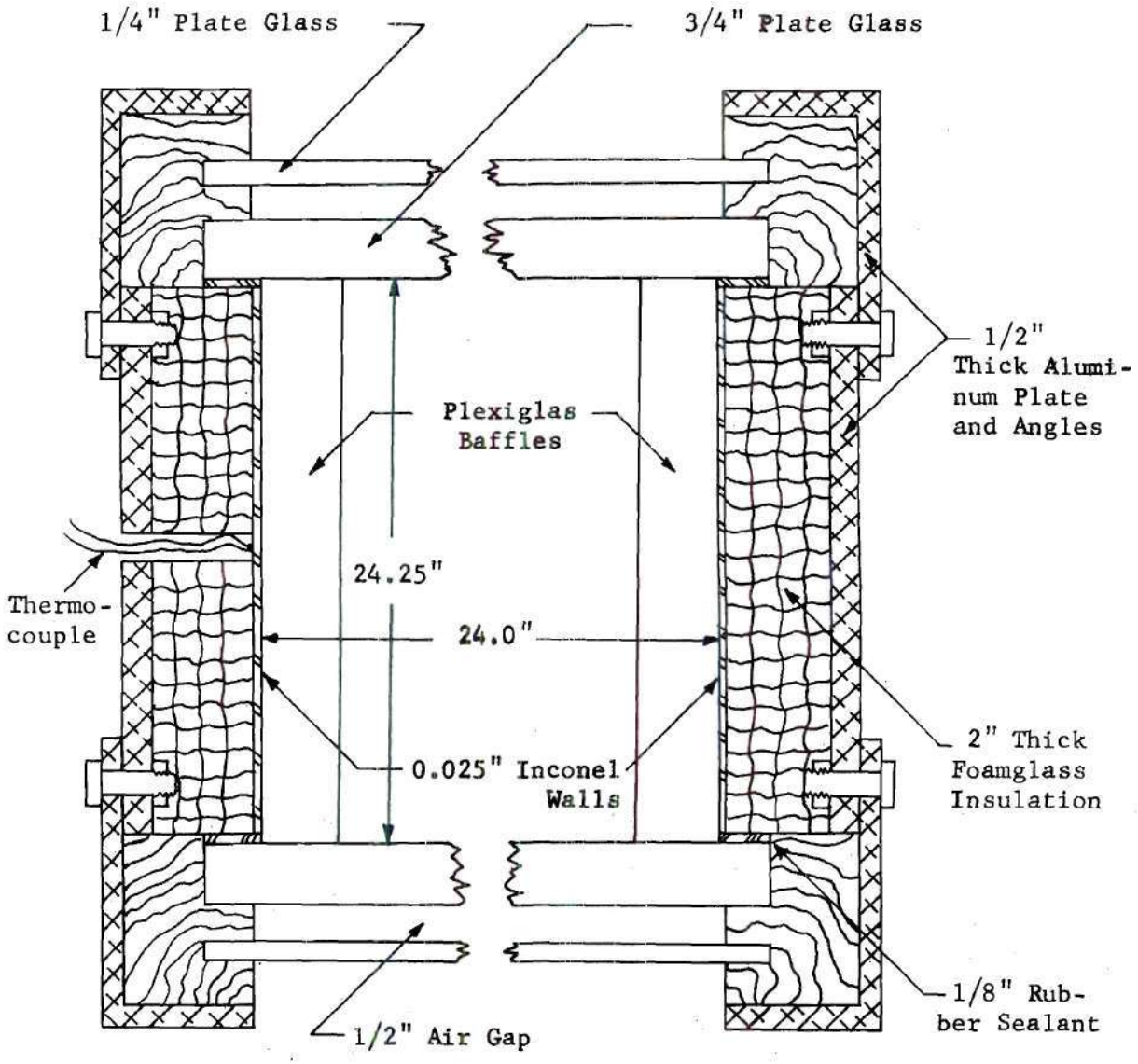

Figure 3. Vertical Cross-Sectional View of Test Tank

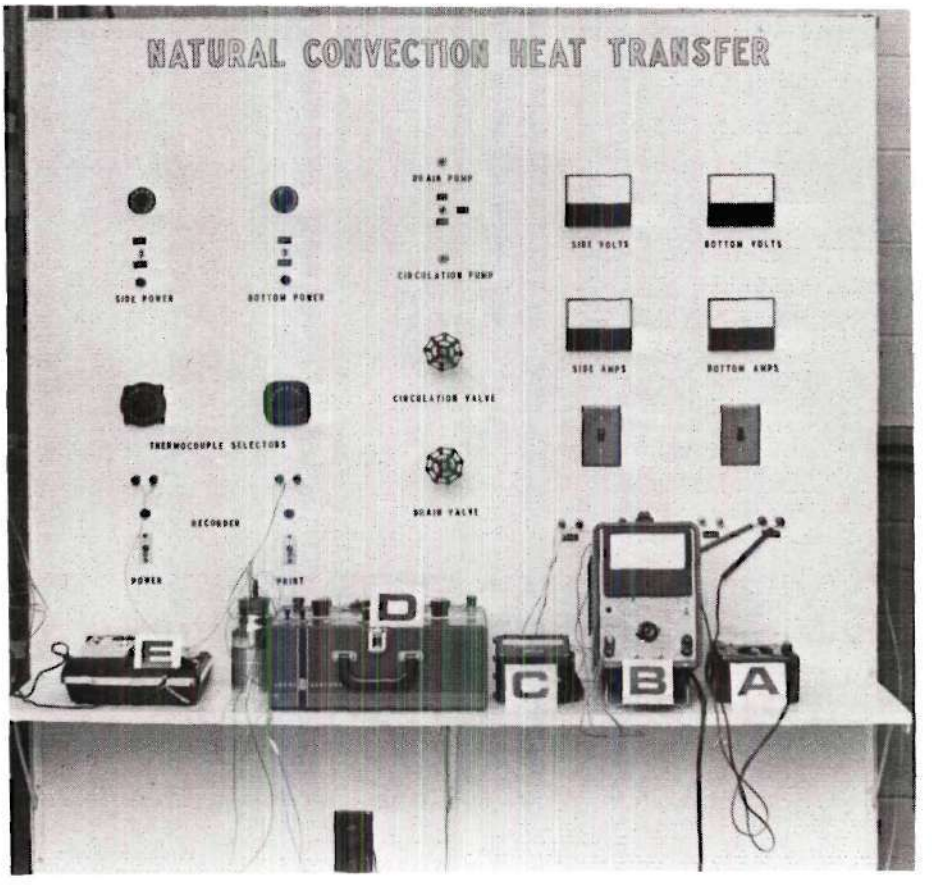

Legend.

A. Voltmeter for Bottom
B. Voltmeter for Side
C. Ammeter
D. Potentiometer
E. Recorder

Figure 4. Control Panel.

Inconel steel and is 119 inches deep, 24 inches wide, and 24.5 inches in breadth. A cross-sectional view of the tank is shown in Figure 3. The tank dimensions were so chosen by Tatom to allow for turbulent flow over about 80 percent of the sidewall when water is used as the test medium. The tank width and breadth dimensions were so chosen as to be approximately ten times the maximum predicted turbulent boundary layer thickness. Thus, end and corner effects could be neglected.

Two opposite sides and the bottom of the tank are used in heating the test fluid. The Inconel heating surfaces on the sides are 0.025 inch thick, backed by a two inch layer of Pittsburgh-Corning Foamglass insulation, and a 0.25 inch aluminum plate. The Inconel sheet, on the side, was held in place by the supports for electrical contacts and it was also cemented, with a rubber base cement, to the foamglass insulation. An 0.018 inch thick Inconel sheet was used on the bottom so that a higher electrical resistance would be obtained in order that reasonable current values could be used. This heating surface was also backed by two inches of Foamglass and 0.25 inch of aluminum. The bottom panel was also cemented to the foamglass insulation. Foamglass insulation was used because of its low water absorption.

The two transparent sides of the test tank were made of Libby-Owens-Ford plate glass. Each side consisted of two panels separated by a one-half inch air gap to reduce heat loss from the test fluid. The outside plate is one-fourth inch glass, while the plate next to the fluid is three-fourths inch. The one-half inch air gap was chosen to minimize the heat loss and the maximum heat loss from the tank for a 10°F average bulk

temperature above ambient is approximately 0.06 KW.

As noted by Tatom, sealing the tank for leaks was one of the most difficult problems. However, this difficulty was overcome in this investigation when a plastic tape, Vogue Stickum, was employed. It was found that this tape sticks to almost any dry surface and has the unique feature of not becoming brittle after prolonged usage as do some of the rubber and epoxy sealants. Also shown in Figure 2 are the horizontal support ribs. These ribs are used to stiffen the tank, particularly the glass plates.

One problem of extreme importance in the present investigation was that of placing the baffles within the tank. The problem was not very difficult when small baffles (as measured from the wall) were used, since these were easily placed on the tank wall and cemented by hand using Dow Corning Silicone Rubber. With the large six inch baffles, only one or two at the time could be cemented on the tank walls and then allowed to dry. The baffles were held in place during the cementing process by using masking tape and blocks. Any excess cement was removed after it had dried. Before a test series in which photographs were to be taken, all traces of the silicon rubber cement on the glass surfaces were removed so that the particles next to the baffle surfaces could be clearly seen.

The baffles used throughout all of the tests were constructed from one-fourth inch Plexiglas, hence they were unheated. In reality, tank baffles may be heated but the amount of heat transfer from the baffles is generally small when compared to that from the side walls. Baffle

dimensions chosen for the present investigation include widths of two, four, and six inches on both heated walls so that a broad range of the baffle to tank width ratio would be analyzed. No baffles were placed on the flat, horizontal bottom.

Control Panel and Instrumentation

Complete operation of the tank during testing was possible from the control panel shown in Figure 4. The panel board contains the power control switches for both the side and bottom heating plates along with the panel volt and ampere meters for the respective heating surfaces. It also contains the drain and circulation pump switches and valves. The fill valve is located at the wall to the right of the panel. Wall thermocouple selector switches and the bulk temperature recorder switches are located on the panel. Plugs for the various auxiliary equipment used during testing are also contained on the panel.

The bottom and side heating currents were measured at the panel with a Weston model 433 ammeter in conjunction with two 1000:5 ratio General Electric type JCP-0 current transformers. The Weston ammeter was factory calibrated with an accuracy of ± 0.25 percent of full deflection. The current transformers were also factory calibrated and within the range of currents used, the correction factor was negligible. The voltage drop across the bottom heater was measured with a Triplett model 630-NA volt-ohm-milliammeter with a rated accuracy of ± 4.0 percent. The side voltage drop was measured with a Hewlett-Packard Vacuum Tube Voltmeter, model 400H with an accuracy of ± 3.0 percent of full scale.

The wall temperature time data were taken at the control panel by

using a Leeds and Northrup Millivolt Potentiometer Catalog No. 8686 and a stopwatch. These measurements were audibly read into an RCA portable tape recorder at various time intervals. Later, the tape was replayed, and the wall temperature-time readings were tabulated. Figures 5 and 6 show the location of the wall thermocouples on the test tank. These thermocouples were made from Thermo-Electric Company, 30 B&S gage copper-constantan wire with Teflon insulation.

The thermocouples were attached to the walls by using a Baldwin-Lima-Hamilton model VTW-34 spot welder. Leads from the wall thermocouples run to the two thermocouple switches located on the control panel. To minimize conduction effects in the wall thermocouples, approximately one inch of each thermocouple wire was coiled and pressed against the heater walls as recommended by Jakob (17). The foamglass insulation removed when placing the thermocouples on the walls was replaced by a fiber glass type insulation of comparable thermal conductivity.

The bulk liquid temperature data were taken by using a vertical thermocouple probe and a 24-channel Honeywell Electronik 16 multipoint strip chart recorder. Factory accuracy of the recorder is $\pm$ 0.25°F. However, as explained in Appendix B, better accuracy was obtained by calibrating the recorder with the thermocouples within the system.

The bulk thermocouple probe used in all the tests was designed and built by Tatom (5). It consists of a two inch diameter Plexiglas tube 119 inches long with 59 thermocouples spaced at various intervals along the tube length. In the L/W equal to one and three tests, two additional thermocouples were added to the probe close to the bottom to give more

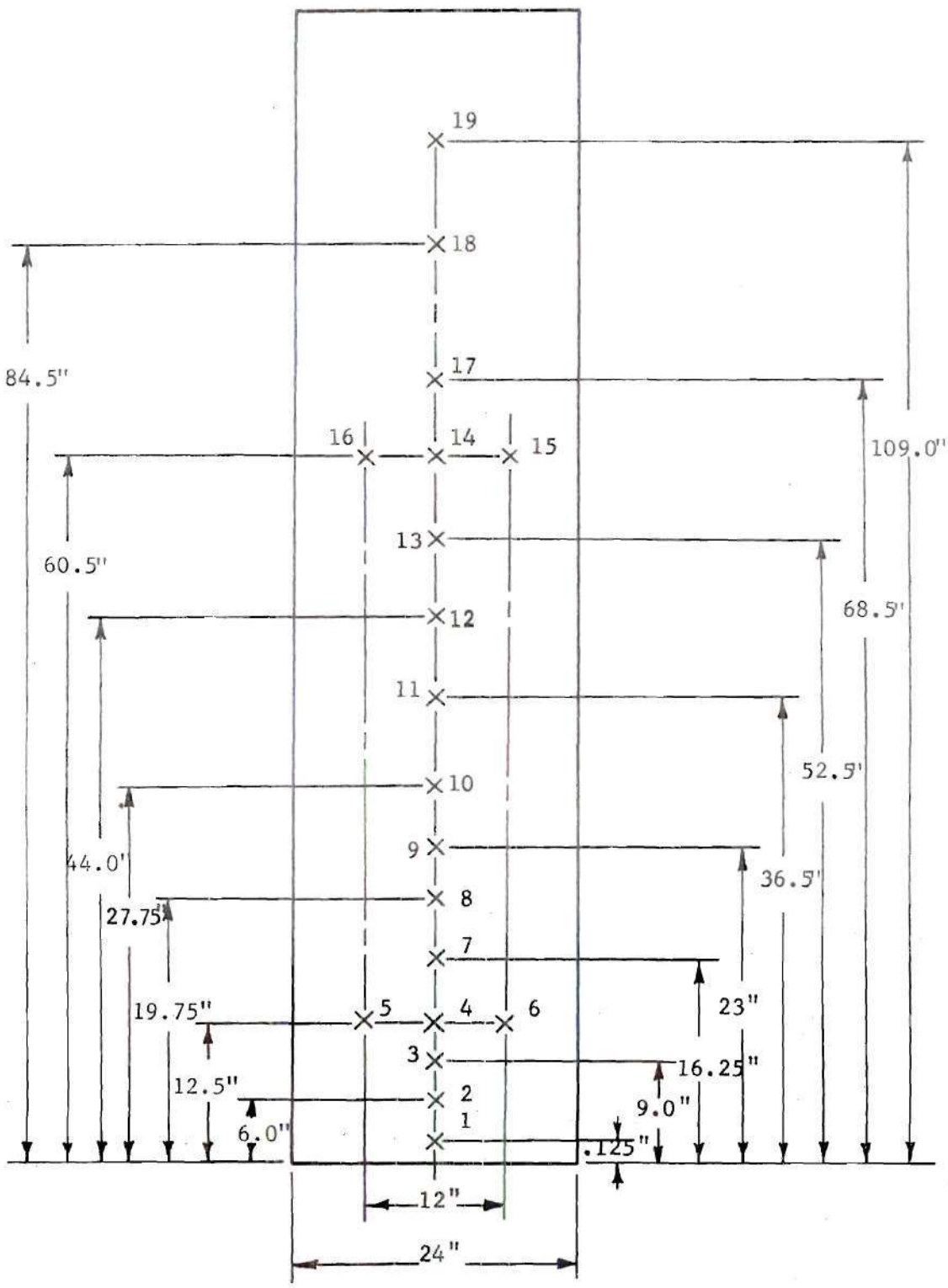

Figure 5. Location of Side Wall Thermocouples

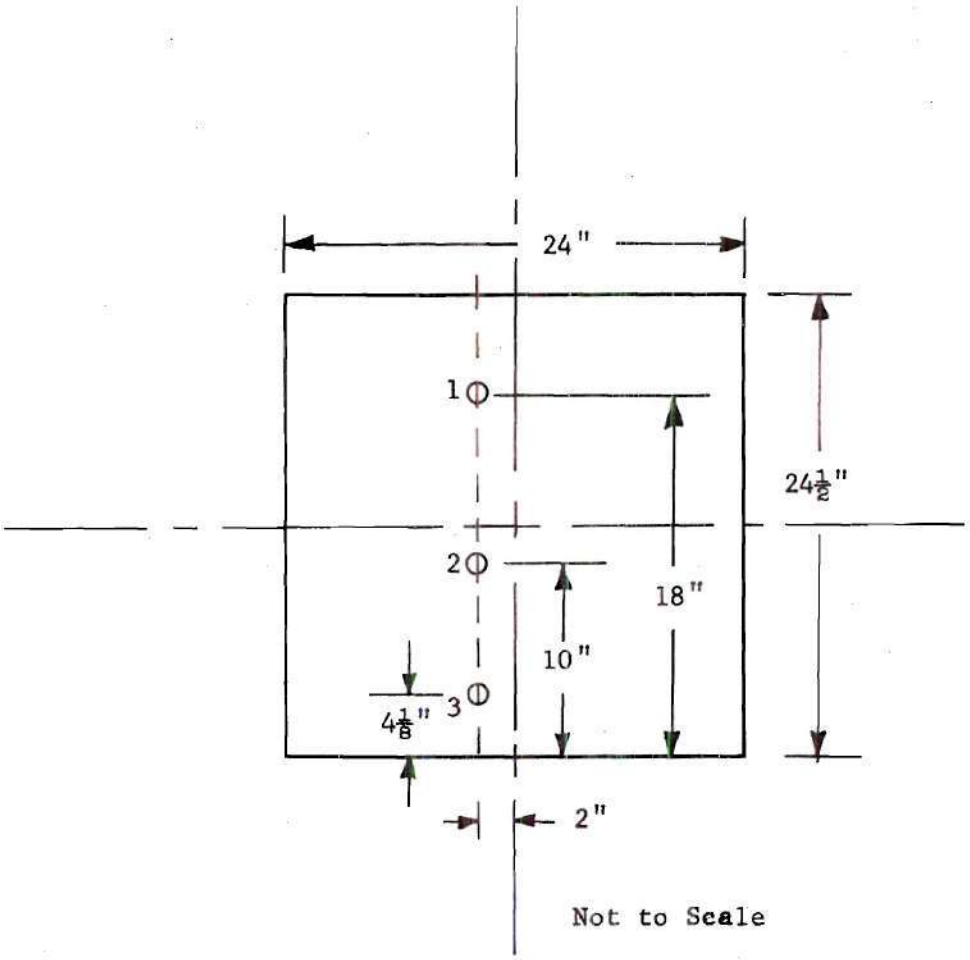

Figure 6. Location of Bottom Thermocouples

information on the bulk profile in the lower part of the tank. Table 1 gives the location of the thermocouples for each aspect ratio. The thermocouple spacing was chosen so as to give an adequate number of thermocouples in the region of the most severe thermal gradients.

Table 1. Thermocouple Locations

Sensor Number	2 Foot Tests Location (Inches from Bottom)	6 Foot Tests Location (Inches from Bottom)	9.75 Foot Tests Location (Inches from Bottom)
1	1	1	1
2	2	6	6
3	4	12	12
4	6	18	24
5	9	24	36
6	12	30	48
7	14	36	60
8	16	42	68
9	18	48	78
10	19	54	88
11	20	64	96
12	21	66	102
13	22	68	108
14	23	70	112
15	23.5	71	116
16	Surface	Surface	Surface

The bulk thermocouples were made from Honeywell 20 gage copper-constantan wire with a double coating of polyvinyl insulation. The reason

for choosing this stiff wire was so that the thermocouple junctions would remain fixed after installation. The thermocouple junctions are located two inches from the Plexiglas probe so that any probe effects should be small. The thermocouples were cemented in place using a silicone rubber cement. The probe is located within the tank, such that the thermocouple junctions form an imaginary centerline of the vertical axis. The thermocouple wires ran through the center of the Plexiglas tube and out at the tank top, then through the probe support arm and into the junction box. At the junction box, 24 extension wires are used to feed the data to the multipoint recorder.

Previously, questions have been raised as to the effect, if any, that the size of the bulk probe has on the temperature measurements. Schneider (26) has recently shown that the overall effect on temperature reading using probes of this diameter as well as larger diameter probes is negligibly small. Another possible source of error in using the bulk temperature probe is the conduction effect from the relatively large wire. Tatom (5) noted that, by removing approximately 1.5 inches of the wire insulation on the thermocouples in the top one foot of the tank, the conduction effect produced an error no greater than ± 0.04°F and hence is negligible.

Photographic System

The system used to obtain the qualitative information of the flow in the tank consisted of a Yashica TL Super 35 mm single lens reflex camera, light box, and Schlieren system. The camera used had an f 1.4, 50 mm lens. The film used throughout all the tests was Kodak Tri-X and

was developed in Acufine developer.

The particle streak photographs were taken by using a one second time exposure and reducing the f number during the exposure. However, this arrangement made particle streaks appear large at the start of the exposure and small at the end. Thus, in later photographs, the f number was started at a high number and reduced to the lowest setting. This procedure made the streaks increase in size in the flow direction. In obtaining the particle streak photographs an intense light system was employed at the tank top. The light system as shown in Figure 7 consists of four 1000 watt Sylvania Quartz Iodine lamps and a converging lens arrangement. The light system was designed so that a thin parallel beam of light could be directed either from the top of the tank, i.e., parallel to and midway between the glass plates, or perpendicular to the tank, in which case the photographs are taken at the tank top.

In photographing the particles from the tank top, the light source must be placed such that the light beam is located within the top three feet of the fluid. Particles at greater depths cannot be photographed because the test fluid absorbs or attenuates the light reflected from the particles.

Brooks (27), Tatom (5), and Schneider (26) have previously used particles of this type. The particles are called Eccosheres and are manufactured by Emerson and Cuming, Inc. They are hollow glass spheres with a specific gravity very close to water and reflect light very well. The diameter of the particles used in the tests varied in size from $0.0024 \leqq D \leqq 0.0035$ inch.

The Schlieren photographs were made by using a six inch Schlieren

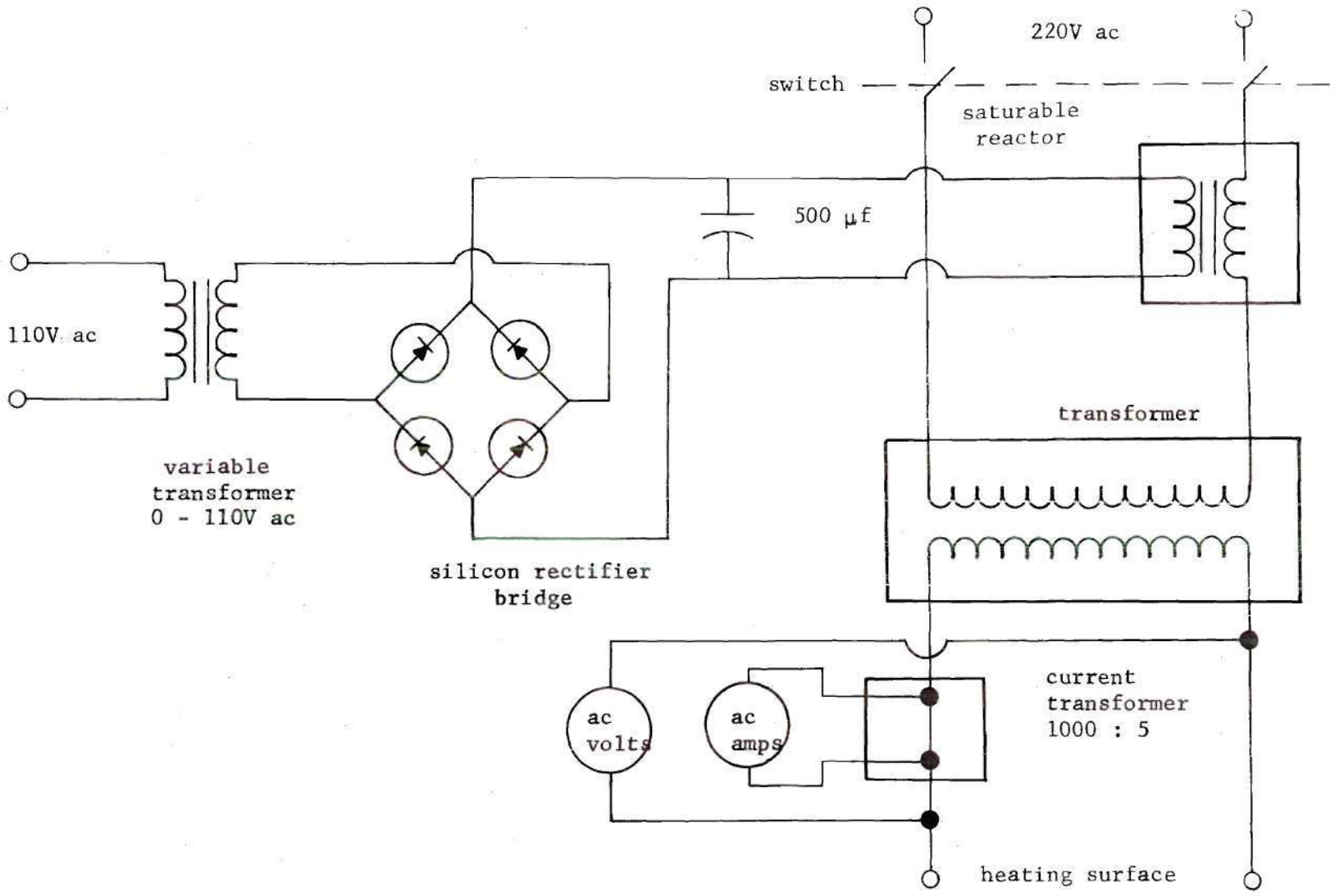

Figure 7. Schematic Drawing of Power System

system manufactured by the Aerolab Supply Company. Since the mirrors on the basic system were relatively fixed, a second mirror system consisting of four 10 by 14 inch front-surface mirrors was used in obtaining photographs at various elevations in the tank. One series of shadowgraph photographs was taken by employing the Schlieren light source, one concave mirror and an opaque sheet of paper attached to the glass plate. However, these photographs revealed little new information of the flow characteristics and were discontinued.

Power Supply and Control

Heating of the panels within the tank was accomplished by allowing a low voltage, high amperage alternating current to flow through the Inconel sheets. Since the electrical resistance of the heating panels is low, a large current is necessary to provide adequate heating rates. The high currents, up to 600 amps, were possible by using a stepdown dry type transformer and saturable reactor. As shown in Figure 4, the bottom and side panels were heated by separate systems.

The side heating system utilizes a 7.5 KVA transformer and a 5.0 KVA saturable reactor. The saturable reactor is controlled by using a variable direct current voltage from a small variable A.C. transformer and a silicon rectifier bridge. The bottom power utilizes a 7.5 KVA transformer and a 2.0 KVA saturable reactor and is controlled like the side power. Figure 8 shows an electrical diagram of the side power supply circuit. The circuit for the bottom power is identical except for the different reactors.

Fill, Drain, and Filtration System

In filling the test tank, tap water is used. However, the water

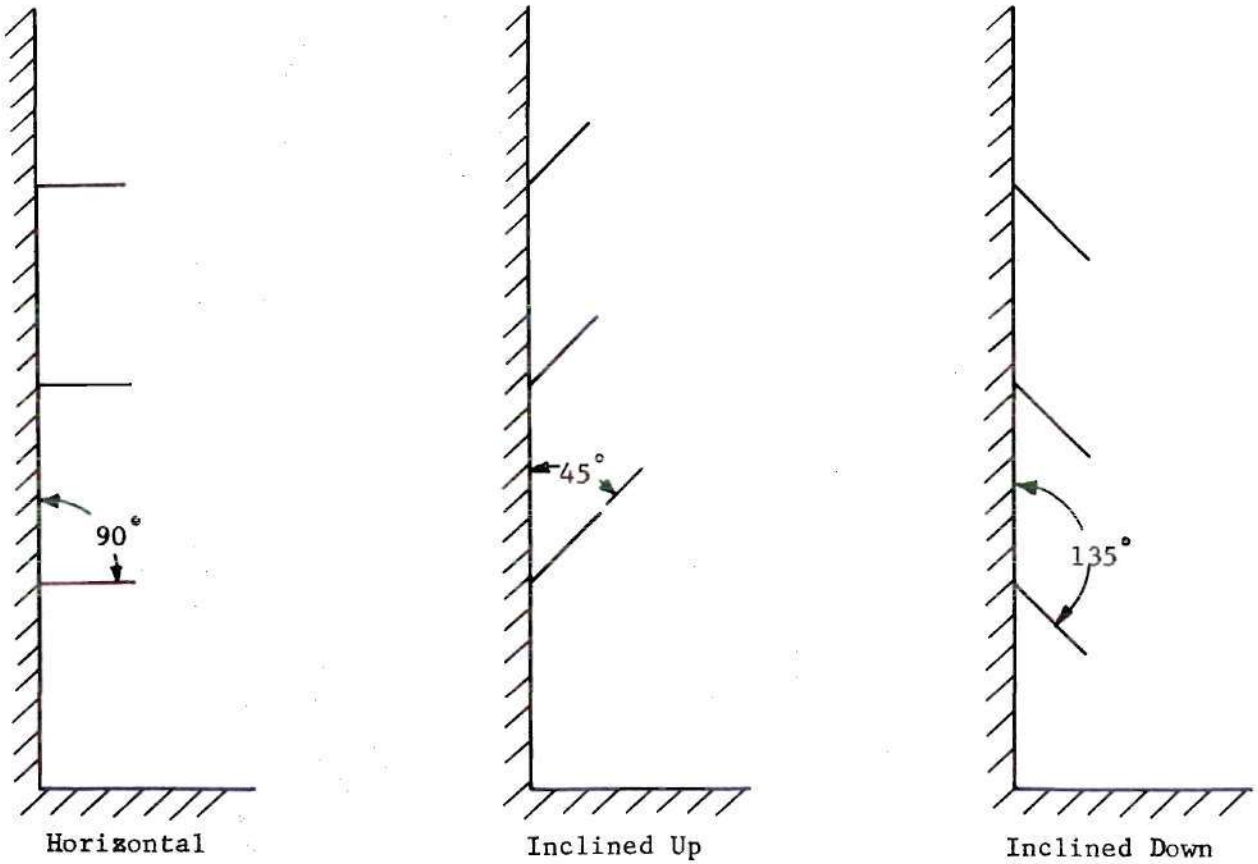

Figure 8. Baffle Configurations

is filtered before entering the tank by a Cuno Micro Klean filter unit. This unit filters out particles as small as five microns in diameter; hence, it is sufficient in providing clear water for the photographs. To drain the tank, two lengths of garden hose, attached at one end of a one inch pipe, are lowered into the tank. A three-quarter horsepower Worthington Monabloc pump is used to remove the fluid. The fluid within the tank may be circulated to obtain either a uniform temperature or to remove extraneous particles. This process is accomplished by opening the circulation valve on the control panel, placing the intake and exhaust hoses within the tank and then turning on the circulation pump, which is also a three-quarter horsepower Worthington Monobloc pump. During some tests, the combined features of draining and filling were employed so that a lower uniform temperature would be obtained.

Tap water was used as the test fluid because of its availability and relative pureness. Upon checking the electrical resistivity of several samples, it was found that the resistance per unit volume for the tap water was approximately 4.7×10^5 ohms per cm^3, while for distilled water it is 5.0×10^5 ohms per cm^3 (28).

The fill system consists of two valves located at the wall next to the control panel. A combination of hot and cold tap water or either one separately may be used in filling the tank. The hot water line was added so that a higher initial bulk temperature could be obtained.

Experimental Procedure

Temperature Data

In obtaining the wall and bulk temperature data, the desired liquid

level within the tank was established and the liquid circulated to obtain a uniform thermal equilibrium state. If the tank had been previously drained, the filling process usually resulted in a uniform thermal state and the liquid was not circulated. The procedure of filling and circulating the liquid within the tank, to obtain a uniform thermal condition, was relatively easy at depths of two and six feet, but at depths of 9.75 feet it was quite difficult.

Approximately one-half hour before making a test, the strip chart recorder power was turned on so that the instrument internal temperature would be stabilized before any data were taken. A zero time reading of the bulk temperature was taken on the recorder while a zero time reading of the wall temperature was taken using the potentiometer. After completion of all initial readings, a check of the data was made to determine if the tank and fluid were at a uniform temperature. Occasionally, a slight gradient in both the bulk and wall temperature existed. However, this gradient never amounted to more than a $\pm$ 0.5°F temperature difference between the bottom and top thermocouples within and on the test tank. With this small gradient, the tank was considered to be in a uniform thermal state.

About five minutes were required to make and check the initial reading for each test so the fluid within the tank was always in a quiescent state before the power was turned on. After the initial reading was made, the recorder was again started, the power was turned on to the tank and the stopwatch was started simultaneously. Frequently during a test the power to the heating panels was adjusted in order to keep the heating rate uniform. This procedure required either increasing or decreasing

the current to the saturable reactors via the small variable transformers on the control panel. Values of the heating panel current and voltage were tabulated along with the variac settings. The wall temperature-time data were recorded every five minutes using the potentiometer, stopwatch, and tape recorder. The test was completed when the thermal gradients within the tank reached a quasi-steady state with the bulk temperature differences increasing linearly with time.

During the first series of tests, the wall temperature on both walls was recorded. However, upon checking the data, the temperatures of the walls were relatively close to each other, being no more than ± 1.0°F difference. These measurements indicated that the walls were transferring almost identical amounts of heat. Thus, in later tests only the temperature data from one wall were recorded.

As a further check on the heating rates from each wall, the voltage drop across each wall was measured during several tests. It was found that the maximum percent error in the voltage drop occurred when testing at low power. The maximum error in voltage drop for the two walls was no greater than 7.26 percent at the low power settings. This value dropped to about 5.0 percent during the highest power test.

Photographic Data

To obtain the photographic data, duplicate tests were run since operation of the camera and potentiometer, without outside assistance, during the same tests was not possible. Also, by running duplicate tests, a check on the reproducibility of the bulk temperature data could be made. The initial preparations for the photographic tests were more elaborate than for the temperature tests. The details of the initial preparations

are discussed by Brooks (27) and Tatom (5). Briefly, they consisted of emptying, cleaning, and refilling the test tank with filtered water. At the beginning of the filling process the particles were placed in the tank so that during the filling process, the particles would be more uniformly mixed within the bulk liquid. The amount of particles placed within the tank varied with each test, but the number recommended by Tatom (5) appears to give satisfactory results.

After completion of the filling process, the camera was positioned and focused and all initial data recorded. This procedure usually required about five minutes which was sufficient time for the particles and fluid within the tank to be in a quiescent state. Once the test was started, a record of the time and exposure number was made along with any other visually observed phenomena. During each exposure, the f number was manually increased or decreased to give a sense of direction to the particle streaks. The Schlieren photographs utilized the same procedure except that no particles were used and the f number remained constant.

The film used in making all of the photographs was Kodak Tri-X Pan film with an ASA 400 rating. However, the exposures were made with an ASA 800 rating. The film was developed in Acufine developer. It was found that this procedure produced a fine grain which gave a better contrast to the photographs.

CHAPTER III

TEST RESULTS

Thermal Analysis

In this study of baffles and their effect on thermal stratification a total of 119 tests with and without baffles was conducted. These tests covered a modified Grashof number range from 7.5×10^8 to 4.6×10^{15} with the fluid properties in the Grashof number evaluated at the wall temperature. During these tests, the tank height to width ratio, often called the aspect ratio, L/W, varied between 1 and 4.88. Table 4 in Appendix D presents a summary of the test program. Figure 8 illustrates the various baffle configurations tested. To insure that the test results were accurate, many of the test conditions were rerun several times. For example, tests T-2, T-5, and T-6 were run under identical conditions. A check of the experimental data showed that bulk temperature profiles at the specific time intervals were almost identical. Deviations between temperature differences for the tests for the different thermocouple locations were no more than ± 5 percent at equal time values. Also, the difference between the integrated average bulk temperature and initial temperature for specified time intervals was compared and found to agree ± 2 percent.

In this investigation, for a given aspect ratio, the effects of different numbers and sizes of baffles and baffle inclination for several heat flux ratios was studied. Since the aspect ratio appears to play a

major role in the shape of the bulk temperature profile and since three different aspect ratios, with and without baffles, were investigated, it was felt that the experimental results should be presented as follows:

1. No baffle tests, $L/W = 4.88$
2. Baffle tests, $L/W = 4.88$
3. No baffle tests, $L/W = 3.0$
4. Baffle tests, $L/W = 3.0$
5. No baffle tests, $L/W = 1.0$
6. Baffle tests, $L/W = 1.0$

No Baffle Tests, $L/W = 4.88$

For a fluid level of 9.75 feet, typical measured bulk temperature profiles without baffles for different time intervals are illustrated in Figures 9, 10, and 11. As previously noted by Tatom (5) for the case of side heating only, the bottom bulk temperatures remain essentially constant at the initial temperature of the fluid. An analysis of Figure 9 reveals that a temperature gradient is immediately set up after heat is applied at the side walls and penetrates deeper into the bulk fluid with increasing time. From Figure 10, it is seen that, with the addition of bottom heating, the temperature gradient within the bulk fluid is not as severe as for the case of side heating only, except at the tank top. However, the gradient near the top is reduced when bottom heat is applied. With the addition of a larger quantity of heat at the bottom than at the sides, that is, for large values of q_b/q_s, a temperature inversion is set up at the bottom of the tank as illustrated in Figure 11. However, this temperature difference is not as large as that formed at the top. The reason for such severe thermal gradients in the bulk fluid, for the case

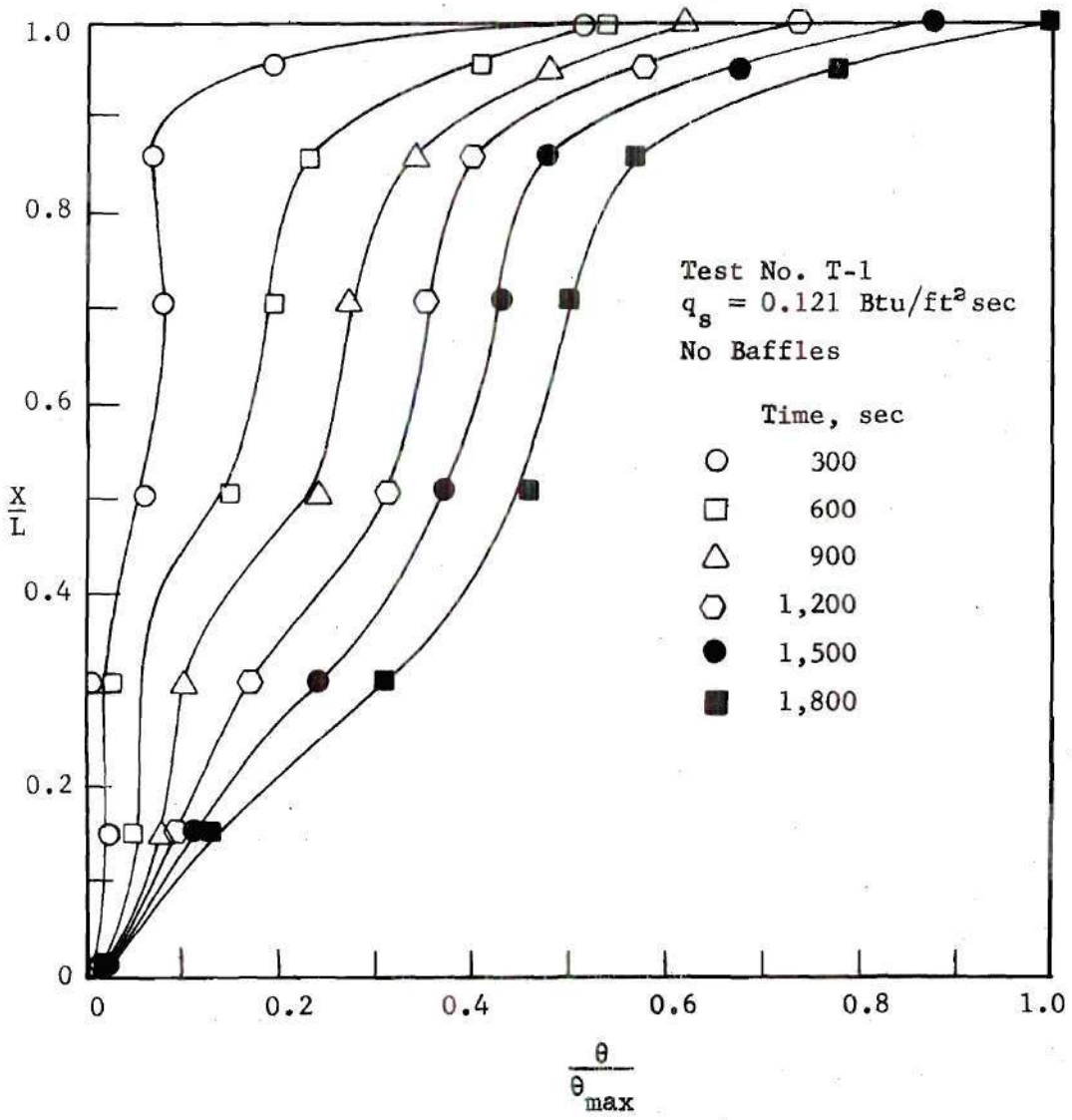

Figure 9. Container Height versus Bulk Temperature; $L/W = 4.88$; $q_b/q_s = 0.0$

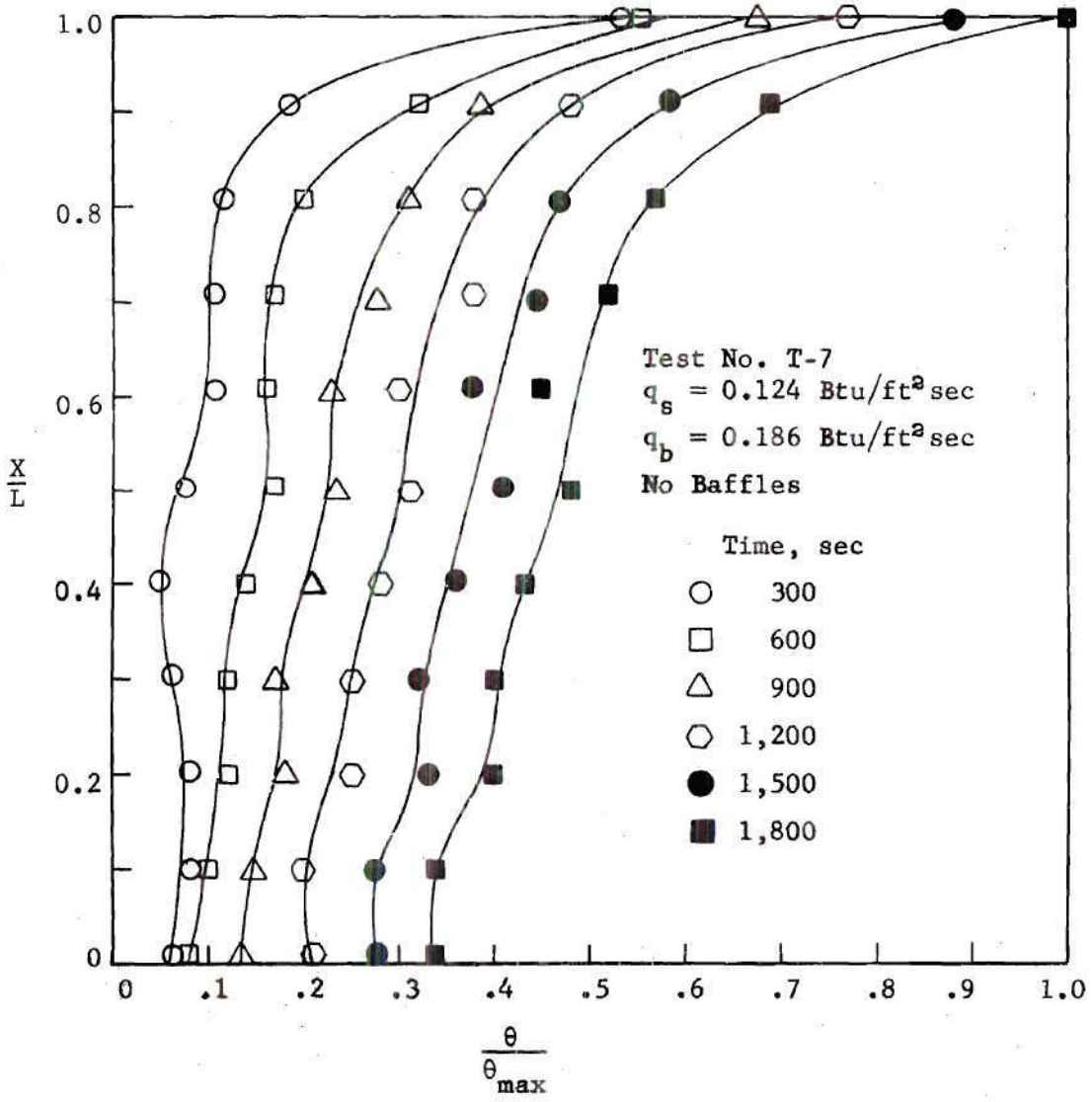

Figure 10. Container Height versus Bulk Temperature; $L/W = 4.88$, $q_b/q_s = 1.52$

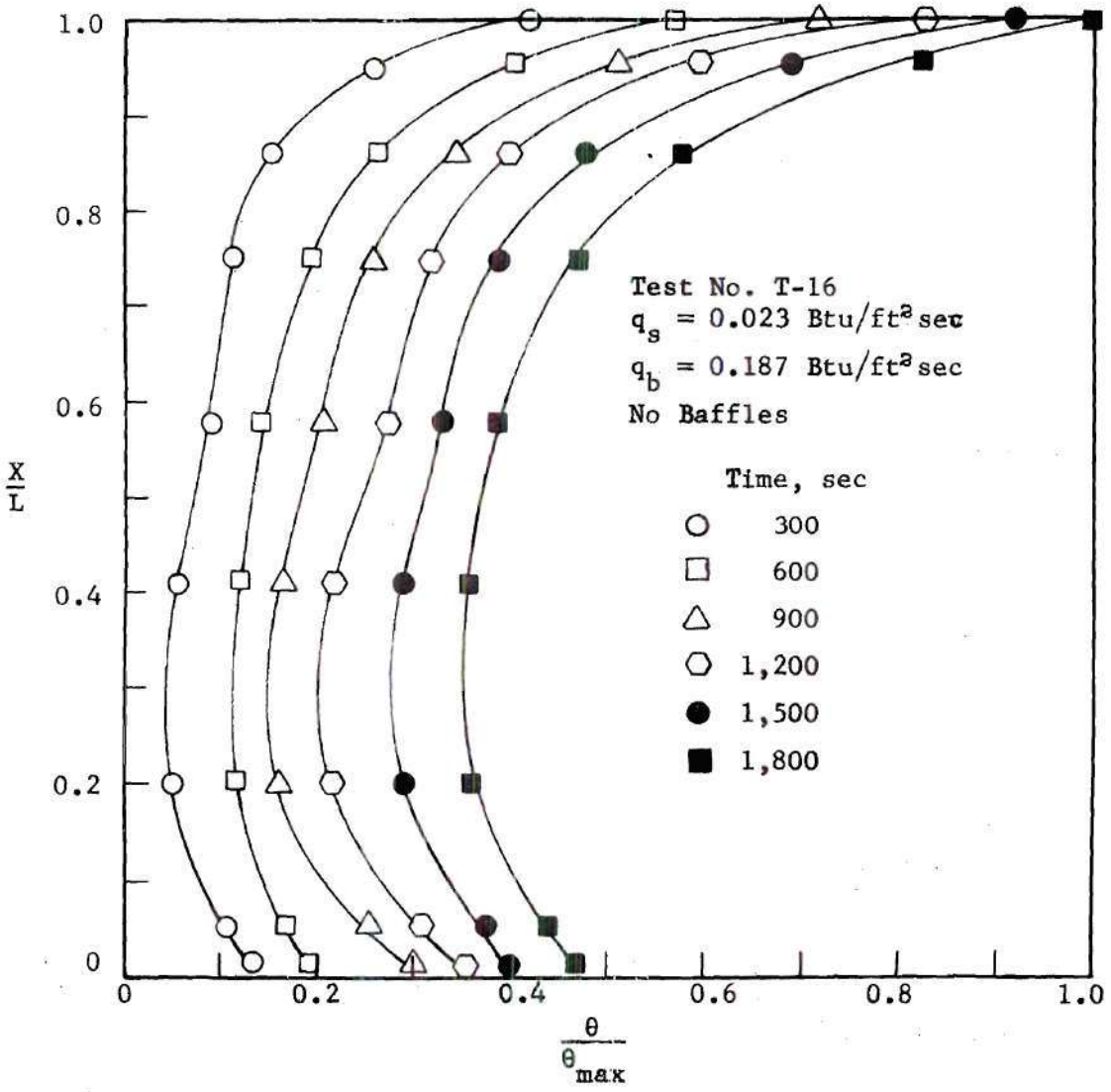

Figure 11. Container Height versus Bulk Temperature; $L/W = 4.88$, $q_b/q_s = 8.09$

of no baffles and no bottom heat flux is that the fluid heated at the tank side walls flows up these walls uninterrupted and mixes only at the tank top as illustrated in the model of Figure 1. Tatom, in his analysis of stratification, noted that some mixing occurs between the bulk and boundary layer flow which has an effect of reducing the size of gradient near the middle of the fluid. This mixing action is a result of the counterflow that exists between the boundary layer and bulk fluid. In the immediate vicinity of the two flow processes, large vortices are generated which greatly assist in the mixing process. The addition of bottom heat flux tends to make the boundary layer along the side wall extremely turbulent, thus assisting in the mixing of the boundary layer flow with the bulk fluid. Also, it tends to increase the turbulence within the bulk liquid itself, particularly near the bottom. In several of the tests, the temperature near the bottom fluctuated due to the induced turbulence; hence, the data shown in Figures 10 and 11 are instantaneous values. Fluctuations on the order of 0.5°F were experienced near the tank bottom.

The aspect ratio plays a role in the shape of the bulk temperature profiles as is indicated by a comparison of Figures 9, 20, and 29. In the high aspect ratio tests, an S-shape bulk profile is set up and is generally maintained for the duration of the tests. Usually, these profiles become more distinctive with increasing time as the stratification progresses deeper into bulk fluid. Such S-shaped profiles have been obtained previously by Neff (6), Bailey (29), and Tatom (5), when testing vessels with large aspect ratios. The difference between these bulk temperature profiles for the low and high aspect ratio tests is probably a result of the turbulent flow which occurs in the large aspect ratio.

The addition of bottom heating, for $L/W = 4.88$ and 3.0 tends to destroy the S-shaped bulk profile and make the bulk temperature more uniform as illustrated in Figures 10 and 11.

Baffle Tests, $L/W = 4.88$

In adding baffles to the sides of the tank walls, one must realize the different variables which are added to the problem. For example, the size and the number of baffles, along with the angle which the baffles make with the vertical walls, will each affect the bulk temperature profile. Thus, each variable must be investigated separately. For this reason, several tests for various values of q_b/q_s at each aspect ratio with different number and sizes of baffles on the vertical walls of the tank were performed. Figures 9, 12, 13, and 14 illustrate how the number and size of the baffles affect the bulk temperature profiles for the case of side heating only. In comparing these figures, one finds that the typical S-shaped profile of Figure 9, for the no baffle case, is not as pronounced when baffles are added to the tank. Thus, regardless of the baffle size, there appears to be some mixing taking place between the boundary layer flow and the bulk fluid when baffles are added on the vertical walls.

Im comparing Figure 9 with Figures 12, 13, and 14, the maximum temperature difference, θ_{max}, is not the same in all four cases. Generally, the tests with baffles have a higher value of θ_{max} as indicated in the figures. The reason for higher values of θ_{max}, when baffles are added, is that the baffles retard the boundary layer flow and reduce the bulk mixing at the top of the tank. That is, if no baffles are present, the boundary layer flow moves along the vertical side walls uninterrupted and

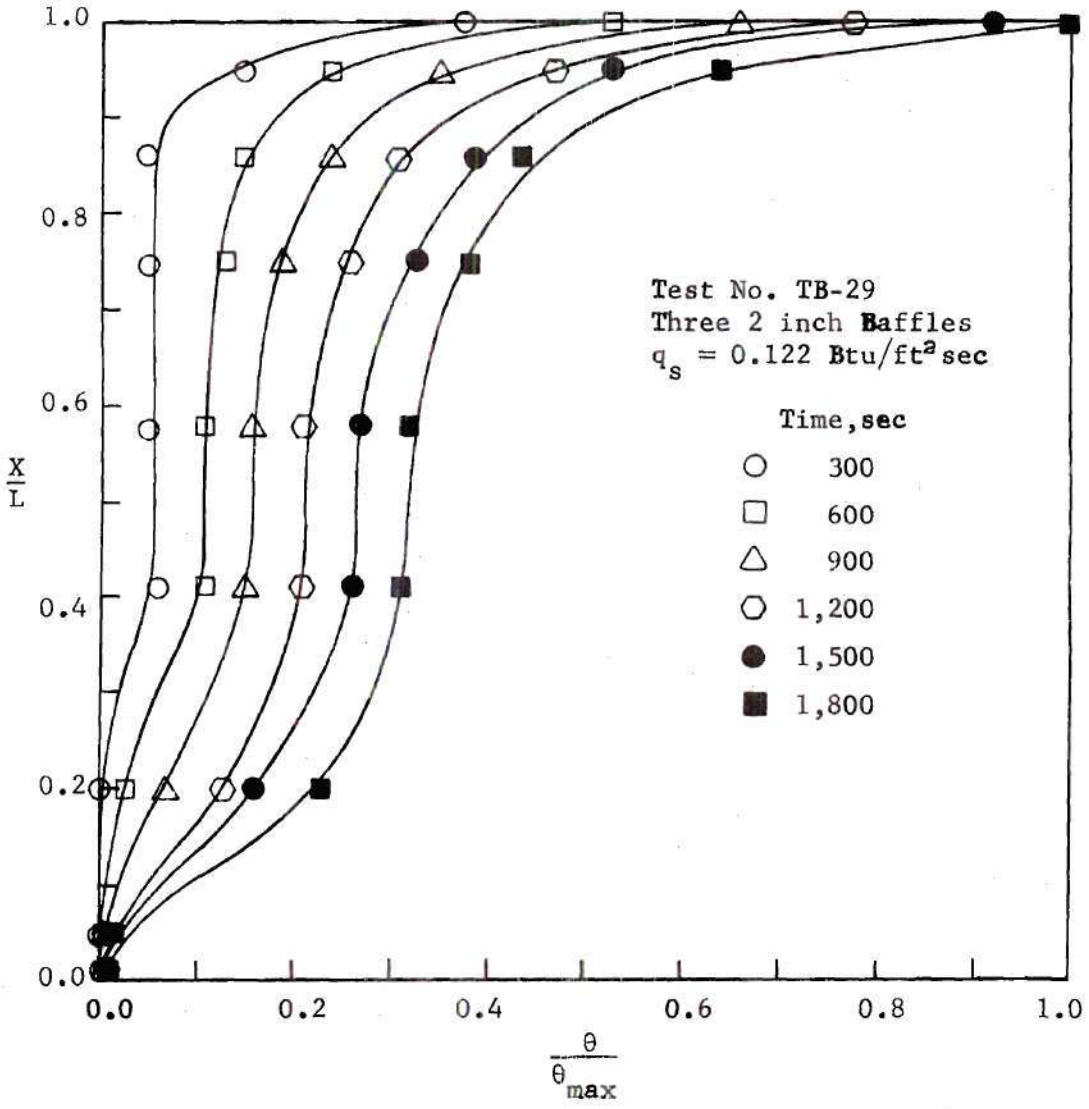

Figure 12. Container Height versus Bulk Temperature; $L/W = 4.88$, $q_b/q_s = 0.0$

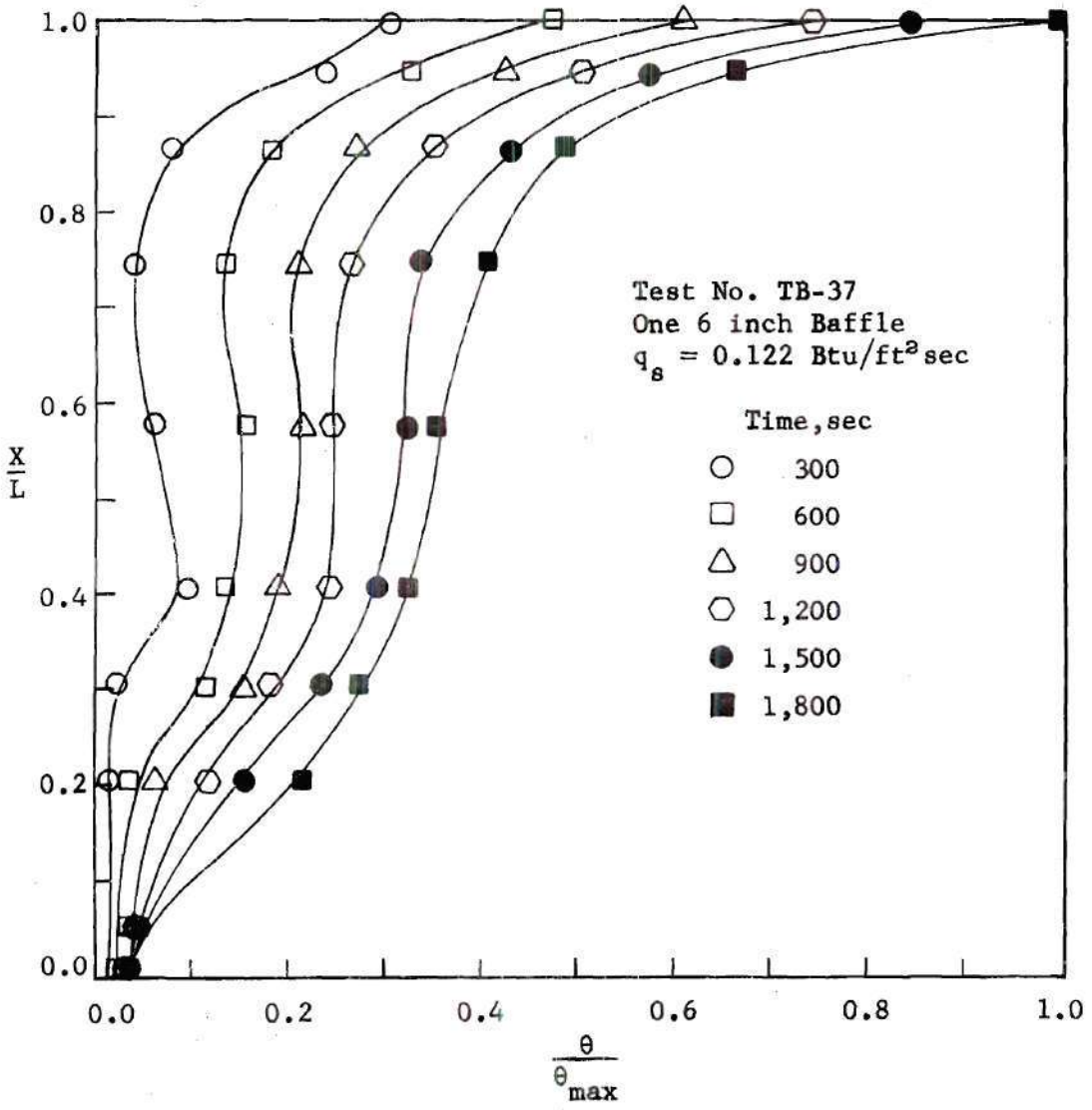

Figure 13. Container Height versus Bulk Temperature; $L/W = 4.88$, $q_b/q_s = 0.0$

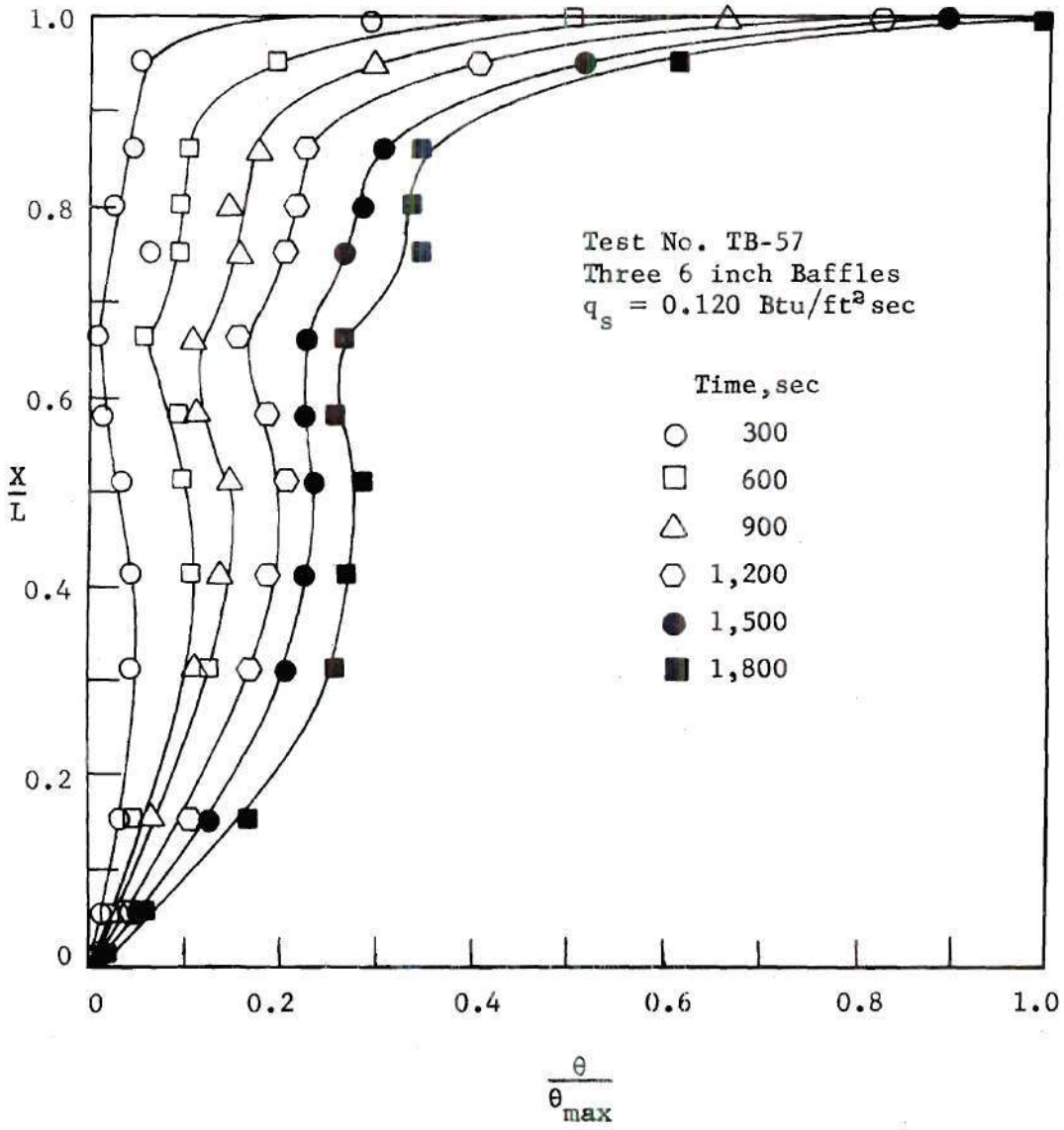

Figure 14. Container Height versus Bulk Temperature; $L/W = 4.88$, $q_b/q_s = 0.0$

acquires a larger velocity than is obtained when baffles are present. When this flow reaches the top of the fluid level, a rapid mixing takes place as the fluid turns the corner. When baffles are added, the boundary layer flow is slowed down considerably and hence, the bulk mixing near the tank top is not as turbulent. Thus, the hot fluid tends to remain on top, creating a large value for θ_{max}.

Perhaps a better explanation of how the baffles promote bulk mixing may be seen from Figure 15, where θ_B, bulk temperature difference, is plotted against x/L for tests number T-7 and TB-58. In this figure only two time intervals are illustrated since all other values of time are bracketed by these intervals. From this figure it is seen that the baffles have the effect of mixing the heated boundary layer fluid with the bulk fluid in the lower portions of the tank. Hence, a more uniform temperature profile results over a major portion of the tank height. Essentially, the baffles promote more mixing near the bottom and within the bulk fluid and less mixing near the top. That is, the energy going into the bulk fluid is distributed more uniformly when baffles are present.

Increasing the size of the baffle does not always result in a bulk temperature profile as uniform as when the number of baffles is increased. This fact is seen by again comparing Figures 12, 13, and 14 where, in the ranges of x/L from 0.15 to 0.85, a more uniform temperature profile results when the number of baffles is increased and not when the size is increased. From these figures it appears that the number of baffles is one of the more important parameters. However, if too many baffles are placed on the vertical walls, the flow around these baffles will be slowed down to such an extent that in most cases reattachment of the flow on the

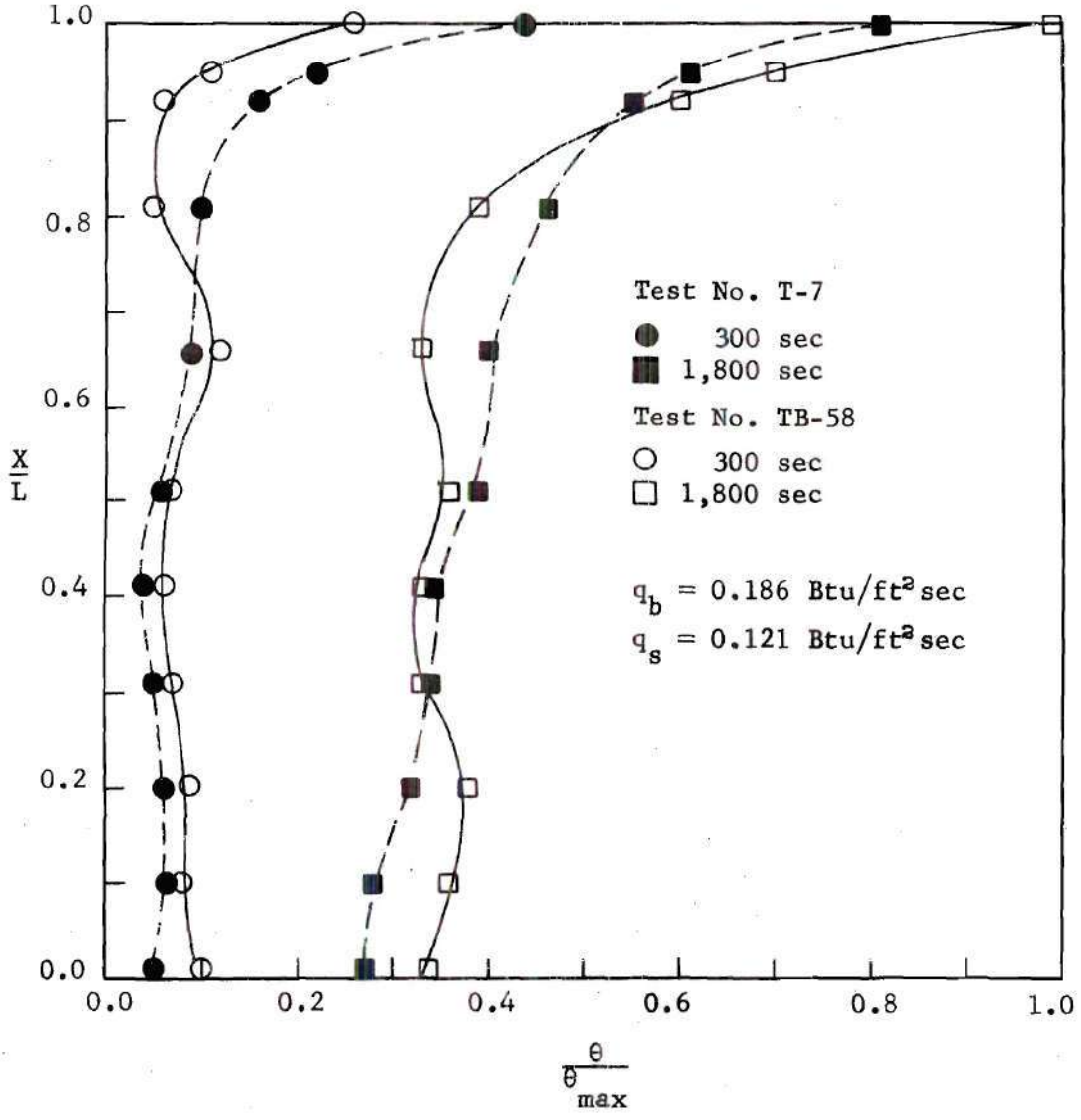

Figure 15. Container Height versus Bulk Temperature for Tests T-7 and TB-58; L/W = 4.88, q_b/q_s = 1.52

backside of the baffle will occur. With reattachment, the mixing action normally associated with the separating flow is reduced and the baffles lose their effectiveness. Vliet (8) in several of his tests observed that the flow around the baffles reattached to the backside of the baffle, reducing the mixing action. However, the distance between successive baffles in his tank was small; thus, only laminar flow existed between the baffles. In most all tests of this investigation, except for the low aspect ratio tests, the distance between successive baffles was large enough to promote turbulent flow over a portion of the vertical walls. Thus, the velocity of the boundary layer flow was large enough in most instances to promote separation from the baffle.

The effect of baffle inclination can be seen by comparing Figures 16 and 17 with Figures 9, 12, and 14. With the baffles inclined up, at an angle 45° to the vertical walls, very little difference in the bulk temperature profile is realized. That is, baffles inclined up do not assist in mixing the flow any more than those perpendicular to the walls. One series of the tests with four 6 inch baffles inclined down at 45° was run and again it was found that this design had about the same effect as the horizontal baffles. At first, it appears that the inclined down baffles might be more effective in promoting mixing since this design would tend to send the heated boundary layer flow into the bulk fluid. However, as previously noted by Neff (6), with increasing time the space between the wall and the concave down baffles becomes filled with the hot boundary layer fluid and they begin to divert the boundary layer flow like horizontal baffles. From analysis of Schlieren and particle photographs

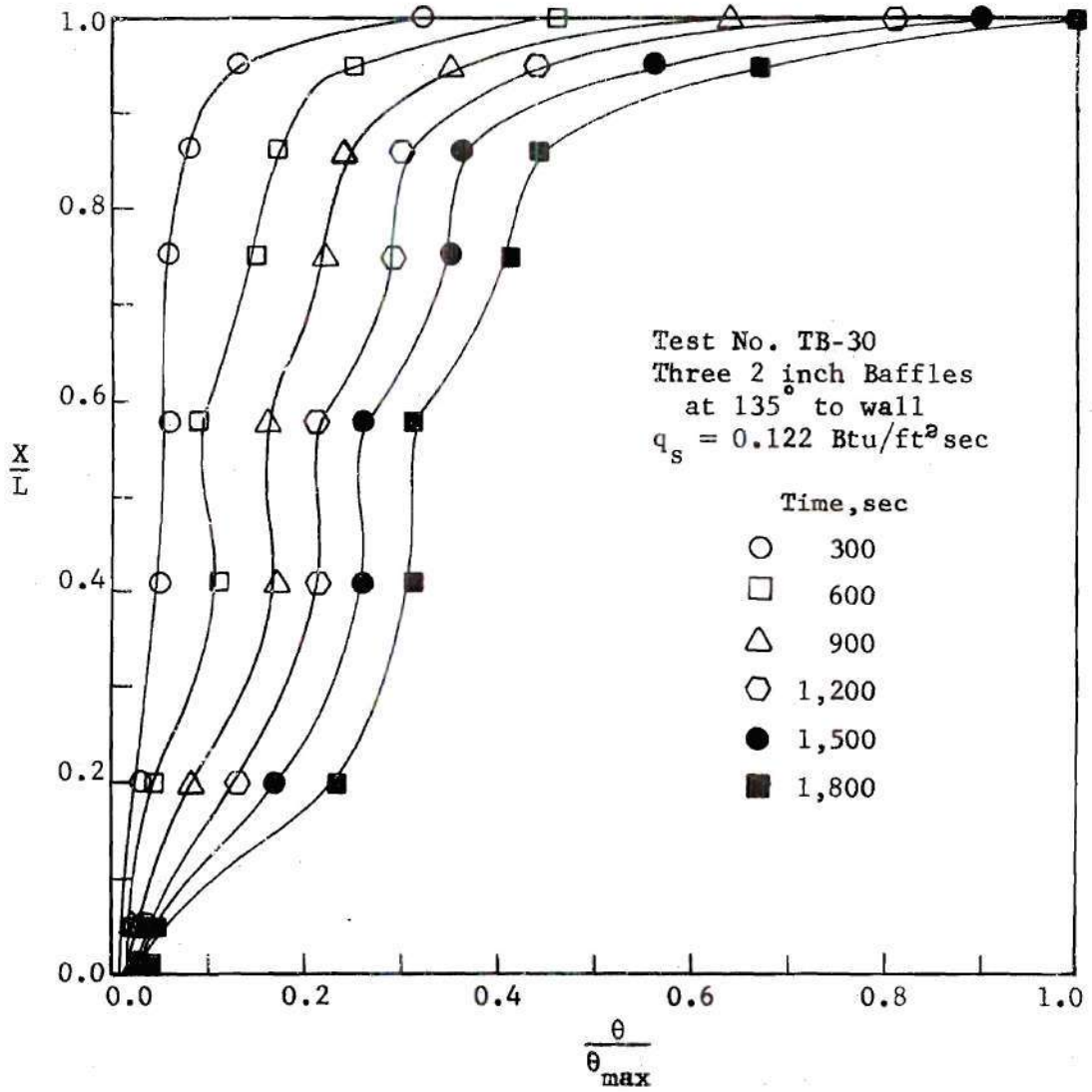

Figure 16. Container Height versus Bulk Temperature; L/W = 4.88, q_b/q_s = 0.0

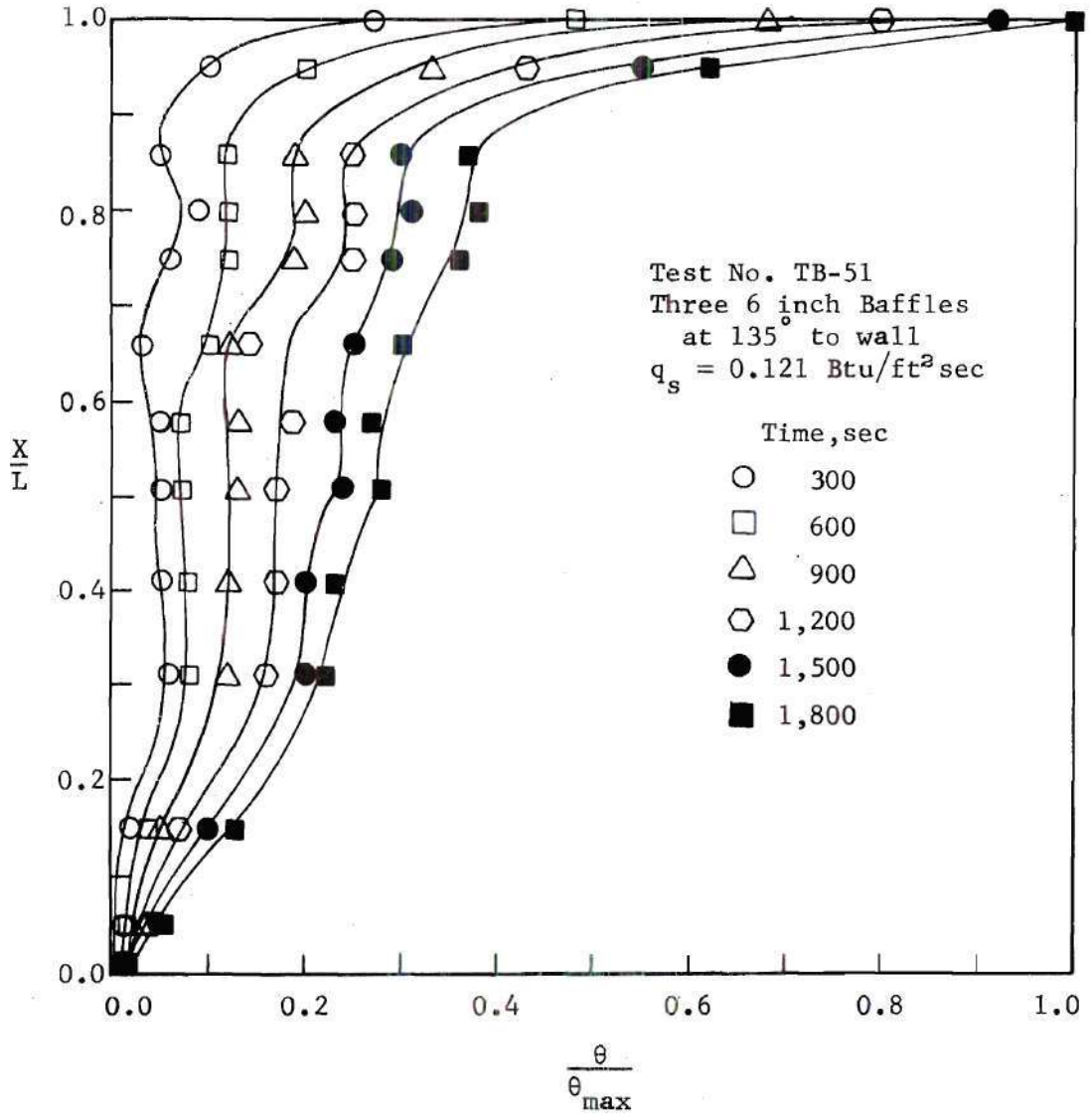

Figure 17. Container Height versus Bulk Temperature; $L/W = 4.88$, $q_b/q_s = 0.0$

of the concave down baffles, it was found that, at times, the baffles do effectively divert the boundary layer flow down. However, this is a periodic type phenomenon and is not steady enough to be any more effective than the flow separation from the horizontal baffles.

The effect of heat flux ratio, q_b/q_s, with baffles added on the walls can be seen by comparing Figures 18 and 19 with Figure 13. For heat flux ratios close to one, an almost uniform bulk temperature results for all values of time with a severe gradient only near the fluid surface. With a further increase of the heat flux ratio to a value around 8.0, a thermal inversion situation is created where the fluid near the heated bottom is at a higher temperature than the rest of the fluid except near the top. This situation is illustrated in Figure 18 for the case of three 6 inch baffles at 90° to the vertical walls. This situation is just as undesirable as the other extreme created with no bottom heat flux. It appears that for large values of the heat flux ratio, the baffles are not effective in promoting mixing but retard the bottom heated fluid, trapping it in the lower region of the tank as is illustrated in Figure 18. Increasing the amount of bottom heat with baffles does not increase the overall bulk mixing. From the experimental data, it appears that the ideal values for the flux ratio, to insure proper mixing of the bulk fluid at the bottom, are around $q_b/q_s = 1.5$ for the aspect ratio of 4.88. Also, from an analysis of the data, the ideal size and number of baffles for the $L/W = 4.88$ tests and for high values of side heating only, appear to be four 4 inch or 6 inch baffles at 90° to the vertical walls. Four baffles on each wall at 90° was not investigated, since placing large numbers of baffles within the tank proved to be quite difficult.

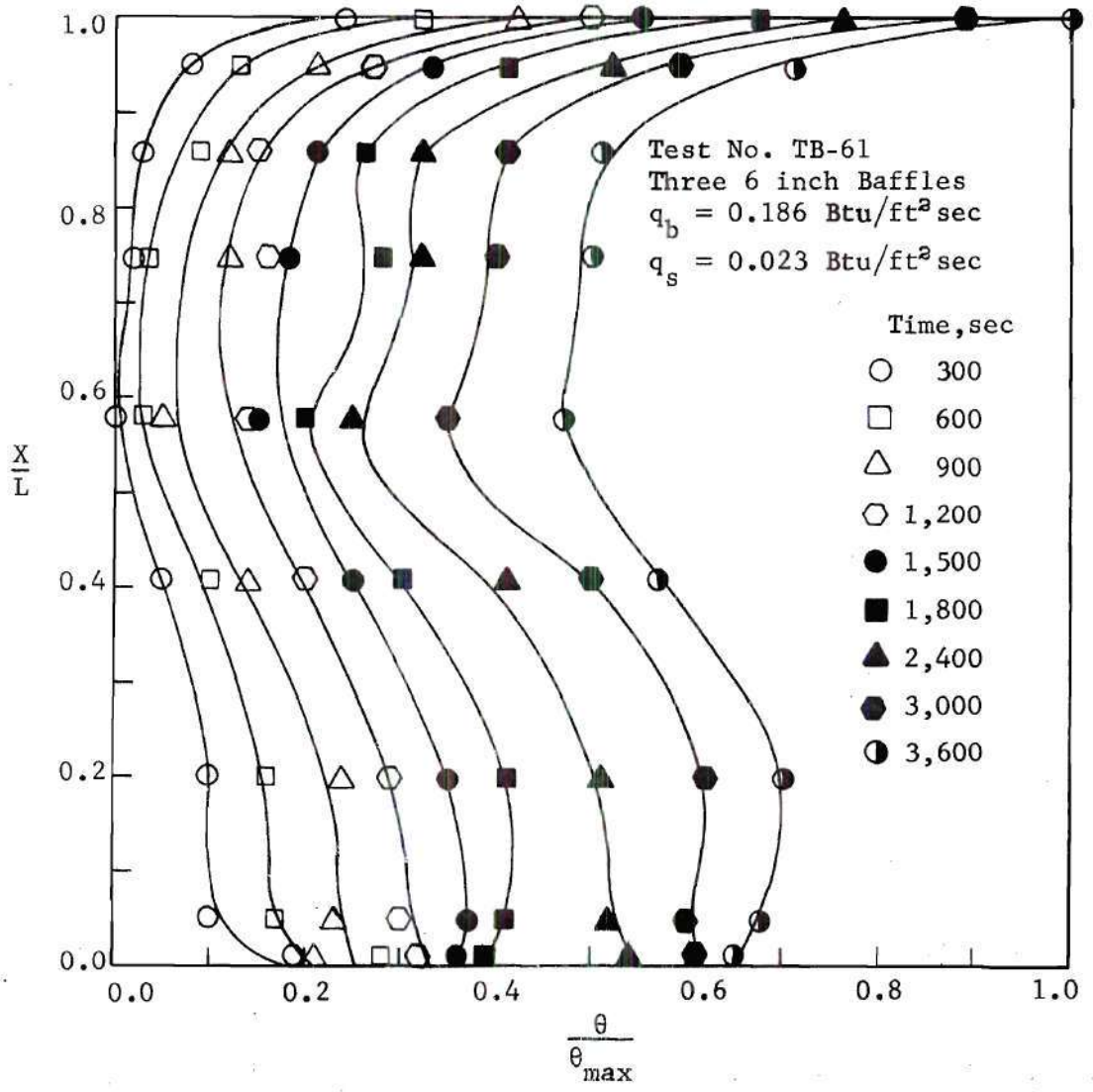

Figure 18. Container Height versus Bulk Temperature; L/W = 4.88, q_b/q_s = 8.09

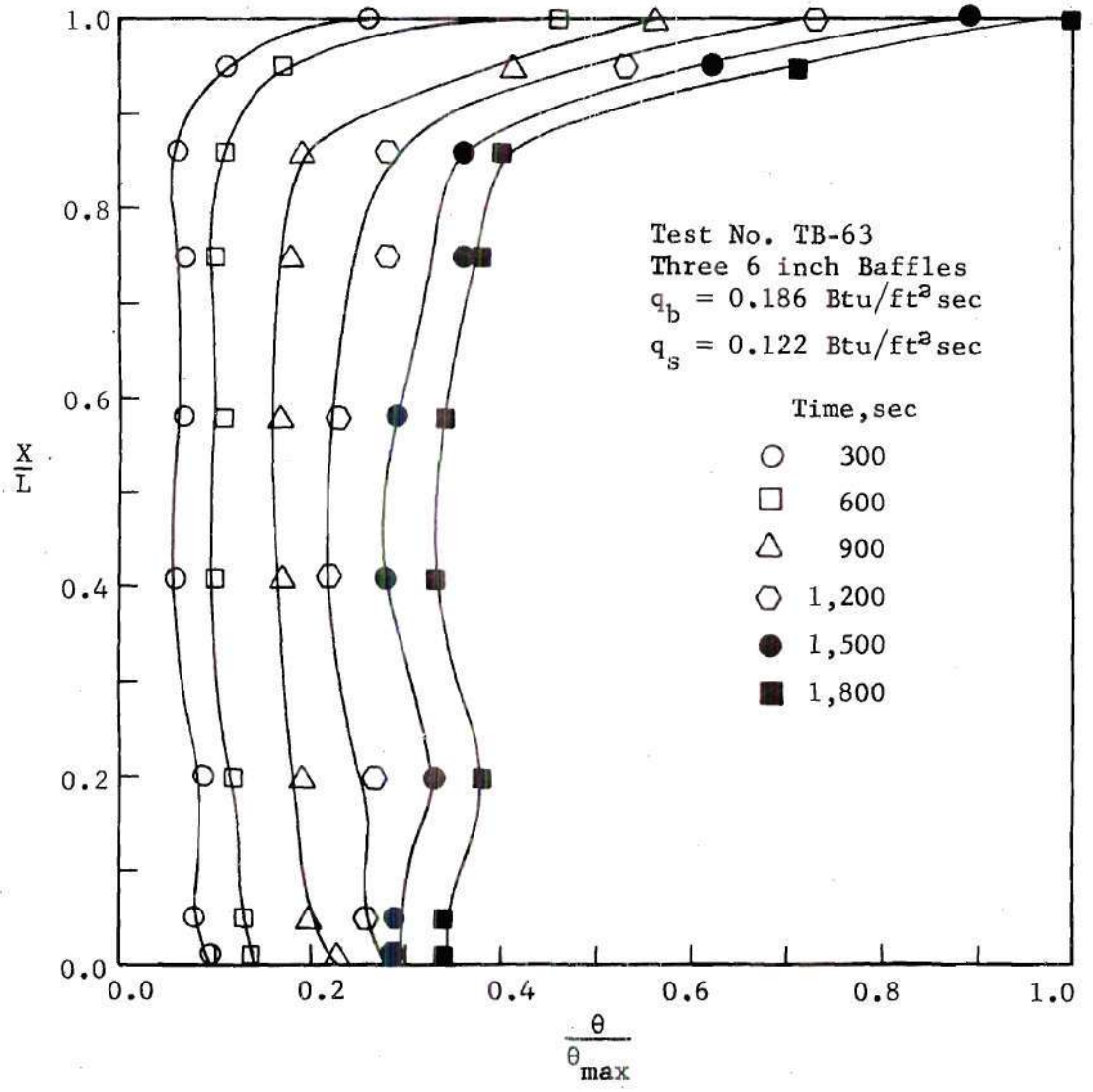

Figure 19. Container Height versus Bulk Temperature; L/W = 4.88, q_b/q_s = 1.52

From the above discussion, it is evident that the size, the number of baffles, and the heat flux ratio are important variables to be considered in design criteria. The magnitude of the individual heat fluxes appears to be of lesser importance, unless a change of phase is taking place near the surface, since these variables are included in the modified Rayleigh or Grashof numbers. A large magnitude of side heat flux promotes a more rapid boundary layer and bulk flow. For a large value of bottom heat flux, on a flat bottom, the cellular convection process extends further into the bulk fluid and interferes with the downdraft bulk flow process. When baffles are added close to the bottom, the effect is to reduce the bulk flow within the tank center in the lower region as is illustrated in Figures 18 and 30.

No Baffle Tests, $L/W = 3.0$

For an aspect ratio of 3.0, Figures 20, 21, and 22 illustrate representative bulk temperature profiles with height. As can be seen from these figures, the profiles bear a similar shape to those exhibited in the larger aspect ratio tests. Due to the difference in side heat flux for these series of tests, the bulk temperature profiles for a heat flux ratio, $q_b/q_s = 0.0$ and $L/W = 3.0$ possess a sharper gradient in temperature in the lower region of the container than those for $L/W = 4.88$. See Figure 9 for a comparison. Also, this gradient increases in severity and depth with time. In Figure 20, the heat flux is greater than in Figure 9. This is a result of running the tests at maximum power to produce maximum mass flow up the container walls.

As in the larger aspect ratio tests, the addition of bottom heating

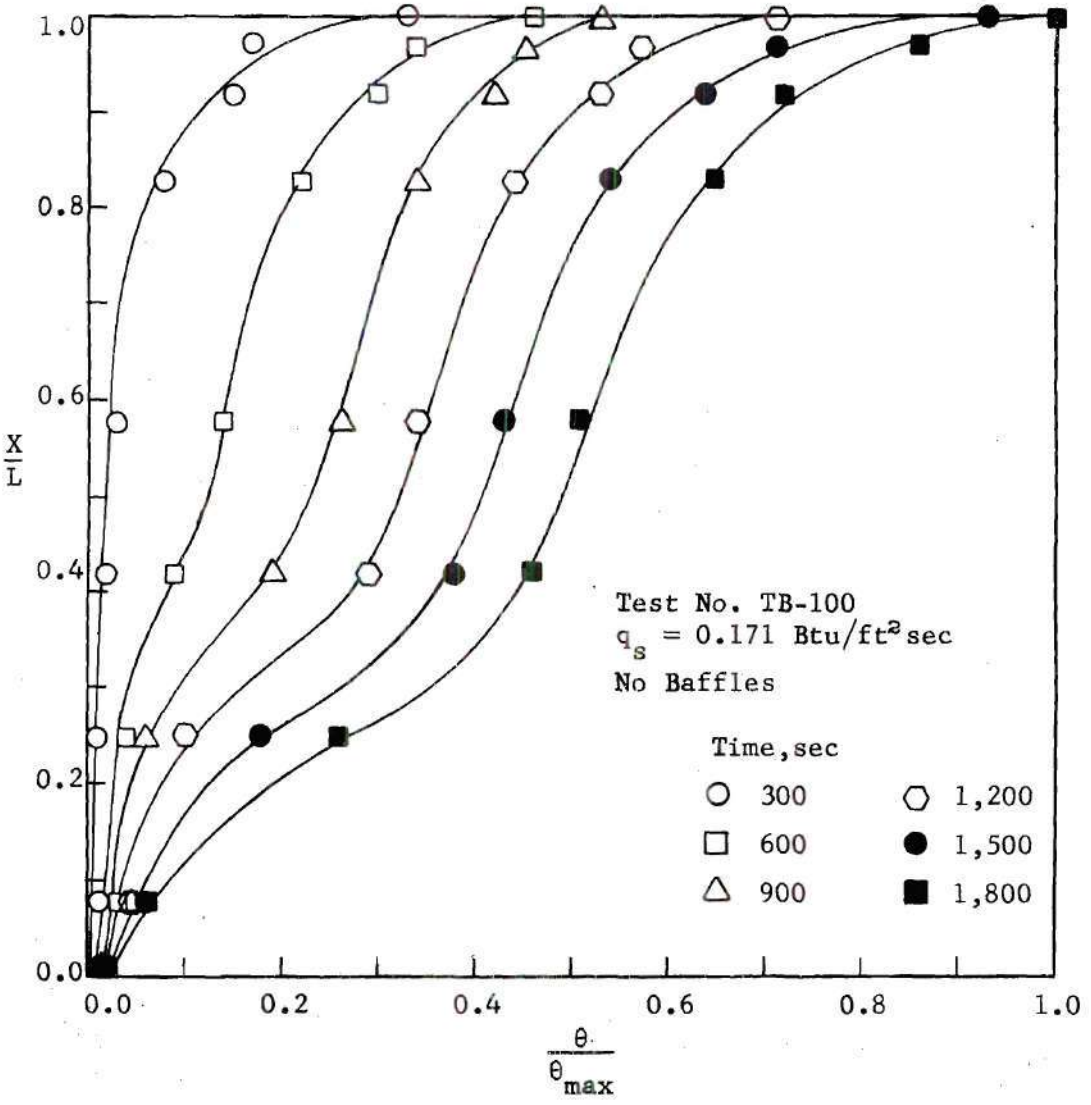

Figure 20. Container Height versus Bulk Temperature; $L/W = 3.0$, $q_b/q_s = 0.0$

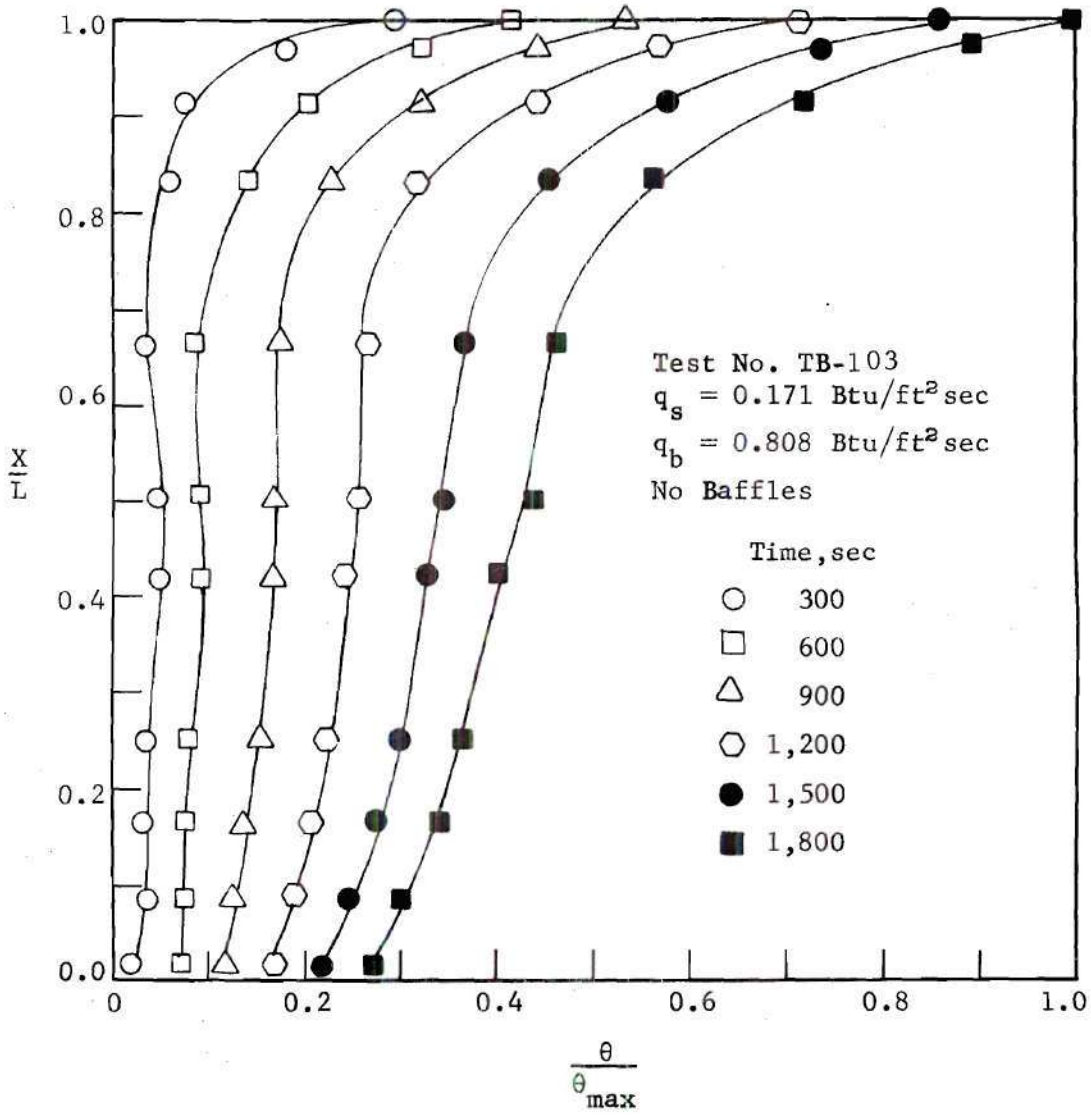

Figure 21. Container Height versus Bulk Temperature; $L/W = 3.0$, $q_b/q_s = 0.465$

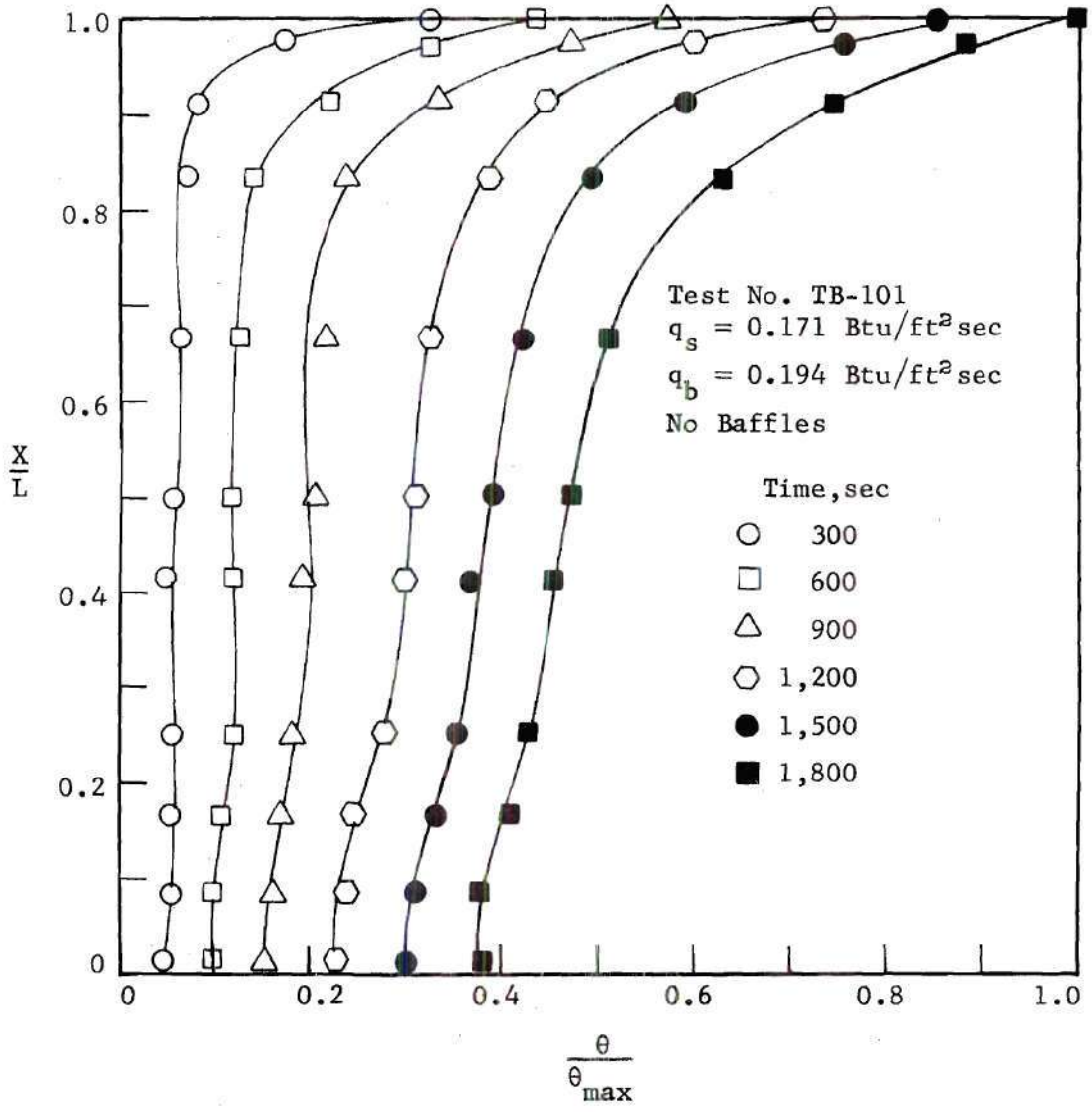

Figure 22. Container Height versus Bulk Temperature; $L/W = 3.0$, $q_b/q_s = 1.13$

reduces the gradient in the lower portion of the tank as seen from Figures 21 and 22. For this aspect ratio, tests involving $q_b/q_s >> 1$ were not run since previous testing had shown this condition to be undesirable and the baffles had little effect. From Figure 22 it can be seen that, for heat flux ratios close to 1.0, some degree of thermal inversion begins. Changing the magnitude of the bottom and/or side heat flux produces results which are similar to Figures 20, 21, and 22 with only a slight decrease in the severity of the bulk temperature gradient.

Baffle Tests, L/W = 3.0

Tests with baffles for this aspect ratio included: two 4 inch, three 4 inch, one 6 inch, and three 6 inch baffles perpendicular to the container walls. No tests were run with baffles placed at angles of 45° or 135° since previous tests had indicated little difference in the overall effectiveness. Table 6 in Appendix D presents a summary of these tests.

As seen by comparing the results of Figures 20, 23, and 24 for $q_b/q_s = 0.0$, the two 4 inch baffles have a smaller effect on the bulk temperature profile than do the three 4 inch baffles. By effect is meant the distributing of the heat input to reduce the bulk temperature gradient over the tank height. The best baffle arrangement tested for this aspect ratio was three 6 inch baffles equally spaced on each wall. The results of this arrangement are illustrated in Figure 27. In comparing the results of Figures 20, 26, and 27, one must keep in mind the results obtained in the larger aspect ratio tests. For L/W = 4.88, the six inch baffles were found to produce the more uniform profiles.

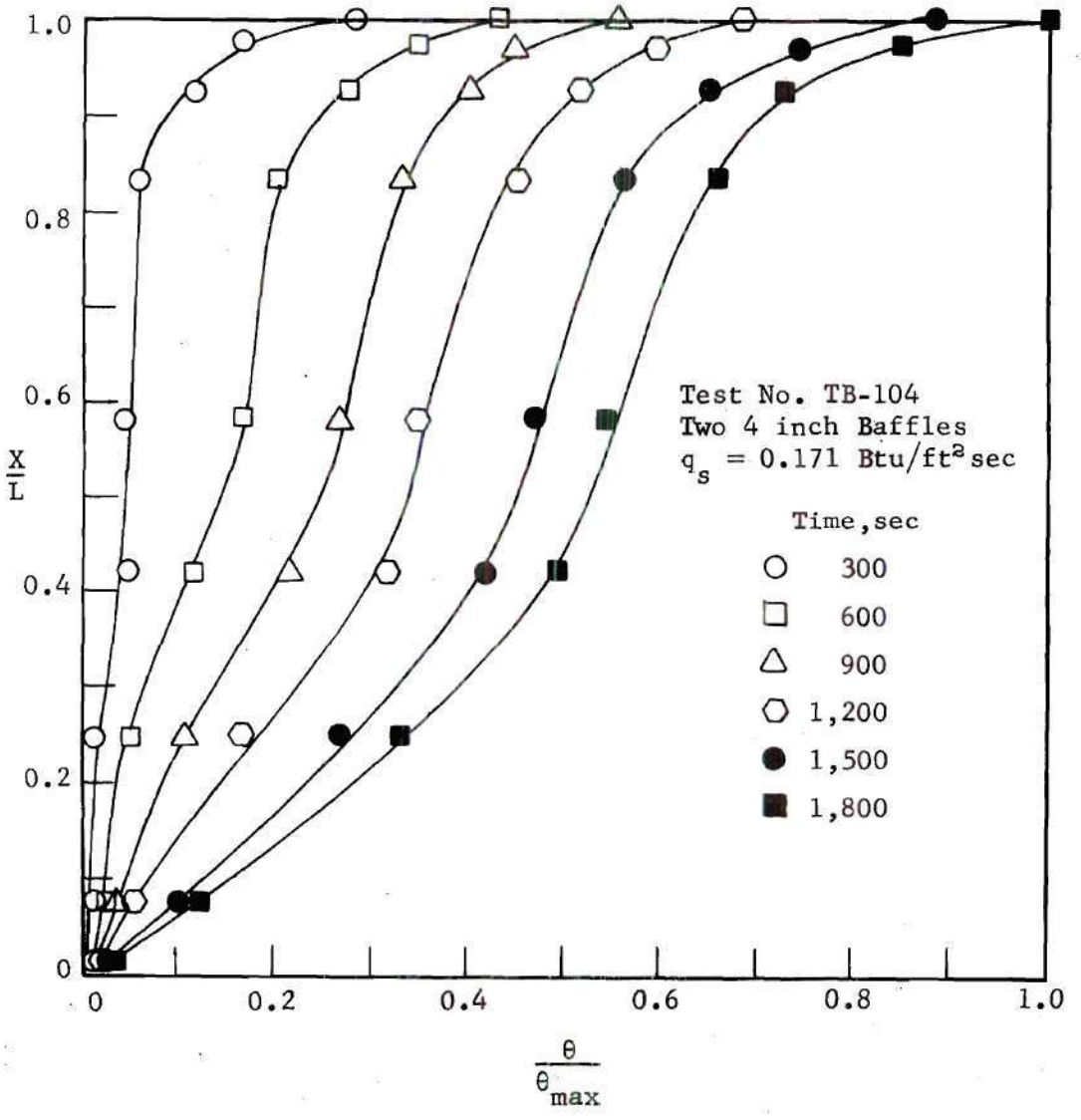

Figure 23. Container Height versus Bulk Temperature; $L/W = 3.0$, $q_b/q_s = 0.0$

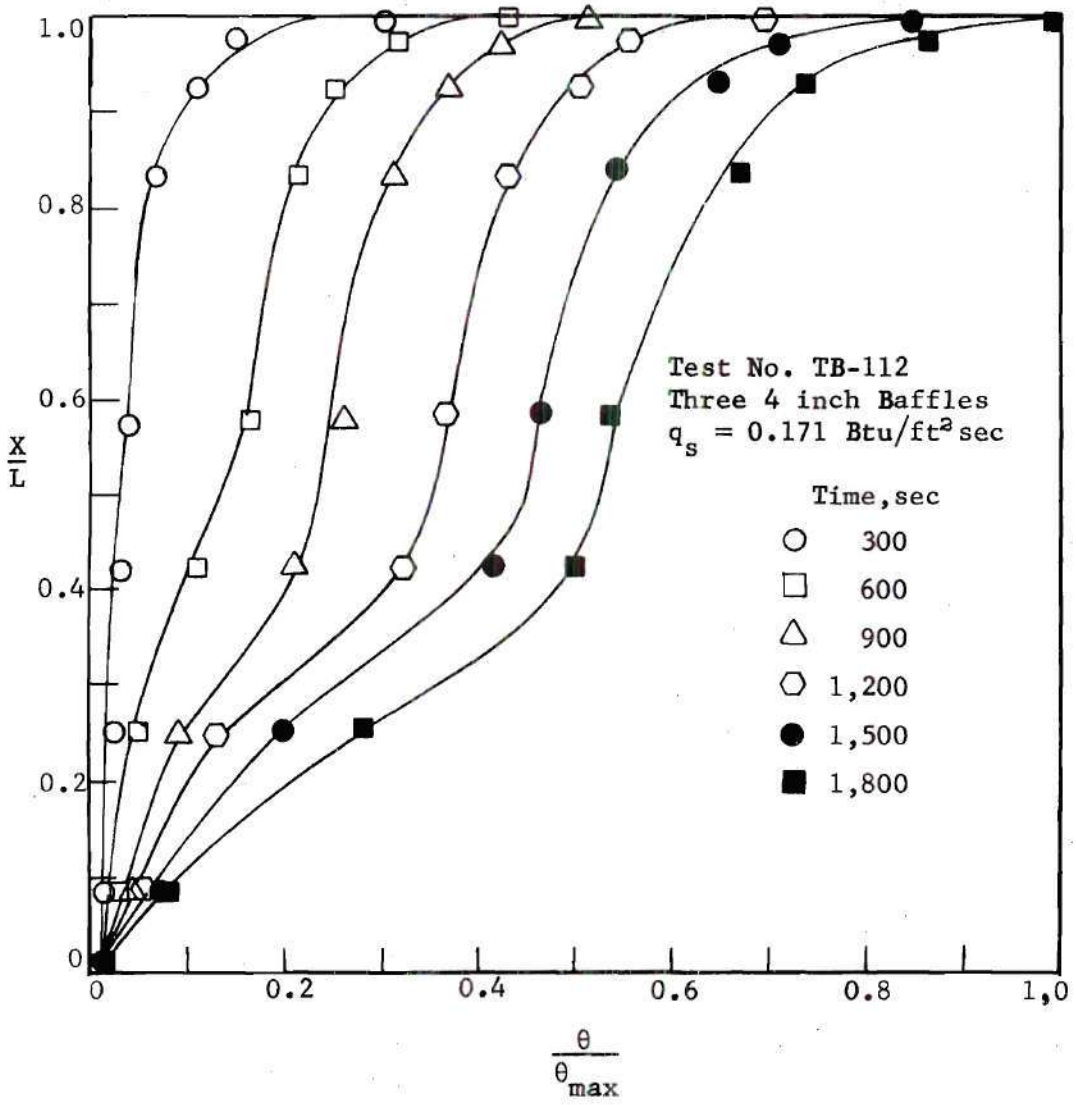

Figure 24. Container Height versus Bulk Temperature; $L/W = 3.0$, $q_b/q_s = 0.0$

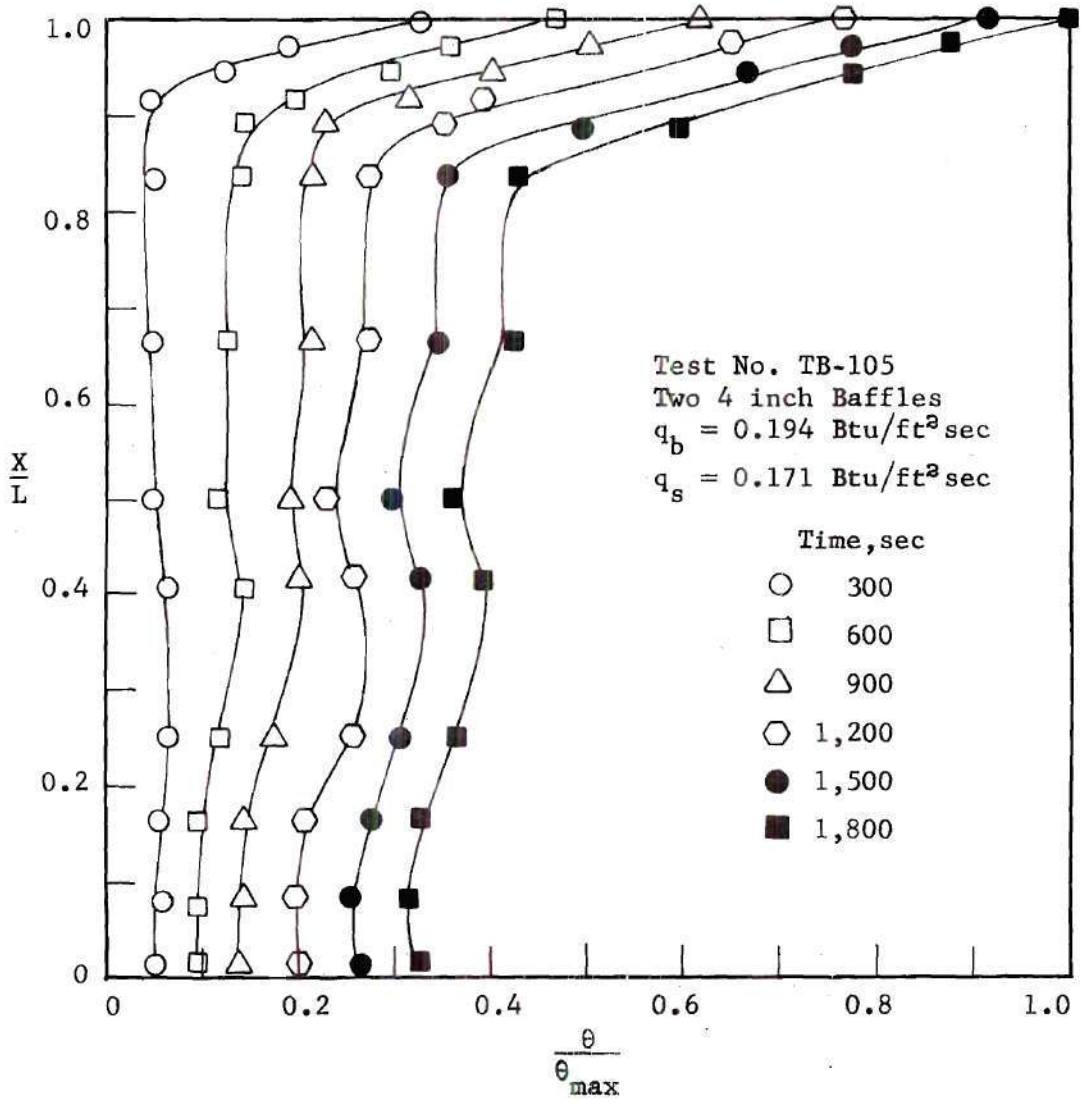

Figure 25. Container Height versus Bulk Temperature; $L/W = 3.0$, $q_b/q_s = 1.13$

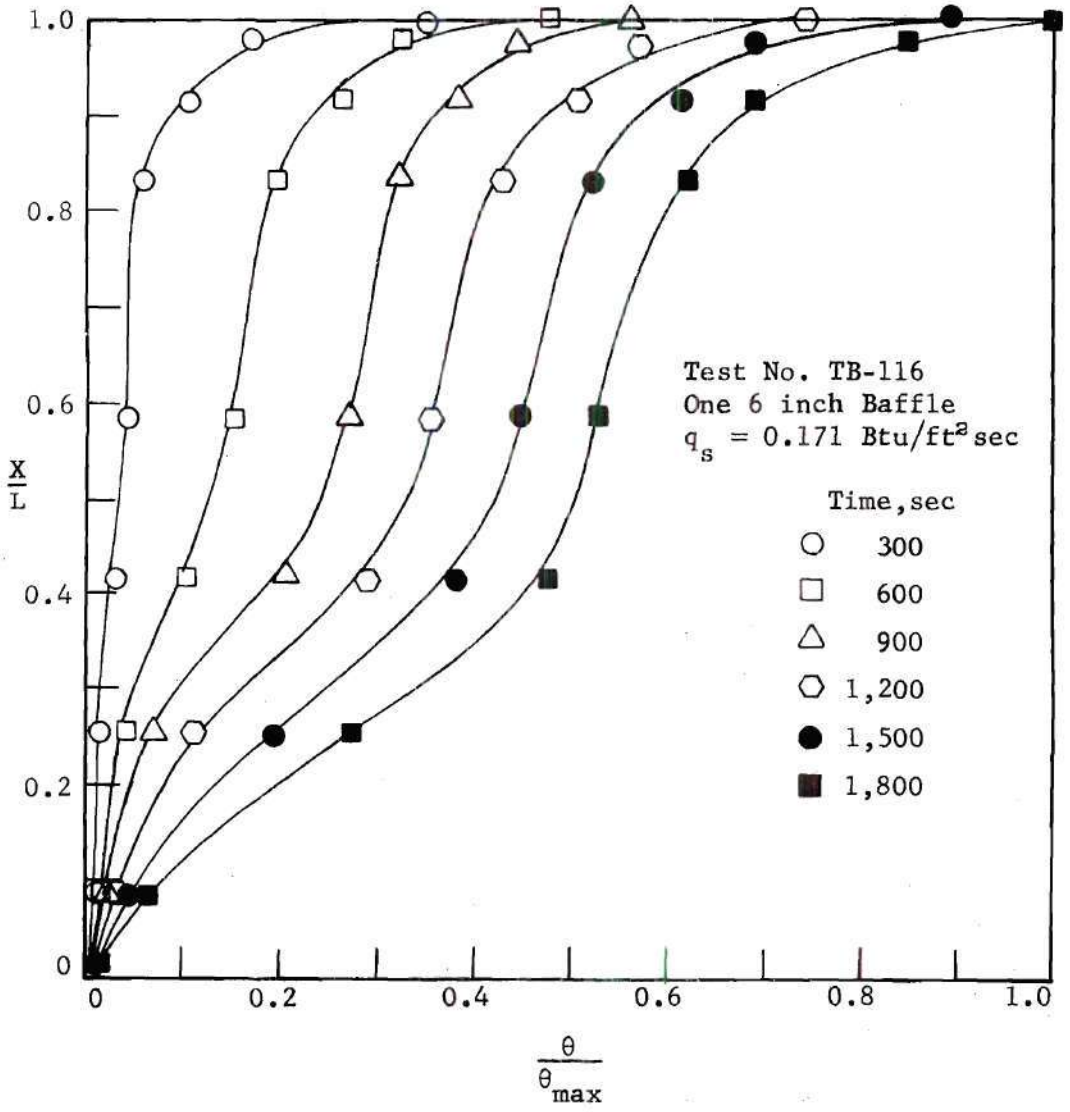

Figure 26. Container Height versus Bulk Temperature; $L/W = 3.0$, $q_b/q_s = 0.0$

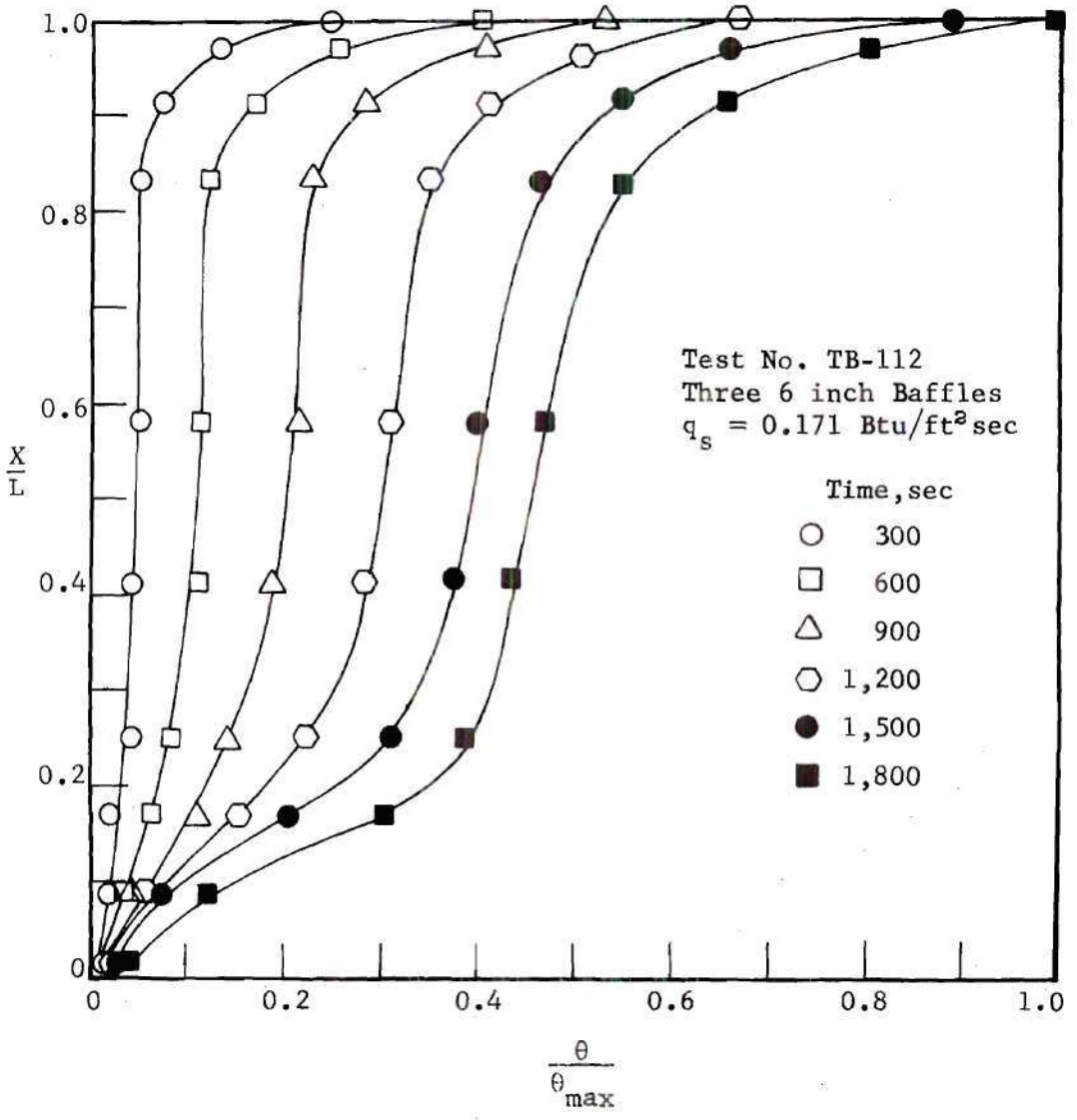

Figure 27. Container Height versus Bulk Temperature; $L/W = 3.0$, $q_b/q_s = 0.0$

This results, as explained earlier, because of the increased bulk mixing with the larger baffles.

For increasing values of the heat flux ratio, a more uniform bulk temperature is realized as in the higher aspect ratio tests. Figures 25 and 28 illustrate representative bulk temperature profiles for $q_b/q_s > 0$. For $q_b/q_s = 1.13$ and three 6 inch baffles, an almost uniform bulk temperature profile is realized. Again, as for the larger aspect ratio tests, certain combinations of baffles and bottom and side heating will produce, through bulk mixing, an almost uniform bulk temperature.

No Baffles Tests, L/W = 1.0

Figures 29, 30, and 31 illustrate representative bulk temperature profiles when no baffles are present for the three different heat flux ratios of 0.0, 0.44, and 1.08 for a liquid level of two feet. From Figure 29, for no bottom heat flux, it is seen that several of the bottom thermocouples do not realize much of a response or change in bulk temperature, which had not been noted previously in the L/W = 4.88 and 3 tests. That is, in the low aspect ratio tests, the major part of the temperature change is restricted to the top half of the tank. Only for large values of time does the fluid near the bottom of the tank experience a temperature change of appreciable magnitude. In these tests, the bulk profiles gradually approach a linear function of the tank height. To begin with, they are convex toward the fluid surface. After long periods of time, the profiles will become concave with respect to the fluid surface. In these low aspect ratio tests, laminar flow exists over most of the vertical side wall, since there was not sufficient mixing with the bulk fluid taking place as the fluid flowed along the side walls.

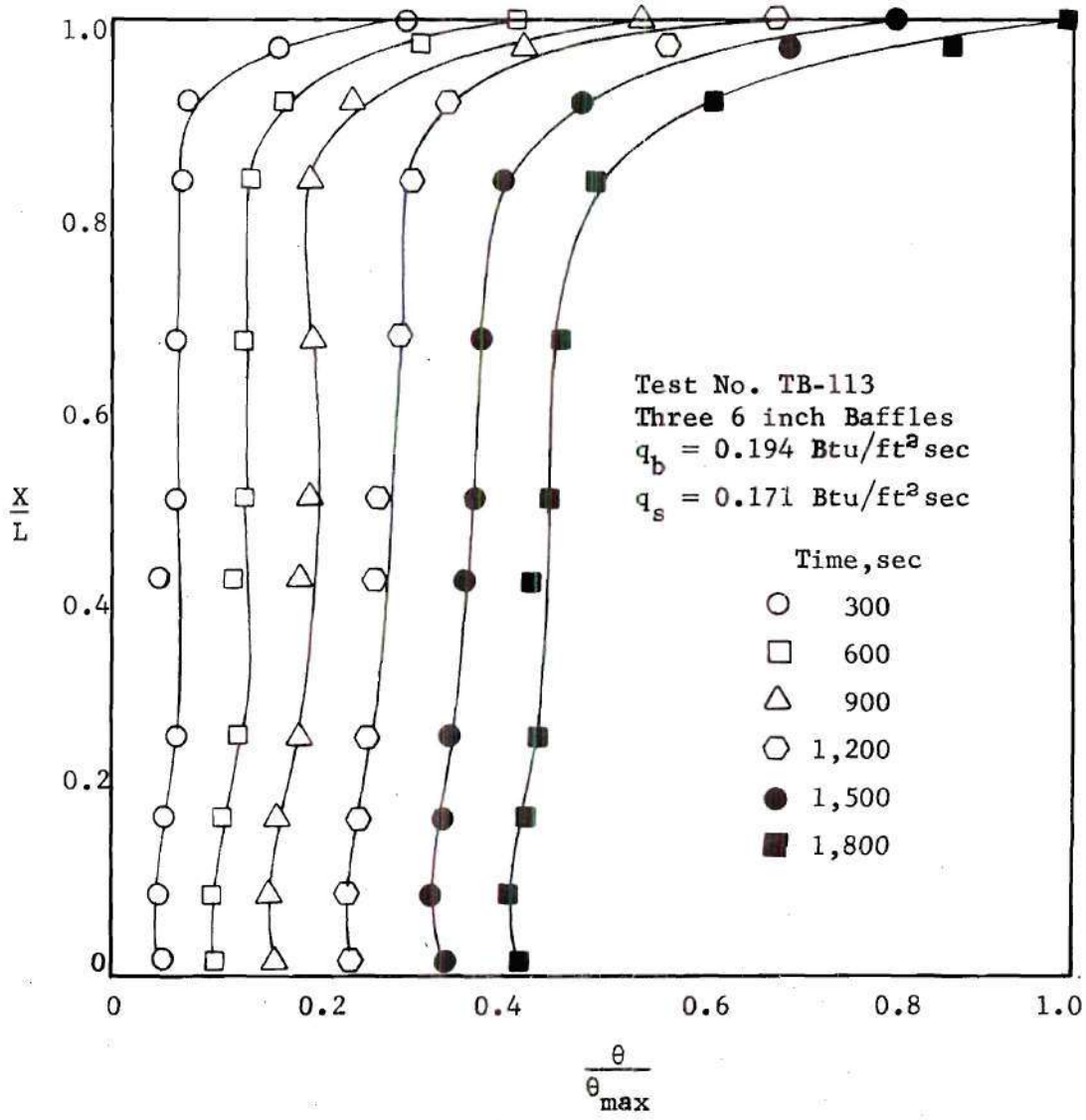

Figure 28. Container Height versus Bulk Temperature; $L/W = 3.0$, $q_b/q_s = 1.13$

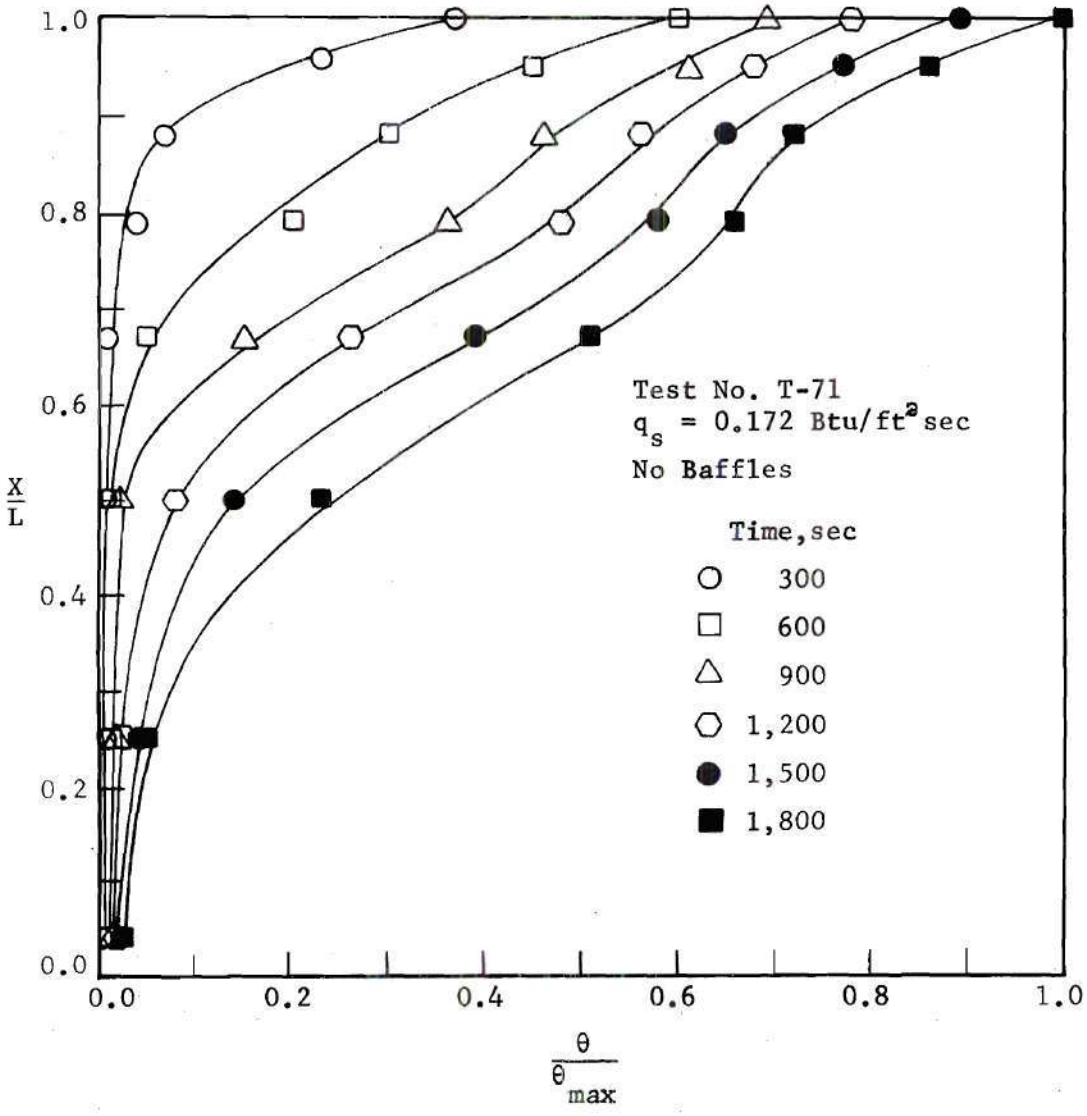

Figure 29. Container Height versus Bulk Temperature; L/W = 1.0; $q_b/q_s = 0.0$

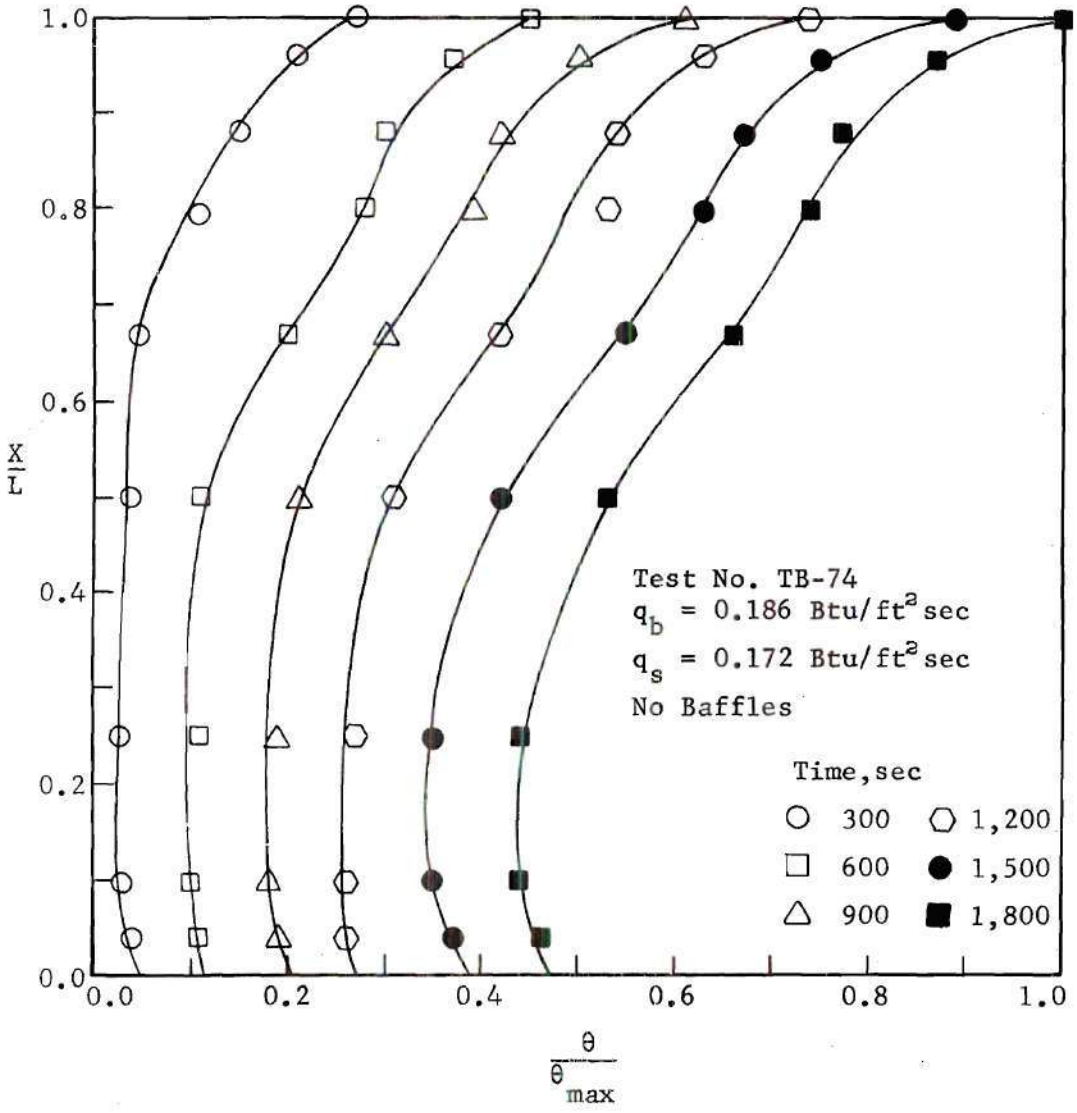

Figure 30. Container Height versus Bulk Temperature; L/W = 1.0; q_b/q_s = 1.08

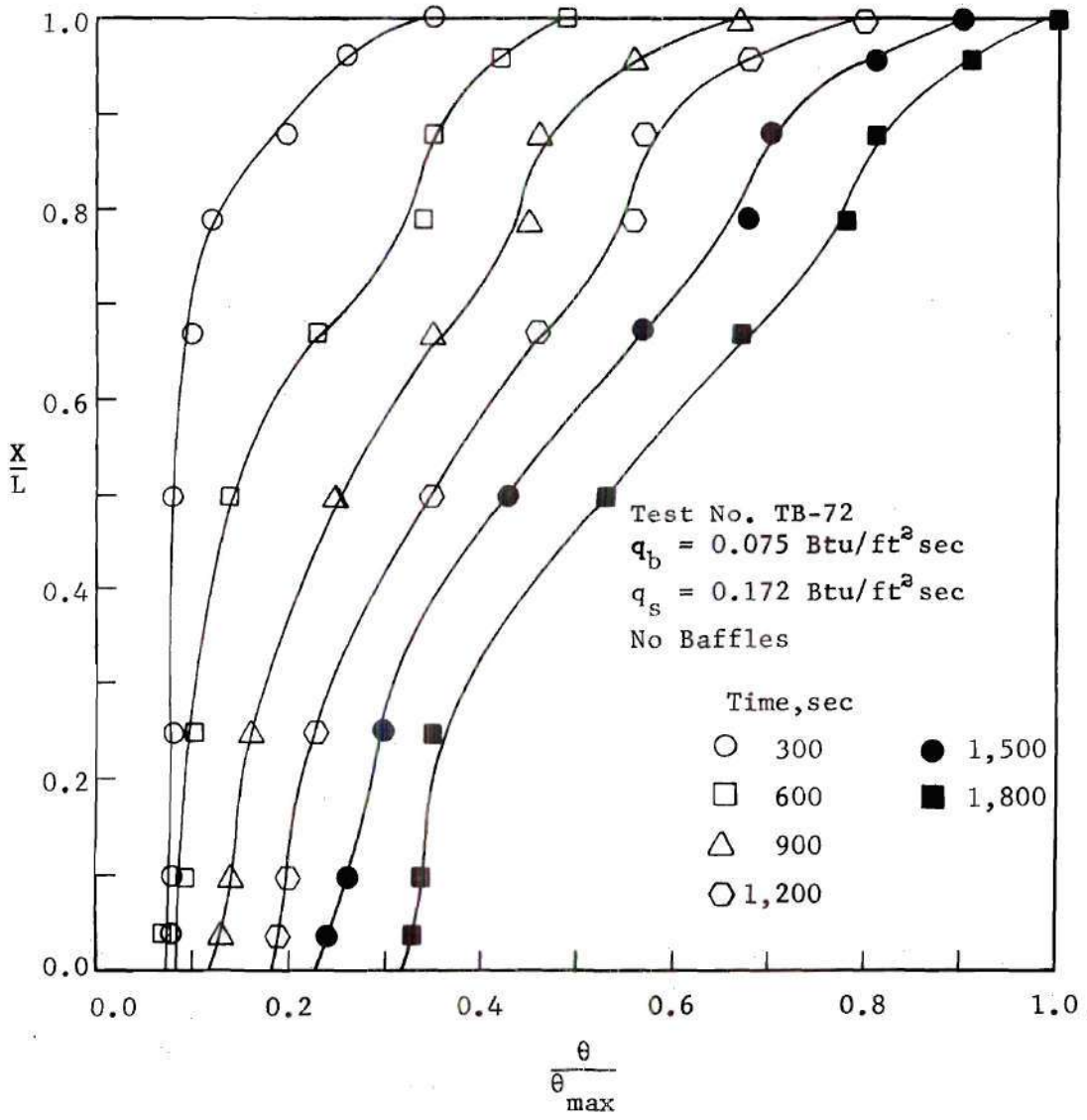

Figure 31. Container Height versus Bulk Temperature; L/W = 1.0; q_b/q_s = 0.44

In this situation, the stratification starts at the top and progresses gradually into the bulk fluid.

In the low aspect ratio tests, the addition of bottom heat has a pronounced effect on the bulk temperature profile as illustrated in Figures 30 and 31. With the addition of approximately one-half the magnitude of the side heat flux at the bottom, $q_b/q_s = 0.44$, the bulk temperature profiles tend to be uniform, over half the tank height, for the first 15 minutes. With a further increase of the heat flux ratio to a value of 1.08, a slight temperature inversion condition is set up at the tank bottom. Hence the ideal value of the bottom heat flux would be somewhere around 0.50 which is one-third the value for an aspect ratio of 4.88.

The effect of aspect ratio on the bulk temperature profile for the no baffle cases and no bottom heating can be seen from Figures 9, 20, and 29. During several of the tests, the boundary layer along the vertical walls was examined with a Schlieren system. It was found that, for the low aspect ratio tests, laminar flow existed over most of the vertical wall with transition trying to take place in the last few inches. For aspect ratios of 3 and 4.88, it was found that the flow along the vertical walls changed from laminar to turbulent at a height of two to three feet. In the high aspect ratio tests, the turbulence was generally more rapid in mixing which is responsible for the difference in the shapes of the bulk profile as mentioned previously. When bottom heat is applied, the low aspect ratio tests show the most significant improvement. The reason for this is that, in bottom heating tests, the bottom heat flux was the same regardless of the aspect ratio. Since this heat flux affects a

certain portion of the bottom bulk fluid, its effect is best realized in the low liquid level tests.

Baffle Tests, L/W = 1.0

Figures 32, 33, and 34 illustrate how the number and size of the baffles affect the bulk temperature profile in the low aspect ratio tests. In comparing Figures 29, 32, and 34, it is apparent that the addition of baffles on the vertical walls has an effect on the bulk temperature profile, especially near the bottom of the tank. By increasing the number of baffles as seen from Figures 32 and 33, more of the bulk fluid is affected by the mixing resulting from the baffles. From a Schlieren analysis of several tests, it was found that the flow around the baffles for the low aspect ratio tests was considerably slower in velocity than the flow at the higher aspect ratios. This should be expected since, for a fluid level of two feet, the natural convection boundary layer flow is slow for moderate temperature differences even when baffles are not present. With the addition of baffles on the vertical walls, the length of the wall over which the boundary layer flow develops is greatly reduced, particularly when the number of baffles is large. Also, continued increase in the size of the baffle may not result in additional mixing as was the case for the other aspect ratios. This fact can be seen by comparing the results of Figures 33 and 34, where all conditions are the same except the size of the baffles. From the figures, it is evident that no more of the bulk fluid is affected by the increase in the size of the baffles. From an observation of the flow around the large eight inch baffles in the low aspect ratio tests, it was found that the flow along the under side of

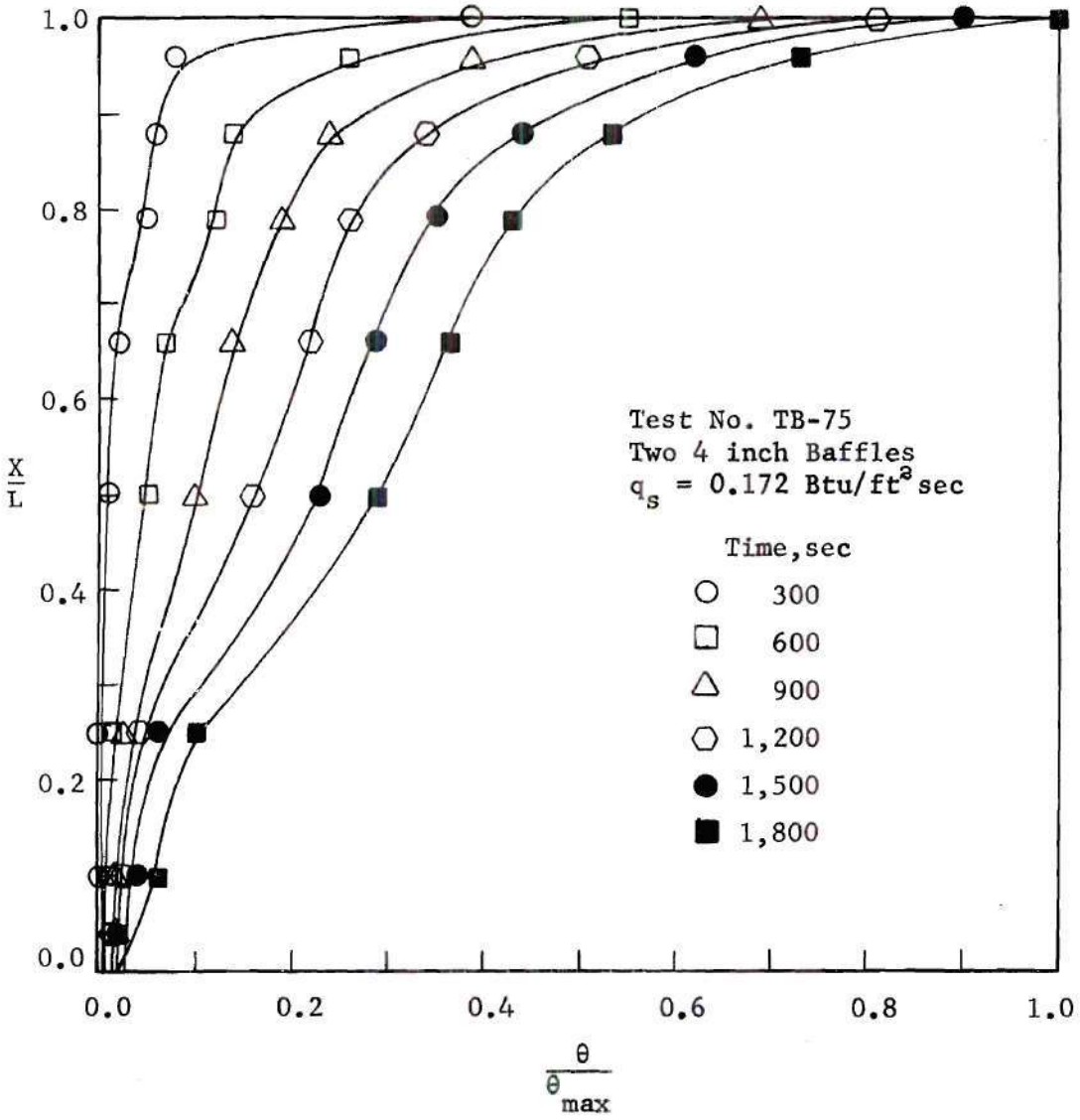

Figure 32. Container Height versus Bulk Temperature; L/W = 1.0, q_b/q_s = 0.0

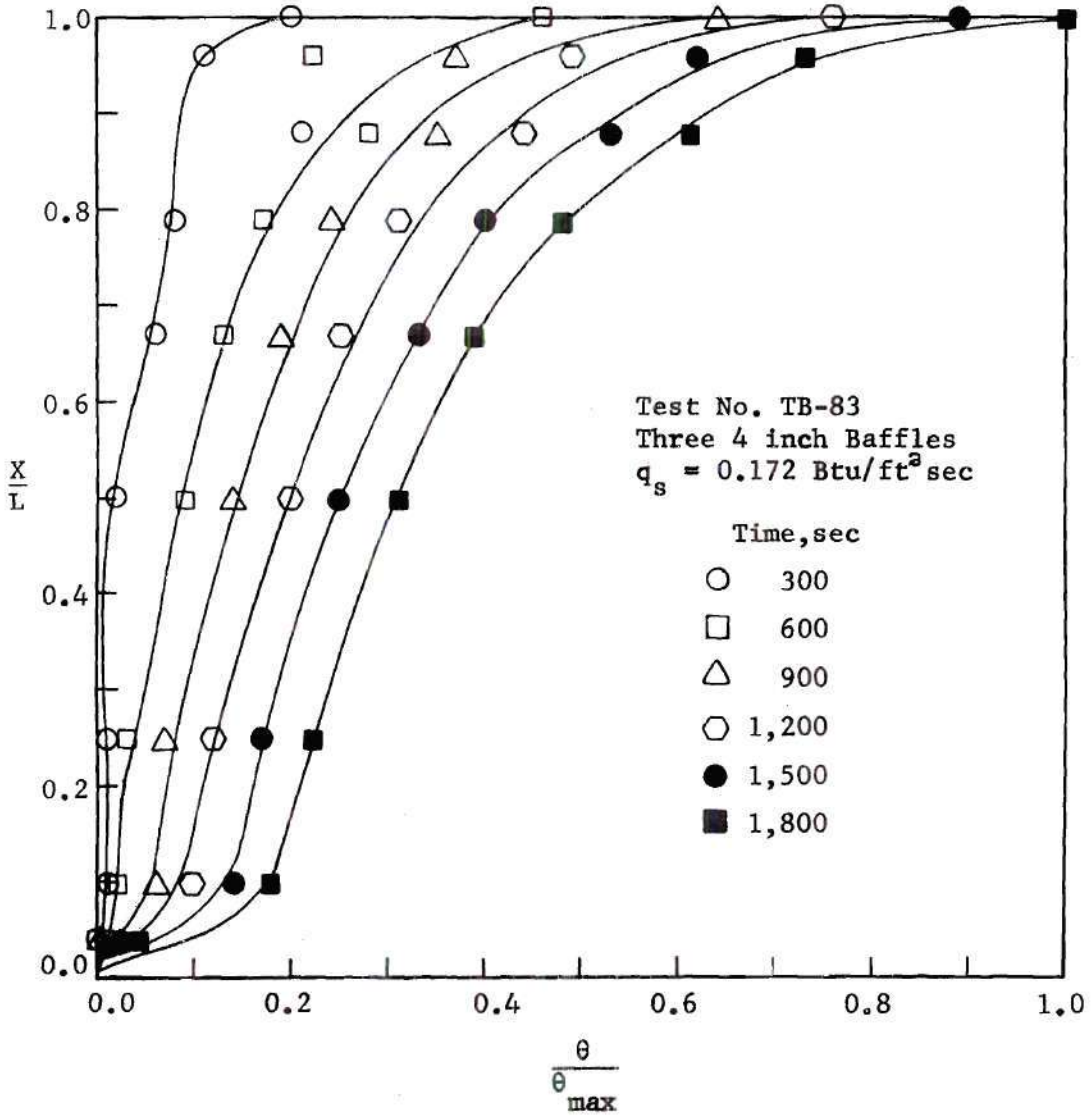

Figure 33. Container Height versus Bulk Temperature; $L/W = 1.0$, $q_b/q_s = 0.0$

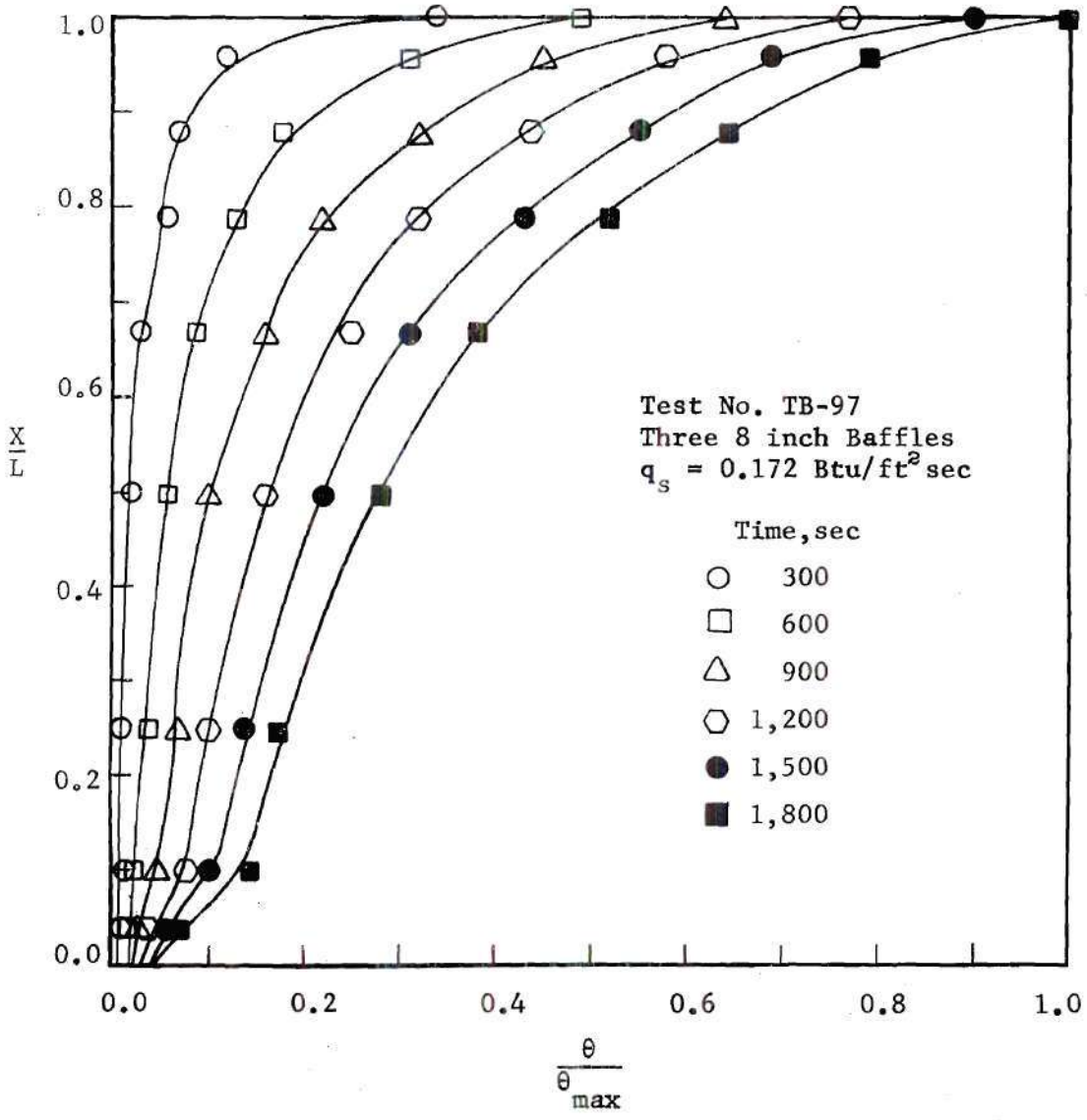

Figure 34. Container Height versus Bulk Temperature; L/W = 1.0, q_b/q_s = 0.0

these baffles was always laminar and slow. However, in most all cases, the flow separated from the baffle tip.

Figure 35 is representative of the bulk temperature results with the baffles inclined at an angle of 45° to the walls of the tank. From a comparison of Figures 35 and 33, it can be seen that baffles inclined up have actually less effect on the bulk temperature than those perpendicular to the walls. This fact is particularly true in the lower region of the tank. The reason for this result is that, for baffles inclined upward, the boundary layer flow is retarded very little when it reaches the baffle. Although the flow is much more turbulent at the baffle tip, the turbulence does not extend far enough into the bulk liquid to be effective in promoting bulk mixing. The momentum or velocity associated with the boundary layer flow is not as great in the low aspect ratio tests; thus, the fluid is not pushed into the center of the tank as previously noted in the high aspect ratio tests. With concave down baffles, the trapping of hot fluid between the baffle and wall is more pronounced than in the other aspect ratio tests, and this shape of baffle quickly resembles a flat horizontal baffle. The reason for this is realized when one considers the velocity within the boundary layer flowing along the vertical walls. With a large number of concave down baffles placed on these walls, the boundary layer velocity is reduced to such an extent that practically none of the wall heated fluid is diverted down into the bulk liquid as might be expected.

The effect of heat flux ratio when baffles are present within the tank can be seen from Figures 33 and 36. For a heat flux ratio of 1.08

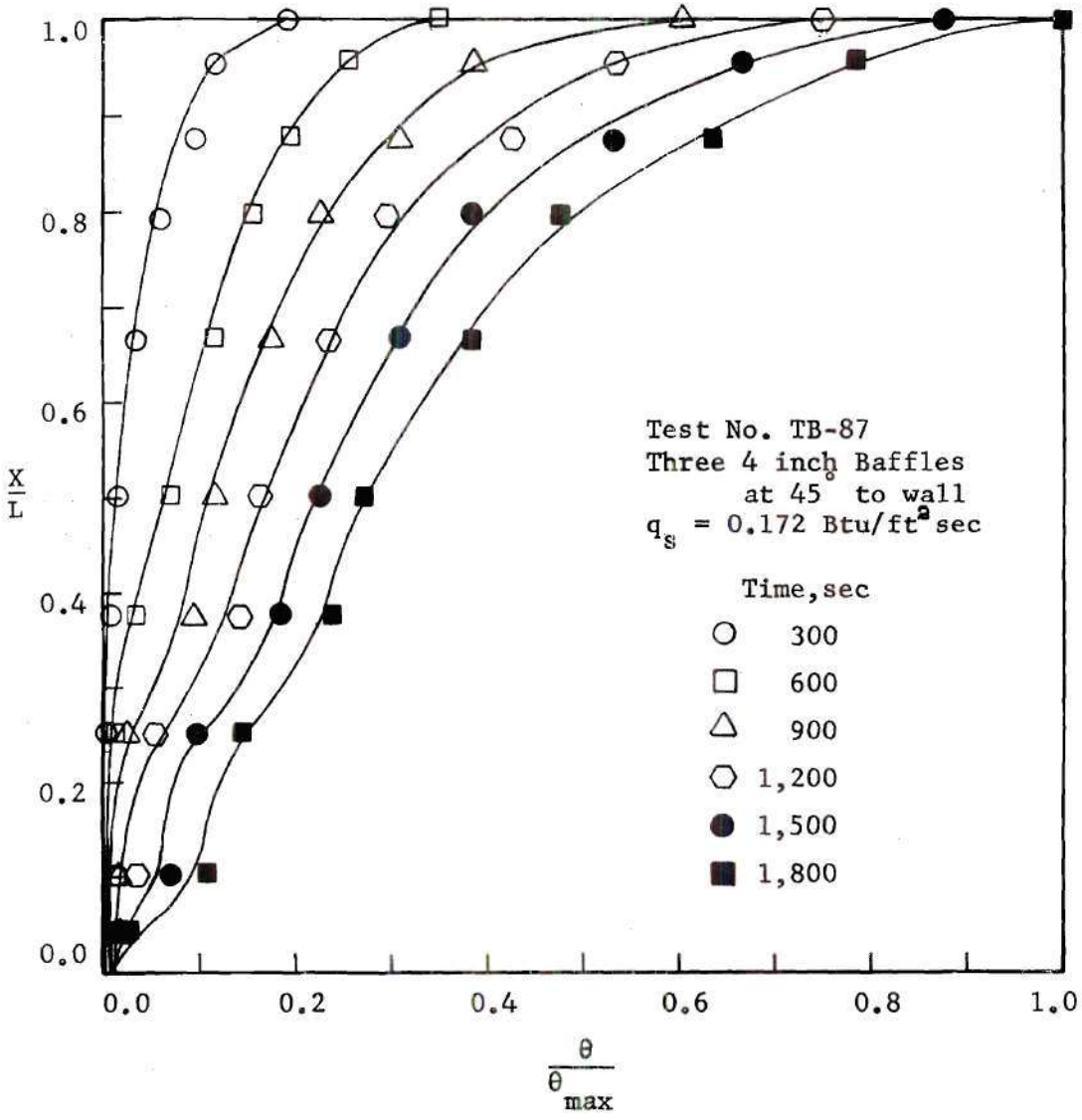

Figure 35. Container Height versus Bulk Temperature; L/W = 1.0, q_b/q_s = 0.0

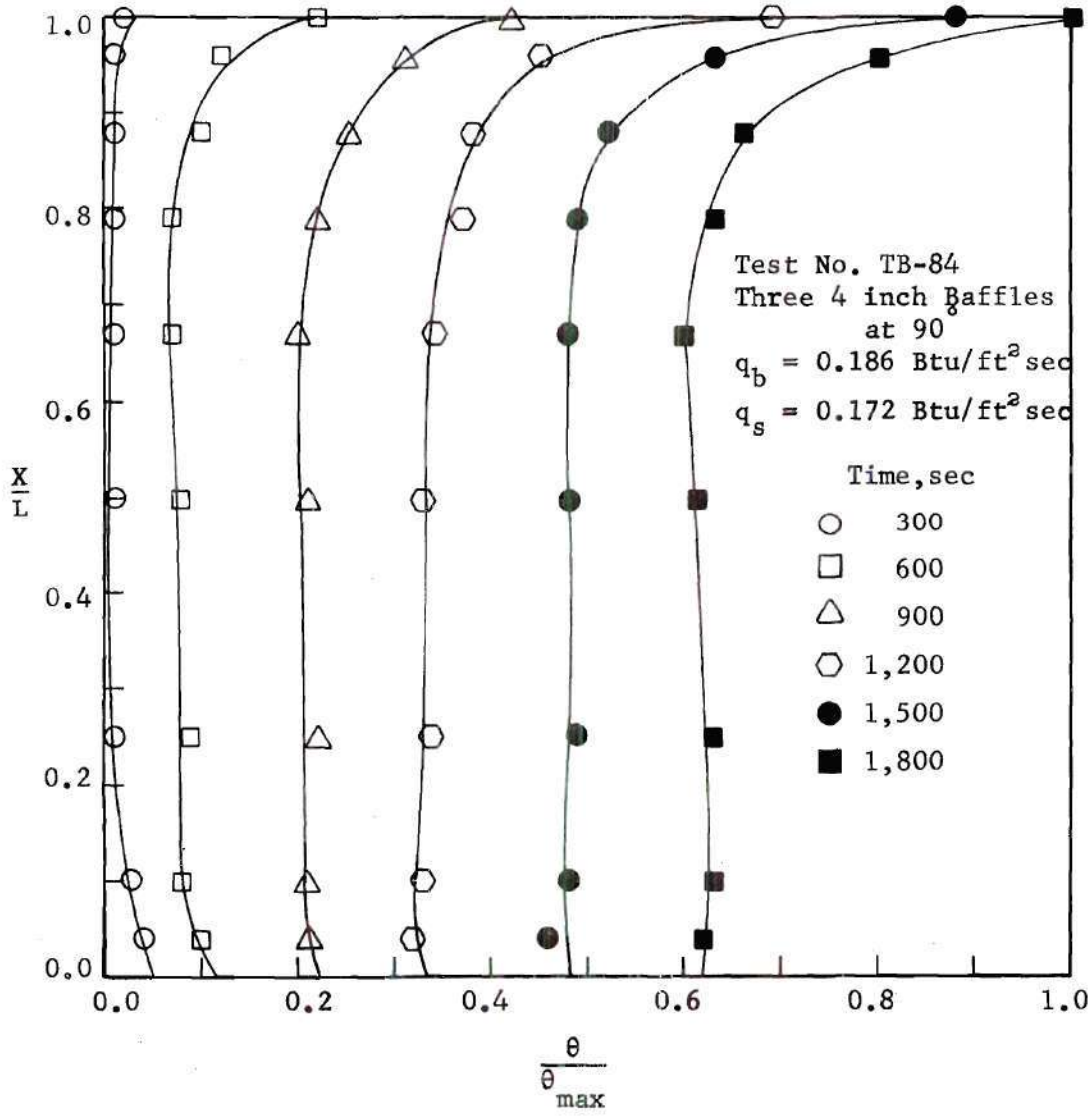

Figure 36. Container Height versus Bulk Temperature; L/W = 1.0, q_b/q_s = 1.08

and three 4 inch baffles at 90° to the wall, a uniform bulk temperature is realized over approximately 80 percent of the tank height for all values of time. Thus, it appears that, with certain combinations of baffles and bottom heat flux, an almost uniform bulk temperature will result. It is believed, by this investigator, that it is impossible to mix the bulk fluid at the top with any baffle design. Hence, some form of temperature gradient will persist in this region. It is possible to have a uniform bulk profile with some type of mixing even when the bulk fluid is not at thermal equilibrium with the environment. That is, regardless of whether the bulk temperature is uniform or not, if a temperature difference exists between the bulk and wall, a natural convection flow situation is set up along the walls of the container unless the mixing process is sufficiently strong to destroy the natural convection process. If this were the case, the heat transfer process would then be forced convection.

In the next chapter, a qualitative analysis of the results discussed in this chapter will be presented. The results presented in the next chapter are an integral part of the overall analysis.

Photographic Analysis

During the course of this investigation, several photographs of the flow around the different baffle designs were taken. However, only the results of tests for $L/W = 4.88$ and 1.0 will be discussed, since the results for $L/W = 3.0$ were found to be closely related to $L/W = 4.88$. Photographs using both a Schlieren system and neutral density particles suspended in the test fluid revealed that, for the high aspect ratio tests,

the flow seldom became reattached to the back side of the baffles. Vliet (8) and Vliet and Brogan (7) had earlier noted that baffles became less effective with increasing time because of the reattachment of the boundary layer flow to the backside of the baffle. In Figure 37, the flow around the middle baffle, located at $X/L = 0.5$, with three 2 inch baffles on each wall, reveals that some of the flow is reattached for small values of time after the initiation of heat. However, for extended values of time, the flow separates from the baffles and remains separated for the duration of the tests. The coarse turbulence noted below the baffles for extended values of time is a result of the turbulent boundary layer, plus the turbulence created by the baffle below this baffle. During the course of a test, several of the baffles were examined to see if the flow around each baffle was identical. Except for the lowest baffle on the walls, the flow was essentially the same around all other baffles. The first baffle usually experienced a more uniform flow since there was no baffle below it to create any irregular bulk turbulence. However, a slight turbulence existed before the first baffle as a result of the turbulent free convection boundary layer. Tatom (5) observed photographically the boundary layer on the tank walls without baffles present and found that a coarse turbulence is induced along the vertical walls. The boundary layer appears to be made up of a fine turbulence close to the walls with the presence of vortices at the outer edge. Fujii (12) and Szewczyk (30) have previously observed a double layer vortex motion of free convection boundary layers. Szewczyk noted that the outer layer vortex motion is predominant and sets in first, well in advance of the turbulence of the inner layer. The outer layer turbulence

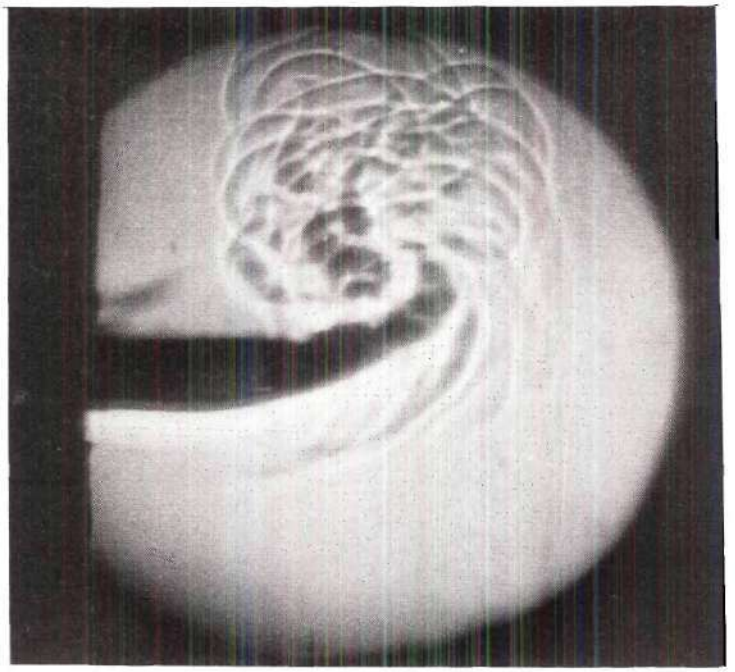

τ = 15 seconds

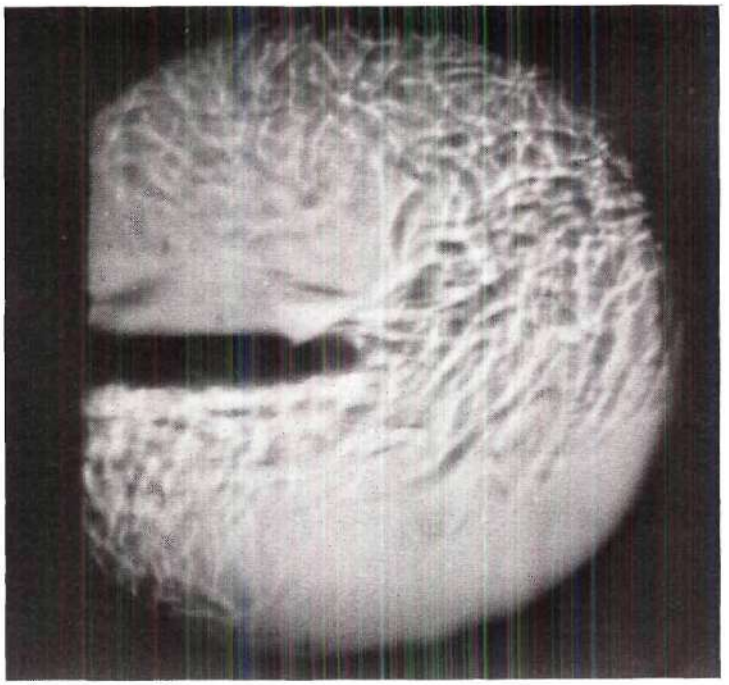

τ = 60 seconds

Figure 37. Flow Around Two Inch Baffles at Different Times; L/W = 4.88, q_b/q_s = 0.0, Three 2 Inch Baffles.

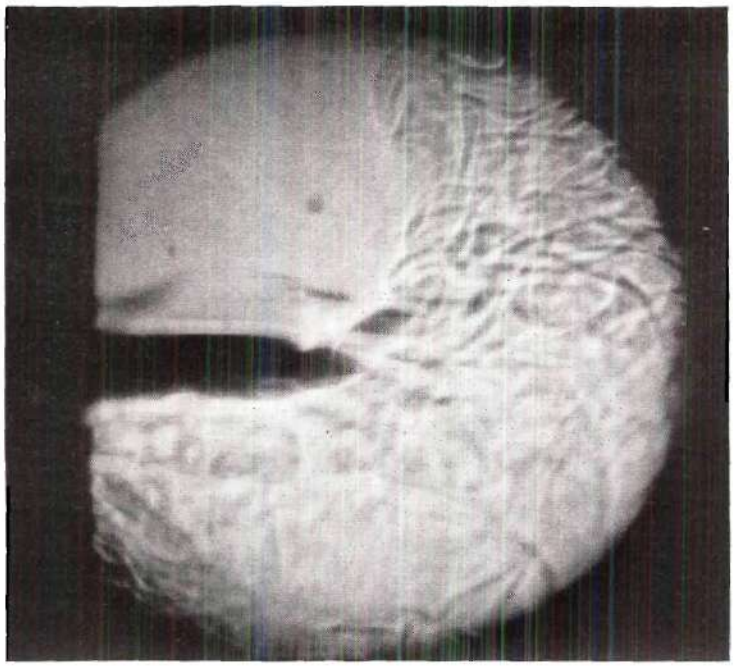

τ = 180 seconds

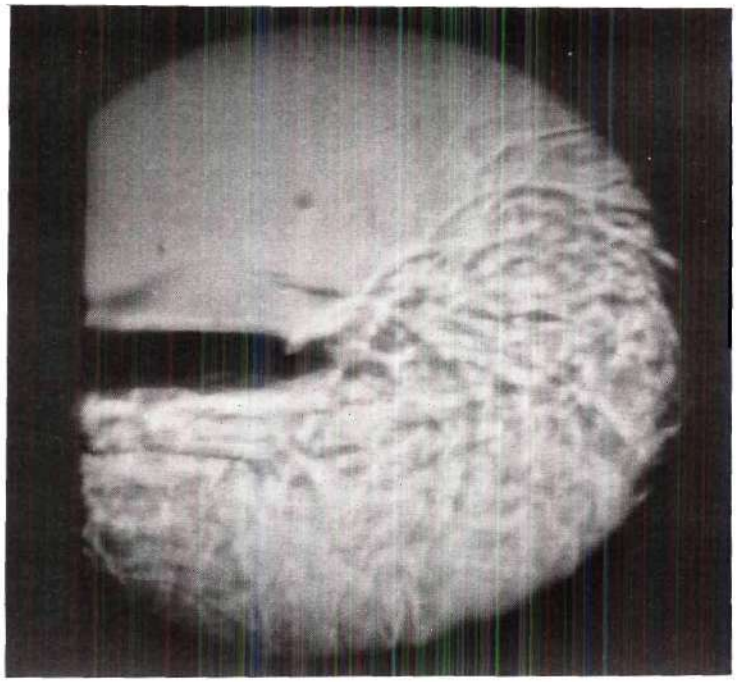

τ = 300 seconds

Figure 37. Continued

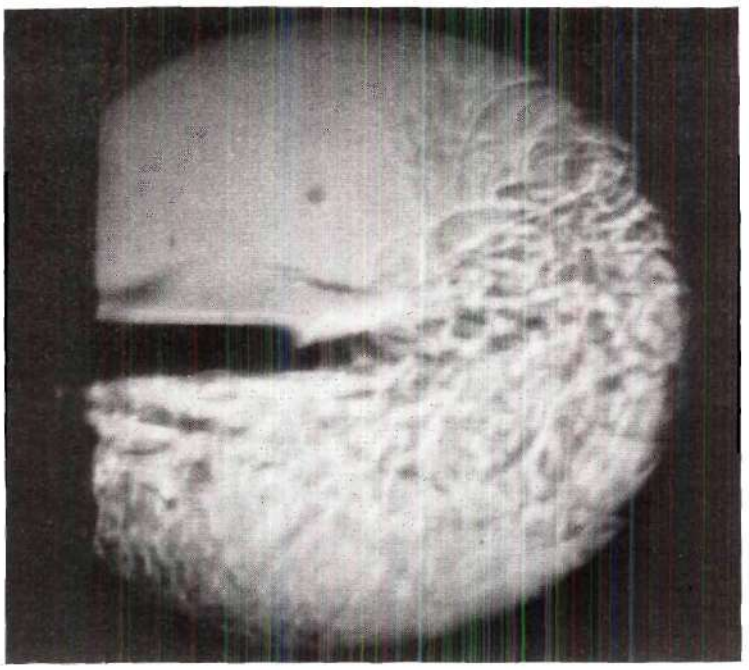

τ = 600 seconds

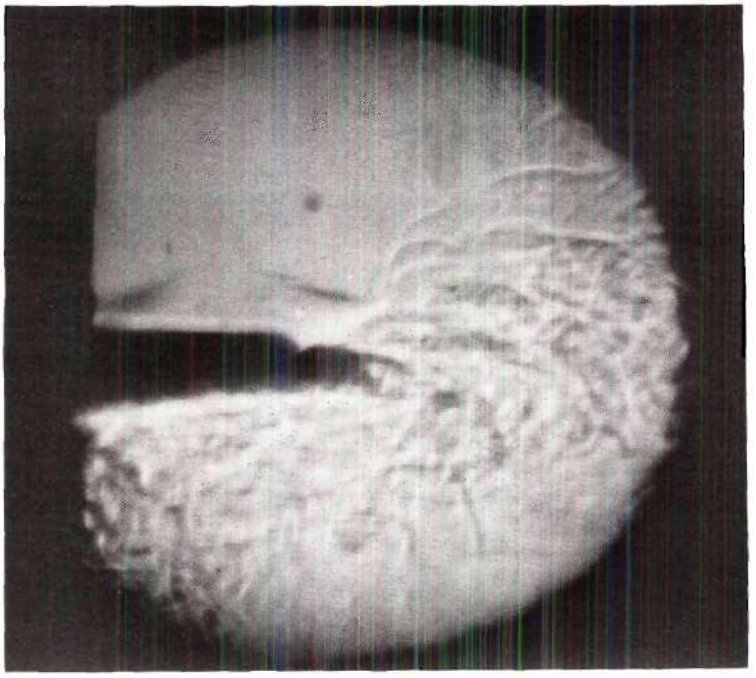

τ = 1200 seconds

Figure 37. Concluded

was found to be responsible for instabilities of the inner layer, hence, making the experimental Grashof number lower than the theoretical, which is calculated from the inner layer instability.

The flow around baffles of larger size can be seen in the particle photographs of Figure 38. Again, it is seen that very little back flow is obtained. However, when flow behind the large baffles occurred, it was intermittant and lasted for only a short time. From these photographs, it can be seen that the distinct advantage large baffles have is that they shove the heated boundary layer fluid further into the bulk liquid. Another characteristic possessed by the larger baffles is the fact that they have more of a tendency to create vortices at the tip of the baffles. These vortices in many cases extended into the middle of the bulk fluid which gave the desired effect of reducing the bulk temperature gradient. The string and washer shown at the left in the photographs is located approximately eight inches from both the wall and glass front. The string was used to focus the camera at a specific depth.

In Figure 38, the heat flux ratio is 4.05. For lower values of the heat flux ratio, a more rapid and turbulent flow is realized around the baffles. Particle photographs, for $q_b/q_s = 0.0$, show that generally larger vortices with a larger rotation velocity are present at the baffle tips for lower heat flux ratios than for high values of this parameter. The photographic sequence of Figure 39 illustrates the flow around a six inch baffle for low values of the heat flux ratio, $q_b/q_s = 0.0$. For several values of time, it is seen that large vortices are generated above or below the baffles as the boundary layer flow is turned into the bulk

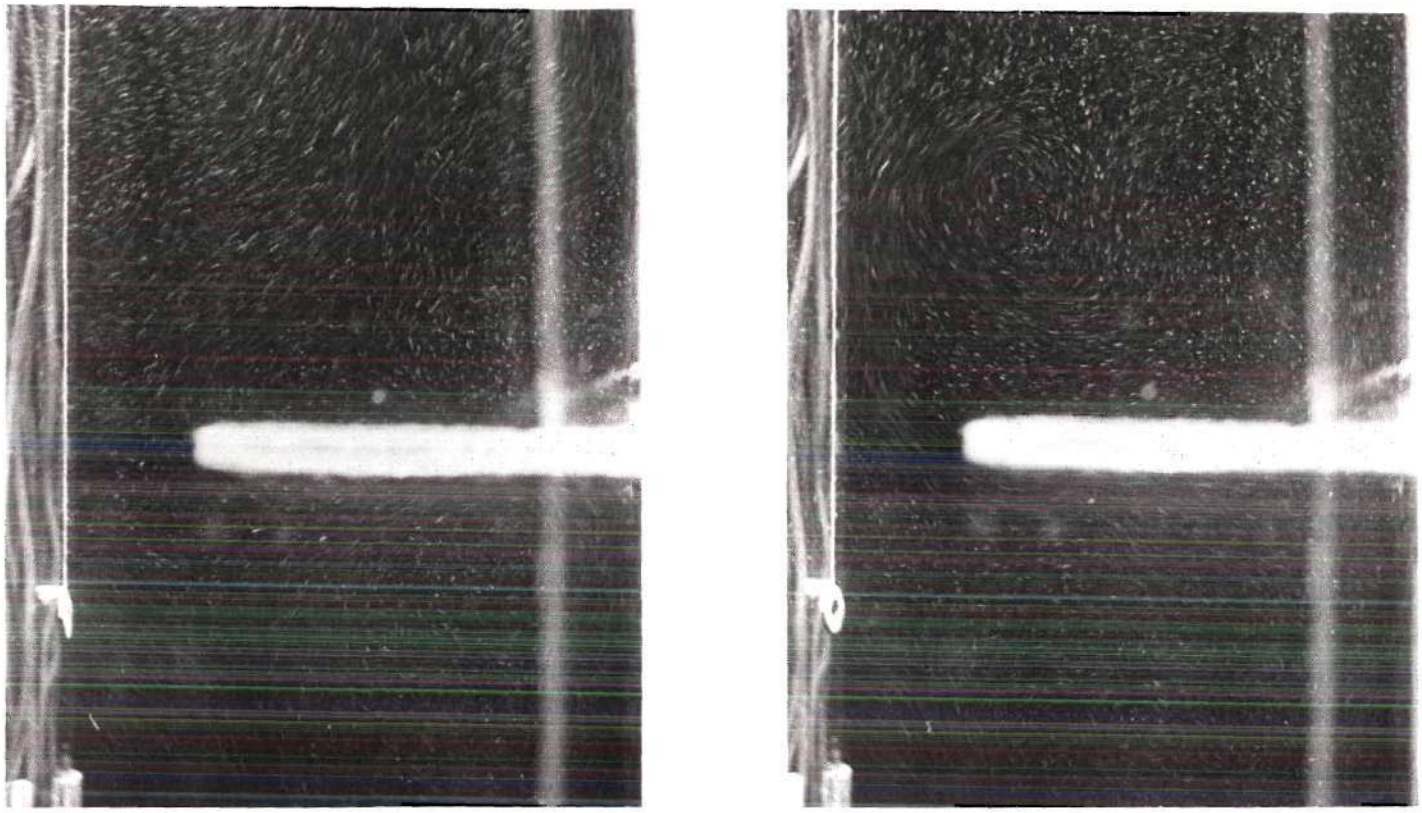

τ = 300 seconds

τ = 600 seconds

Figure 38 Flow Around Six Inch Baffles at Different Times; L/W = 4.88, q_b/q_s = 4.05, Three 6 Inch Baffles

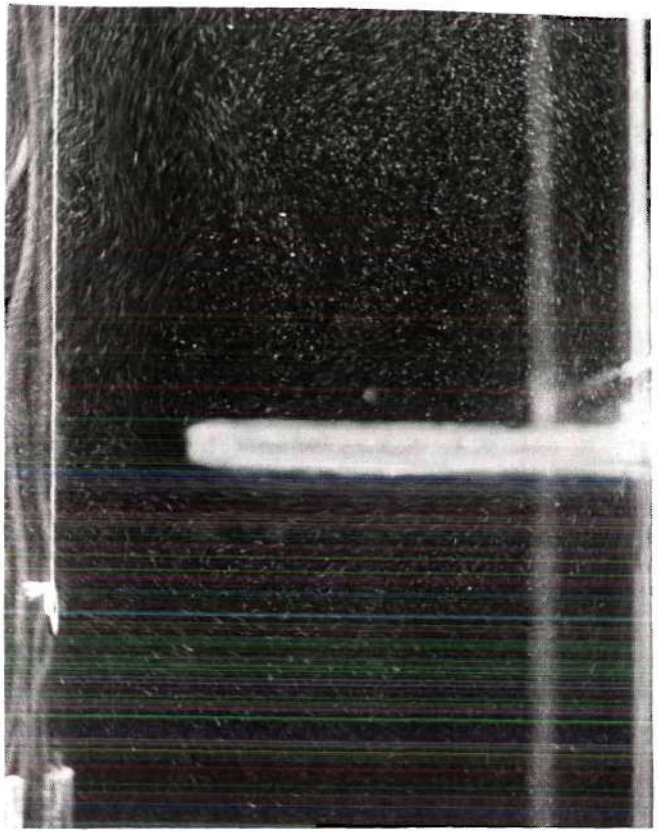

τ = 1800 seconds

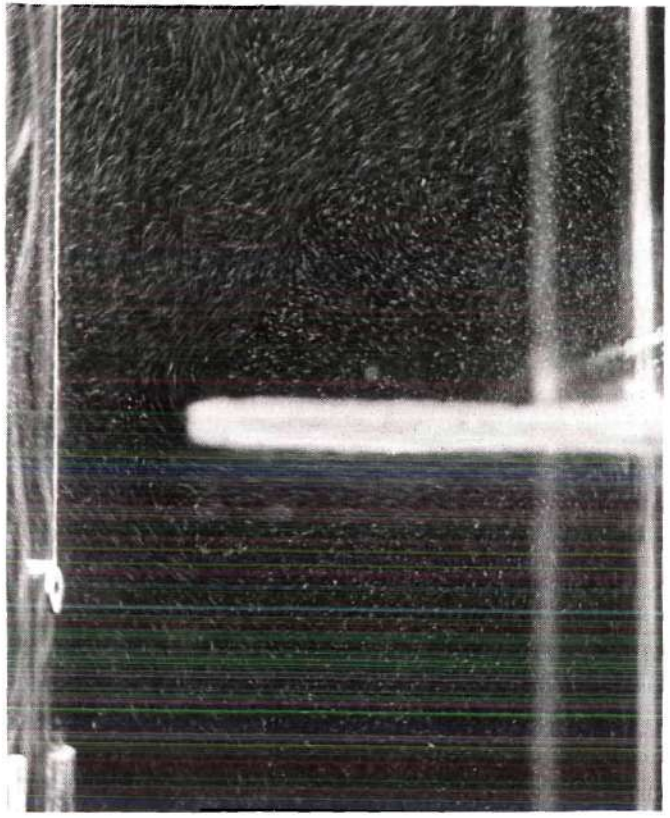

τ = 2400 seconds

Figure 38. Concluded

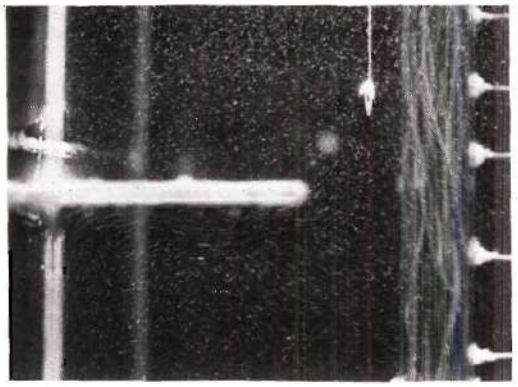

τ = 30 seconds

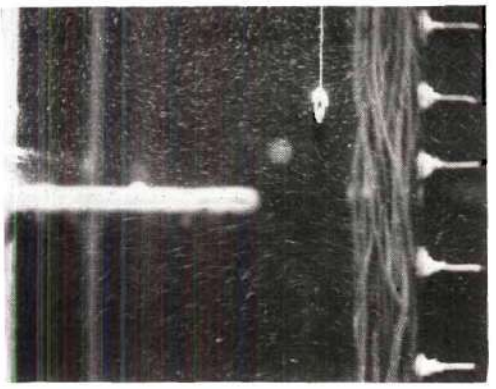

τ = 1048 seconds

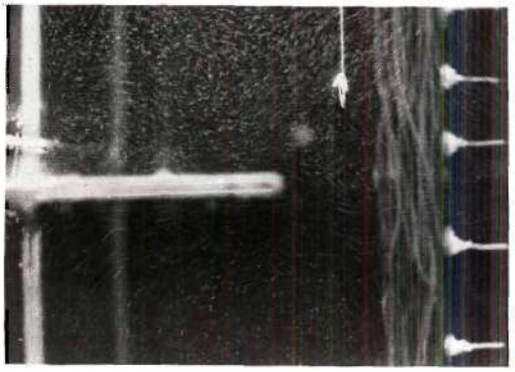

τ = 240 seconds

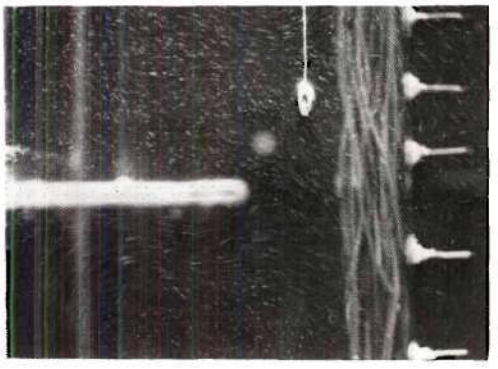

τ = 1500 seconds

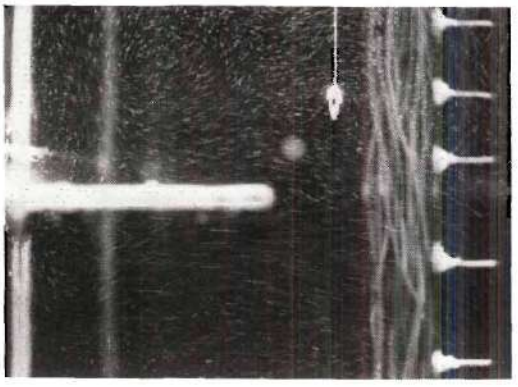

τ = 720 seconds

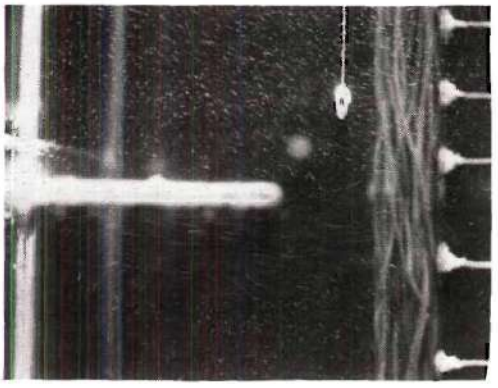

τ = 1800 seconds

Figure 39. Flow Around Six Inch Baffles at Different Times: L/W = 4.88, q_b/q_s = 0.0, Three 6 Inch Baffles

liquid. From the photographs it is also seen that the flow from both walls meets approximately at the tank center and turns either up or down. Usually the flow below the baffle turns down, while the flow above turns up at the center. It should be mentioned that the flow associated with the different baffle designs is not regular with time. Even for identical test conditions, that is, duplicate tests, the flow around the baffles was not the same for identical values of time. Also, in a few of the large baffle tests, some oscillation in the flow from the two walls was observed. For example, at one instant of time, the flow around a baffle on one wall appeared to be larger than the flow from the baffle directly across the tank. A few seconds later, this flow situation had reversed itself. Such oscillations are believed to be a result of the bulk flow disturbance which results when large baffles are used. When no baffles are present on the vertical walls, a uniform flow down the center of the container is experienced. If large baffles are placed on the walls, this downward motion is disturbed and becomes irregular.

Eichorn (31) has shown that with small particles, free convection velocities can be accurately determined. However, an approximation of the magnitude of the velocities may be obtained by measuring the length of the particle streaks and dividing by the exposure time. The camera exposure for all particle photographs was 1.0 second. Thus, the length of a particle streak, multiplied by a scale factor and divided by the time, will give an approximate velocity of the fluid at the streak location. A more elaborate and accurate calculation procedure for the velocity of the particles is given by Eichorn (31) and by Tatom (5). In his analysis, the defraction through the water, glass plates, and air is

taken into account. Also, the response of the particle to buoyancy and unsteady accelerations is calculated.

The effect of baffle inclination can be seen by comparing the photographs of Figure 37 with those of Figure 40. In both cases, the number and size of the baffles was the same. Also, the aspect ratio and heat flux was identical. In Figure 40, after the first minute of heating, the flow separates from the baffle and never reattaches to the back side for the duration of tests. However, reattachment in some tests occurred further up the wall. It is interesting to note that, as the flow leaves the baffle, part of it is turned down and mixes with the bulk fluid. This is a result of the vortex motion created by the flow when it separates from the baffle and the downward motion normally associated with the stratification phenomena when baffles are not present. The boundary layer flow leaving the baffle resembles somewhat the expansion of a fluid after passing through a nozzle. The top portion of the fluid continues, for a few inches, into the bulk liquid at about the angle it leaves the baffle. Again, as previously mentioned, the flow before the baffle is coarsely turbulent. This is a result of the turbulent boundary layer and the turbulence created by the baffle lower in the tank. In most cases, the turbulence between two baffles was greater than when the baffles were not present. That is, the small baffles act like turbulence generators along vertical walls.

Adding heat to the bottom of the tank has a pronounced effect on the flow around the baffles. This fact has been previously mentioned when discussing the large six inch baffles. However, bottom heat has more effect

τ = 35 seconds

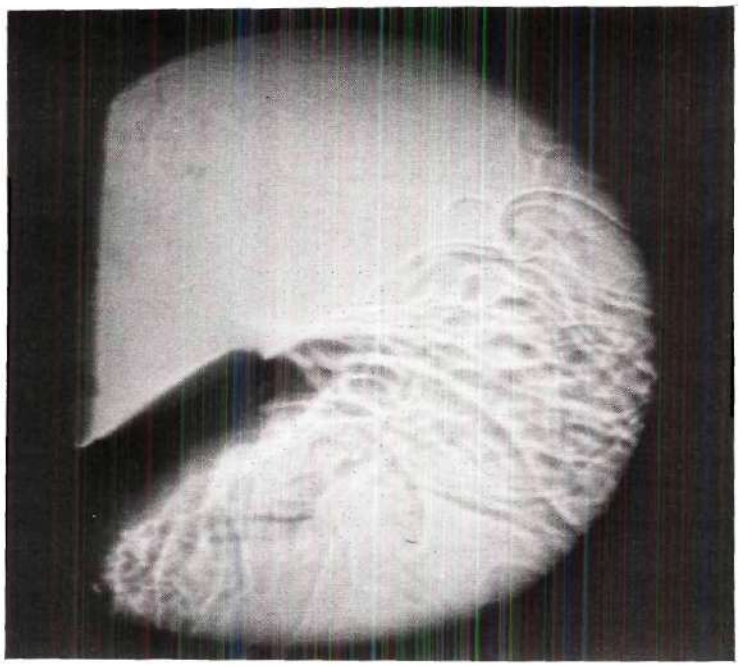

τ = 2 minutes

Figure 40. Flow Around Two Inch Baffles at 45° to the Wall for Different Values of Time; L/W = 4.88, q_b/q_s = 0.0, Three 2 inch Baffles

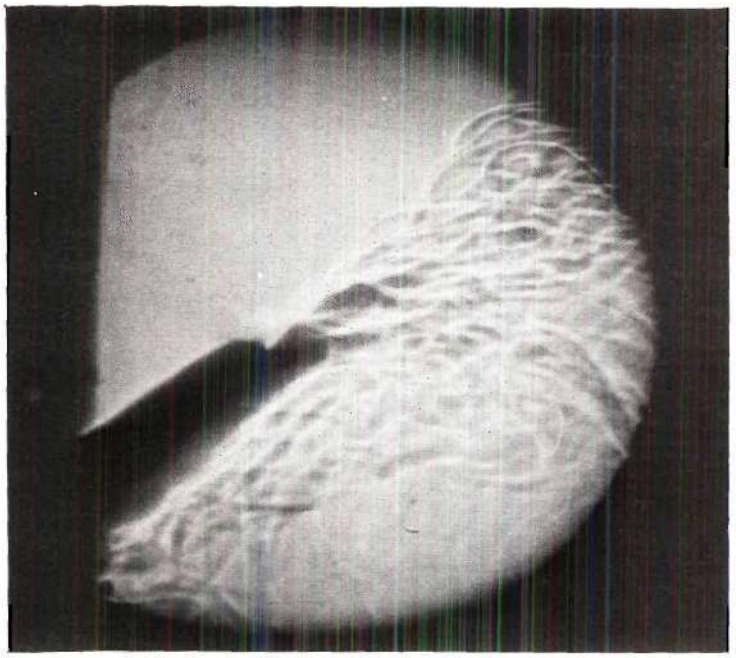

τ = 5 minutes

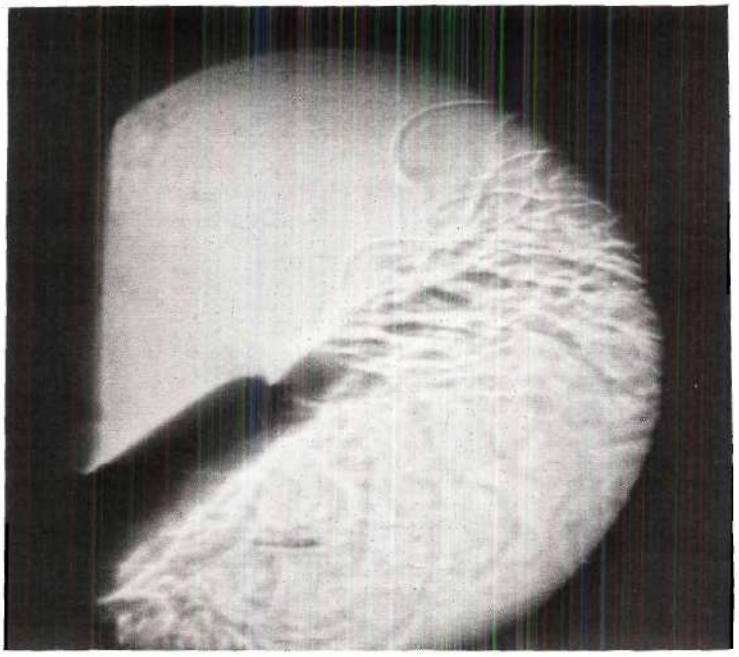

τ = 15 minutes

Figure 40. Continued

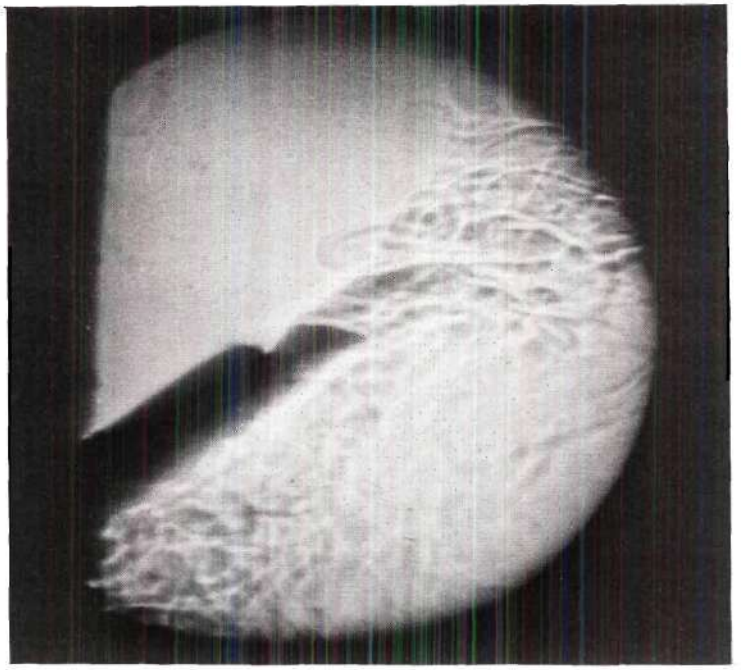

τ = 25 minutes

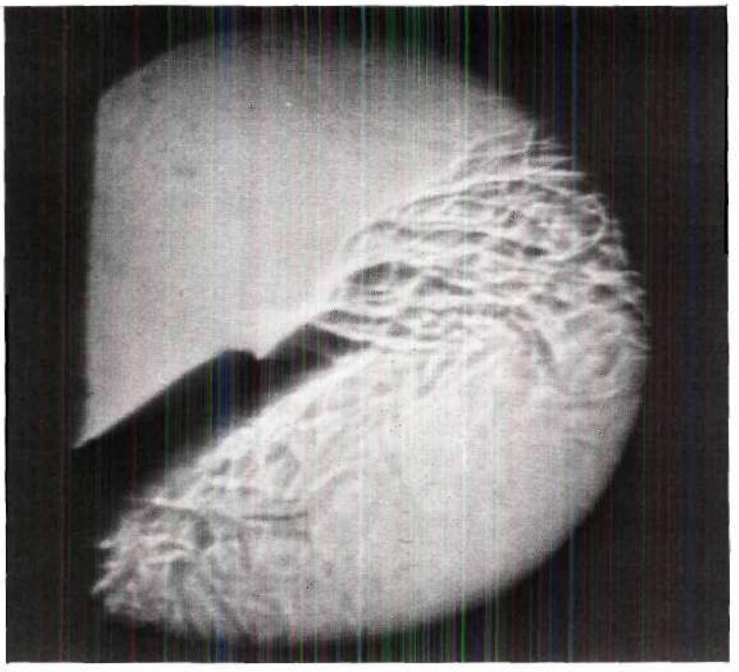

τ = 30 minutes

Figure 40. Concluded

on the flow when the size of the baffle is small. The Schlieren photographs of Figure 41 show that, when bottom heat is applied, the flow around the baffles is more turbulent and back flow persists for a major part of the total test time. Also, the flow along the wall is increased in turbulence over the case when no bottom heat was applied. It is felt that this increase in turbulence with what appears to be a thickening of the boundary layer causes the flow around the small two inch baffles to reattach to the wall quicker.

For larger baffles inclined up, the effect of bottom heat is not as great. Representative particle photographs of flow around a six inch baffle at 45° to the wall are shown in Figures 42 and 43. The flow in this case had a tendency to reattach itself to the wall about 12 inches up the wall from the baffle. Also, with the addition of bottom heat flux, the flow around the inclined baffles had a tendency to be in an upward instead of outward direction. In both figures it is noted that a slight turbulence exists before the baffles. However, the turbulence appears to be less than that experienced by the two inch baffles.

The sequence of photographs shown in Figures 44 and 45 for $L/W = 1.0$ illustrates the same type of flow separation as experienced in the larger aspect ratio tests. However, the flow around the baffles in the low aspect ratio tests was much slower. Also, the flow in most all cases appeared to be laminar in nature. The reason for this is that the distance between successive baffles is smaller in the low aspect ratio tests, hence restricting the modified Grashof number to small values. Even with the slower motion associated with the low aspect ratio tests, the flow at

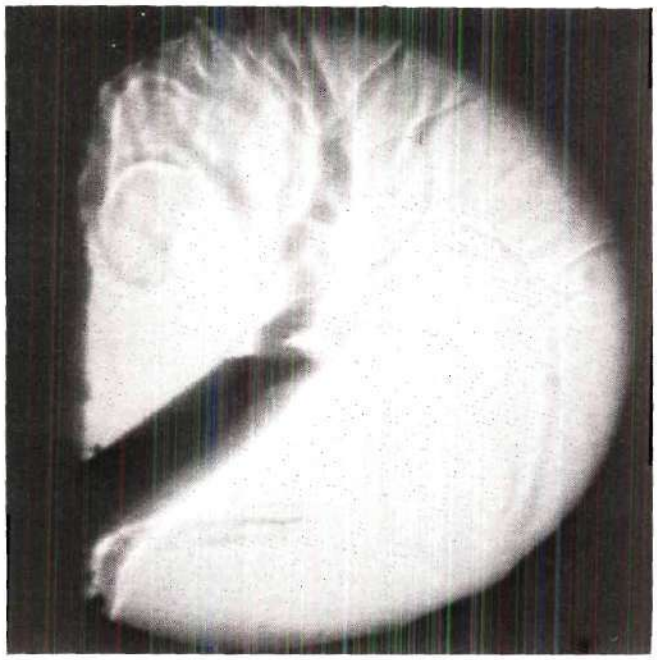

τ = 30 seconds

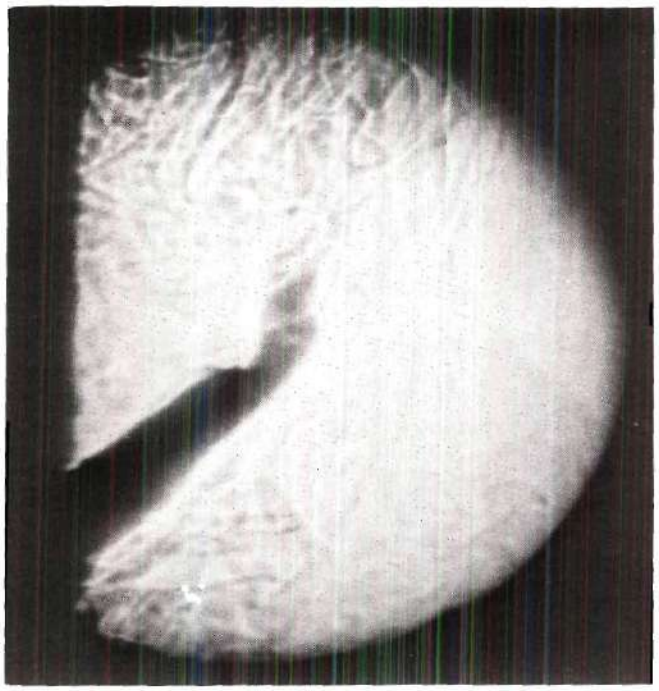

τ = 2 minutes

Figure 41. Flow Around Two Inch Baffles at 45° to the Wall for Different Values of Time; L/W = 4.88, q_b/q_s = 1.51, Three 2 inch Baffles

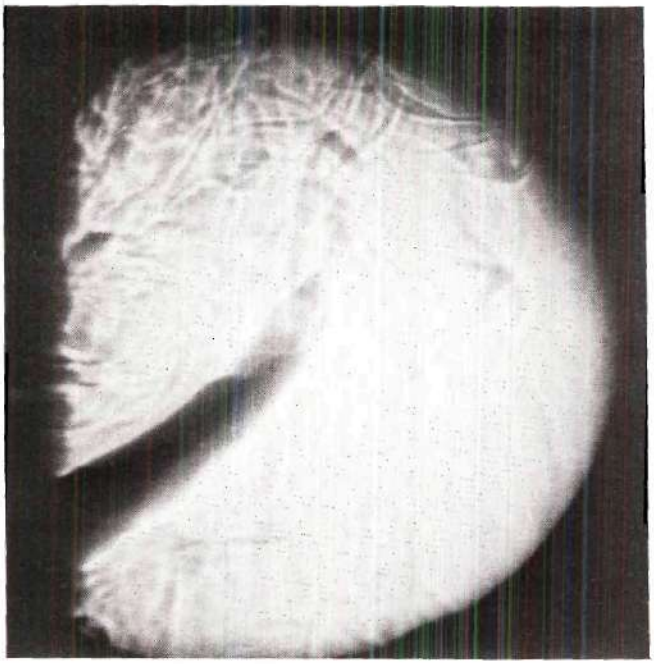

τ = 5 minutes

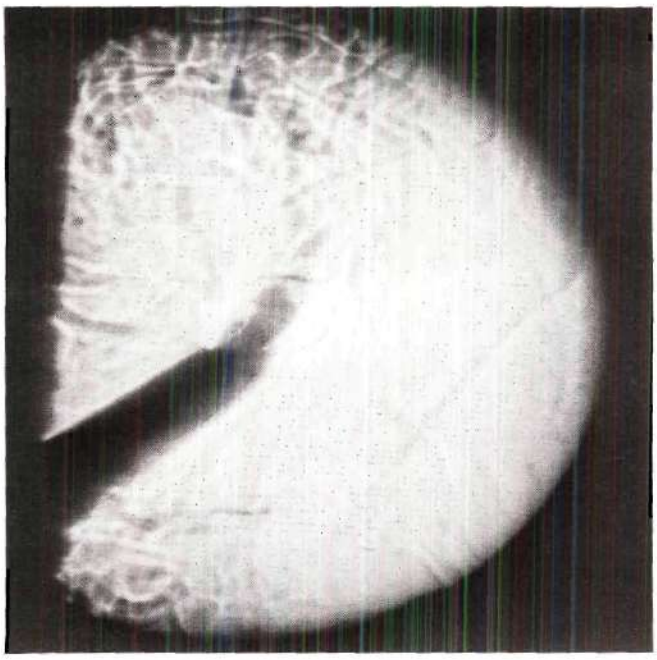

τ = 10 minutes

Figure 41. Continued

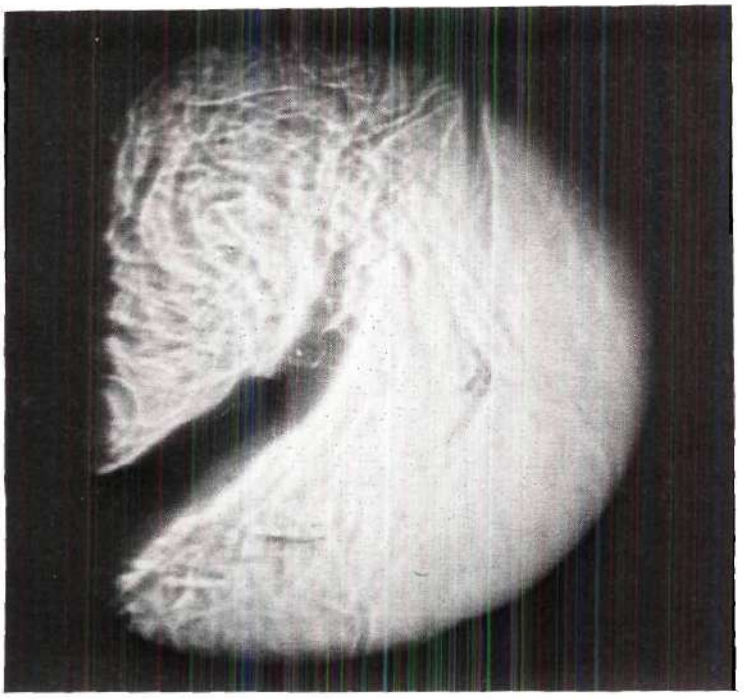

τ = 20 minutes

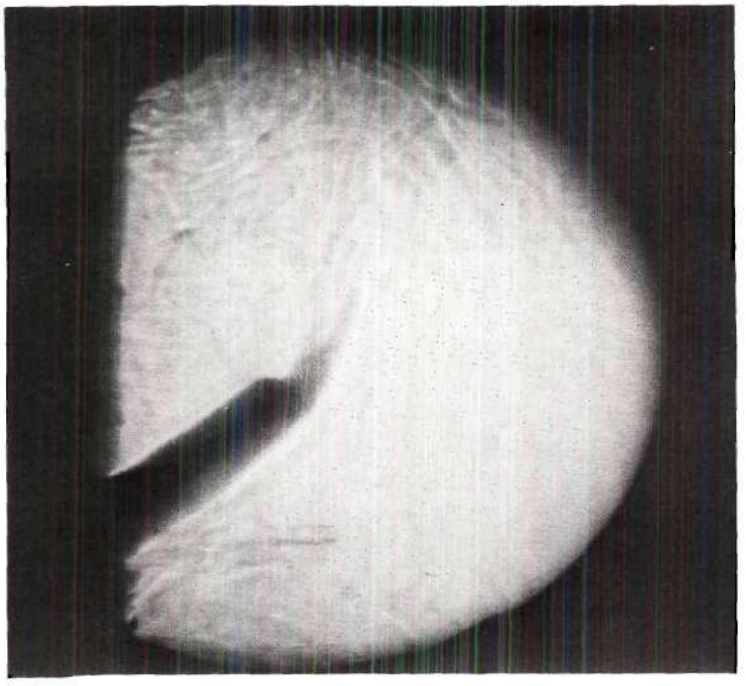

τ = 30 minutes

Figure 41. Concluded

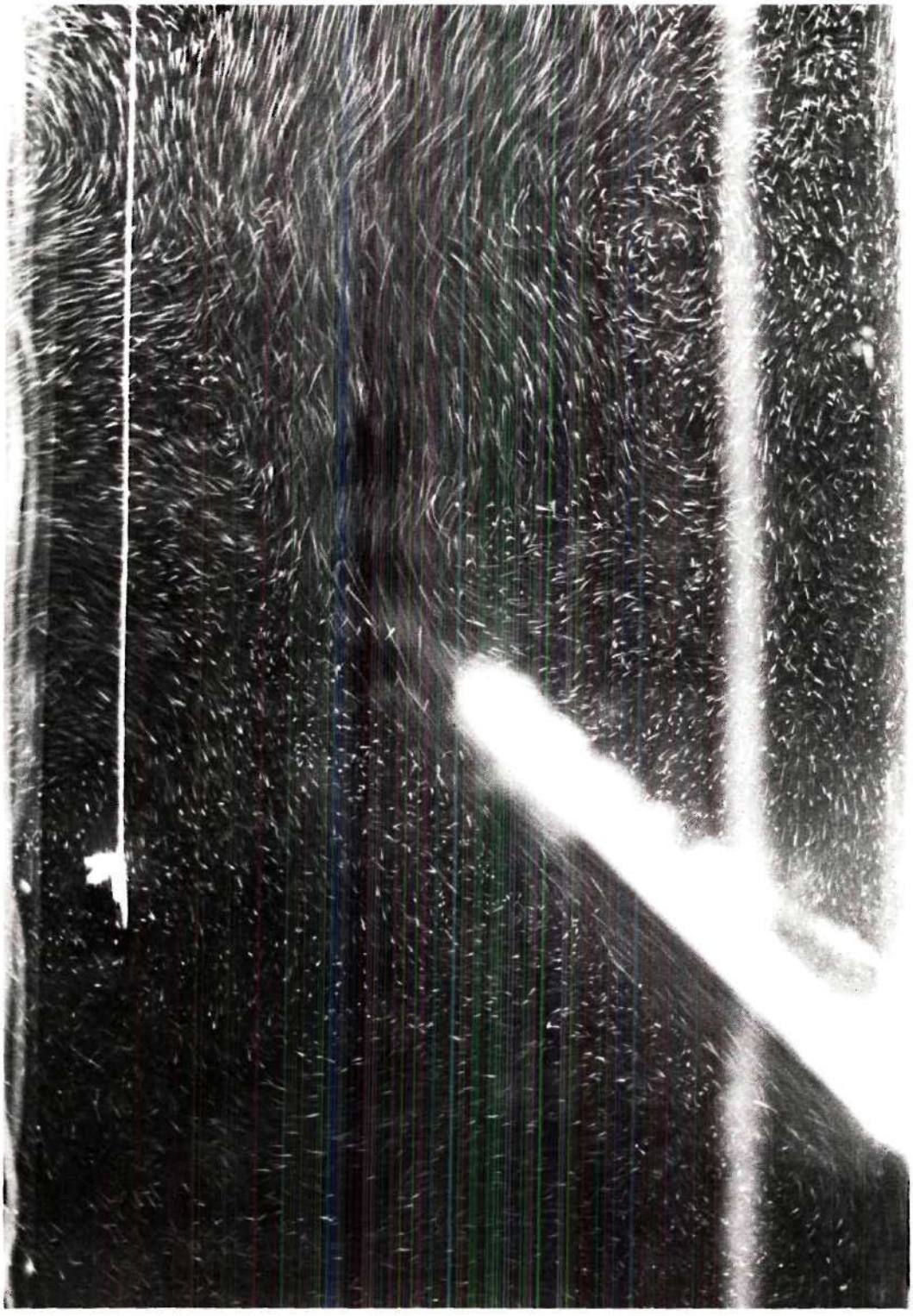

Figure 42. Flow Around a Six Inch Baffle After Two Seconds; $\theta = 45^{\circ}$, $q_b/q_s = 0.45$, L/W = 4.88, Test No. TB-67

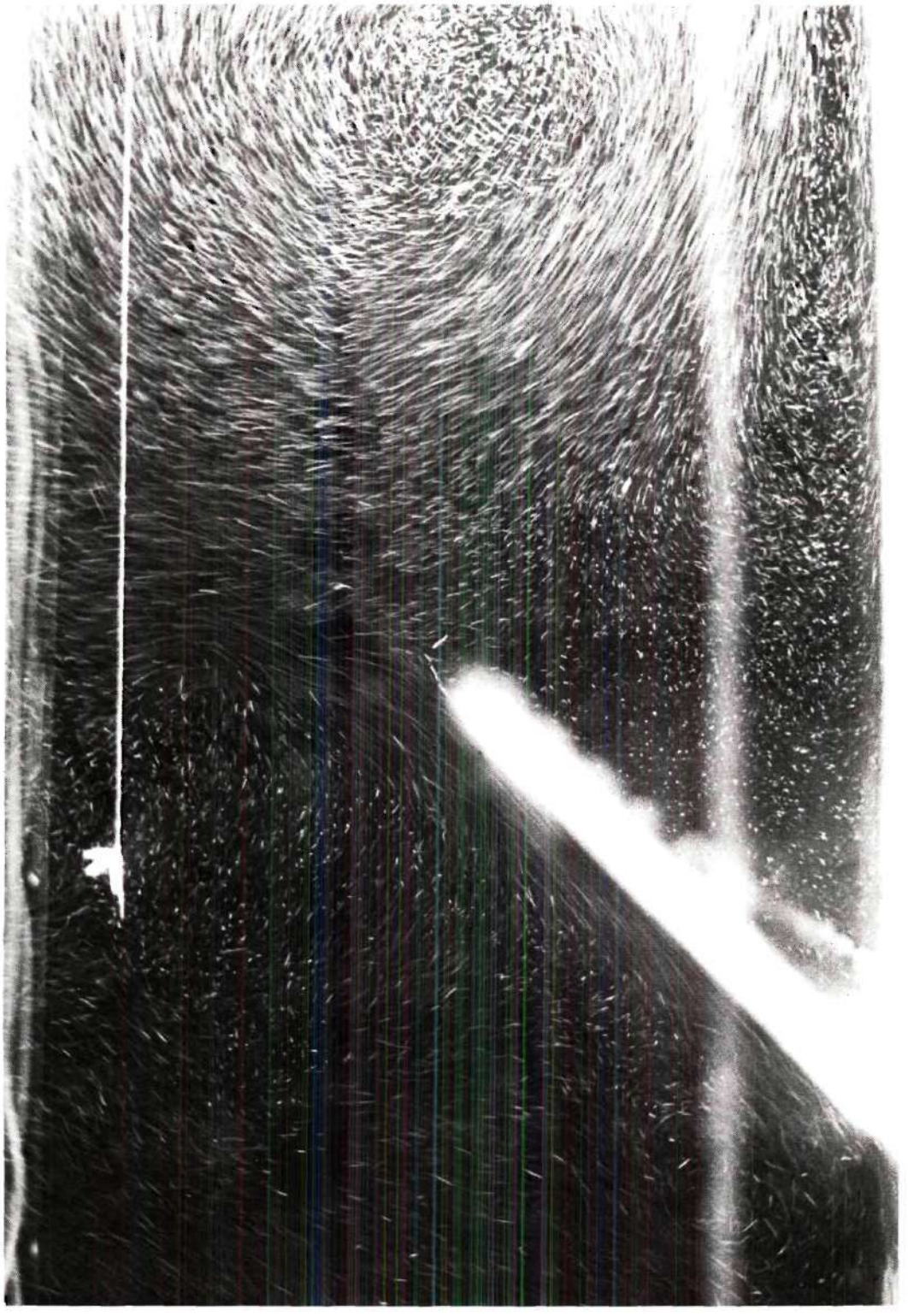

Figure 43. Flow Around a Six Inch Baffle After 20 Seconds; $\theta = 45°$, $q_b/q_s = 0.45$, L/W = 4.88, Test No. TB-67

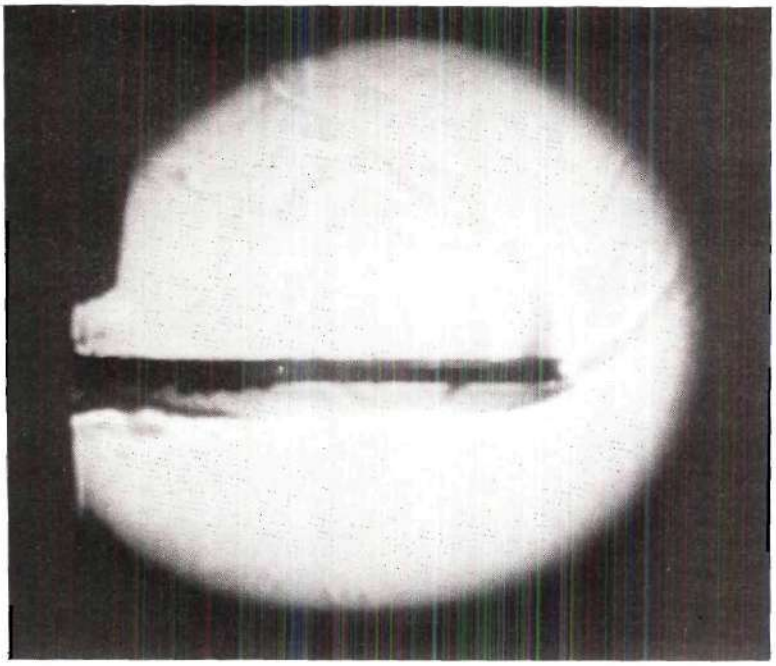

τ = 65 seconds

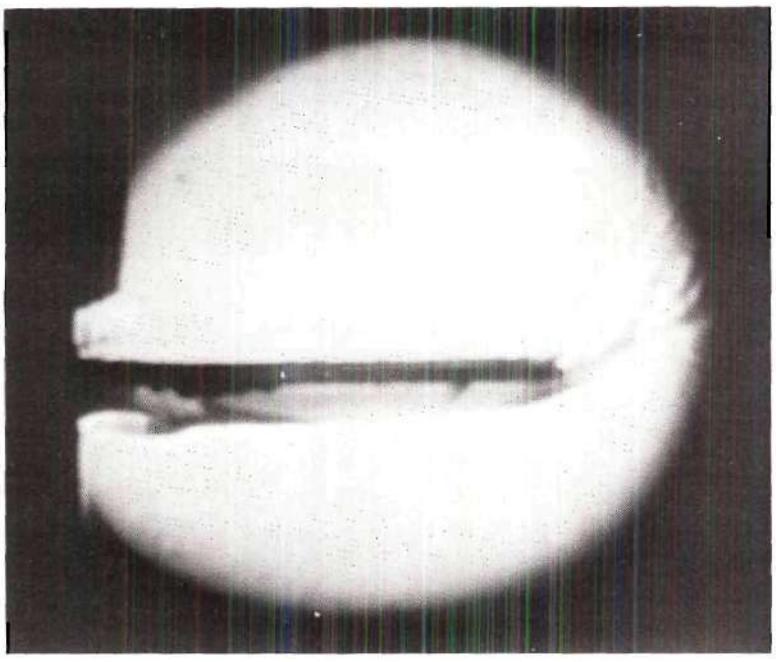

τ = 3 minutes

Figure 44. Flow Around Four Inch Baffles at Different Times; L/W = 1.0, q_b/q_s = 0.0, Three 4 inch Baffles

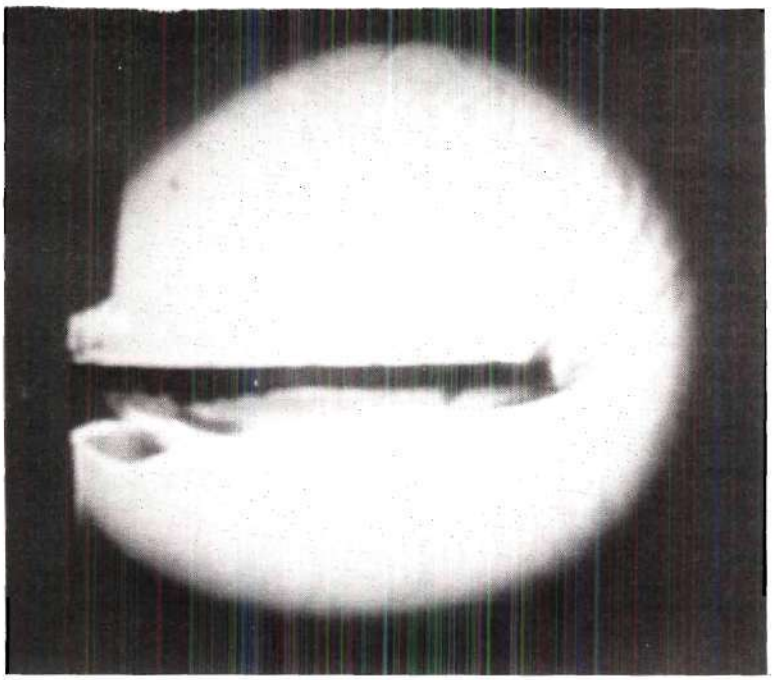

τ = 5 minutes

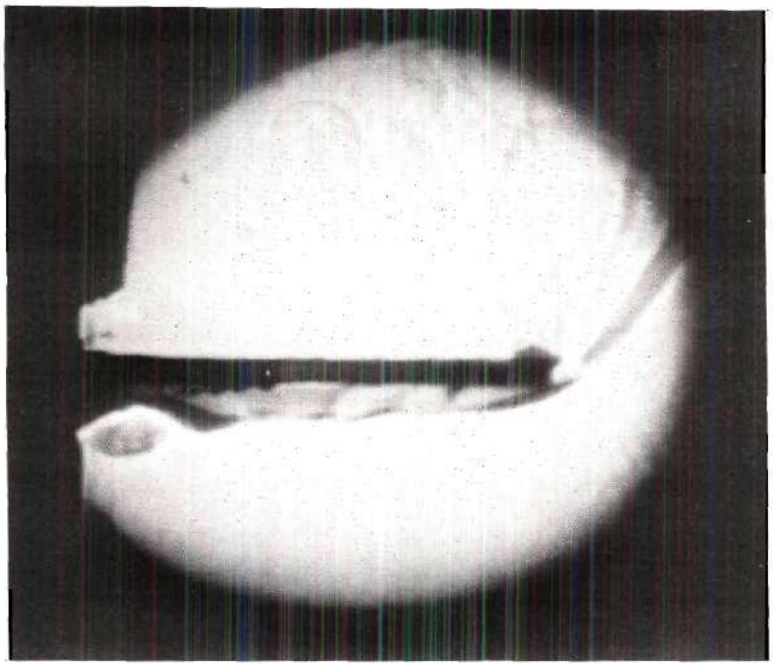

τ = 10 minutes

Figure 44. Continued

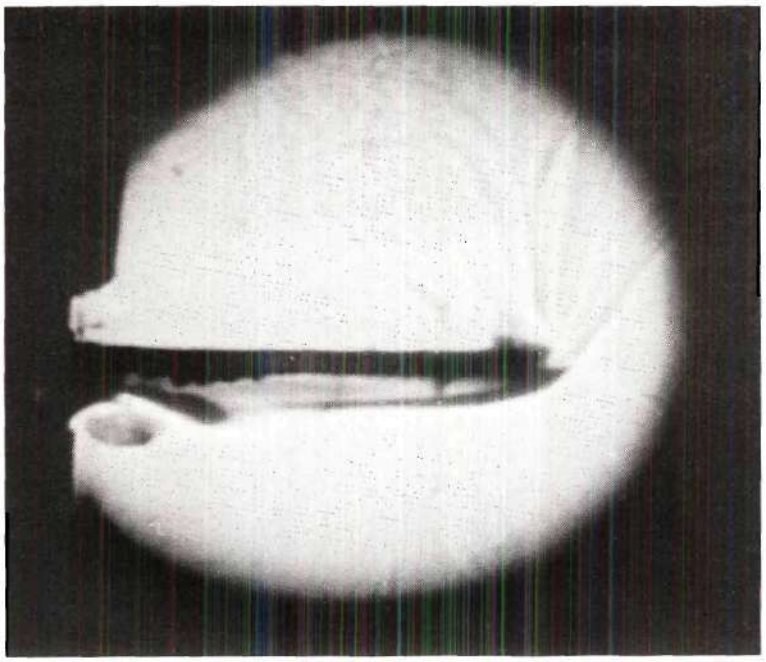

τ = 30 minutes

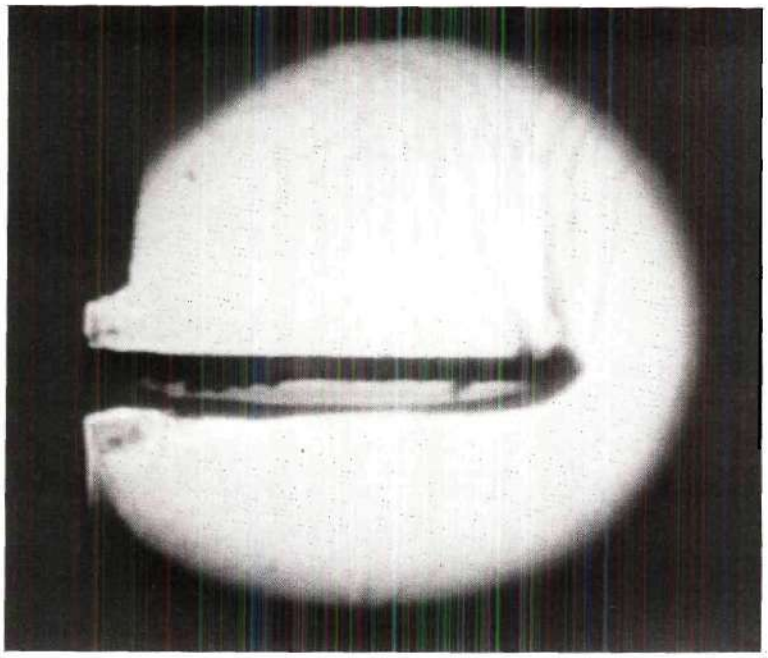

τ = 20 minutes

Figure 44. Concluded

the tip of the baffles separated from the baffle and mixed with the bulk fluid. With even larger baffles placed on the walls of the tank, the flow along the baffles is further reduced. For example, in some of the eight inch baffle tests, at lower values of the side heat flux, the flow has a tendency to reattach to the back side of the baffle, thus reducing the mixing action which is desired. Photographs of the eight inch baffles are not presented since the Schlieren system employed had a six inch field of view which was not large enough to examine the whole baffle at one instant of time. With the addition of bottom heat, the flow around the large baffles, particularly near the center of the wall, was further reduced and very little mixing action was created in the bulk fluid.

In Figure 44, the heat flux ratio is equal to 0.0 while in Figure 45 it is 0.59. From a comparison of these figures, it is seen that the addition of bottom heat has the effect of reducing the flow beneath the baffles which in turn promotes reattachment. This was particularly true when low values of the side heat flux were used in tests with high values of the bottom heat flux. For the higher heat flux ratios, the flow tends to curl around the baffle and reattach to the wall about six inches up the wall from the baffle. In the low heat flux ratio tests it appeared from the Schlieren and particle photograph that more of boundary layer flow was diverted into the center region of the tank.

When baffles are added to walls of a tank, the bulk temperature profiles are no longer constant across the tank cross section. Measurements without baffles indicate an almost constant cross sectional temperature except in regions close to the heated walls or near the tank bottom. For this reason, the assumption of two-dimensional flow within such tanks

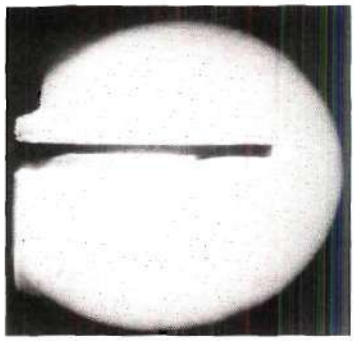

τ = 15 seconds

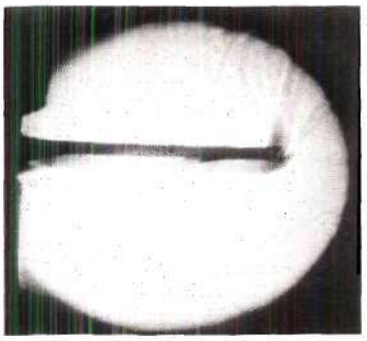

τ = 20 minutes

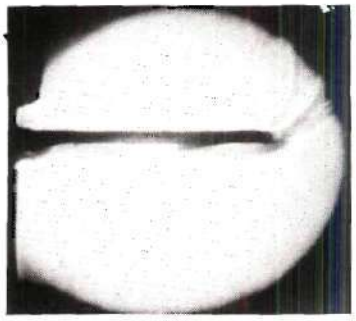

τ = 2 minutes

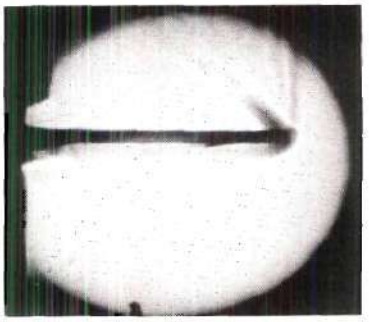

τ = 25 minutes

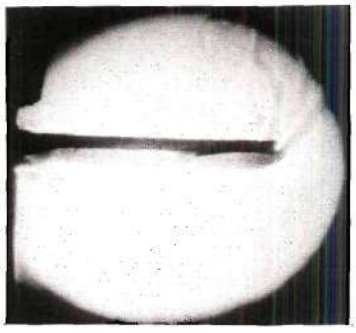

τ = 10 minutes

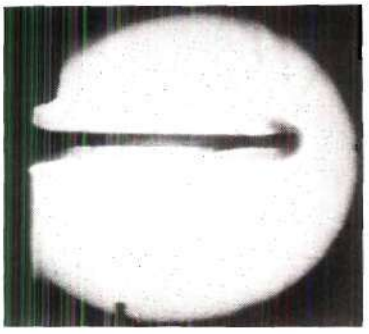

τ = 30 minutes

Figure 45. Flow Around Four Inch Baffles at Different Times; L/W = 1.0, q_b/q_s = 0.53, Three 4 inch Baffles

had been used in developing analytical models. Schneider (26) photographically studied the flow in both large and small tanks and found the assumption of two-dimensional flow to be valid for the small tanks, but questionable in the upper regions of large tanks such as the one used in this investigation. With the addition of baffles on the vertical walls of large tanks, the flow is more likely to be three-dimensional throughout, hence making an analytical solution to the problem extremely difficult.

CHAPTER IV

CORRELATION OF DATA

Baffle Effectiveness

In the previous chapter, various bulk temperature profiles with and without baffles were presented. From these figures, it can be seen that baffles have the general effect of promoting a more uniform bulk temperature throughout a greater part of the bulk fluid. To measure this effect Vliet (8) defined the term baffle effectiveness, E, and derived an equation for this term which is presented in Chapter I. In Vliet's original equation, the temperature moment about the bottom of the vessel was made dimensionless with respect to the uniformly mixed case according to the equation

$$M_T^* = \frac{M_T - \bar{T}_N L^2}{\frac{T_N L^2}{2}} \tag{4.1}$$

In the above equation, M_T is defined in terms of a local temperature difference $(T - T_i)$ which is then being compared with a temperature moment based on an average bulk temperature, $\bar{T}$. It was felt by the author that a better comparison could be obtained by using an average temperature difference, θ, instead of the average temperature. Using an average temperature difference, Eq. (4.1) becomes

$$M_\theta^* = \frac{M_T - \frac{\bar{\theta} L^2}{2}}{\frac{\bar{\theta} L^2}{2}} \tag{4.2}$$

with the baffle effectiveness, E, defined as

$$E = 1 - \frac{M_\theta^*}{M_{\theta N}^*} \tag{4.3}$$

On substituting for M_θ and $M_{\theta N}$, this equation becomes

$$E = \frac{M_{\theta N} - \frac{\bar{\theta}}{\bar{\theta}_N} M_\theta}{M_{\theta N} - \frac{\bar{\theta}_L^2}{2}} = \frac{M_{\theta N} - M_\theta}{M_{\theta N} - \frac{\bar{\theta}_L^2}{2}} \tag{4.4}$$

since $\bar{\theta} = \bar{\theta}_N$.

The significance of the effectiveness parameter has previously been discussed in Chapter I.

An Algol computer program, using Eqs. (4.1), (4.2), and (4.4) along with Simpson's numerical method of integration, was written and run on a Burrough's B-5500 computer. The effectiveness values calculated for many of the tests are illustrated in the following sections. A listing of the computer program is presented in Appendix E.

Baffle Effectiveness, L/W = 4.88

Representative effectiveness values for the high aspect ratio tests are illustrated in Figures 46, 47, and 48. From Figure 46, for a heat flux ratio of zero, it is seen that for early values of time, the most effective baffle design tested was either three 2 inch baffles or one 6 inch baffle at 90° to the vertical wall. However, the effectiveness of the two inch baffles decreases rapidly with increasing time. The most effective baffle design for the entire test appears to be three 6 inch baffles on each wall.

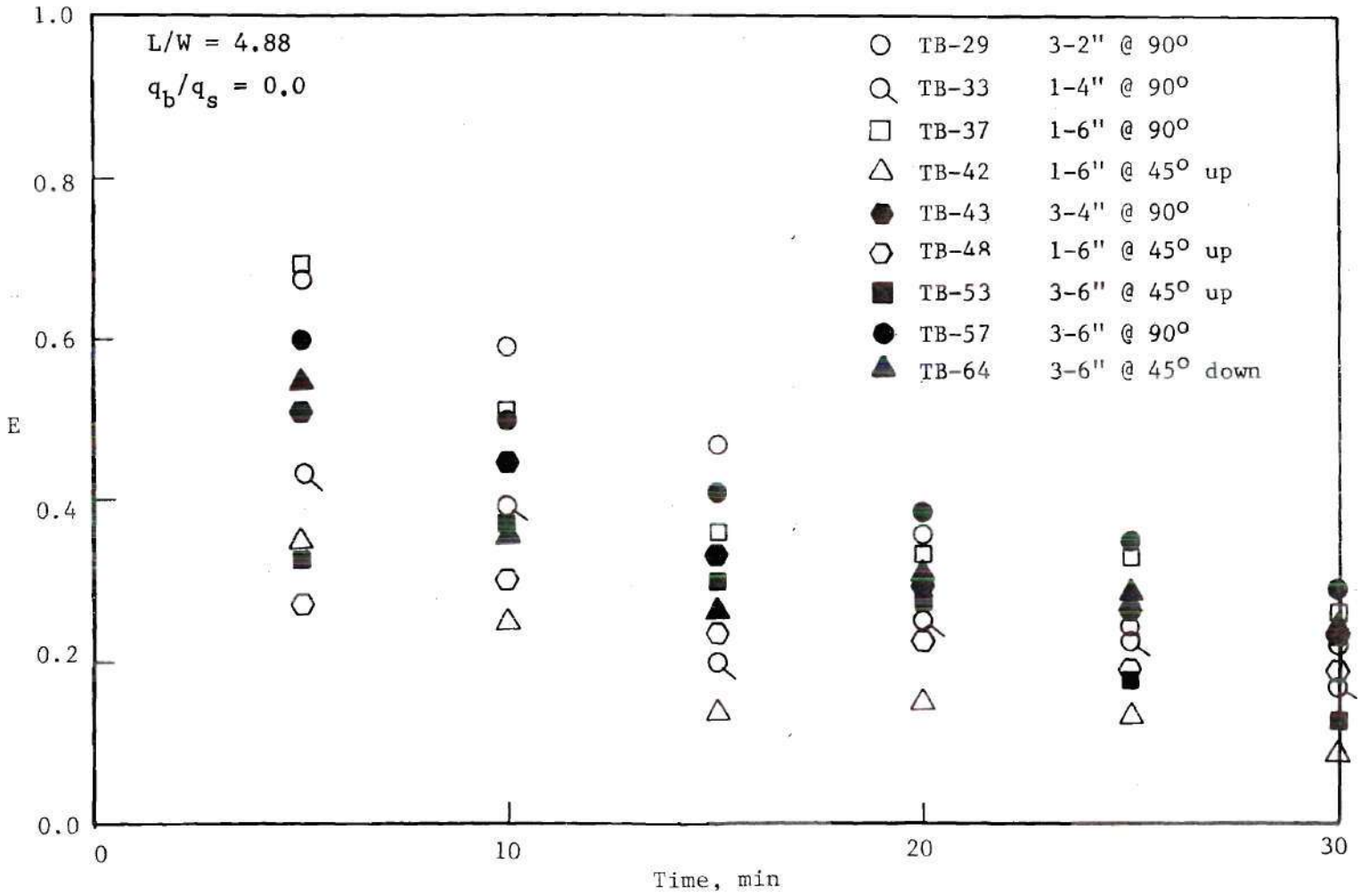

Figure 46. Effectiveness versus Time for Various Baffle Designs

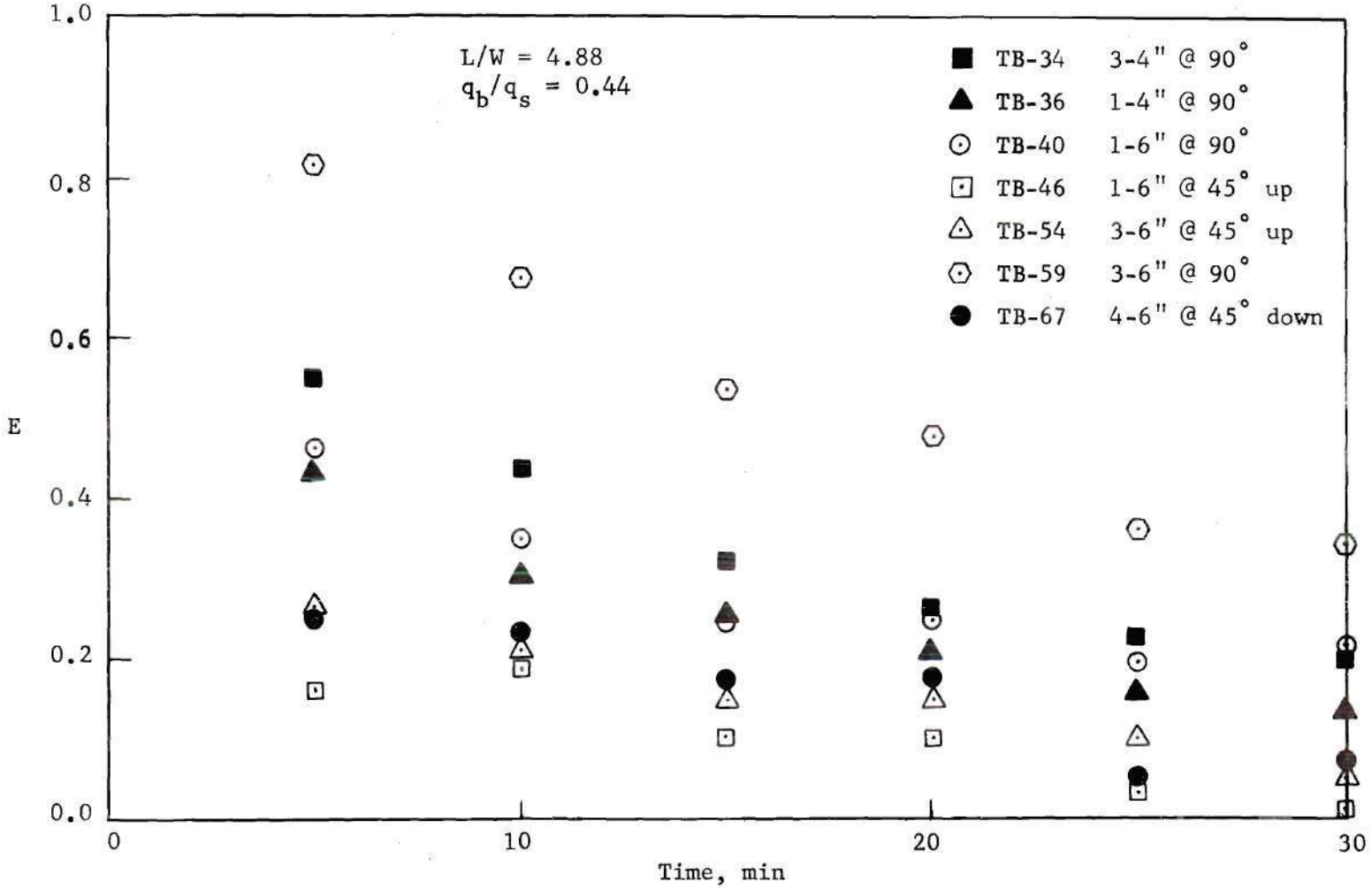

Figure 47. Effectiveness versus Time for Various Baffle Designs

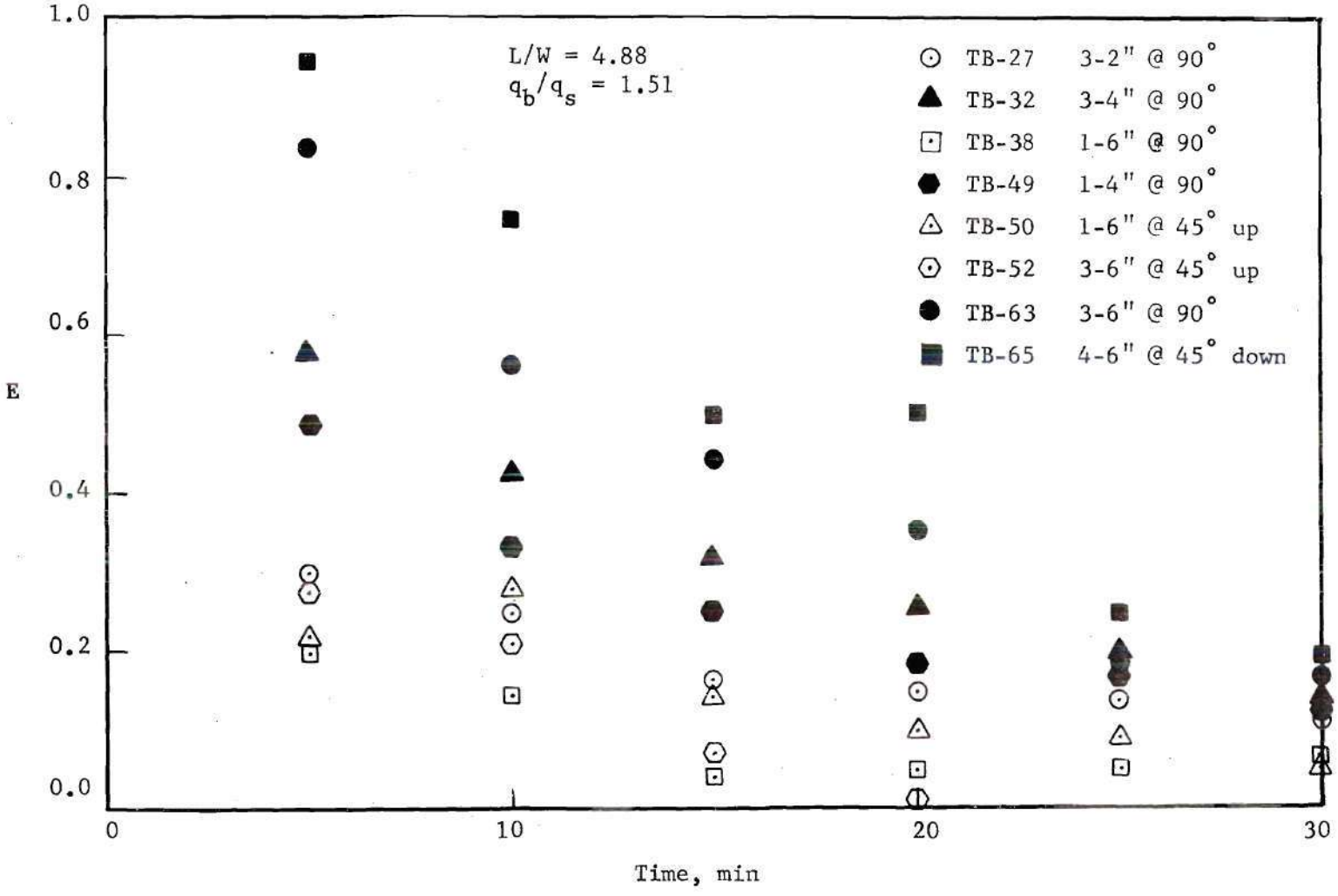

Figure 48. Effectiveness versus Time for Various Baffle Designs

Although this design appears to be slightly less effective for the first five minutes, its effectiveness is higher for extended values of time as shown in the figure. The results of three 4 inch baffles on each wall are consistently below those of the three 6 inch baffles for all values of time. All the curves, however, have the same general trend of becoming less effective as time increases. During the effectiveness calculations, it was observed that a small error in temperature, especially near the top of the fluid, could make a considerably larger error in the baffle effectiveness, because of the temperature moment calculation, Near the tank top, the lever arm for the moment calculation about the bottom of the vessel is large, therefore a larger or smaller moment will be calculated depending on whether or not the measured bulk temperature is larger or smaller than the true bulk temperature. This fact could have caused the two inch baffle to appear more effective than the larger baffles.

Also, from Figures 47 and 48, it is noted that the concave up baffles are less effective at the beginning of the tests. Further, from the figures, it is seen that three 6 inch baffles concave up at 45° to the vertical walls are about as effective as one 6 inch baffle. It is also seen from Figure 46, by a comparison of Test TB-42 and TB-48, that some degree of repeatability is obtained. Although the values are not identical for all values of time, they do follow a general pattern and are relatively close. A greater effectiveness is obtained with four 6 inch baffles concave down at 45° than for the concave up baffles. The reason for this result is understandable when one notes that the concave up baffles tend to assist the boundary layer flow instead of mixing it as do the

concave downward and horizontal baffles. It is seen from Figures 46, 47, and 48 that the concave down baffles have approximately the same effectiveness as an equal number at 90° to the wall for extended values of time. In Figure 48 the four 6 inch baffles concave down initially have a high effectiveness which drops off considerably with increasing time. This verifies the earlier observation that the concave down baffles resemble the horizontal baffles in diverting the boundary layer flow.

By comparing Figure 46 with Figures 47 and 48, it is seen that increasing the heat flux ratio generally reduces the baffles' effectiveness. Except for outstanding cases, the effectiveness of baffles for $q_b/q_s > 1$ is below the lower heat flux values for all values of time. The reason for this appears to be that the addition of bottom heat, when baffles are present, reduces the mixing which is obtained when no heat is applied. This fact was previously observed in the photographic analysis of flow around the baffles. When bottom heat was applied, it was noted that the flow around the baffles was considerably reduced and, in some cases, the flow reattached to the back side of the baffles. The addition of a small amount of bottom heat for the three 6 inch baffle design increased the effectiveness, while for the three 4 inch baffles, there was little change.

Baffle Effectiveness, L/W = 3.0

Figures 49 through 52 illustrate baffle effectiveness for the medium aspect ratio. The heat flux ratio for this series of tests ranged between 0.0 and 2.42. For a heat flux ratio of 0.0, the most effective baffle design is three 6 inch baffles on each wall, as illustrated in Figure 49. Also, from the figure, one can see that there is not a large

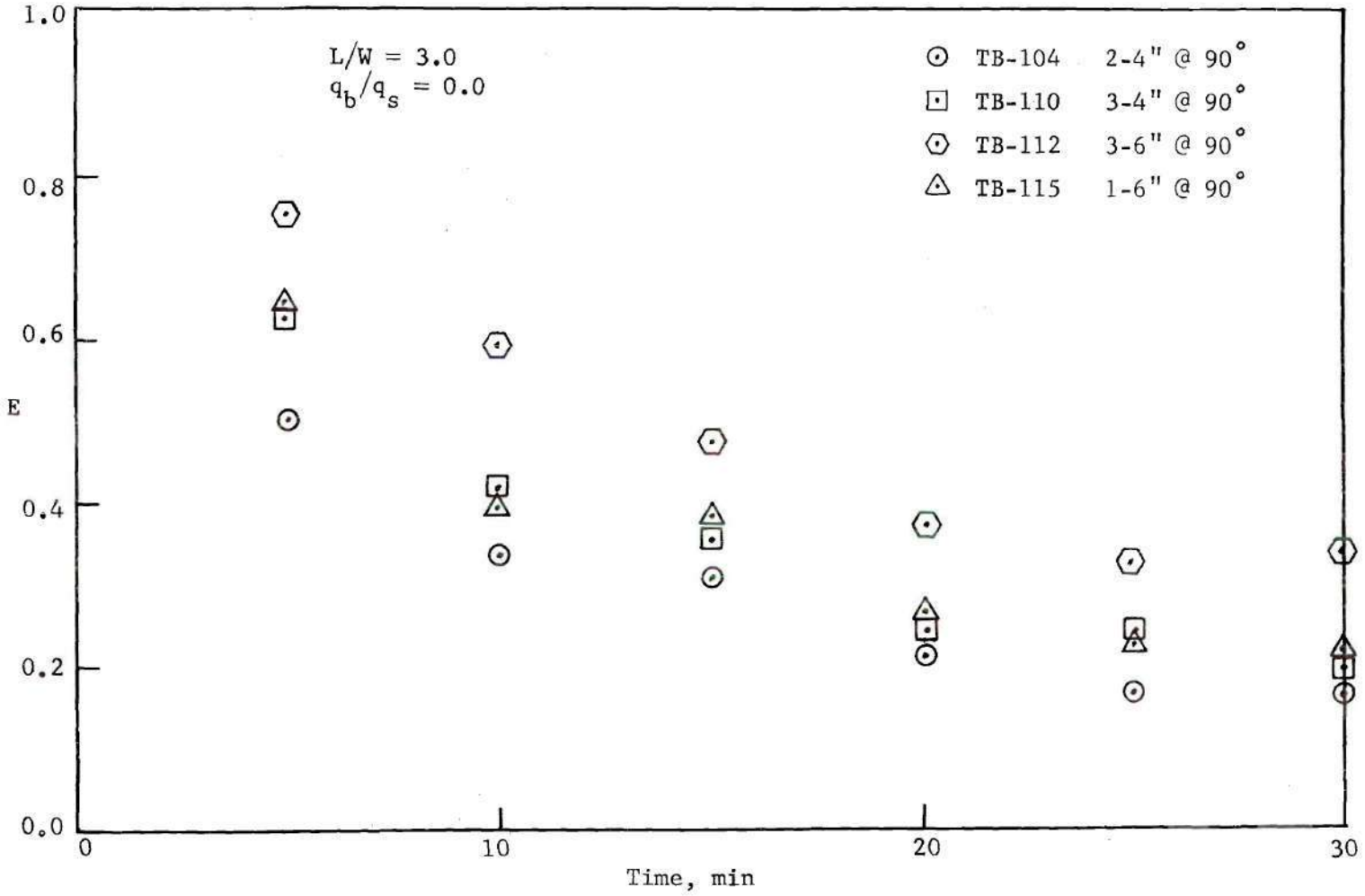

Figure 49. Effectiveness versus Time for Various Baffle Designs

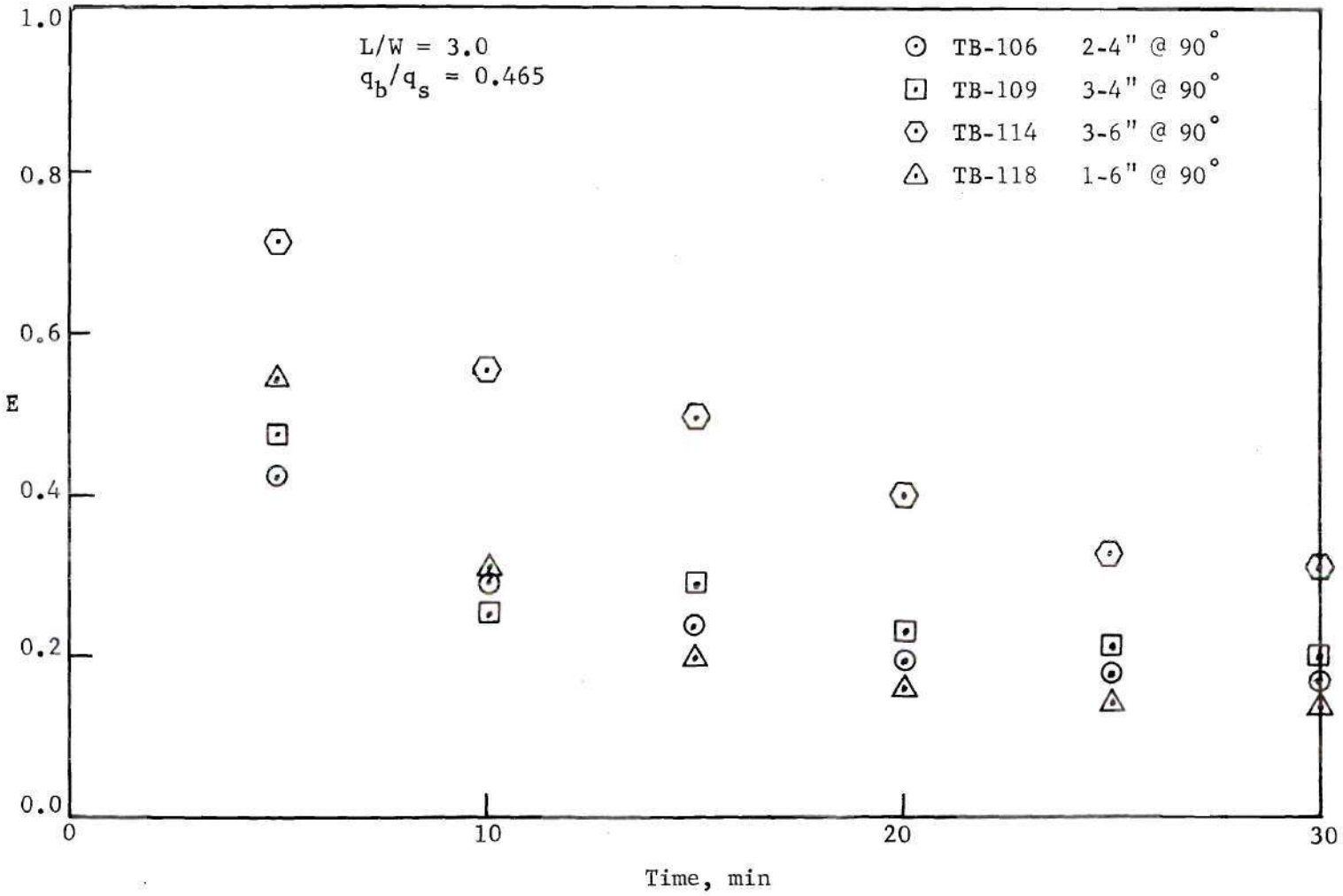

Figure 50. Effectiveness versus Time for Various Baffle Designs

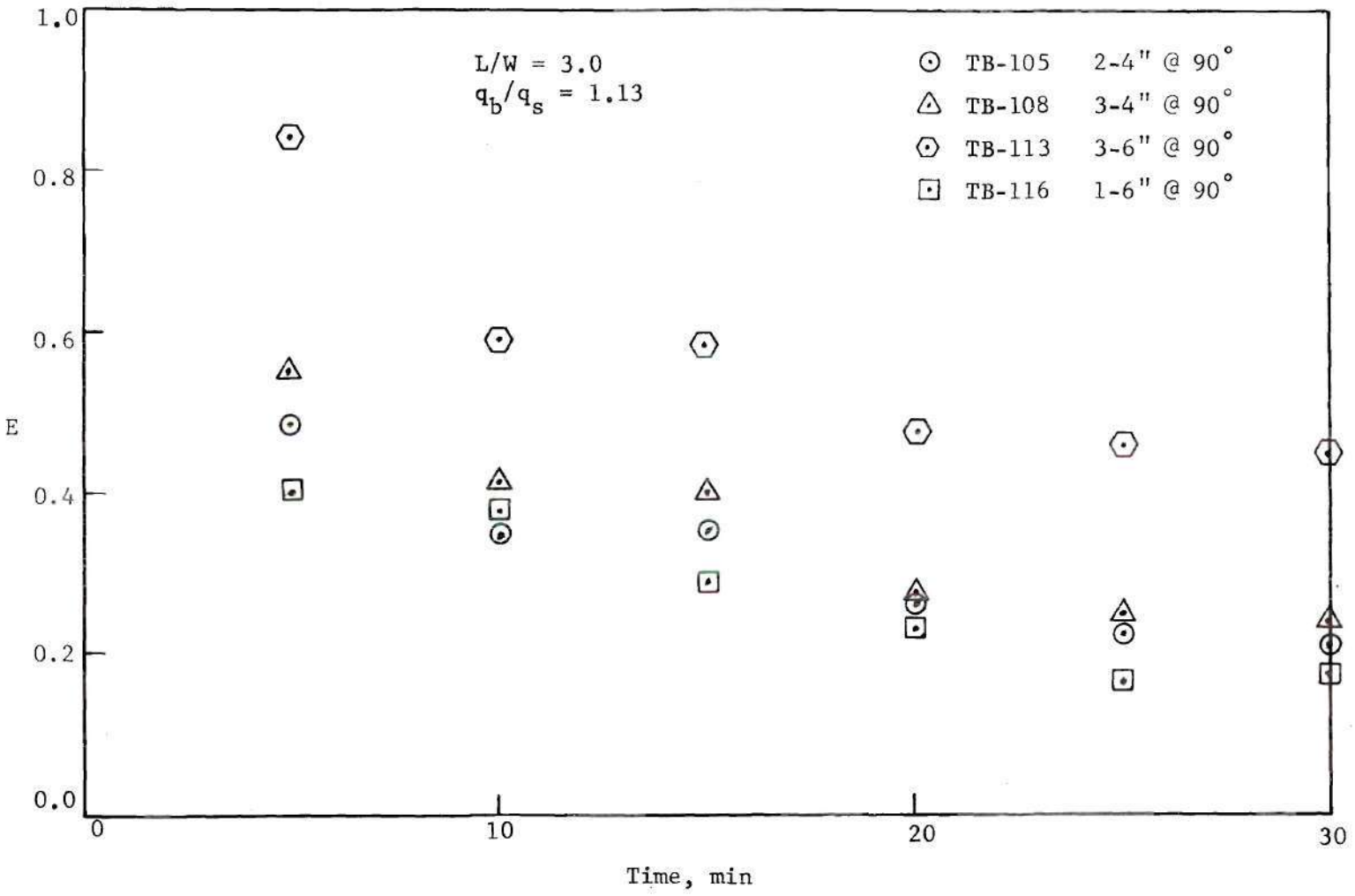

Figure 51. Effectiveness versus Time for Various Baffle Designs

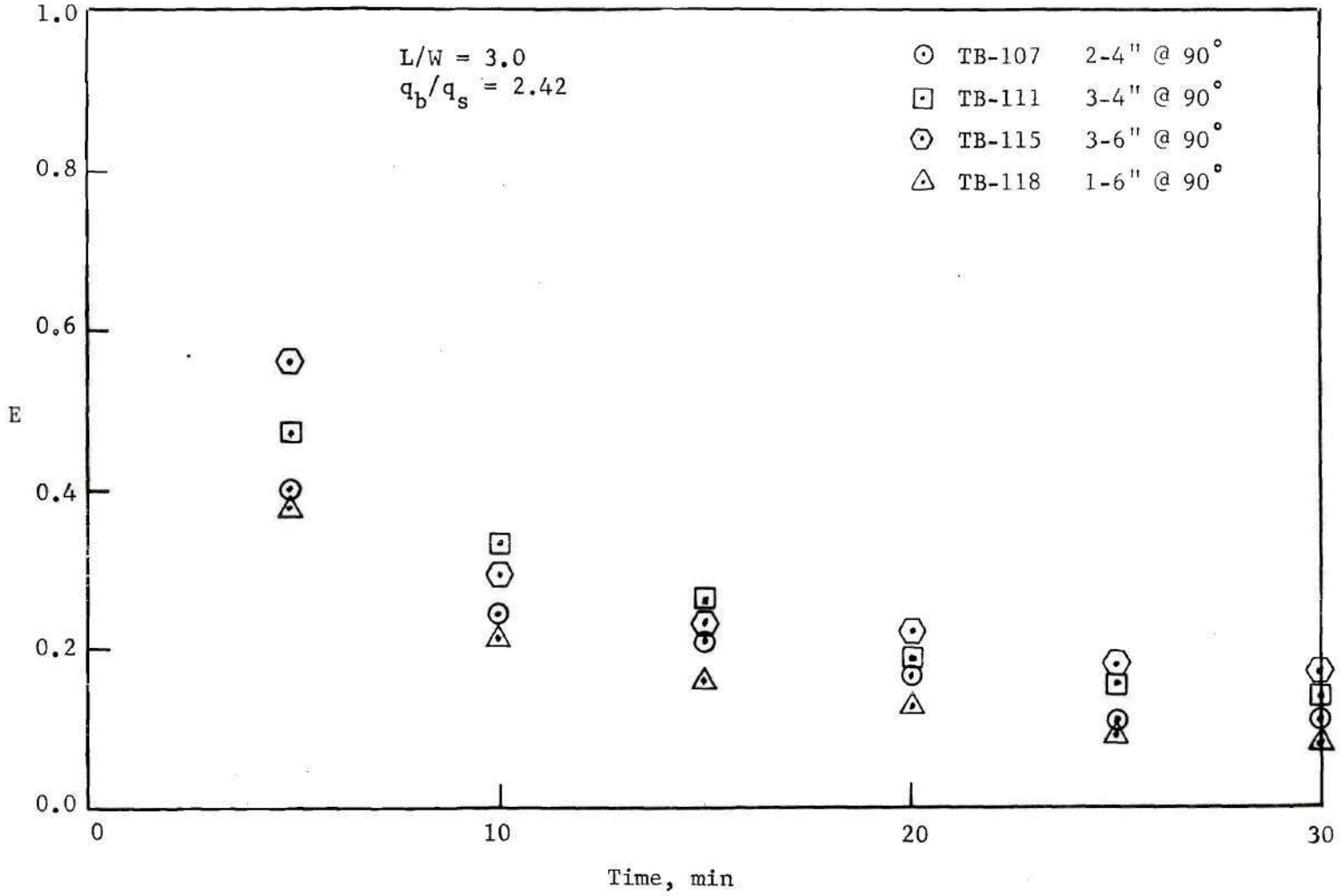

Figure 52. Effectiveness versus Time for Various Baffle Designs

difference between the effectiveness of one 6 inch or three 4 inch baffles. The least effective design for this aspect and heat flux ratio is the two 4 inch baffles. Again, the probable reason for this is that the two 4 inch baffles are not quite large enough in size to induce mixing into the center of the tank as do the larger baffles.

For an aspect ratio of 3.0, the addition of bottom heat of about one-half the magnitude of the side heat flux, generally produced little effect. The results can be seen by comparing Figures 49 and 50. The effect in general was to reduce slightly the effectiveness of all baffles tested. However, increasing the heat flux ratio close to 1.0 results in effectiveness values which are approximately the same as those for a ratio of zero. With further increase in the heat flux ratio, the effectiveness continues to decrease. This result can be seen in Figure 52. In two of the tests, at the large heat flux ratio, the effectiveness almost remained constant.

By comparing Figures 49, 50, 51, and 52, the most effective baffle design tested was the three 6 inch baffles at 90° to the heat walls. As for the aspect ratio of 4.88, the most effective heat flux appears to be zero. During the series of tests at this aspect ratio, no tests on the effect of baffle angle were performed. This variable was dropped because of the extreme complexity it added to the data analysis. It was felt that the qualitative analysis of the angle effect at the high aspect ratio would be sufficient for its description.

Baffle Effectiveness, $L/W = 1.0$

Figures 53 and 54 illustrate the baffle effectiveness for the low

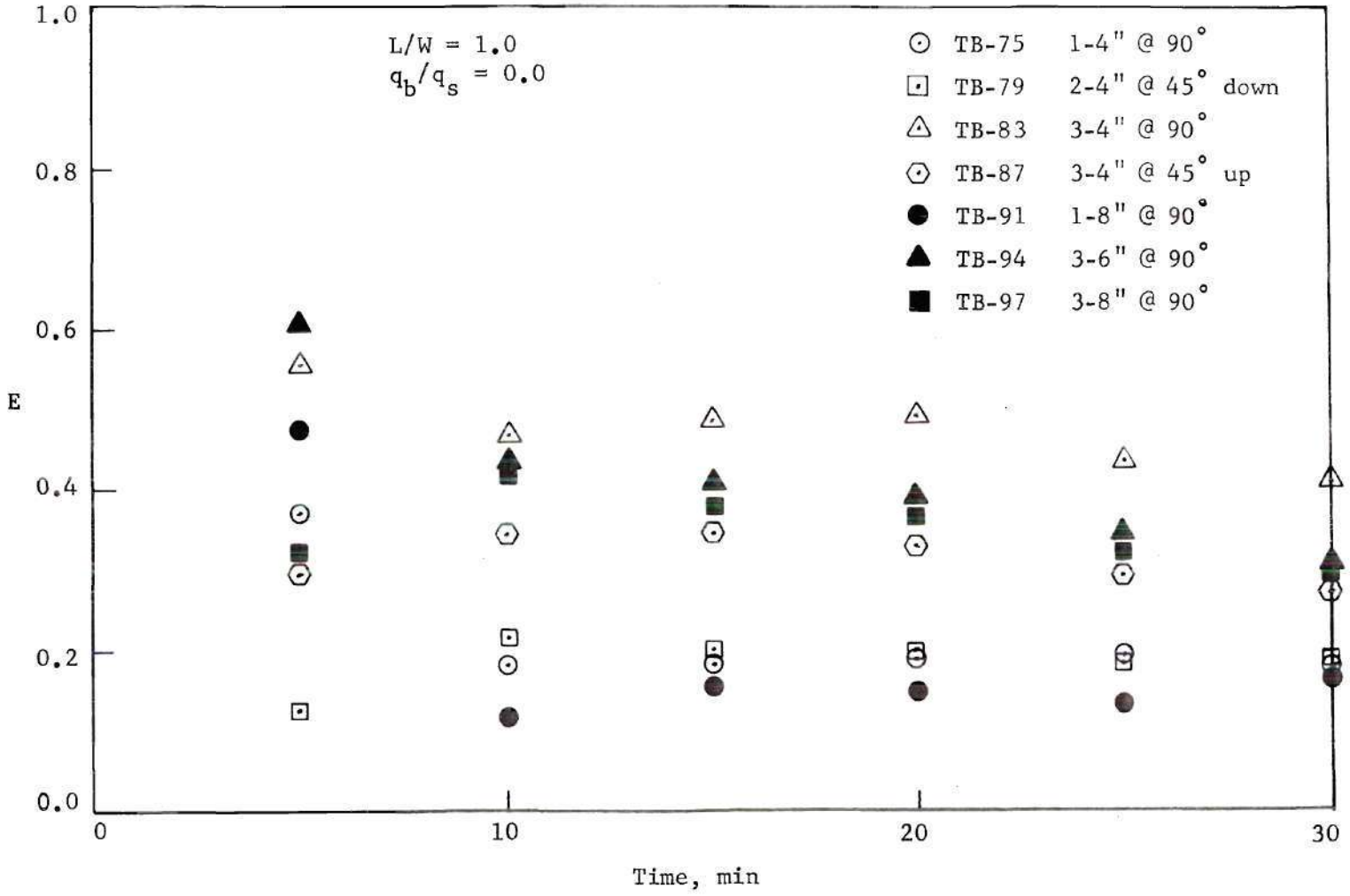

Figure 53. Effectiveness versus Time for Various Baffle Designs

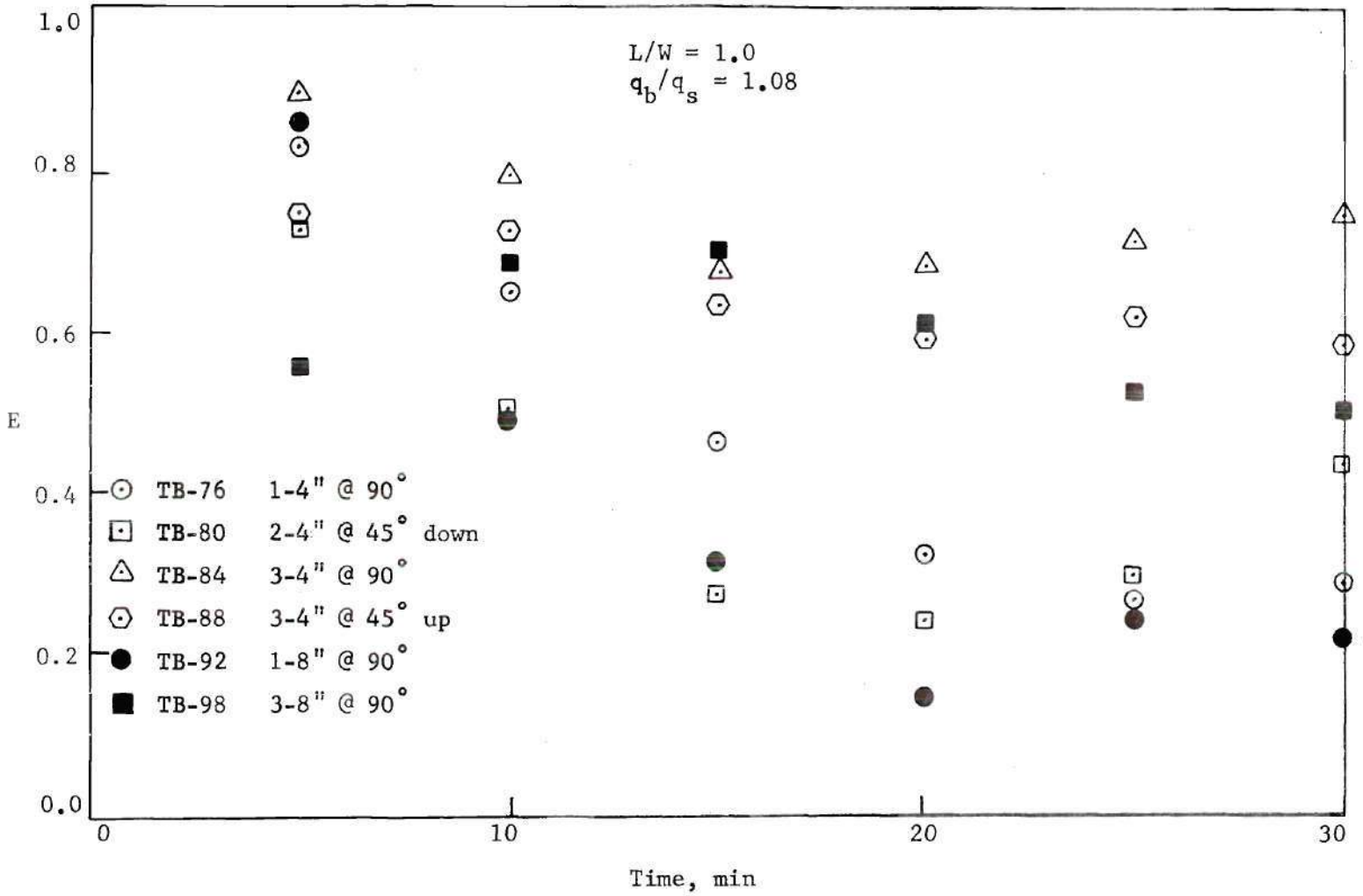

Figure 54. Effectiveness versus Time for Various Baffle Designs

aspect ratio tests. During this series of tests, the heat flux ratio was varied from 0.0 to 0.93. From Figure 52 for a heat flux ratio of zero, it is seen that the most effective baffle designs tested were the three 4 inch baffles on each wall with three 6 inch baffles following closely. The results of the higher aspect ratio tests indicated that the larger baffles were generally more effective. However, for low values of L/W, the flow around the larger baffles is slower, thus, there is less mixing and the effectiveness is reduced. Again, it is seen from the figure that baffles concave up or down are generally less effective than those horizontal to the walls. However, in the low aspect ratio tests, for the heat flux ratios tested, the baffles concave up were more effective than those concave down. It should also be noted that, for the low aspect ratio tests, the initial values of effectiveness are generally higher than for the large aspect ratio tests.

In Figure 54 for the higher heat flux ratios, the four inch baffles proved to be more effective than the large eight inch baffles. Also, increasing the number of larger baffles increases the effectiveness as seen by comparing tests TB-92 and TB-98. Initially, the single baffle appears to be more effective, however, after the first five minutes, the effectiveness of three baffles is larger. This result was true for both the four inch and eight inch baffles. Further, in the low aspect ratio tests, the effectiveness values are generally higher when bottom heat is added. This is contrary to the results obtained in the high aspect ratio tests. The reason for this appears to be a result of the increased mixing that takes place when bottom heat is applied. In the low aspect ratio tests, baffles

are located much closer to the bottom of the vessel. It is the close proximity of the first baffles on the vertical walls with the vessel bottom which assists in increasing the mixing in this region while at the same time diverting the boundary layer flow from the fluid surface.

Correlation of Effectiveness

For the results of this work to be a value for design purposes, it was felt that an equation which correlates the data should be presented. During the testing, trends were observed and noted as to the effect of each variable on the bulk temperature profiles. Four prominent variables excluding time, were considered. These are: (1) heat flux ratio, q_b/q_s; (2) aspect ratio, L/W; (3) baffle to tank with ratio, $\frac{B}{W}$; and (4) the number of baffles on one side, N. Each of these variables is related to the container geometry. For example, to obtain maximum flow up the walls of the container, the heat flux ratio for the three aspect ratios was not exactly the same. It was felt before testing that, for the baffles to be effective, maximum boundary layer flow up the container walls was a necessity. Testing at low values of side heat flux proved this statement to be correct. At low side heat fluxes, the flow around the baffles was slow and bulk mixing did not result.

Since the phenomenon under investigation is transient in nature, the time, τ, is also an important variable that must be considered. An analysis of the effectiveness versus time curves in the first portion of this chapter illustrates the effect time has on baffle effectiveness.

In developing correlation equations, one of the basic rules, according to Mackey (32), is to observe the characteristic shape of the

graphs and find some mathematical relation with constants which fits the general trend of the graphs. For example, the data in Figures 46 through 54 slope to the right in similar fashion to the curve

$$y = e^{-x} \tag{4.5}$$

Using the assumption that the data fit such a curve as Eq. (4.5), the data in Figures 46 through 54 were plotted on semi-log coordinates as illustrated in Figure 55 except that effectiveness, E, versus time, τ, was first plotted. Most of the data fell on straight lines with slopes varying between -0.07 and -0.20, with an average slope of -0.14. The y or E intercept varied depending on the aspect ratio, baffle tank width ratio, heat flux ratio, and number of baffles. Most of the curves were parallel as indicated in Figure 55. Thus, it was assumed that the other variable mentioned above had the effect of shifting the curves up or down and thus entered into a general correlation equation as product terms. That is, the correlation equation took the form

$$E = A\, e^{-by} \left(\frac{L}{W}\right)^m \left(\frac{B}{W}\right)^n N^o (1+q_b/q_s)^p \tag{4.6}$$

To refine the above equation, a second attempt at plotting the data with effectiveness, E, versus the product, $\tau/(L/W)^{\frac{1}{2}}$, was performed. Again, straight lines resulted but with a little less scatter than was previously observed. This is the actual results indicated in Figure 55 for several tests. The slopes of these curves vary for the different tests, so a value of the slope was used which best fit the majority of the data. With the above modification incorporated into Eq. (4.6), the form of the corre-

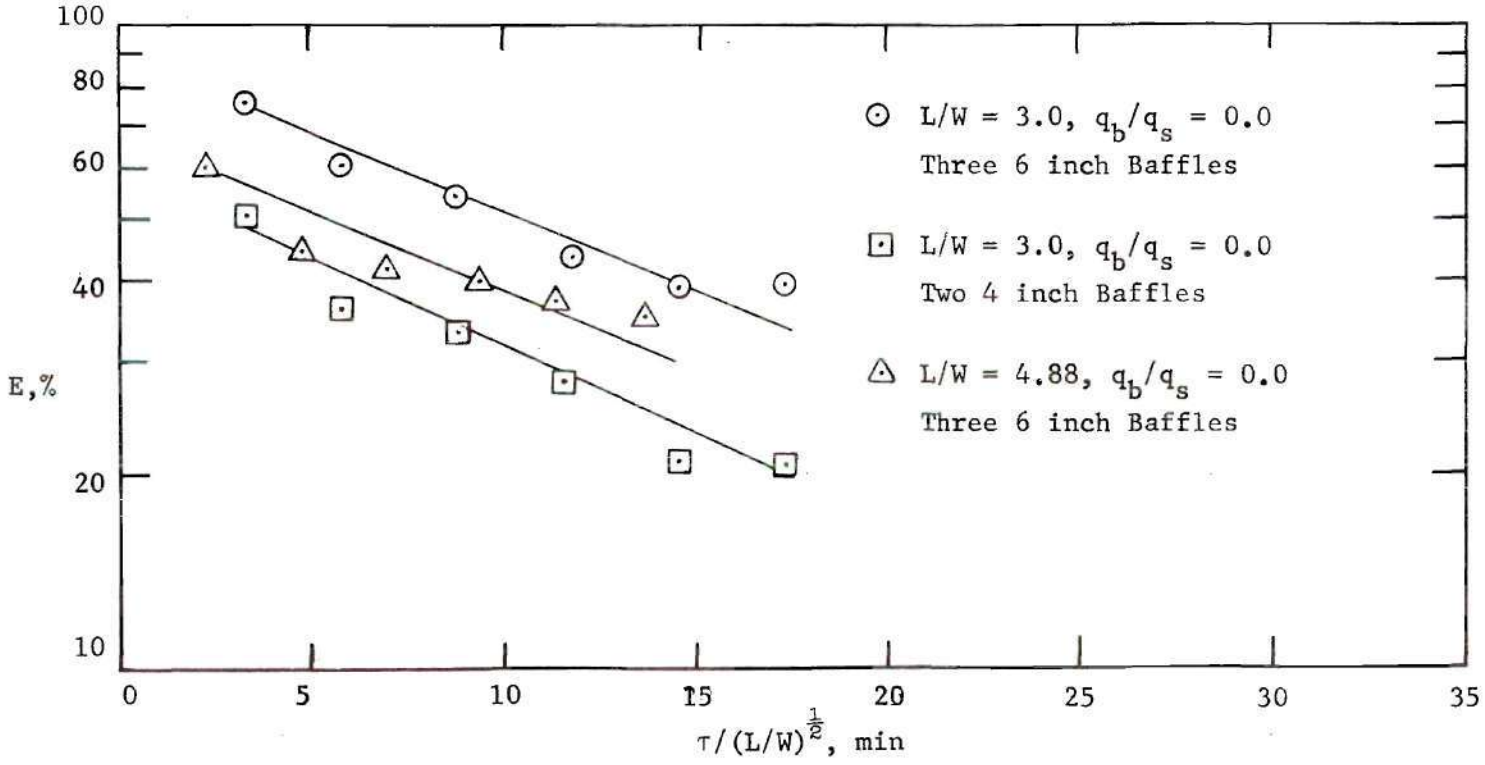

Figure 55. Effectiveness versus $\tau/(L/W)^{\frac{1}{2}}$ for Various Baffle Designs

lation equation is

$$E \propto e^{-b\tau/(L/W)^{\frac{1}{2}}} \left(\frac{B}{W}\right)^{n} N^{o}(1+q_b/q_s)^{p} \qquad (4.7)$$

The reason for the term $(1+q_b/q_s)$ is so that for $q_b/q_s = 0$, E does not equal zero.

To find the constant coefficient c and the exponents n, o, and p, an Algol computer program using Eq. (4.7) was written and run on the Burroughs B-5500 computer. See Appendix E for a listing of the program. This program was designed so that several values of b, n, o, and p were chosen and the right hand side of Eq. (4.7) was calculated for six values of time from five to 30 minutes. Values of n, o, and p varied from one-eighth to one-half, while b varied between 0.03 and 0.06. In essence, the approach is one of trial and error, with values of the coefficient and exponents chosen which appeared to bracket the data. With the aid of the program, it was found that the equation that best fits the data for all values of the variables is

$$E \propto e^{-0.055\ \tau/(L/W)^{\frac{1}{2}}} \left(\frac{B}{W}\right)^{\frac{1}{2}} N^{\frac{1}{8}}(1+q_b/q_s)^{\frac{1}{8}} \qquad (4.8)$$

The results of Eq. (4.8) are shown for an aspect ratio of 4.88 in Figure 56. The results for L/W = 1.0 and 3.0 are quite similar to this figure. To make Eq. (4.8) an identical expression, a proportionality factor, A, must be found. This factor is equal to the slope of the line which best fits the data. A best fit line through each set of data reveals that a single value of the slope does not fit all cases.

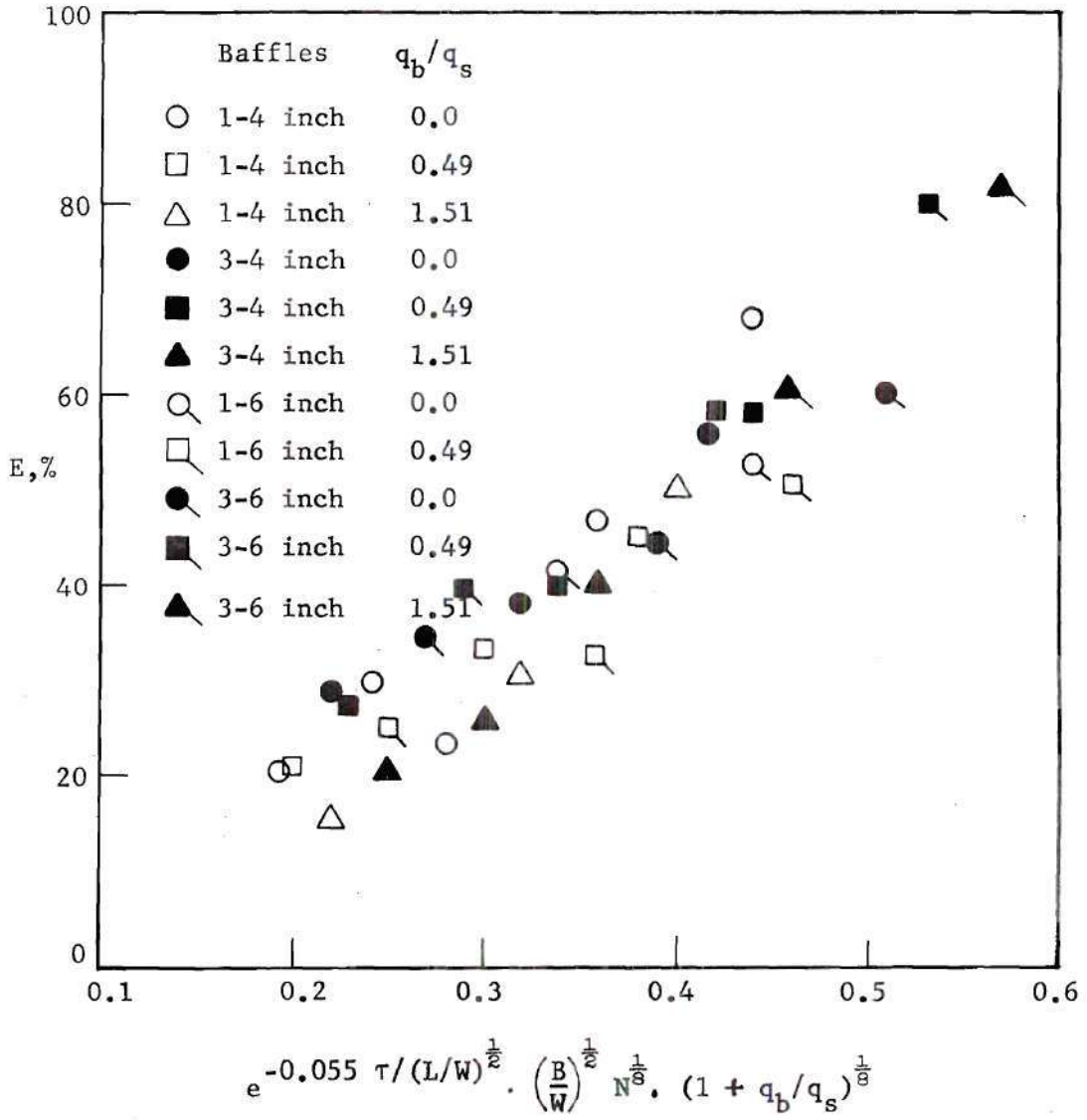

Figure 56. Correlation of Effectiveness for L/W = 4.88

The best curve through all the data is not a straight line but a curved line concaved downward. The data were replotted on semi-log coordinates as illustrated in Figures 57, 58, and 59. Here it is seen that the data lie approximately on a single straight line with a slope of 1.10. Thus, the correlation equation which best fits all the data, excluding angle effects, is represented by the equation

$$\text{Ln } E = 1.10\ e^{-0.055\,\tau/(L/W)^{\frac{1}{2}}}\ (\frac{B}{W})^{\frac{1}{2}}\ N^{\frac{1}{8}}(1+q_b/q_s)^{\frac{1}{8}} \qquad (4.9)$$

From this expression, one can see that the heat flux ratio and number of baffles do not influence the effectiveness of baffles to the extent that aspect ratio and baffle size do. Some of the data in Figure 59 are from the investigation by Neff (6). As seen from the figure, the results are in fair agreement with this investigation. Also shown in the figures are the error limits of ± 20 percent. Most of the data of this investigation fall within these limits which for most design purposes is tolerable.

The scatter of the data in Figure 59 for some tests is a result of the increase in baffle effectiveness experienced for later values of time as illustrated in Figure 54. This increase is evidently related in a more complex form, to either the heat flux ratio or time, than what has been presented above.

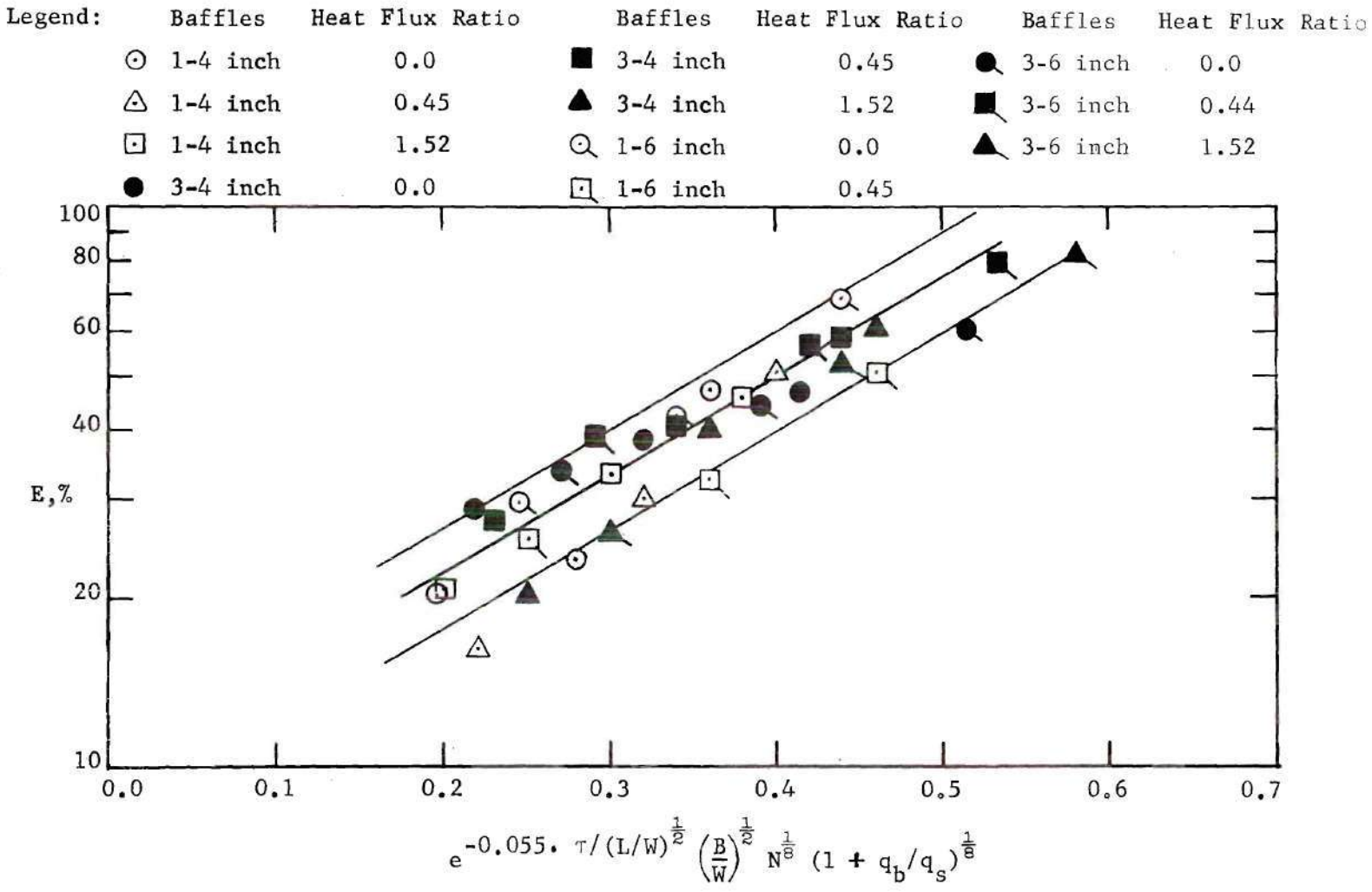

Figure 57. Correlation of Effectiveness for L/W = 4.88

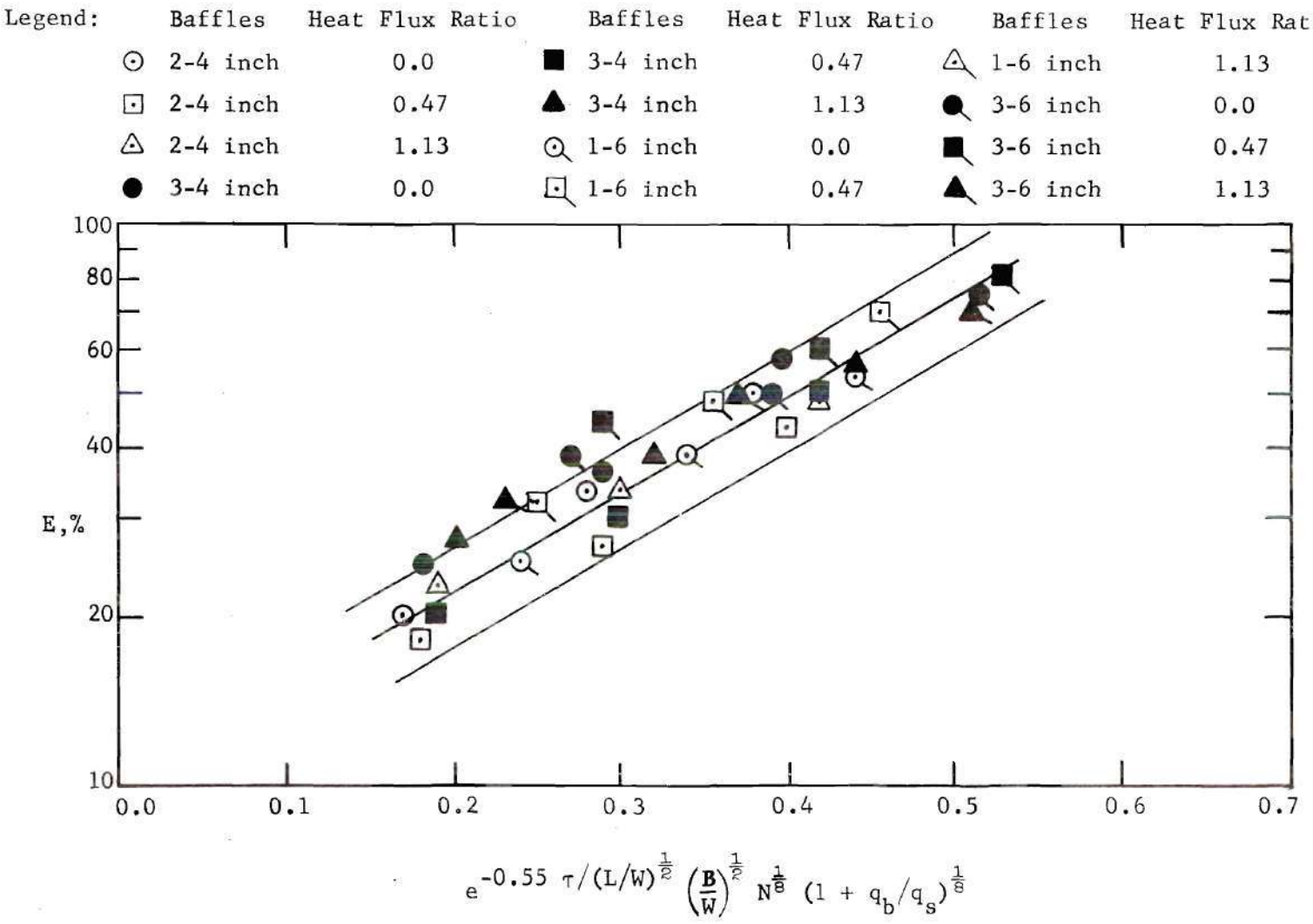

Figure 58. Correlation of Effectiveness for L/W = 3.0

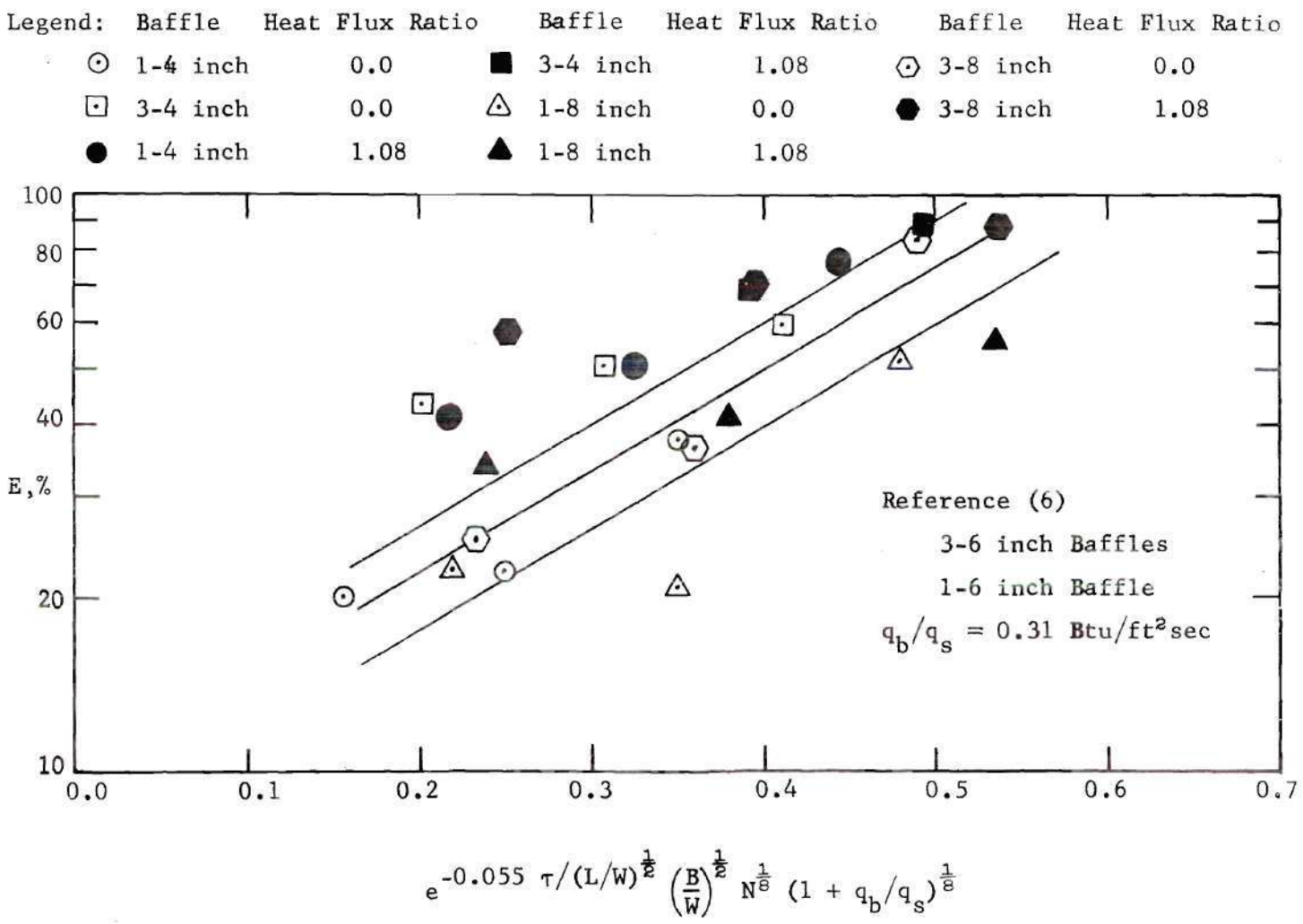

Figure 59. Correlation of Effectiveness for L/W = 1.0

CHAPTER V

HEAT TRANSFER CORRELATION

In many of the tests, wall temperatures were taken along with bulk temperature measurements. Representative wall temperature distributions for the case of no baffles on the vertical walls can be seen in Figures 60, 61, and 62. From these figures, it can be seen that the wall temperature first decreases then increases for increasing values of x/L, except for the first five minutes. As previously mentioned, the system took approximately five minutes to become quasi-steady. After the initiation of heat at the sides, the wall temperature increases with time. The greatest increase being near the tank top because it is in this region that the greatest increase in bulk temperature is experienced. A comparison of the three figures reveals that the wall temperature profiles for the low and high aspect ratios are considerably different. In the low aspect ratio tests, after the first five minutes, the wall temperature is almost a linear function of x/L. But, with increasing time, wall temperatures in the upper and extreme lower portion of the tank increase at a greater rate than does the temperature in the middle. The reason for the large increase near the bottom is because of the low velocity and reduced mixing in this area. Also, it can be seen from a comparison of Figures 60, 61, and 62 that, in the large aspect ratio tests, the wall temperature in the top 60 percent of the container increases at a greater rate with time than in the low aspect ratio tests. The reason for this

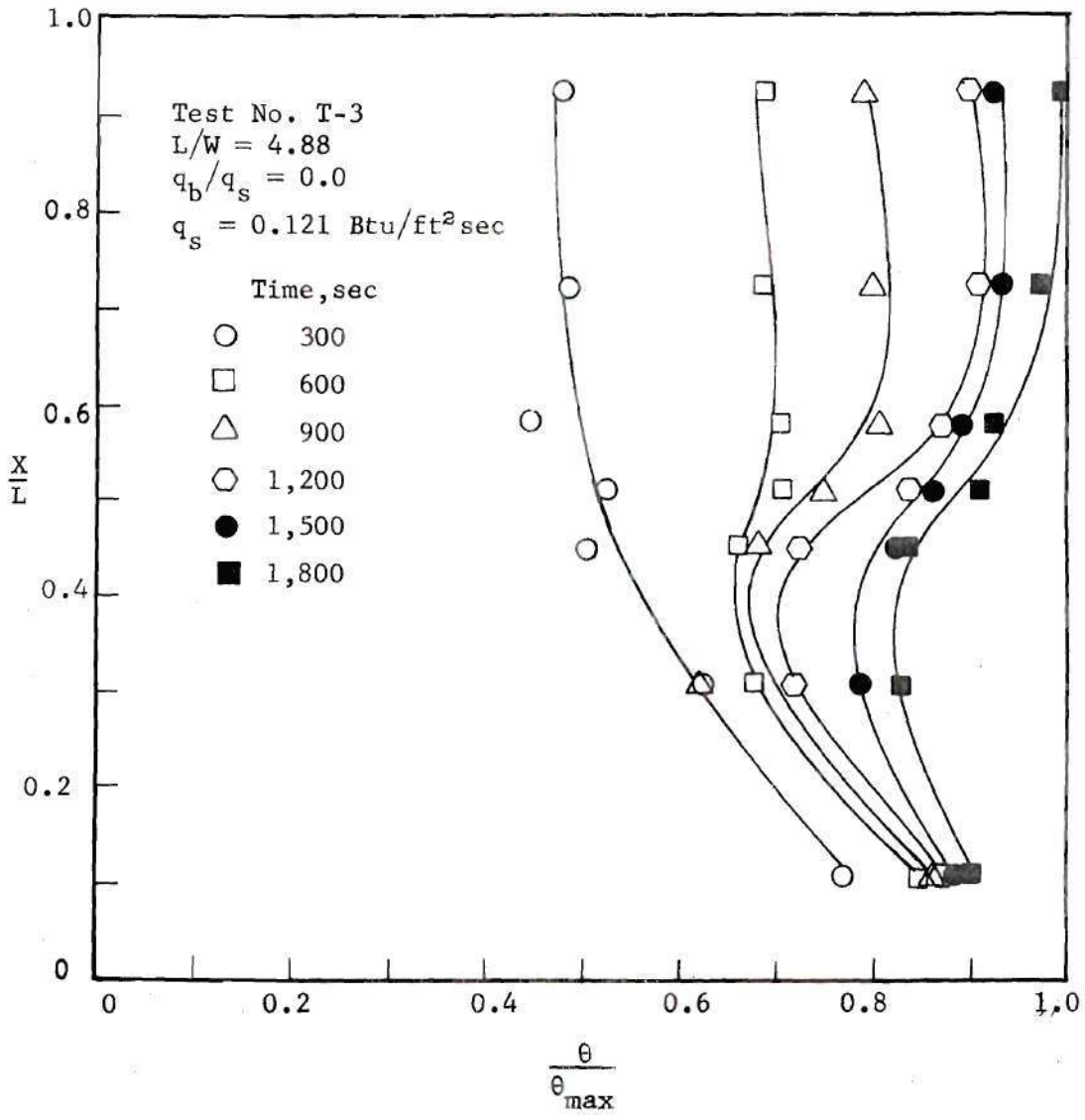

Figure 60. Container Height versus Wall Temperature; No Baffles

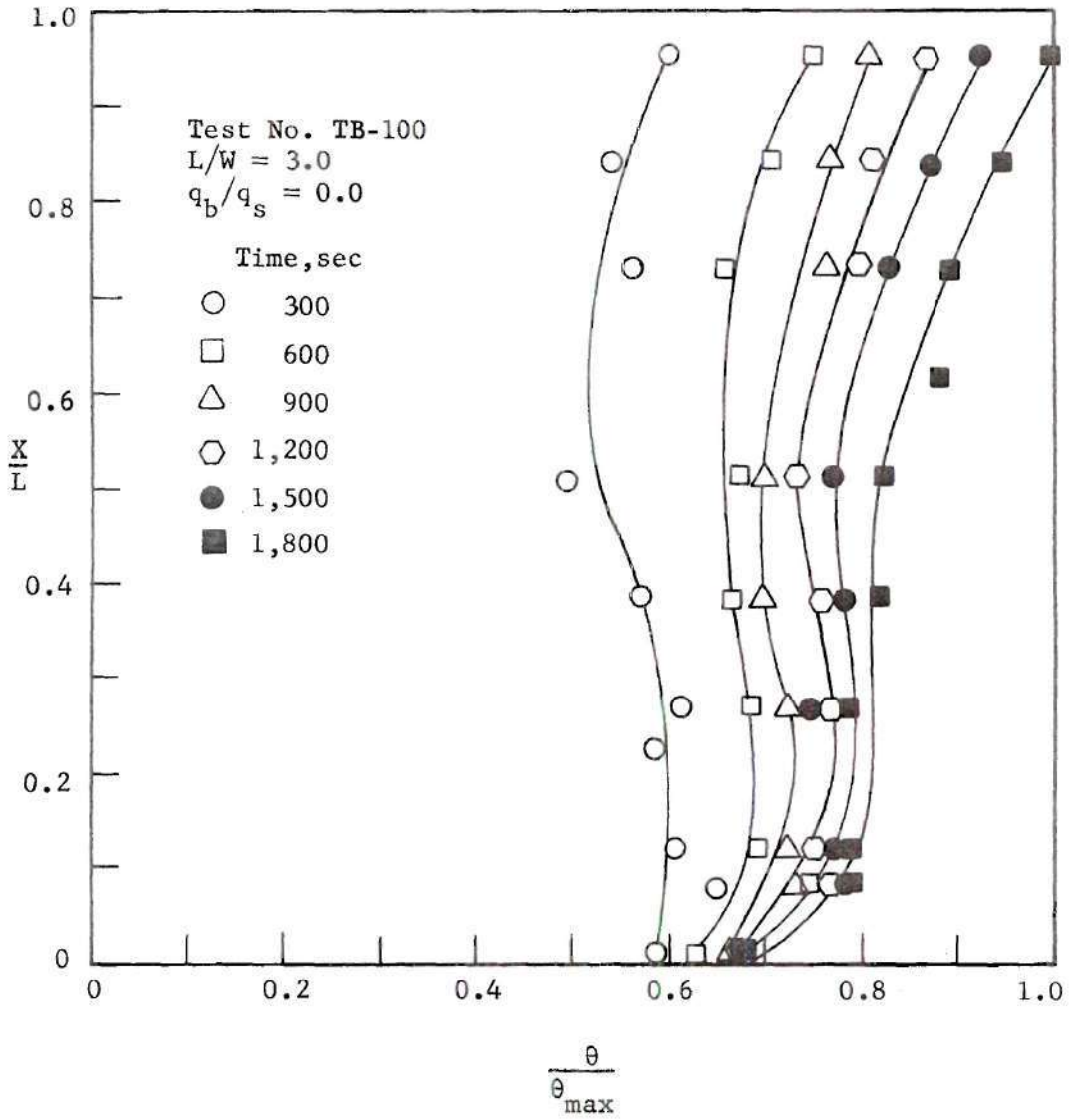

Figure 61. Container Height versus Wall Temperature; No Baffles

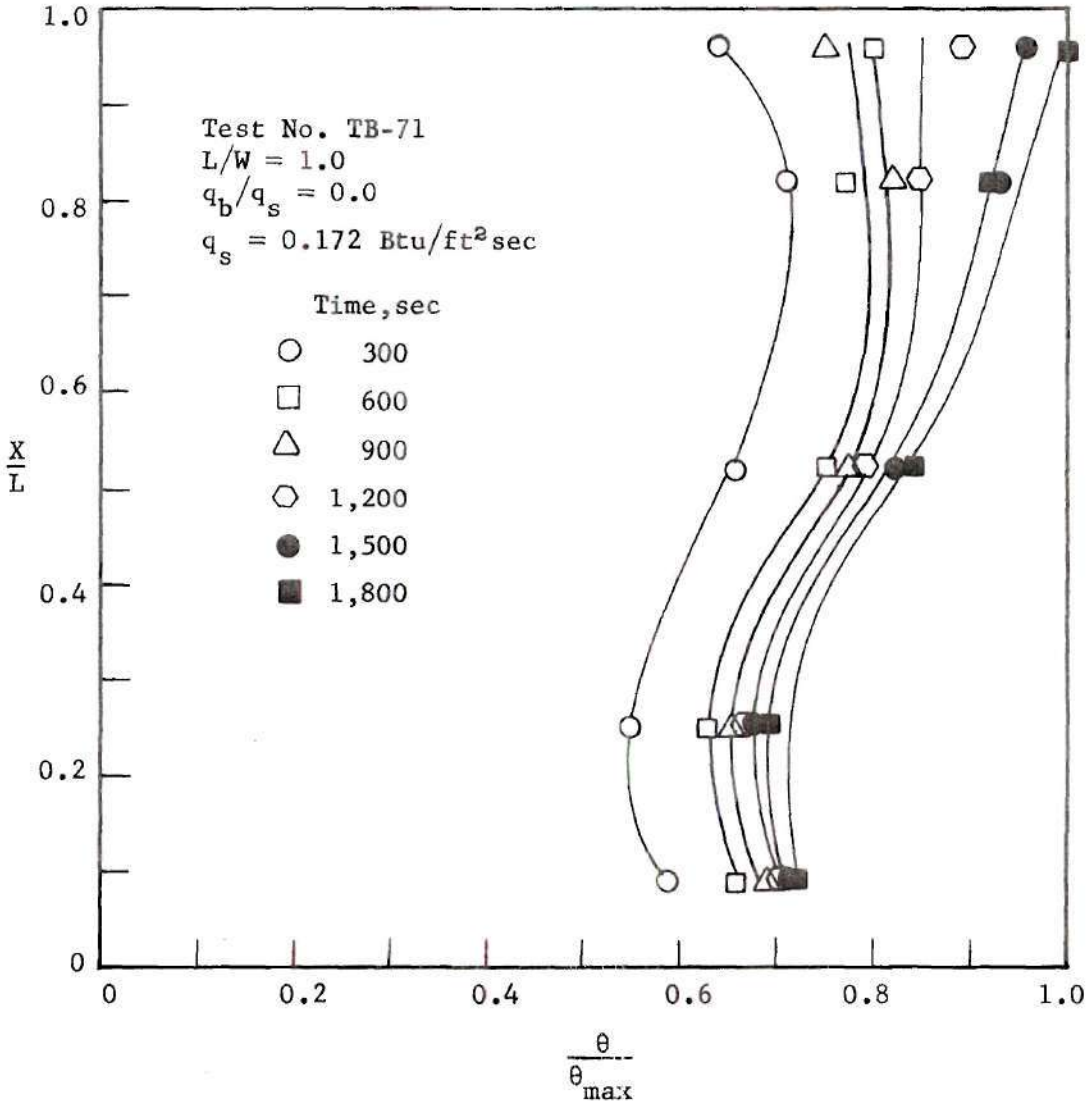

Figure 62. Container Height versus Wall Temperature; No Baffles

higher rate of increase is because the bulk fluid is increasing in temperature at a greater rate in the higher aspect ratio tests.

For length to width ratios of 4.88 and 3.0, the difference between the local wall and average bulk temperature at a given height, $(T_w-T_b)_x$, follows closely the one-fifth power law which is associated with laminar flow over a wall heated with a constant heat flux in the laminar flow area. An illustration of the temperature difference for two values of time is shown in Figure 63. The temperature difference for other values of time falls within these two limits. The one-fifth power law, derived by Sparrow and Gregg (33) is for a uniformly heated plate in an infinite fluid, thus, it should not be expected to describe exactly the results for a confined and finite fluid which is being heated only.

It appears that, for the L/W = 4.88 tests, transition occurs somewhere between x/L of 0.20 and 0.35. For the L/W = 3.0 tests, at high values of side heating only, the transition to turbulent flow occurs between x/L = 0.28 and 0.41. The transition region is indicated in Figure 63 by the dotted portion of the curve. For the low aspect ratio tests, transition to turbulent flow never occurred, even for higher values of the side heat flux tested. However, it was observed that, in a few tests, the flow along the walls near the top of the fluid had a tendency to become turbulent. A representative wall-average bulk temperature difference curve for L/W = 1.0, for two values of time, is shown in Figure 64. The decrease in temperature difference after the first 300 seconds as observed in Figures 63 and 64 is because the flow within the container during this time interval is not in a quasi-steady state. As previously noted in Chapter I,

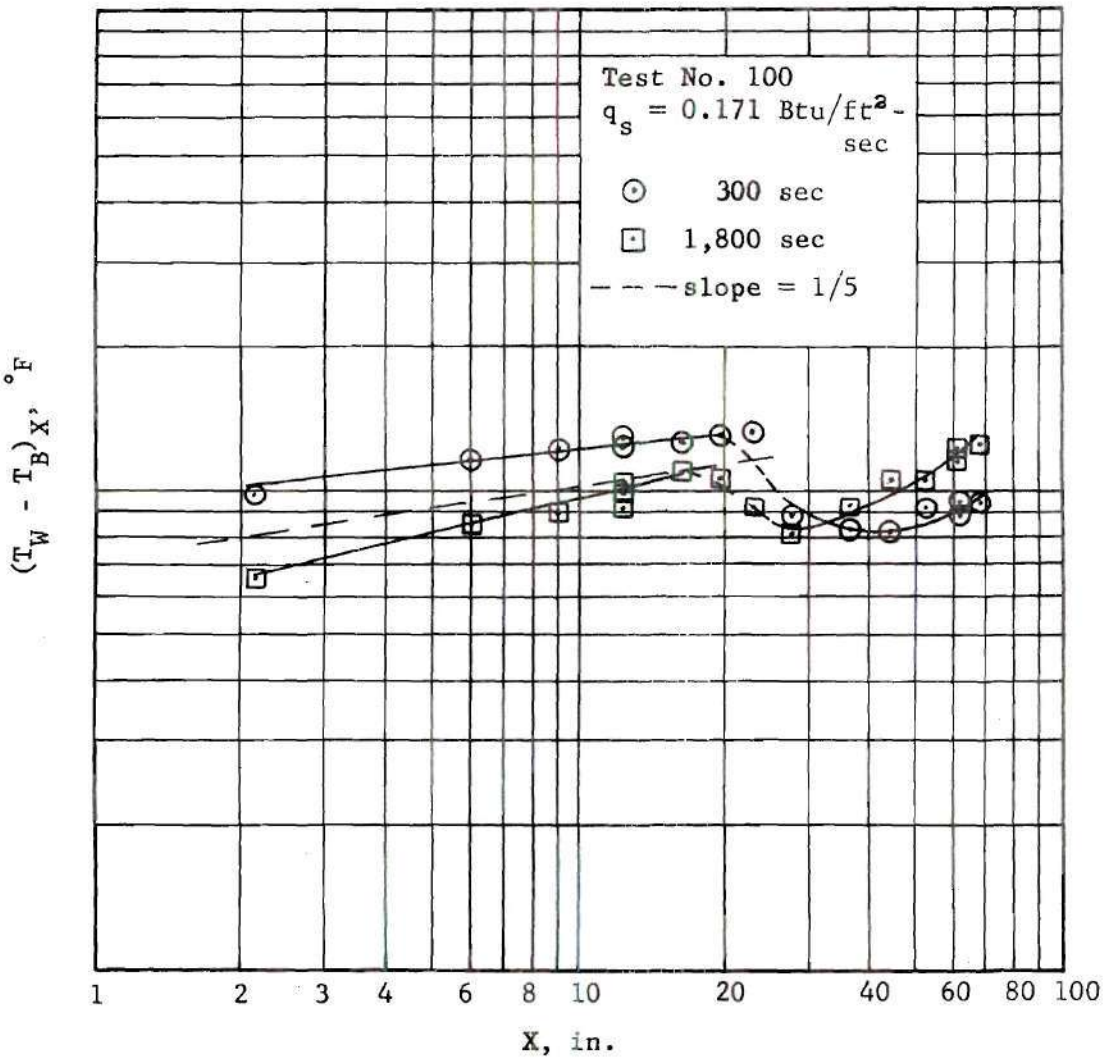

Figure 63. Local Temperature Difference versus Container Height; L/W = 3.0, No Baffles

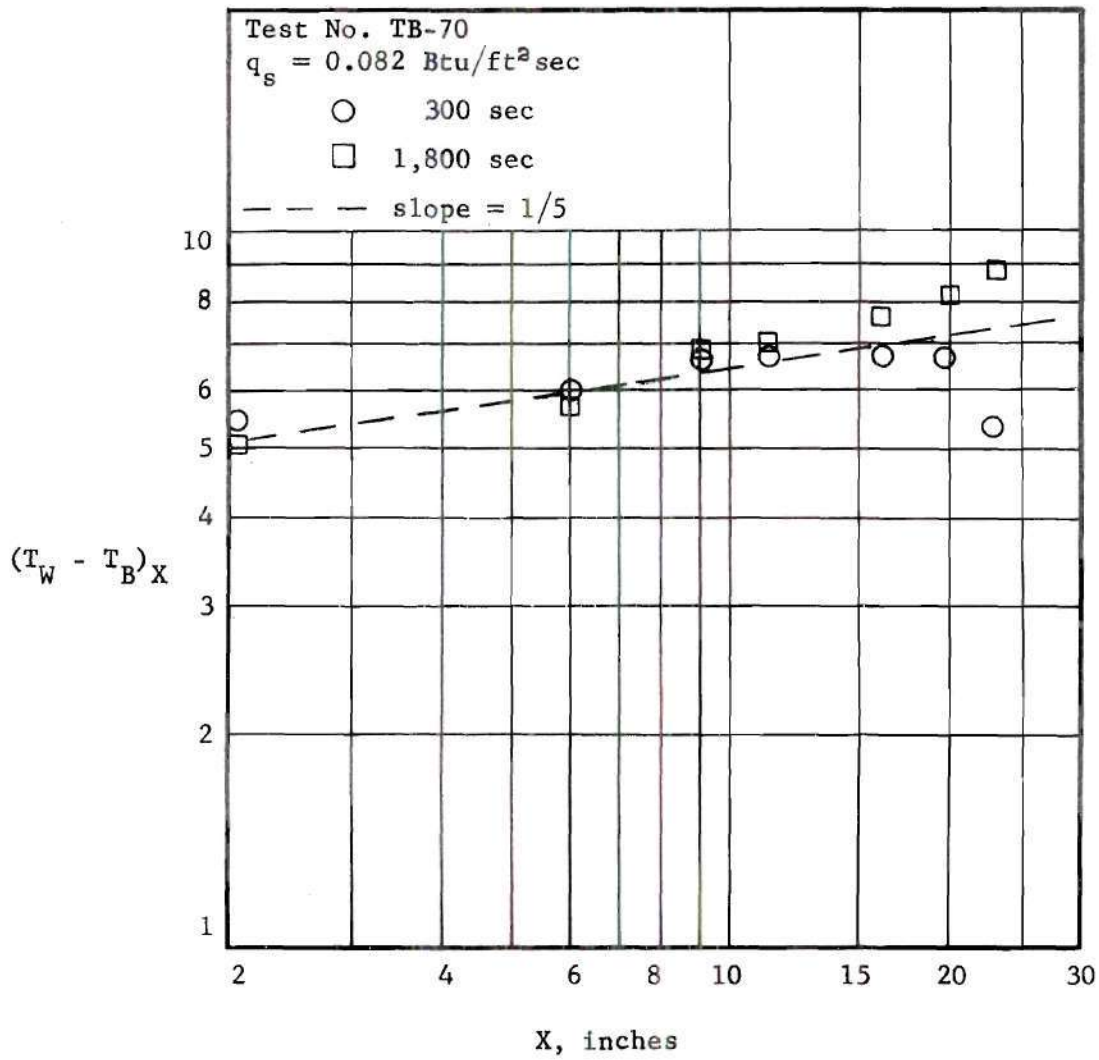

Figure 64. Local Temperature Difference versus Container Height; L/W = 1.0, No Baffles

Kolar (20) observed that it took at least 180 seconds for his small container to reach a quasi-steady state. From an analysis of the wall and bulk temperature data, for high values of the side heat flux, it appears that 300 to 400 seconds are needed for the system to reach quasi-steady state for all values of the aspect ratio.

In both Figures 63 and 64, it is seen that the temperature difference decreases for increasing values of time over the first half of the curve. After transition, the difference between the two curves then increases. The decrease, which is associated with the lower portion of the container, is a result of a more uniform and rapid bulk flow process being set up in the lower portion of the vessel. The increase in flow velocity tends to cool the wall and reduce the temperature. The increase in the top portion, as explained earlier, is a result of the increase in bulk temperature in this region, see for example, Figures 9 and 29. In the upper region the turbulent flow cannot exchange the heat with the bulk fluid at the rate it could if the fluid were infinite in extent with a uniform bulk temperature.

For a uniformly heated plate, in an infinite medium over which the flow is turbulent, an equation describing the wall temperature distribution with length is derived in Appendix A. The equation is

$$\frac{(T_w - T_\infty)_x}{(T_w - T_\infty)_L} = \left(\frac{x}{L}\right)^{-\frac{1}{7}} \tag{5.1}$$

and, except for a difference in the exponent, it is exactly the equation derived by Sparrow and Gregg for the case of laminar flow. In the L/W = 4.88 and 3.0 tests, the last part of the wall-average bulk temperature

difference curves do not follow the negative one-seventh power law for a uniformly heated wall experiencing turbulent flow. However, some affirmation of this equation is obtained from Figure 2 of the paper by Siegel and Norris (34). In the investigation, Siegel measured the wall temperatures on a 70 inch high uniformly heated plate. The laminar part of the temperature difference curve followed closely the one-fifth power law. Transition occurred around 12 inches. In the turbulent portion of the curve, the experimental data closely fit a slope of minus one-seventh. To the author's knowledge, there are no other published data in the open literature for turbulent flow over a flat uniformly heated plate in an infinite fluid with which to compare the above equation.

From the measurement of wall and bulk temperature, knowing the amount of heat generated within the walls, the local heat transfer coefficient can be obtained from the steady-state equation

$$h_x = 1/[(T_w - \overline{T}_B)_x/q - t/k_w] \qquad (5.2)$$

The second term in the denominator is negligibly small, since the term containing the wall thickness, t, which is equal to 0.00208 foot, is small.

Transient heat transfer coefficients, for small values of the Biot number, Bi, can be calculated from the equation recommended by Jakob (17),

$$T(x,y) - T_\infty = \frac{q \cdot t}{h} (1 - e^{-Fo \cdot Bi}) \qquad (5.3)$$

However, the Fourier number, Fo, for the time intervals of interest in

this investigation, is exceptionally large. Hence, the exponential term is negligible and Eq. (5.3) reduces to the well known Newton's law. In the above expression, T_∞ is assumed constant. Kudryavtsev (35) derived an expression similar to Eq. (5.3) with the temperature at infinity, a linear function of time according to the equation

$$T_\infty(\tau) = T_\infty(\tau=0) + r\cdot\tau \tag{5.4}$$

With this expression for the temperature at infinity, the expression for the temperature difference for any time at a given position is,

$$T_w(\tau) - T_\infty(\tau=0) = \left(\frac{q}{Ah} - \frac{rpc\tau}{h}\right)\left(1 - e^{-Bi\cdot Fo}\right) \tag{5.5}$$

To solve for h from either Eq. (5.3) or Eq. (5.5), one must use either a trial and error or iteration technique. However, since the Fourier number is large,

$$Fo = \frac{\alpha\tau}{t^2} >> 100$$

Eq. (5.5) reduces to

$$T_w(\tau) - T_\infty(\tau=0) = \left(\frac{q}{Ah} - \frac{rpc\tau}{h}\right) \tag{5.6}$$

Again, comparing the sizes of the two terms on the right, the second term is small unless r, the bulk temperature slope coefficient, is large. In all tests, the temperature slope was less than 0.1, making the second term small. Thus, Eq. (5.6) also reduces to Newton's law.

In Eq. (5.3) or Eq. (5.6), if the temperature at infinity is assumed to be the average bulk temperature for a given time interval according to the equation

$$\overline{T}_{B,\infty} = \frac{1}{L}\int_{o}^{L} T_{B,x}\, dx \tag{5.7}$$

then both equations reduct to the equation

$$h_x = \frac{(T_w - \overline{T}_B)_x}{q_s} \tag{5.8}$$

Using this equation, the local values of the Nusselt number shown in Figures 65 and 66 were calculated for several intervals of time. The physical properties in the modified Grashof number were calculated at the wall temperature from the relations presented in Appendix F at an average temperature for the tests. The wall temperature was used, since, in practical situations, this temperature is generally known. An Algol computer program to calculate local heat transfer coefficients from the three previous equations was written. This program consists of quadratic interpolation equations to calculate the bulk and wall temperatures for specific values of time. Also included is a linear interpolation of the bulk temperature, at a given time, with position. This step is necessary so that bulk temperatures at corresponding liquid levels could be used in calculating the film coefficient.

It can be seen from Figure 65 that, for the low aspect ratio tests, the local Nusselt number closely follows the theoretical curve

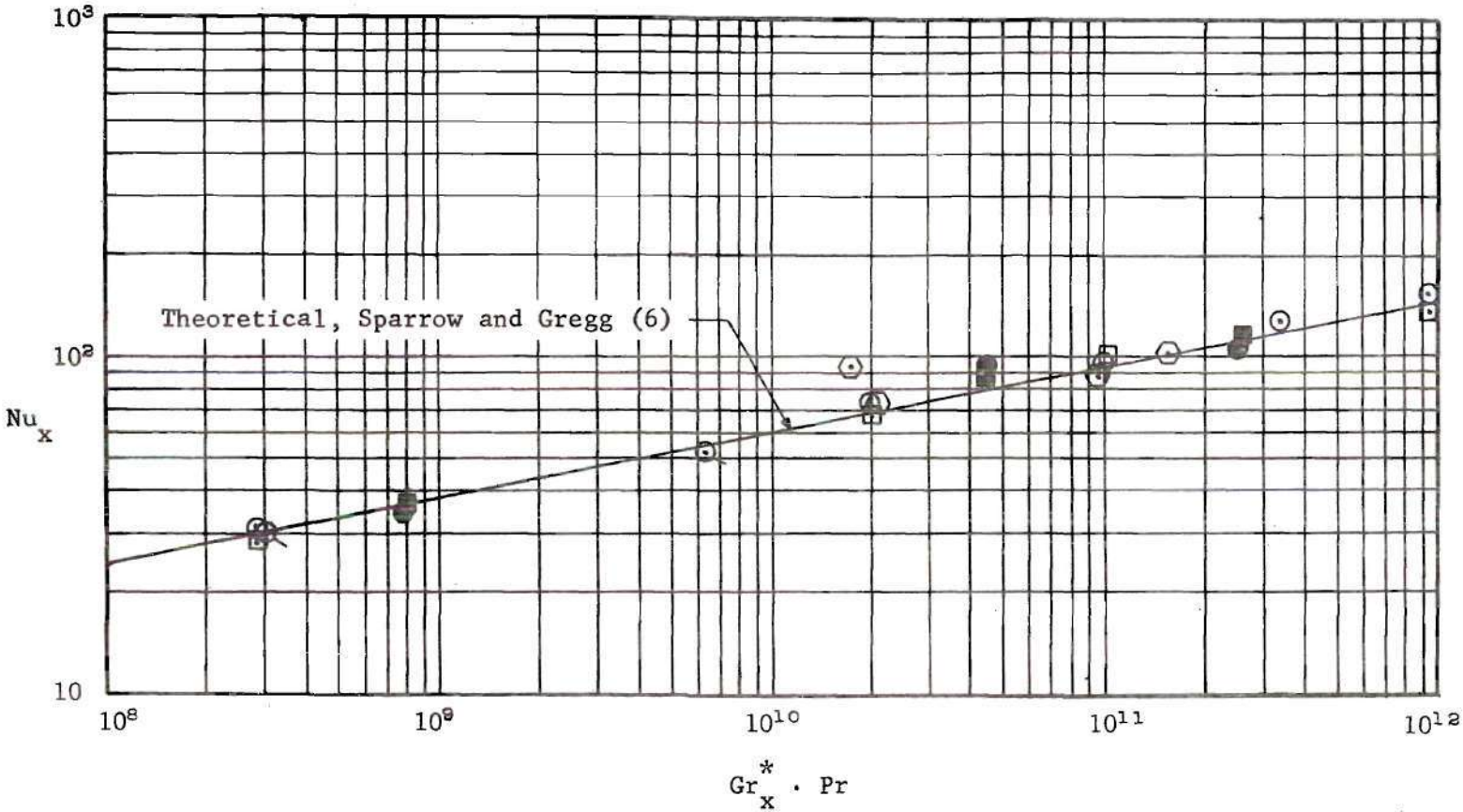

Legend: Test No. TB-70 at 600 sec - ⊙ ; at 1,800 sec - ⊡ ; Test No. TB-71 at 300 sec - ● ; at 1,800 sec - ■ ; Eckert and Goldstein (17) - ⊙ ; Kolar (15) - ⊙

Figure 65. Local Nusselt Numbers for Laminar and Transitional Flow

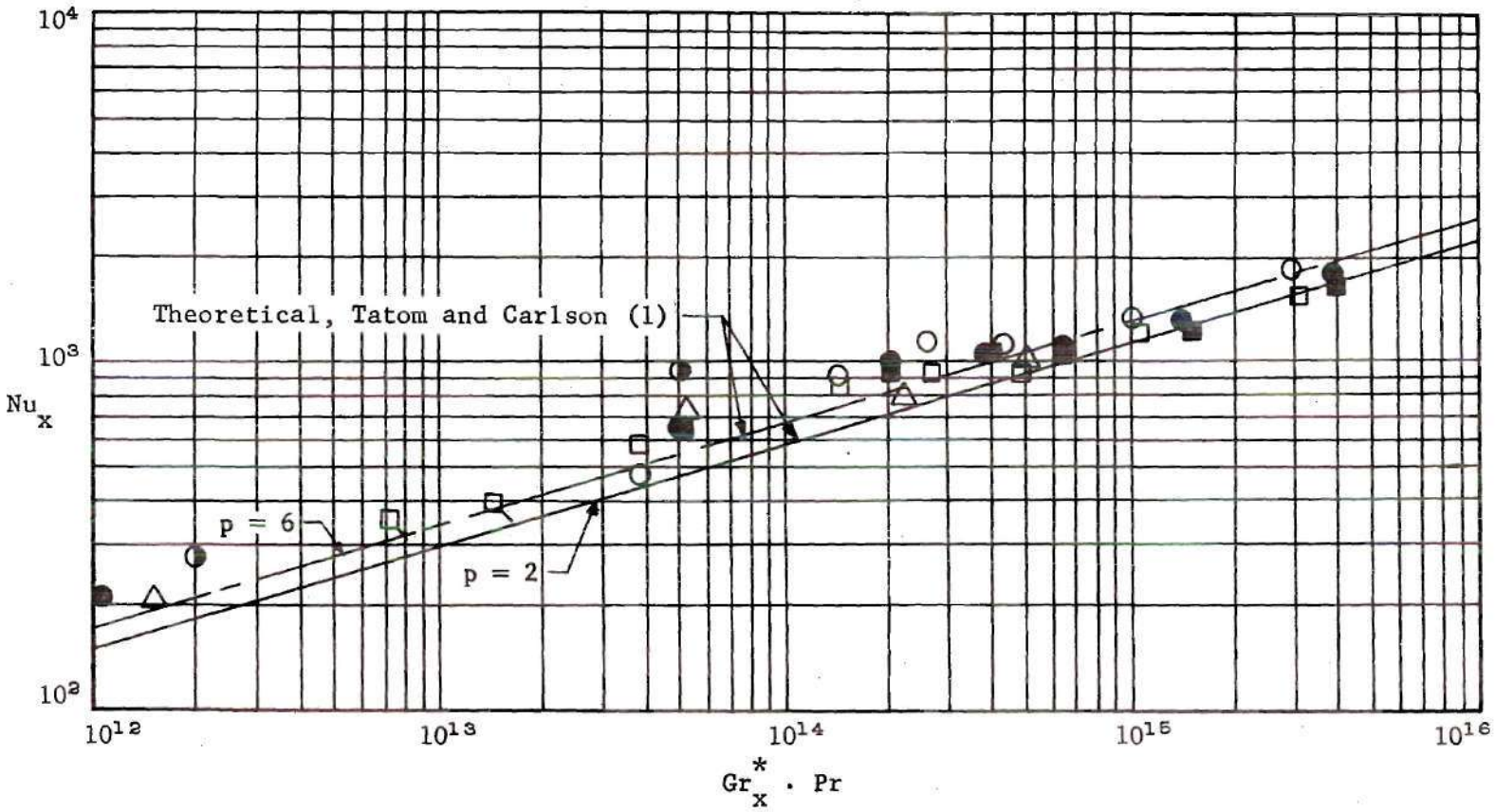

Legend: Text No. T-1 at 300 sec - ○ ; at 1,800 sec - □ ; Test No. T-3 at 600 sec - ● ; at 1,500 sec - ■ ; Test No. T-2 at 1,200 sec - △ ; Hartnett and Welsh (17) - ◑ ; Cheesewright (16) - □

Figure 66. Local Nusselt Numbers for Turbulent Flow

$$Nu_x = \frac{2}{(360)^{\frac{1}{5}}} \left[\frac{Pr^2}{0.8+Pr}\right]^{\frac{1}{5}} Gr_x^{*\frac{1}{5}} \tag{5.9}$$

which is obtained from the work of Sparrow and Gregg (33) for a Prandtl number of five. This result should be expected, since the temperature distribution follows closely the theoretical curve. Most of the data for the laminar portion of the curve are within ± 20 percent of the theoretical value. Transition to turbulent flow occurs between $Pr \cdot Gr_x^*$ equals 10^{11} to 10^{12} for a uniformly heated wall. Hartnett and Welch (19) list a value of 2.6×10^{11} for the critical value of $Pr \cdot Gr_x^*$. This corresponds to a critical value of 2×10^9 for the constant temperature wall case.

The results for turbulent flow over the vertical walls of the container are not as close to the theoretical equation as were the laminar results. The theoretical expression for the local Nusselt number, for the case of turbulent flow over a uniformly heated plate, can be obtained by using the integral techniques of von Kárman for the boundary layer flow. Eckert and Jackson (10) employed this technique for the case of a constant temperature wall. Following Eckert and Jackson, Tatom (5) integrated the momentum and energy integrals with the following boundary layer velocity and temperature profiles

$$\frac{u}{U} = \left(\frac{y}{\delta}\right)^{\frac{1}{7}} \left(1 - \frac{y}{\delta}\right)^p \tag{5.10}$$

and

$$\frac{\theta}{\theta_w} = \left[1 - \left(\frac{y}{\delta}\right)^{\frac{1}{7}}\right] \tag{5.11}$$

In using these profiles, the Prandtl number has been assumed to be equal

to one. However, the results can be applied with reasonable accuracy to fluids with Prandtl numbers close to one. From Appendix A, the local Nusselt number for turbulent flow over a uniformly heated wall is

$$Nu_x = \left[\frac{(0.0225)^4}{64 \cdot J_2}\right] \cdot Pr^{\frac{1}{3}} \left[\frac{Gr_x^*}{1.572 \cdot \frac{J_1}{J_2} + Pr^{\frac{2}{3}}}\right]^{\frac{2}{7}} \tag{5.12}$$

where J_1 and J_2 are functions of the exponent, p, in Eq. (5.10). For a Prandtl number of five and p = 2 and 6, Eq. (5.12) becomes

$$Nu_x = 0.0576 \ (Gr_x^* \cdot Pr)^{\frac{2}{7}} \ ; \quad p = 2 \tag{5.13}$$

and

$$Nu_x = 0.0665 \ (Gr_x^* \cdot Pr)^{\frac{2}{7}} \ ; \quad p = 6 \tag{5.14}$$

Equations (5.13) and (5.14) are illustrated in Figure 66 along with the experimental data of several tests for various values of time. From the figure, it appears that a value of p = 6 is the best exponent for the velocity profile. This value of p indicates that the boundary layer is thicker for the flow in a container than for an infinite flat plate.

From Eq. (A-8), of Appendix A, the local value of the heat transfer coefficient may be written as

$$h_x = C_H \cdot x^{\frac{1}{7}} \tag{5.15}$$

Integrating this expression, the average coefficient becomes

$$\bar{h}_L = \frac{7}{8} C_H L^{\frac{1}{7}} = \frac{7}{8} h_x \tag{5.16}$$

In integrating Eq. (5.15) it was assumed that the boundary layer was turbulent over the whole plate length. In reality, this is not true, for a laminar region usually proceeds the turbulent region. However, if the plate is extremely long, or the heat flux is extremely high, such that the modified Grashof number is large, then Eq. (5.16) is a good approximation to the true value of h_L. The limit for the modified Grashof number appears to be near $Gr^* = 2 \times 10^{12}$. For modified Grashof numbers higher than this value, the average Nusselt number then becomes

$$\bar{Nu}_L = \frac{hL}{k} = \frac{7}{8}\left[\frac{(0.0225)^4}{64 \cdot J_2}\right] \cdot Pr^{\frac{1}{3}}\left[\frac{Gr_L^*}{1.572\,\frac{J_1}{J_2} + Pr^{\frac{2}{3}}}\right]^{\frac{2}{7}} \tag{5.17}$$

For a Prandtl number of five, and with the exponent, p, in the velocity profile equal to six, this equation reduces to,

$$\bar{Nu}_L = 0.0583\ (Gr_L^* Pr)^{\frac{2}{7}} \tag{5.18}$$

Figure 67 illustrates a comparison of the results from the above equation with the averaged Nusselt number calculated for several tests. Not only were the Nusselt number values averaged with respect to distance along the tank walls in Figure 67, but they were also averaged with respect to time according to the equation

$$h_L = \frac{1}{\tau_0}\int_0^{\tau} h_L \cdot d\tau \tag{5.19}$$

where τ_0 is the total length of time over which the tests were conducted. From the figure it is seen that the average values of the Nusselt numbers are higher than predicted by the flat plate, infinite medium theory.

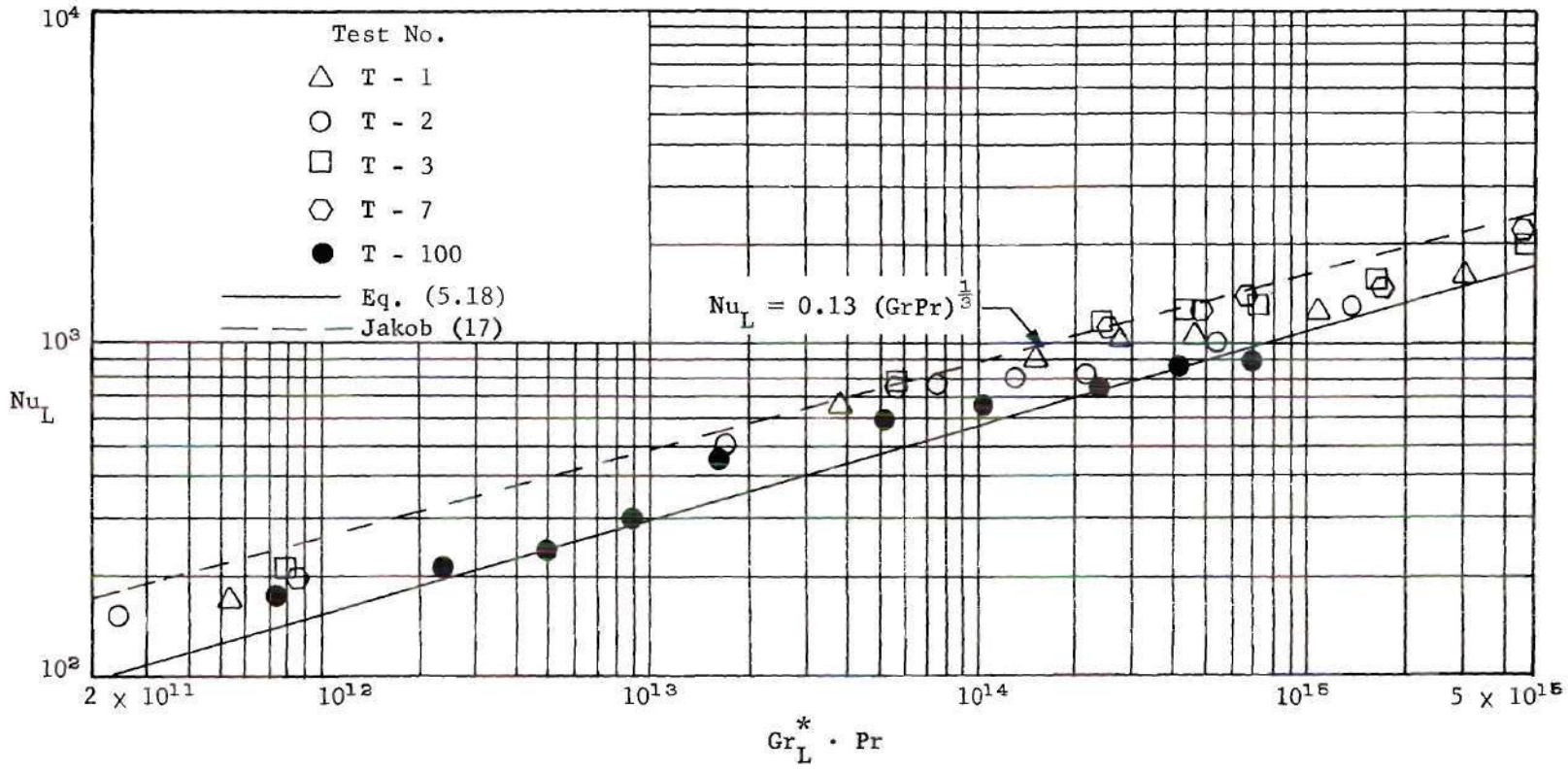

Figure 67. Average Nusselt Numbers for Flow Within a Container

The modification of Jakob's equation by McAdams, as presented in Chapter I, predicts values which are higher than were obtained experimentally while Eq. (5.17) predicts values which are lower. Two possible ways of correcting this difference would be to select another temperature difference to calculate the Nusselt number or apply a correction to Eq. (5.17) for the Prandtl numbers different from one.

Siegel and Norris (34) conducted steady-state tests on air and found that the local film coefficients were lower than predicted by an empirical equation developed by Jakob (17). However, in these tests, the heated boundary layer fluid was allowed to exit from the top of the rectangular container and cool air entered at the top through the middle. Although the tests were quite similar to those performed by Martin (16) and Hartnett and Welsh (18), they used the ambient temperature of the room instead of the local or average bulk temperature in calculating values of h. The difference between the wall and room temperature was always greater than the local temperature difference. Hence, for a given heat flux, the film coefficient was lower. In this investigation, if the initial or ambient temperature had been used in calculating the wall to bulk fluid temperature difference, then the local and average Nusselt number values would be less than shown in the preceding figures.

Wall temperature and heat transfer data with baffles on the walls are not presented. With baffles placed along the walls, the local wall temperature in many tests was quite erratic in nature depending on the nearest baffle. Also, the wall temperature along the whole length varied considerably depending again on baffle location and the number of baffles.

For a few baffle tests, film coefficients were close to the case of no baffles. One might suspect that this should be true, since a comparison of the total energy transferred to the bulk fluid revealed that the same amount of energy is transferred with or without baffles.

CHAPTER VI

RESULTS AND CONCLUSIONS

Experimental studies on the effectiveness of baffles in reducing thermal stratification were conducted over a range of modified Grashof numbers to include both the laminar and turbulent flow regimes. The important results of this investigation are summarized as follows:

1. The effectiveness of most baffle designs tested decreases as time increases, approaching asymptotic values.

2. The degree of stratification depends on the heat flux ratio, decreasing as this ratio increases to values near one. For much larger values of q_b/q_s, a thermal inversion situation is created and the effectiveness of baffles is decreased.

3. Higher effectiveness values were obtained in this investigation than previously reported. This is due to the increased bulk mixing produced by the baffles. Instead of the wall-heated fluid reattaching to the back side of the baffles with increasing time, as previously reported, the flow generally separated from the baffles.

4. For a given baffle size, there is an optimum number of baffles. The number of baffles needed depends not only on the aspect ratio but on the baffle to tank width ratio and heat flux ratio. If the distance between successive baffles is considerably reduced, separation of the boundary layer flow will not occur and the effectiveness is decreased. For a given number of baffles, there is an optimum size for each aspect ratio. The optimum size appears to decrease with decreasing aspect ratio.

5. Horizontal baffles were found to be generally more effective than baffles inclined up or down. Inclined up baffles tended to promote reattachment of the boundary layer flow.

6. A correlation equation to determine baffle effectiveness was derived. The equation predicts baffle effectiveness within ± 20 percent.

7. The system investigated can be assumed to be in a quasi-steady state after the first five minutes of heating. The approach to quasi-steady state is a function of the heat flux magnitude and container size.

8. Heat transfer measurements on the vertical walls of the container indicate local Nusselt numbers in the turbulent regime which are slightly higher than predicted by theory for a vertical surface in an infinite medium.

9. Correlation between equations to predict film coefficients on vertical surfaces for the cases of uniform temperature and heat flux are presented.

10. The temperature distribution along a vertical surface undergoing turbulent free convection was shown to fit an equation similar to that of laminar flow but with an exponent of one-seventh.

CHAPTER VII

RECOMMENDATIONS

The test apparatus used in this investigation could be modified in several ways to extend the study of transient free convection. First, an investigation into the effect of different bottom shapes on the convection process within the tank and their role as possible stratification reduction techniques should be undertaken. Second, a further and more comprehensive investigation of the turbulent boundary layer within the container would be desirable. Such an investigation would undertake the measurements of boundary layer temperature and velocity profiles as a function of container height and time. With such measurements, one could describe more accurately the time variation of the local film coefficients. Also, the boundary layer velocity and temperature profiles could be better defined instead of guessing, which is being done at present.

Another possible area of investigation, if instrumentation were available, is the initial starting transient of the flow up the walls of the container. Such an investigation would necessitate the use of a high speed multi-channel recorder. Incremented levels in the tank would need to be measured for bulk, wall, and boundary layer temperature.

APPENDIX A

HEAT TRANSFER CORRELATIONS

In correlating free convection heat transfer data, the results are usually presented in a non-dimensional Nusselt, Prandtl, and Grashof number equation. Ostrach (36) developed an analytical expression for the Nusselt number as a function of the Prandtl and Grashof number for the case of laminar flow over a constant temperature wall. Later, Sparrow and Gregg (33) derived an expression for the Nusselt number for laminar flow over a uniformly heated wall. Comparison of the two results by Sparrow and Gregg (33) revealed that the boundary condition on the wall made very little difference in the values of the Nusselt number. For Prandtl numbers between 0.1 and 100, the results for a constant temperature wall were found to be within eight percent of the results for a uniformly heated wall for which the wall to fluid temperature difference was assumed to be an integrated average. With the uniformly heated wall temperature based on the temperature at the midpoint of the wall, even closer agreement with the constant temperature case was obtained. The above results can be seen from Tables 1 and 2 of reference (33).

Siegel (34) has reportedly shown similar agreement for the case of laminar and turbulent flow. However, the results of his work, to the author's knowledge, have not been published in the open literature. From reference (34), the agreement between constant heat flux and constant wall

temperature for the case of turbulent flow appears to be based on the empirical formula developed by Jakob (17). During this investigation it was found that such agreement could be shown analytically by using the results of Eckert and Jackson (10) and Tatom (5).

Using von Karman's integrated momentum equation and the energy integral equation for the boundary layer on a vertical flat wall with the following velocity and temperature distributions within the boundary layer

$$\frac{u}{U} = \left(\frac{y}{\delta}\right)^{\frac{1}{7}} \left[1 - \frac{y}{\delta}\right] \tag{A-1}$$

and

$$\frac{\theta}{\theta_w} = \left[1 - \left(\frac{y}{\delta}\right)^{\frac{1}{7}}\right] \tag{A-2}$$

Eckert and Jackson (10) derived the following expression for the local Nusselt number

$$Nu_x = 0.0295 \left[1 + 0.494\ Pr^{\frac{2}{3}}\right]^{-\frac{2}{5}} Pr^{\frac{7}{15}}\ Gr_x^{\frac{2}{5}} \tag{A-3}$$

In using the above profiles, it was assumed that the Prandtl number was equal to one.

Tatom (5) employed the same integral technique for the case of a constant heat flux wall, but with the velocity profile in the more general form

$$\frac{u}{U} = \left(\frac{y}{\delta}\right)^{\frac{1}{7}} \left[1 - \frac{y}{\delta}\right]^{p} \tag{A-4}$$

Substituting Eqs. (A-2) and (A-4) in the integral forms of the momentum

and energy equation and using Reynolds analogy with the forced convection relations employed by (10), Tatom obtained the following equation for the wall temperature distribution

$$\theta_w = \left[\frac{64 \cdot J_2}{(0.0225)^4}\right] \cdot \frac{q}{k Pr^{\frac{1}{3}}} \cdot \left[\frac{Gr_x^*}{1.572 \cdot \frac{J_1}{J_2} + Pr^{\frac{2}{3}}}\right]^{-\frac{2}{7}} \cdot x \qquad \text{(A-5)}$$

where the parameters J_1 and J_2 are defined as:

$$J_1 = \frac{\Gamma(9/7) \cdot \Gamma(1+2p)}{\Gamma(1+9/7+2p)} \qquad \text{(A-6)}$$

and

$$J_2 = \frac{\Gamma(8/7) \cdot \Gamma(1+p)}{\Gamma(1+8/7+p)} - \frac{\Gamma(9/7)\,\Gamma(1+p)}{\Gamma(1+9/7+p)} \qquad \text{(A-7)}$$

The local Nusselt number then becomes

$$Nu_x = \left[\frac{(0.0225)^4}{64 \cdot J_2}\right]^{\frac{1}{7}} \cdot Pr^{\frac{1}{3}} \left[\frac{Gr_x^*}{1.572 \cdot \frac{J_1}{J_2} + Pr^{\frac{2}{3}}}\right]^{\frac{2}{7}} \qquad \text{(A-8)}$$

Comparison of this equation with Eq. (A-3) shows that they are quite similar since, for a given value of p, J_1 and J_2 become constants. Also, recognizing the fact that

$$Gr_x^* = Gr_x \cdot Nu_x \qquad \text{(A-9)}$$

then the Grashof number in Eq. (A-3) can be transformed into the modified Grashof number of equal power in Eq. (A-8).

A value for the average heat transfer coefficient can be obtained

from Eq. (A-8) by introducing the expressions for the local Nusselt and modified Grashof numbers. Also, with the assumption that the boundary layer is turbulent from the leading edge, the average heat transfer coefficient becomes,

$$h_L = \frac{1}{L}\int_0^L h_x dx = \frac{C_H}{L}\int_0^L x^{\frac{1}{7}}\, dx = \frac{7}{8}\, h_x \qquad \text{(A-10)}$$

Usually a laminar region precedes the turbulent region, thus the preceding expression for the turbulent heat transfer coefficient can be expected to represent the actual value only for modified Grashof numbers so large that the laminar portion of the boundary layer may be neglected compared with the turbulent portion. Eckert and Jackson (10) noted that, for the constant temperature wall case, this limit for the Grashof number appeared to be near 10^{10}. This corresponds to a value near 10^{12} for the constant heat flux case. For modified Grashof numbers higher than this value, the average Nusselt number can be calculated from Eq. (A-10)

$$Nu_L = \frac{7}{8}\left[\frac{(0.0225)^4}{64\cdot J_2}\right]^{\frac{1}{7}} Pr^{\frac{1}{3}}\left[\frac{Gr_x^*}{1.572\,\frac{J_1}{J_2} + Pr^{\frac{2}{3}}}\right]^{\frac{2}{7}} \qquad \text{(A-11)}$$

for a Prandtl number of one and p = 4 in Eq. (4), this equation reduces to,

$$Nu_L = 0.064\cdot(Gr_L^* Pr)^{\frac{2}{7}} \qquad \text{(A-12)}$$

For p = 2 and 6 with Pr = 1.0, the coefficient on the right hand side of Eq. (A-12) becomes 0.058 and 0.068, respectively.

Sparrow and Gregg (33) in their investigation found that the wall temperature distribution for laminar flow followed a one-fifth power law according to the equation

$$\frac{(T_w - T_\infty)_x}{(T_w - T_\infty)_L} = \left(\frac{x}{L}\right)^{\frac{1}{5}} \tag{A-13}$$

A similar equation for turbulent flow over a uniformly heated plate can be obtained from Eq. (A-5). For a given heat flux and fluid, this equation can be written as

$$\theta_w = (T_w - T_\infty)_x = C_1 \cdot x^{-\frac{1}{7}} \tag{A-14}$$

the value of θ_w at $x = L$ is

$$\theta_{w,L} = (T_w - T_\infty)_L = C_1 \cdot L^{-\frac{1}{7}} \tag{A-15}$$

where T_∞ is the ambient fluid temperature. Dividing Eq. (A-15) into (A-14) gives

$$\frac{(T_w - T_\infty)_x}{(T_w - T_\infty)_L} = \left(\frac{x}{L}\right)^{-\frac{1}{7}} \tag{A-16}$$

Again, it has been assumed that the boundary layer is turbulent over the whole plate. As noted in Chapter V, only a limited amount of data exists with which to compare this equation. Figure 68 illustrates the variation of wall temperature difference with distance along the plate as calculated from Eq. (A-16). Also shown are the experimental points calculated from

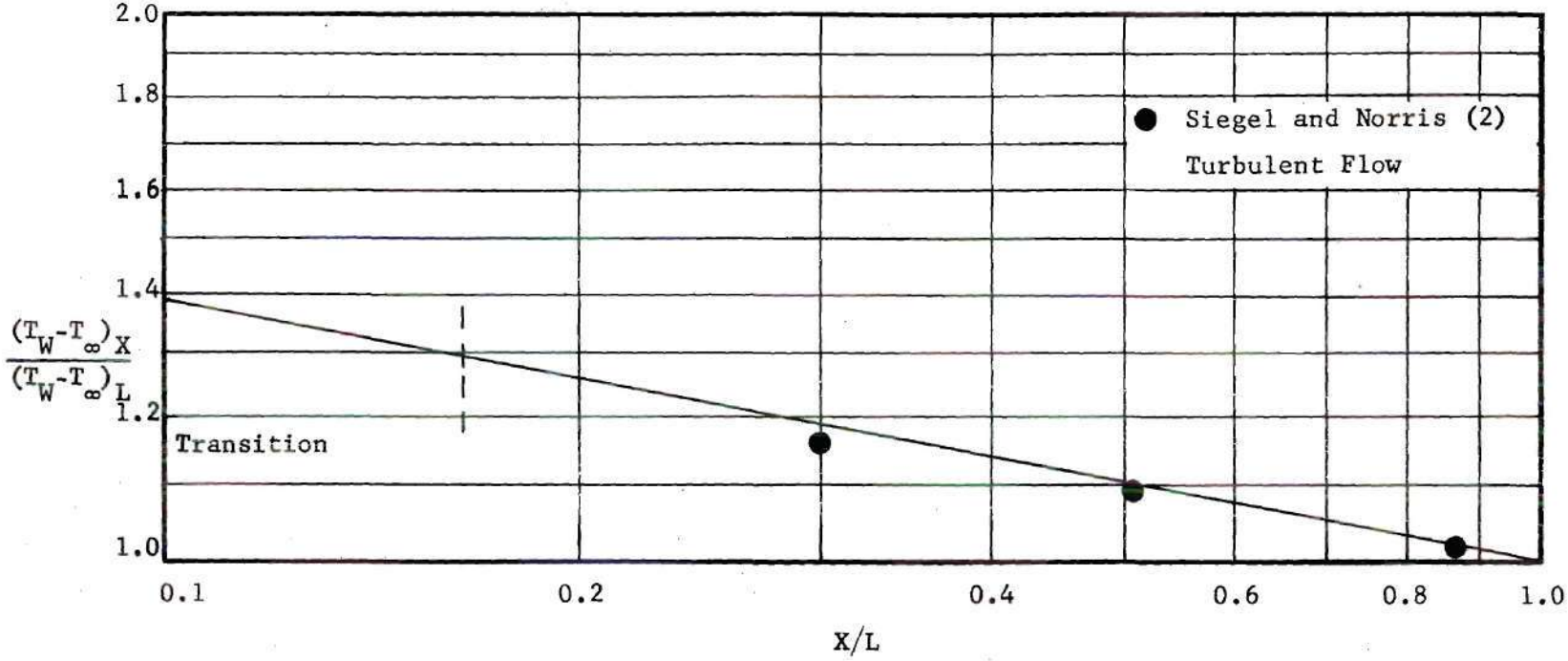

Figure 68. Temperature Distribution as a Function of Distance Along Plate Surface

the work by Siegel. From Eq. (A-16) it is noted that a discontinuity exists at x = 0. However, a laminar region usually precedes the turbulent region, thus, the discontinuity can be avoided.

Average Nusselt Numbers

For a uniformly heated wall, there is no one characteristic temperature difference with which to compute an average heat transfer coefficient and hence and average Nusselt number. The choice is arbitrary. However, Sparrow and Gregg (33) noted that, for laminar flow, usually the average wall temperature difference or the temperature difference half way along the plate was used in calculating the average value of Nu. To compare the average Nusselt number for the constant temperature wall with that for a constant heat flux, the above two methods were used.

The average temperature difference on a surface, over which the flow is completely turbulent, may be calculated from Eq. (A-16).

$$(T_w - T_\infty)_{av} = (T_w - T_\infty)_L \int_0^1 \left(\frac{x}{L}\right)^{-\frac{1}{7}} d\left(\frac{x}{L}\right) = \frac{7}{6} (T_w - T_\infty)_L \qquad \text{(A-17)}$$

Using this temperature difference an average heat transfer coefficient can be calculated from the equation

$$q = h_{av} (T_w - T_\infty)_{av} \qquad \text{(A-18)}$$

From Eq. (A-5) the value of $(T_w - T_\infty)_L$

$$\frac{(T_w - T_\infty)_L \cdot Gr^{*\frac{2}{7}}}{\frac{q \cdot L}{k}} = \frac{C_1}{C_2} \cdot Pr^{-\frac{1}{3}} \qquad \text{(A-19)}$$

Substituting for q and $(T_w - T_\infty)_{av}$ from Eqs. (18), this equation becomes,

$$\frac{Gr_L^{*\frac{2}{7}}}{Nu_L \cdot \frac{7}{6}} = \frac{C_1}{C_2} \cdot Pr^{\frac{1}{3}} \qquad \text{(A-20)}$$

But,

$$Gr_L^* = Gr_L \cdot Nu_L$$

Therefore

$$Nu_L = \left(\frac{6}{7} \cdot \frac{C_2}{C_1}\right)^{\frac{7}{5}} \cdot Pr^{\frac{7}{15}} \cdot Gr_L^{\frac{2}{5}} \qquad \text{(A-21)}$$

With p = 4, the terms C_1 and C_2 become

$$C_1 = \left[\frac{64 \cdot J_2}{(0.0225)^4}\right]^{\frac{1}{7}} = 12.02$$

and

$$C_2 = [1.572 \cdot 0.35873 + Pr^{\frac{2}{3}}]^{-\frac{2}{7}} = [0.564 + Pr^{\frac{2}{3}}]^{-\frac{2}{7}}$$

and Eq. (A-21) reduces to

$$Nu_L = 0.0248 \cdot [0.564 + Pr^{\frac{2}{3}}]^{-\frac{2}{5}} \cdot Pr^{\frac{7}{15}} \cdot Gr_L^{\frac{2}{5}} \qquad \text{(A-22)}$$

The average Nusselt numbers as calculated from the constant temperature wall equation by Eckert and Jackson are compared with Eq. (22) in Table 2 for various Prandtl numbers. It is seen from this table that, for Prandtl numbers close to one, $Nu_L/(Pr \cdot Gr_L)^{\frac{2}{5}}$ evaluated at the average value of $(T_w - T_\infty)_{av}$ for a plate having a uniform surface heat flux differs less than three percent from the value for a plate having a constant wall tem-

perature. For Prandtl numbers not close to one, the error between the two equations becomes greater, for example, for Pr = 5, the error is 14 percent. However, this deviation is often within the limits of experimental accuracy.

Table 2. Nusselt Number Comparison Based on Average Temperature Difference at L/2

Pr	$Nu_L/(Pr \cdot Gr_L)^{2/5}$, EQ. (A-22)			
	p = 2	p = 4	p = 6	Ref. (11)
0.72	0.0185	0.0214	0.0234	0.0210
1.0	0.0180	0.0207	0.0226	0.0211
5.0	0.0148	0.0167	0.0181	0.0194

A similar analysis, but employing the temperature difference at x = L/2, can be calculated by using the equation

$$(T_w - T_\infty)_{L/2} = (T_w - T_\infty) \cdot (\tfrac{1}{2})^{-\frac{1}{7}} \qquad \text{(A-23)}$$

Again, an average heat-transfer coefficient can be defined using this temperature difference

$$q = h_{av} (T_w - T_\infty)_{L/2}$$

Following the previous procedure, it is found that

$$Nu_L = 0.0269 \left[0.564 + Pr^{\frac{2}{3}}\right]^{-\frac{2}{5}} \cdot Pr^{\frac{7}{15}} \cdot Gr^{\frac{2}{5}} \qquad \text{(A-24)}$$

Equation (A-24) is compared with the results for the constant temperature wall in Table 3.

Table 3. Nusselt Number Comparison Based on Average Temperature Difference at L/2

Pr	$Nu_L/(Pr \cdot Gr_L)^{2/5}$, EQ. (A-24)			
	p = 2	p = 4	p = 6	Ref. (11)
0.72	0.0200	0.0230	0.0253	0.0210
1.0	0.0195	0.0224	0.0244	0.0211
5.0	0.0160	0.0181	0.0196	0.0194

From Table 3 it is seen that, for Prandtl numbers close to one, a larger error exists between the two values of $Nu_L/(Pr \cdot Gr_L)^{\frac{2}{5}}$ if the temperature difference in defining an average film coefficient is based on L/2 instead of the average temperature difference. However, the maximum error is less than eight percent even for a Prandtl number of five. So, the agreement between the experimental results for turbulent flow over a uniform wall temperature and a uniform surface heat flux is made valid.

APPENDIX B

THERMOCOUPLE CALIBRATION

The probe used in measuring the bulk temperatures within the test tank was constructed and calibrated by Tatom (5). However, his calibration was performed when the thermocouples were not within the system. Tatom's method of taking experimental data was the same as his calibration procedure. That is, the probe thermocouples were calibrated with a Leeds and Northrup potentiometer while his data were also taken with a potentiometer. However, Tatom's method was not used in this investigation. Instead, a Honeywell Electronic 16 Multipoint recorder was used in recording all bulk temperature data. The recorder had a factory accuracy of ± 0.25 percent within the range of 50°F to 150°F. To obtain good accuracy, in the temperature reading in this investigation, both the recorder and the thermocouples were calibrated. In calibrating the two separately, the errors should be additive. However, errors in the reading may occur by using different extension wires or in the hookup of the thermocouples to the recorder. For this investigation only the thermocouples used with the recorder were calibrated.

There are two methods of calibrating thermocouples: (1) outside the system, such as Tatom employed, and (2) within the system. Each method requires a calibrated reference standard with which the readings are to be compared. The reference standard used in calibrating the bulk and wall thermocouples was a 24 B & S gage copper-constantan thermocouple

calibrated at the two points, 50°F and 100°F, by the Industrial Division of Honeywell, Inc. The calibrated thermocouples had a certified error of -0.05°F and +0.09°F at 100°F. In calibrating the thermocouples at points between the certified points on the reference thermocouple, the error was assumed to be a linear function between the two given points.

The method employed in calibrating the bulk thermocouples and recorder together was as follows:

1. The thermocouples within the level of the fluid to be tested were selected and attached to the recorder terminals.

2. The tank was filled to the corresponding level with water. Also, the recorder was turned on and allowed to warm up for one-half hour.

3. The circulation pump was turned on and the fluid was continually mixed to maintain a uniform temperature. Sometimes a paddle was also used in mixing the fluid.

4. The calibrated thermocouple, which was connected to an ice bath and potentiometer, was placed in the tank and lowered to a position opposite and approximately one-quarter of an inch from the thermocouple to be calibrated.

5. One of the outlets from the circulation pump was directed at the two thermocouple junctions and three readings were taken of both the reference standard and bulk thermocouples. The bulk temperature output was read from the recorder while the reference standard output was read on a Leeds and Northrup model 8686 potentiometer.

6. The three readings from both the bulk and reference thermocouples were average compared to get the error. Steps 4 and 5 were then repeated for each thermocouple.

7. Heat was then applied to the fluid in the tank increasing the bulk temperature. Steps 4, 5, and 6 were then repeated to get an error measurement at a second temperature level. In most all cases the error was approximately constant.

It should be noted that, with the thermocouples exposed to periodic temperature variations within the system, the calibration changes (37). This effect was noted somewhat in the later tests. However, the change was small, approximately $\pm$ 0.10°F, hence, it was considered negligible. With the above procedure, not only were the thermocouples calibrated but the temperature measuring system as a whole was calibrated.

The method of reducing and displaying the temperature results can either magnify or reduce the size of the error as represented on a graph. For example, for a given thermocouple if the temperature-time curves are plotted as bulk temperature, T_B, versus time, τ, then any error in the temperature measurement, even after correction, is portrayed on the graph. But, if the result is plotted as bulk temperature difference, $(T-T_i)_B$, for the same thermocouple, versus time, then the error portrayed on the graph is reduced, since for a given thermocouple, over a limited temperature range, the error is approximately constant (37); hence, the error is subtracted out. For this reason, the latter method was selected in displaying the data in this thesis.

The wall thermocouples were not as easy to calibrate as the bulk thermocouples since they had to be calibrated after welding them to the walls. The method in calibrating the wall thermocouples was as follows:

1. The test tank was filled with water to the desired level. The circulation pump turned on and the water thoroughly mixed to ensure a uniform bulk temperature.

2. Three readings of each wall thermocouple were taken and averaged. These were then compared to the bulk readings at the same location.

3. The water was then heated by the side and bottom heaters until a higher desired temperature was reached. The power was then turned off.

4. The bulk fluid was again mixed to get a uniform bulk temperature and a second set of readings was taken. Usually about 40°F temperature difference separated the two readings.

5. Each set of averaged readings for each wall thermocouple was compared with the bulk readings for the two bulk temperature levels. This gave two extreme points on the error curve for the wall thermocouples.

6. The error was considered to be linear between these points. In most all cases, as with the bulk thermocouples, the error was approximately constant.

Using the above procedure, the wall thermocouples were calibrated to within ± 0.25°F accuracy. Also, the same method was employed in displaying the wall data as was used for the bulk data. Thus, any apparent error in wall temperature is reduced. Tables 4 and 5 illustrate the correction for the bulk and wall thermocouples.

Table 4. Bulk Thermocouple Corrections

$$T_n)_{true} = C_n + T_n)_{read}$$

Where $T_n)_{read}$ = Temperature as indicated by the recorder for the sensor n being measured

Thermocouple Number	Calibration Correction	Thermocouple Number	Calibration Correction	Thermocouple Number	Calibration Correction
n	C_n, °F	n	C_n, °F	n	C_n, °F
1	-0.1	21	0.0	41	+0.1
2	-0.1	22	-0.1	42	-0.1
3	-0.15	23	+0.1	43	-0.1
4	-0.08	24	-0.2	44	-0.2
5	+0.1	25	-0.2	45	+0.08
6	+0.2	26	-0.1	46	+0.2
7	-0.1	27	+0.1	47	+0.3
8	-0.08	28	+0.1	48	-0.1
9	+0.2	29	0.0	49	0.0
10	+0.1	30	0.0	50	0.0
11	+0.2	31	-0.1	51	-0.3
12	-0.1	32	-0.2	52	-0.2
13	0.0	33	-0.08	53	-0.2
14	+0.1	34	+0.1	53	+0.1
15	+0.1	35	0.0	55	+0.1
16	0.0	36	+0.1	56	+0.1
17	-0.1	37	-0.2	57	-0.2
18	0.0	38	-0.1	58	0.0
19	0.0	39	+0.1	59	-0.1
20	+0.08	40	-0.2	Surface	+0.1

Table 5. Wall Thermocouple Corrections

Thermocouple Number	Calibration Correction	Thermocouple Number	Calibration Correction
n	C_n, °F	n	C_n, °F
1	-0.2	13	-0.4
2	-0.3	14	+0.2
3	-0.1	15	+0.1
4	+0.2	16	0.0
5	+0.1	17	+0.2
6	-0.1	18	-0.1
7	-0.2	19	-0.1
8	0.0	Bottom	
9	+0.2	1	-0.2
10	+0.3	2	-0.1
11	-0.2	3	-0.3
12	-0.1		

APPENDIX C

HEAT BALANCE ON TANK

In calculating the effectiveness of the baffles and the heat transfer coefficients, it is important to know and be able to check through calculations where the heat, which is generated in the heater plates, is going. That is, how much of the generated heat is going into the bulk fluid, how much is going to increase the internal energy of the heating walls, and how much is lost to the surroundings of the tank. In the analysis that follows, the test system consists of heater plates, the test fluid (water), and the additional parts of the tank, such as the glass plates and the insulation. Also, air is in contact with the fluid at the tank top. The equation describing the heat balance on the system is,

$$\dot{Q}_T \cdot \tau = Q_P + Q_B + Q_L \qquad \text{(C-1)}$$

In the above equation, $\dot{Q}_T$ is the heat generated in both the bottom and side heater plates, Btu/sec. Q_P is that portion of the heat which is generated which increases the internal energy of the heater plates, Btu. Q_B is that portion of the heat generated which goes to increasing the internal energy of the test fluid, Btu. Q_L is that portion which is lost from the system, Btu. The majority of the heat which is lost may be lost via the bulk fluid, since it is in contact with the glass plates and the air at the tank top.

The expression for the internal energy of the heating plates is,

$$Q_p = \rho_p V_p C_p (\bar{T}-T_i)_p \tag{C-2}$$

and for the test fluid,

$$Q_B = \rho_B V_B C_B (\bar{T}-T_i)_B \tag{C-3}$$

The heat lost from the tank occurs through the glass plates and at the liquid surface. In Chapter II, it was shown that two opposite sides of the tank with glass plates are constructed so that two plates of glass are one-half inch apart. The heat lost through these plates and the enclosed air space can be calculated from the equation

$$q_L = \frac{T_1 - T_\infty}{\frac{t_1}{k} + \frac{1}{h_1} + \frac{t_2}{k} + \frac{1}{\bar{h}_2}} \tag{C-4}$$

In this equation, an inside surface temperature for the glass plates, T_1, which will be close to the average bulk temperature and the ambient temperature, T_∞, of the room must be known. An approximate value of the film coefficient, $\bar{h}_1$, can be found from the work of Eckert and Carlson (38). As an example, in test TB-71, the ambient temperature $T_\infty = 78^\circ F$, the time average bulk temperature was $81.3^\circ F$ at 1800 seconds. Thus, from Eq. (C-4) the heat loss is

$$q_L = 0.0011 \frac{Btu}{ft^2 sec}$$

This amount of heat loss is small when compared to the total heat input. Thus, it was considered negligible. The amount of heat lost at the liquid-air surface is also negligibly small. This fact has been demonstrated by Adams (39), since the velocity of the air flow over the surface is small and the difference between the liquid surface and the air temperature is small, being about 5-10°F. In this situation, the film coefficient is also small. In no tests did the surface temperature come close to saturation, so heat loss by vaporization could be neglected.

In some cases, if the bulk temperatures were exceptionally low, instead of a heat loss, there was a heat gain through the glass plates and air at the surface. However, this gain, like the heat loss, was negligibly small in all cases. Sample calculations showed it to be less than 2.5 Btu/ft^2hr.

Another and perhaps better method of calculating the heat lost during a test is to compare the integrated, average bulk temperature, $\overline{T}_B$, with the bulk temperature computed from Eq. (C-3). The equation for the integrated bulk temperature is

$$\overline{T}_B = \frac{1}{L}\int_0^L T dx \qquad (C-5)$$

where L is the tank height. Equations (C-3) and (C-4) were part of the computer program discussed in Appendix D. Average bulk temperatures for the specified time intervals was computed first from Eq. (C-3). The part of the heat generated which increased the wall temperature was neglected. Then by numerically integrating Eq. (C-5) using the trapezoidal rule and

the average bulk temperature. Upon comparison of many tests, it was found that the percent difference between the two values was no more than ± 1.50 percent. This difference is due in the most part to the energy absorbed or retained by the heating walls themselves.

APPENDIX D

EXPERIMENTAL BULK AND WALL TEMPERATURE-TIME DATA

The data presented in the following table is a test summary obtained from the experimental data. A computer program written in Algol language and run on a Burroughs B-5500 computer was used in reducing the data to the form shown in the body of the thesis. The purpose of the computer program was to take the experimental bulk and wall temperature data, which were obtained at various and different time intervals, and compute the bulk and wall temperature at specified time intervals as presented in the table. The first part of the effectiveness program listed in Appendix E is a copy of the program for the quadratic interpolation of the temperatures.

The bulk temperature data for the program were taken from the recorder print outs. The wall temperature data were in millivolt-time form, since they were taken with a potentiometer and stopwatch. These data were directly written on computer sheets for easy data reduction. In many tests, the wall data were not recorded. Due to the large number of tests, the experimental bulk and wall temperature data are not included in the appendix. A copy of the data is on file in the Georgia Institute of Technology library.

The computer program was designed to do the following:

1. Calculate the wall temperature in ^{O}F from the millivolt data. The bulk temperature was read into the program in ^{O}F form. Correct all reading according to the thermocouple correction data.

2. Compute the bulk temperature at specified time intervals by using Newton's divided difference interpolation, or what is often called quadratic interpolation, with three different time intervals. The particular interpolation procedure is clearly explained in Wylie (40).

3. Compute and print the temperature difference θ_B and $\theta_B/\theta_{B\ max}$ versus x/L for each thermocouple.

4. Compute the wall temperature again using Newton's interpolation formula. Print out θ_w and $\theta_w/\theta_{w\ max}$ versus x/L for each thermocouple.

5. Print out a table of bulk and wall temperature at the specified time intervals, including the thermocouple location.

Table 6. Summary of Tests

Test Number	Baffle Size Inches	Number of Baffles	Bottom Heat Flux Btu/ft^{2}sec	Side Heat Flux Btu/ft^{2}sec	Aspect Ratio	Angle Degrees
T-1	0	0	0	0.121	4.88	
T-2	0	0	0	0.122	4.88	
T-3	0	0	0	0.121	4.88	
T-4	0	0	0.186	0.123	4.88	
T-5	0	0	0	0.124	4.88	
T-6	0	0	0	0.123	4.88	
T-7	0	0	0.186	0.124	4.88	
T-8 through T-12	These series of tests were run for information on boundary layer temperature profiles. No bulk temperature profile was recorded.				4.88	
T-13	0	0	0.055	0.122	4.88	
T-14	0	0	0	0.093	4.88	
T-15	Test terminated early, data no good.				4.88	
T-16	0	0	0.187	0.023	4.88	
T-17	0	0	0.186	0.121	4.88	
T-18	0	0	0.075	0.046	4.88	
TB-19	2	3	0	0.123	4.88	90
TB-20	2	3	0.186	0.123	4.88	90
TB-21	2	3	0	0.093	4.88	90
TB-22	2	3	0.087	0.121	4.88	90

Table 6. (Continued)

Test Number	Baffle Size Inches	Number of Baffles	Bottom Heat Flux Btu/ft^{2}sec	Side Heat Flux Btu/ft^{2}sec	Aspect Ratio	Angle Degrees
TB-23	2	3	0.055	0.122	4.88	90
TB-24	2	3	0.075	0.046	4.88	90
TB-25	Test terminated, data no good.				4.88	90
TB-26	2	3	0	0.122	4.88	90
TB-27	2	3	0.186	0.122	4.88	90
TB-28	2	3	0	0.122	4.88	90
TB-29	2	3	0	0.122	4.88	90
TB-30	2	3	0	0.122	4.88	135
TB-31	2	3	0.186	0.122	4.88	135
TB-32	4	3	0.186	0.122	4.88	90
TB-33	4	1	0	0.121	4.88	90
TB-34	4	3	0.055	0.1215	4.88	90
TB-35	2	3	0.075	0.046	4.88	45
TB-36	4	1	0.055	0.122	4.88	90
TB-37	6	1	0	0.122	4.88	90
TB-38	6	1	0.186	0.122	4.88	90
TB-39	6	1	0.186	0.122	4.88	90
TB-40	6	1	0.055	0.122	4.88	90
TB-41	6	1	0.075	0.046	4.88	90
TB-42	6	1	0	0.122	4.88	135

Table 6. (Continued)

Test Number	Baffle Size Inches	Number of Baffles	Bottom Heat Flux $Btu/ft^2 sec$	Side Heat Flux $Btu/ft^2 sec$	Aspect Ratio	Angle Degrees
TB-43	4	3	0	0.122	4.88	90
TB-44	6	1	0.186	0.122	4.88	135
TB-45	6	1	0.075	0.046	4.88	135
TB-46	6	1	0.055	0.121	4.88	135
TB-47	6	1	0.186	0.023	4.88	135
TB-48	6	1	0	0.122	4.88	135
TB-49	6	1	0.186	0.122	4.88	45
TB-50	4	1	0.186	0.122	4.88	90
TB-51	6	3	0	0.121	4.88	135
TB-52	6	3	0.186	0.122	4.88	135
TB-53	6	3	0	0.121	4.88	135
TB-54	6	3	0.055	0.122	4.88	135
TB-55	6	3	0.075	0.046	4.88	135
TB-56	6	3	0.186	0.023	4.88	135
TB-57	6	3	0	0.122	4.88	90
TB-58	6	3	0.186	0.122	4.88	90
TB-59	6	3	0.055	0.121	4.88	90
TB-60	6	3	0.046	0.075	4.88	90
TB-61	6	3	0.186	0.023	4.88	90
TB-62	6	3	0.186	0.122	4.88	90

Table 6. (Continued)

Test Number	Baffle Size Inches	Number of Baffles	Bottom Heat Flux Btu/ft^2 sec	Side Heat Flux Btu/ft^2 sec	Aspect Ratio	Angle Degrees
TB-63	6	3	0.186	0.122	4.88	45
TB-64	6	4	0	0.121	4.88	45
TB-65	6	4	0.18	0.122	4.88	45
TB-66	6	4	0.186	0.096	4.88	45
TB-67	6	4	0.055	0.122	4.88	45
TB-68	6	4	0.075	0.046	4.88	45
TB-69	0	0	0	0.082	1.0	
TB-70	0	0	0	0.082	1.0	
TB-71	0	0	0	0.172	1.0	
TB-72	0	0	0.076	0.172	1.0	
TB-73	0	0	0.044	0.082	1.0	
TB-74	0	0	0.186	0.172	1.0	
TB-75	4	2	0	0.172	1.0	90
TB-76	4	2	0.186	0.172	1.0	90
TB-77	4	2	0	0.082	1.0	90
TB-78	4	2	0.044	0.082	1.0	90
TB-79	4	2	0	0.172	1.0	45
TB-80	4	2	0.186	0.172	1.0	45
TB-81	4	2	0.076	0.172	1.0	90
TB-82	4	2	0.044	0.182	1.0	90

Table 6. (Continued)

Test Number	Baffle Size Inches	Number of Baffles	Bottom Heat Flux Btu/ft^2 sec	Side Heat Flux Btu/ft^2 sec	Aspect Ratio	Angle Degrees
TB-83	4	3	0	0.172	1.0	90
TB-84	4	3	0.186	0.172	1.0	90
TB-85	4	3	0.076	0.172	1.0	90
TB-86	4	3	0.044	0.082	1.0	90
TB-87	4	3	0	0.172	1.0	135
TB-88	4	3	0.0186	0.172	1.0	135
TB-89	4	3	0.044	0.082	1.0	135
TB-90	4	3	0.076	0.172	1.0	135
TB-91	8	1	0	0.172	1.0	90
TB-92	8	1	0.186	0.172	1.0	90
TB-93	8	1	0.044	0.082	1.0	90
TB-94	8	1	0	0.172	1.0	90
TB-95	8	1	0.076	0.172	1.0	90
TB-96	8	3	0.044	0.082	1.0	90
TB-97	8	3	0	0.172	1.0	90
TB-98	8	3	0.186	0.172	1.0	90
TB-99	8	3	0.076	0.172	1.0	90
TB-100	0	0	0	0.171	3.0	
TB-101	0	0	0.194	0.171	3.0	
TB-102	0	0	0.194	0.082	3.0	

Table 6. (Continued)

Test Number	Baffle Size Inches	Number of Baffles	Bottom Heat Flux Btu/ft^{2}sec	Side Heat Flux Btu/ft^{2}sec	Aspect Ratio	Angle Degrees
TB-103	0	0	0.080	0.171	3.0	
TB-104	4	2	0	0.171	3.0	90
TB-105	4	2	0.194	0.171	3.0	90
TB-106	4	2	0.080	0.171	3.0	90
TB-107	4	2	0.194	0.082	3.0	90
TB-108	4	3	0.194	0.171	3.0	90
TB-109	4	3	0.080	0.171	3.0	90
TB-110	4	3	0.0	0.171	3.0	90
TB-111	4	3	0.194	0.082	3.0	90
TB-112	6	3	0.0	0.171	3.0	90
TB-113	6	3	0.194	0.171	3.0	90
TB-114	6	3	0.080	0.171	3.0	90
TB-115	6	3	0.194	0.082	3.0	90
TB-116	6	1	0.0	0.171	3.0	90
TB-117	6	1	0.194	0.171	3.0	90
TB-118	6	1	0.194	0.082	3.0	90
TB-119	6	1	0.080	0.171	3.0	90

APPENDIX E

EFFECTIVENESS CORRELATION PROGRAM

Calculation of the effectiveness of the various baffle designs as illustrated in the thesis body was accomplished with the computer program listed on the next pages. The comment cards or the cards with a % symbol preceeding them illustrates the various sections of the program. The main variables printed out of this program are effectiveness (EFF) and time.

The other program included in this appendix is for the correlation of the baffle effectiveness. The equations employed in this program have been presented on pages 118 thru 123.

```
                %
                % EFFECTIVENESS CALCULATIONS
                %
     FILE OUT    PRTRBP 16(3,15) ; %
      FILE IN    CARBP (3,10) ; %
      INTEGER    P,N,L,TN,H,A,B,J,E,FF,M1,I1,I,TIME,G,I2,E1,F1,G1 ; %
    REAL    EFF,DX,TBI,X1,X2,X3,X4,X5,EE,NB,BTW,PERC,EF1,PER1,PER2 ; %
        LABEL   L1,L2,L3,L4,L5 ; %
INTEGER ARRAY   TIM1[0:25,0:20] ; %
REAL ARRAY    TBQV,TB,TBQI,T,MT,TAV,TBV,TBQA,T1,TQV[0:50,0:50] ;
   REAL ARRAY   CONST1,X,XI,DF,F,AP,Z[0:150] ; %
   FORMAT OUT   FMT1(//X50,"TIME=",I4,"SEC.") ; %

            FORMAT OUT   FMT2(/5F20.5,2F10.5) ; %

   FORMAT OUT   FMT3(/X2,I8,F19.2,F24.3,F34.3) ; %

        FORMAT OUT  FMT4(/X4,4E15.5) ; %

   FORMAT OUT   FMT5(//X10,"BAFFLE TO TANK WIDTH RATIO =",F9.3) ; %

   FORMAT OUT   FMT6(//X40,"TEST NUMBER =",I4) ; %

        FORMAT TITLE(//X20,"EFFECTIVE AND TEMP.-TIME-POSITION DATA");

          WRITE (PRTRBP,TITLE) ; %
              % L GIVES NO. OF TEST  TO BE RUN
           READ (CARBP,/,L) ; %
                FOR I←1 STEP 1 UNTIL L DO
          BEGIN %
           READ (CARBP,/,TN,H) ; %
          WRITE (PRTRBP,FMT6,TN) ; %
                READ(CARBP,/,TBI,NB,BTW) ; %
                READ(CARBP,/,P,N,I1,E1,F1,G1) ; %
                READ(CARBP,/,FOR A←1 STEP 1 UNTIL P DO[AP[A]]) ; %
                READ(CARBP,/,FOR A←1 STEP 1 UNTIL P DO[CONST1[A],
                X[A]]) ; %
                FOR A←1 STEP 1 UNTIL P DO %
                READ(CARBP,/,FOR B←0 STEP 1 UNTIL N DO[TB[A,B]]) ;
    COMMENT   CALCULATE TIME ; %
                B←0 ; %
                FOR A←1 STEP 1 UNTIL P DO %
                TIM1[A,B]←0 ; %
                B←1 ; %
                FOR A←1 STEP 1 UNTIL P DO %
                TIM1[A,B]←TIM1[A,B-1]+6×AP[A]÷144 ; %
```

```
            FOR B←2 STEP 1 UNTIL N DO %
  BEGIN     FOR A←1 STEP 1 UNTIL P DO %
            TIM1[A,B]←TIM1[A,B-1]+288 ; %
          END ; %
            % CORRECT BULK TEMPERATURE
              FOR A←1 STEP 1 UNTIL P DO %
      BEGIN%
            FOR B←0 STEP 1 UNTIL N DO %
            TB[A,B]← TB[A,B]+CONST1[A] ; %
        END ; %
            % QUADRATIC INTERPOLATION OF TEMPERATURES
             E←300 ; FF←300 ; G←1800 ; %
              B←0 ; M1←0 ; %
L2:           FOR TIME←E STEP FF UNTIL G DO %
      BEGIN %
      WRITE (PRTRBP,FMT1,TIME) ; %
            FOR A←1 STEP 1 UNTIL P DO %
      BEGIN X1←(TIME-TIM1[A,B])/(TIM1[A,B]-TIM1[A,B+1]) ; %
            X2←-X1 ; %
            X3←((TIME-TIM1[A,B])×(TIME-TIM1[A,B+1]))/((
            TIM1[A,B]-TIM1[A,B+1])×(TIM1[A,B]-TIM1[A,B+2])) ; %
            X4←((TIME-TIM1[A,B])×(TIME-TIM1[A,B+1]))/
            ((TIM1[A,B+1]-TIM1[A,B])×(TIM1[A,B+1]-TIM1[A,B+2])); %
            X5←((TIME-TIM1[A,B])×(TIME-TIM1[A,B+1]))/((
            TIM1[A,B+2]-TIM1[A,B])×(TIM1[A,B+2]-TIM1[A,B+1])) ; %
            TBQI[A,B+1]←TB[A,B]+X1×TB[A,B]+X2×TB[A,B+1]+X3×TB[A,B]
                      +X4×TB[A,B+1]+X5×TB[A,B+2] ; %
        END ; %
            B←B+1 ; M1←M1+1 ; %
        END ; %
            IF H>2×B    THEN
  BEGIN     E←E1; FF←F1;G←G1 ; %
            GO TO L2 ; %
       END ; %
            % LINEAR INTERPOLATION OF TEMP. WITH POSITION
            TIME←300 ; %
             DX←X[P]/I1 ; %
             X[0]←0.0 ; %
            XI[0]←0.0 ; %
            FOR B←1 STEP 1 UNTIL M1 DO %
  BEGIN      TBQI[0,B]←TBQI[1,B] ; %
      WRITE (PRTRBP,FMT1,TIME) ; %
             A←1 ; %
             TBQA[A,B]←X[A]×TBQI[A,B] ; %
             FOR A←2 STEP 1 UNTIL P DO %
             TBQA[A,B]←TBQA[A-1,B]+(X[A]-X[A-1])×((TBQI[A,B]+
                  TBQI[A-1,B])/2.0) ; %
             TQV[I,B]←TBQA[P,B]/X[P] ; %
             A←0 ; %
            FOR J←1 STEP 1 UNTIL I1 DO %
      BEGIN %
             XI[J]←XI[J-1]+DX ; %
L1:       IF XI[J]>1.00001×X[A] THEN
      BEGIN A←A+1 ; %
            GO TO L1 ; %
        END ; %
           T1[J,B]←TBQI[A-1,B]+(TBQI[A,B]-TBQI[A-1,B])×
                  ((XI[J]-X[A-1])/(X[A]-X[A-1])) ; %
             IF A>P-2     THEN
             A←A-1 ; %
             IF A>P-2     THEN
             A←A-1 ; %
```

```
                X1←(XI[J]-X[A])/(X[A]-X[A+1]) ; %
                X2←-X1 ; %
                X3←((XI[J]-X[A])×(XI[J]-X[A+1]))/
                   ((X[A]-X[A+1])×(X[A]-X[A+2])) ; %
                X4←((XI[J]-X[A])×(XI[J]-X[A+1]))/
                   ((X[A+1]-X[A])×(X[A+1]-X[A+2])) ; %
                X5←((XI[J]-X[A])×(XI[J]-X[A+1]))/
                   ((X[A+2]-X[A])×(X[A+2]-X[A+1])) ; %
          T[J,B]←TBQI[A,B]+X1×TBQI[A,B]+X2×TBQI[A+1,B]+X3×TBQI[A,B]
                   +X4×TBQI[A+1,B]+X5×TBQI[A+2,B] ; %
                IF I≤1   THEN
                WRITE(PRTRBP,FMT2,T1[J,B],T[J,B],XI[J]) ; %
        END ; %
                I2←I1-1 ; %
                 Z[0]←TBQI[1,B] ; %
                Z[I1]←T[I1,B] ; %
                FOR J←1 STEP 1 UNTIL I2 DO %
                Z[J]←Z[J-1]+2.0×T[J,B] ; %
                TAV[I,B]←(Z[I2]+Z[I1])×DX/(2.0×X[P]) ; %
                PERC←((TAV[I,B]-TQV[I,B])×100.0)/TAV[I,B] ; %
                TBV[I,B]←TAV[I,B]-TBI ; %
                TBQV[I,B]←TQV[I,B]-TBI ; %
                PER1←(TBV[I,B]-TBQV[I,B])×100.0/TBV[I,B] ; %
                 PER2←(TQV[1,B]-TQV[I,B])×100.0/TQV[1,B] ; %
WRITE(PRTRBP,FMT2,TAV[I,B],TQV[I,B],PERC,PER1,TBV[I,B],TBQV[I,B],
                PER2) ; %
                TIME←TIME+300 ; %
        END ; %
           % NUMERICAL INTEGRATION FOR EFFECTIVENESS
             TIME←300 ; %
             FOR B←1 STEP 1 UNTIL M1 DO %
   BEGIN %
             I2←I1-1 ; %
              F[1]←(T[1,B]-TBI)×XI[1]/2.0 ; %
             F[I1]←(T[I1,B]-TBI)×XI[I1]/2.0 ; %
             FOR J←2 STEP 1 UNTIL I2 DO %
 BEGIN       DF[J]←(T[J,B]-TBI)×XI[J] ; %
             F[J]←F[J-1]+DF[J] ; %
      END ; %
             MT[I,B]←DX×(F[I2]+F[I1]) ; %
              WRITE(PRTRBP,FMT2,MT[I,B] ) ; %
             TIME←TIME+300 ; %
       END ; %
              IF I≤1   THEN
              GO TO L5 ; %
              FOR B←1 STEP 1 UNTIL M1 DO %
 BEGIN        TIME←300×B ; %
              EFF←(MT[1,B]-(TQV[1,B]/TQV[I,B])×MT[I,B])/
              (MT[1,B]-(TQV[1,B]×X[P]*2.0)/2.0) ; %
              EE←0.25×(1.0+2.2×EXP(-0.0025×TIME/NB))×BTW*0.5×NB*0.5
              EF1←(MT[1,B]-(TBV[1,B]/TBV[I,B])×MT[I,B])/
              (MT[1,B]-(TBV[1,B]×X[P]*2.0)/2.0) ; %
              WRITE(PRTRBP,FMT4,EFF,EE,TIME,EF1) ; %
              END ; %
L5:     END ; %
    END.
```

```
BEGIN

% EFFECTIVE CORRELATION
FILE OUT PRTRBP 16(3,15) ; %
FILE IN CARBP(3,10) ;
INTEGER I,J,K,I1,I2,I3,I4,J1 ;
REAL ARRAY BW,NO,QR,E,T,LW[0:10] ;
REAL ARRAY N,M,O[0:3,0:3,0:3] ;
FORMAT TITLE (//X20,"EFFECTIVENESS CORRELATION") ;

FORMAT OUT FMT1(/,6F10.5) ;

WRITE (PRTRBP,TITLE) ;
 FOR I←1 STEP 1 UNTIL 3 DO
BEGIN
 FOR J←1 STEP 1 UNTIL 3 DO
BEGIN
 FOR K←1 STEP 1 UNTIL 3 DO
READ (CARBP,/,N[I,J,K],M[I,J,K],O[I,J,K]) ;
END;
END;
READ(CARBP,/,LW[1],LW[2]) ;
FOR J1←1 STEP 1 UNTIL 2 DO
BEGIN
FOR I2←1 STEP 1 UNTIL 2 DO
READ(CARBP,/,BW[I2]) ;
FOR I3←1 STEP 1 UNTIL 2 DO
READ(CARBP,/,NO[I3]) ;
FOR I4←1 STEP 1 UNTIL 2 DO
READ(CARBP,/,QR[I4]) ;
 FOR I2←1 STEP 1 UNTIL 2 DO
BEGIN
 FOR I3←1 STEP 1 UNTIL 2 DO
BEGIN
FOR I4←1 STEP 1 UNTIL 2 DO
BEGIN
 FOR I←1 STEP 1 UNTIL 3 DO
BEGIN
 FOR J←1 STEP 1 UNTIL 3 DO
BEGIN
 FOR K←1 STEP 1 UNTIL 3 DO
BEGIN
I1←1 ;
T[1]←5.0 ;
 FOR I1←1 STEP 1 UNTIL 6 DO
BEGIN E[I1]←BW[I2]*N[I,J,K]*NO[I3]*M[I,J,K]*(1.0+QR[I4])*O[I,J,K]
*EXP (-0.055*T[I1]/(LW[J1]*0.5)) ;
T[I1+1]←T[I1]+5.0;
END;
WRITE(PRTRBP,/,BW[I2],N[I,J,K],NO[I3],M[I,J,K],QR[I4],O[I,J,K]);
WRITE(PRTRBP,FMT1,FOR I1←1 STEP 1 UNTIL 6 DO[E[I1]]);
END;
END;
END;
END;
END;
END;
END.
```

APPENDIX F

PHYSICAL PROPERTIES OF WATER

Figures 69 and 70 illustrate graphically the property values used in this investigation. Viscosity values were obtained from the investigation of Thorpe and Rodgers (41) while values of the thermal conductivity and coefficient of volume expansion were obtained from Jakob (17).

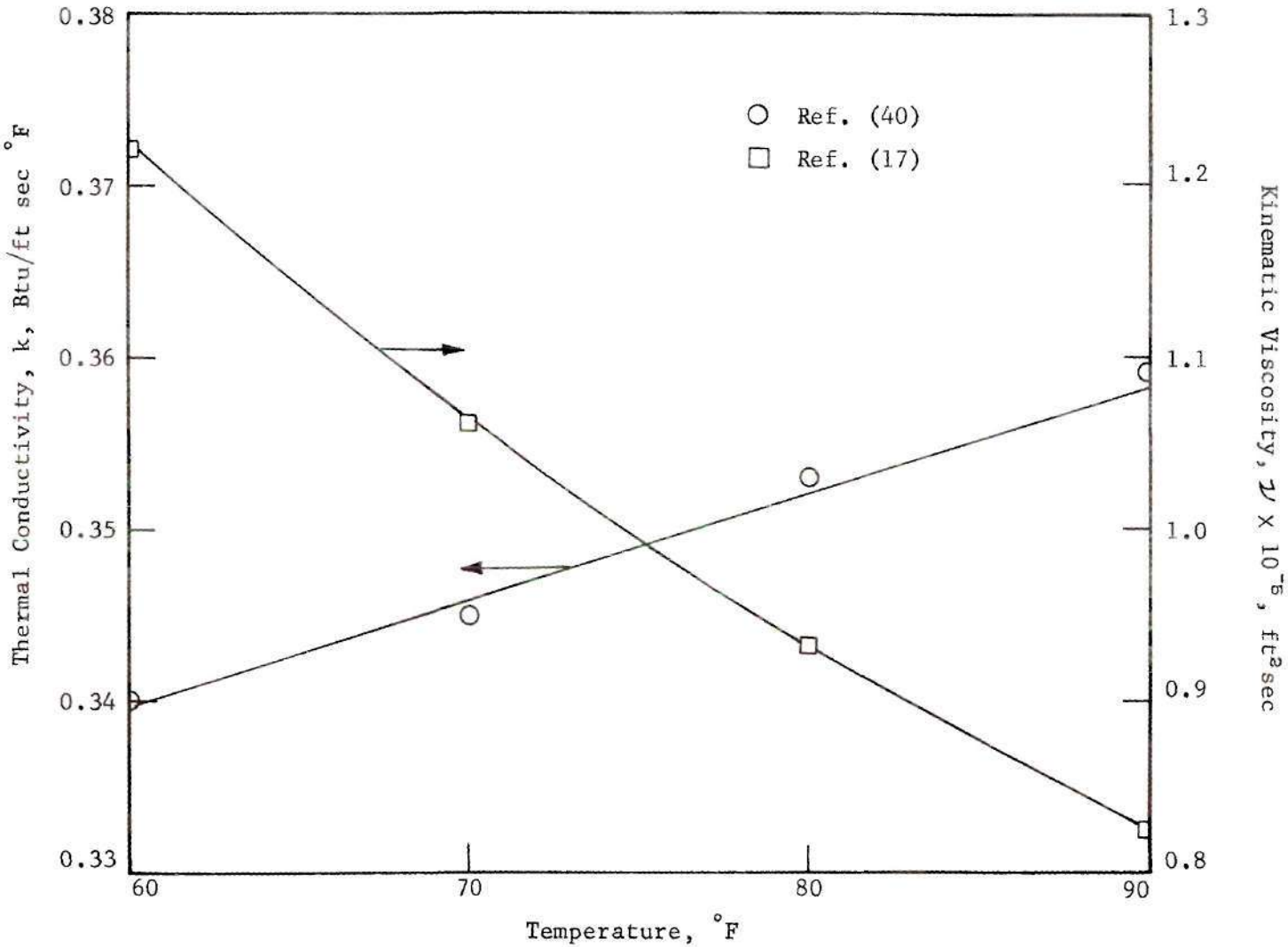

Figure 69. Thermal Conductivity and Kinematic Viscosity versus Temperature for Water

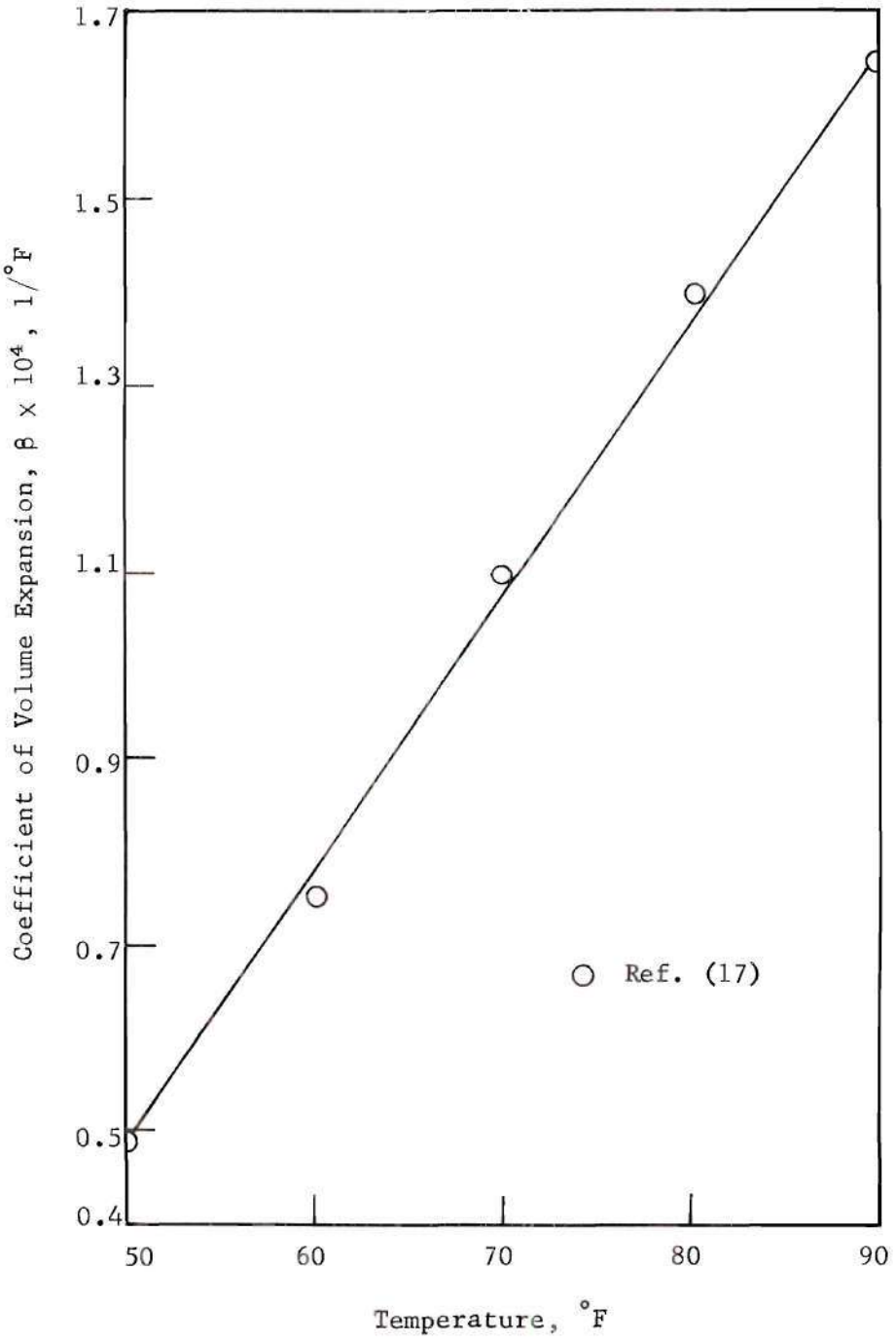

Figure 70. Coefficient of Volume Expansion versus Temperature for Water

REFERENCES CITED

1. Tellep, D. M. and Harper, E. T., "Approximate Analysis of Propellant Stratification," American Institute of Aeronautics and Astronautics Journal, Vol. 1, No. 8, August, 1963, pp. 1954.

2. Tatom, J. W., Brown, W. H., Knight, L. H., and Coxe, E. F., "Analysis of Thermal Stratification of Liquid Hydrogen in Rocket Propellant Tanks," Advances in Cyrogenic Engineering, Vol. 9, pp. 265-272, Plenum Press, New York, 1963.

3. Huntley, S. C., "Temperature-Pressure-Time Relations in a Closed Container," NASA TN 4259 (1959).

4. Robbins, J. H. and Rogers, A. C., Jr., "An Analysis on Predicting Thermal Stratification in Liquid Hydrogen," Presented before AIAA First Annual Meeting, June 29-July 2, 1964.

5. Tatom, J. W., "Transient Free Convection in a Closed Container with Heating at the Bottom and at the Sides," Ph.D. Thesis, Georgia Institute of Technology, Atlanta, Georgia, May, 1966.

6. Neff, B. D., "Study of Cryogenic Propellants Stratification Reduction," Final Report, The Martin Company, Report CR-65-33, under Contract NAS 8-5208, August, 1965.

7. Vliet, G. C. and Brogan, J. J., "Experimental Investigation of the Effects of Baffles on Natural Convection Flow and on Stratification," Proceedings of the Conference on Propellant Tank Pressurization and Stratification, NASA, Huntsville, Alabama, January 20, 21, 1965.

8. Vliet, G. C., "Report of Flow Visualization Studies Concerning the Effect of Baffles on Natural Convection Flow and on Stratification," Aerophysics Research Report, Lockheed Missiles and Space Company, Palo Alto, California, February, 1964.

9. Griffiths, E. and Davis, A. H., "The Transmission of Heat by Radiation and Convection," Special Report No. 9, Food Investigation Board, British Department Science and Industrial Research, 1922, Revised Edition, 1931.

10. Eckert, E. R. G. and Jackson, T. W., "Analysis of Turbulent Free Convection Boundary Layer on Flat Plate," NACA TR 1015, pp. 6, 1951.

REFERENCES CITED (Continued)

11. Eckert, E. R. G. and Jackson, T. W., "Analytical Investigation of Flow and Heat Transfer in Coolant Passages of Free-Convection Liquid-Cooled Turbines," NACA Research Memorandum E50D25, National Advisory Committee for Aeronautics, Washington, July, 1950.

12. Fujii, T., "Experimental Studies of Free Convection Heat Transfer," Japan Society of Mechanical Engineers, Vol. 2, No. 8, pp. 55, 1959.

13. Tritton, D. J., "Turbulent Free-Convection Above a Heated Plate Inclined at a Small Angle to the Horizontal," Journal of Fluid Mechanics, Vol. 16, The University Press, Cambridge, 1963.

14. Bayley, F. J., "An Analysis of Turbulent Free Convection Heat-transfer," Institute of Mechanical Engineer Proceedings, London, Vol. 169, 1955, pp. 361-370.

15. Lighthill, M. J., "Theoretical Considerations on Free Convection in Tubes," Quarterly of Mechanics and Applied Mathematics, 6, pp. 398-439, 1953.

16. Martin, B. W., "Free Convection in an Open Thermosyphon with Special Reference to Turbulent Flow," Proceedings Royal Society A., 230, pp. 502-530, 1955.

17. Jakob, M., Heat Transfer, Vol. 1, John Wiley and Sons, New York, 1949.

18. McAdams, Heat Transmission, McGraw-Hill Book Company, New York, 1954, pp. 170-182.

19. Hartnett, J. P. and Welsh, W. E., "Experimental Studies of Free Convection Heat Transfer in a Vertical Tube with Uniform Wall Heat Flux," Transaction of the American Society of Mechanical Engineers, Vol. 79, New York, pp. 1551-1557.

20. Kolar, M. J., "Experimental Investigation of the Thermal Boundary Layer in a Confined Liquid," NASA Technical Note D-3393, National Aeronautics and Space Administration, Washington, D. C., April, 1966.

21. Gebhart, B. and Adams, D. E., "Measurements of Transient Natural Convection on Flat Vertical Surfaces," Journal of Heat Transfer, Vol. 85, No. 1, February, 1963, pp. 25-28.

22. Siegel, R., "Transient Free Convection from a Vertical Flat Plate," Transaction of the American Society of Mechanical Engineers, Vol. 80, New York, February, 1958, pp. 347-359.

REFERENCES CITED (Continued)

23. Cheesewright, R., "Natural Convection from a Vertical Surface in Non-isothermal Surroundings," International Journal of Heat and Mass Transfer, Vol. 10, Pergamon Press, June, 1967, pp. 1847-1859.

24. Turcotte, D. L., "A Boundary-Layer Theory for Cellular Convection," International Journal of Heat and Mass Transfer, Vol. 10, Pergamon Press, 1967, pp. 1065-1074.

25. Kuo, H. L., "Solution of the Non-Linear Equations of Cellular Convection," Journal of Fluid Mechanics, Vol. 4, 1958, pp. 225-229.

26. Schneider, E. H., "Errors in Experimental Measurements in Free Convection of Fluids in Closed Containers," M.S. Thesis, Georgia Institute of Technology, Atlanta, Georgia, August, 1967.

27. Brooks, R. V., "Free Convection Velocity Measurements by the Use of Neutral Density Particles," M.S. Thesis, Georgia Institute of Technology, June, 1965.

28. Editors, Handbook of Chemistry and Physics, forty-eighth edition, 1966, Cleveland, Ohio, Chemical Rubber Company.

29. Bailey, T. E., Vandekoppel, R., and Skartvedt, G., "Cryogenic Propellant Stratification and Test Data Correlation," AIAA Journal, Vol. 1, No. 1, pp. 1657-1659, January, 1963.

30. Szewczyk, A. A., "Stability and Transition of the Free Convection Layer Along a Vertical Flat Plate," International Journal of Heat and Mass Transfer, Vol. 5, Pergamon Press, 1962, pp. 903-914.

31. Eichorn, R., "Measurements of Low Speed Gas Flows by Particle Trajectories: A New Determination of Free Convection Velocity Profiles," International Journal of Heat and Mass Transfer, Vol. 5, Pergamon Press, 1962, pp. 915-928.

32. Mackey, C. O., Graphical Solutions, second edition, John Wiley and Sons, New York, 1944, pp. 105-130.

33. Sparrow, E. M. and Gregg, J. L., "Laminar Free Convection from a Vertical Flat Plate with Uniform Heat Flux," Trans. ASME, Vol. 78, 1956, pp. 435-440.

34. Siegel, R. and Norris, R. H., "Tests of Free Convection in a Partially Enclosed Space Between Two Heated Plates," Trans. ASME, Vol. 79, 1957, pp. 663-673.

REFERENCES CITED (Concluded)

35. Kudryavtsev, Y. V., Unsteady State Heat Transfer, American Elsevier Publishing Company, New York, 1966.

36. Ostrach, S., "An Analysis of Laminar Free Convection Flow and Heat Transfer About a Flat Plate Parallel to the Direction of the Generating Body Force," NACA TR 1111, 1953.

37. Roeser, Wm. F., and Lonberger, S. T., "Methods of Testing Thermocouples and Thermocouple Materials," NBS Circular No. 590, National Bureau of Standards, United States Department of Commerce, February 1958.

38. Eckert, E. R. G. and Carlson, W. O., "Natural Convection in an Air Layer Enclosed Between Two Vertical Plates with Different Temperatures," International Journal of Heat Transfer, Vol. 2, pp. 106-120, Pergamon Press, 1961.

39. Adams, B. M., "Natural Convection of Air-Liquid Interfaces," Journal of Fluid Mechanics, Vol. 16, pp. 432-437, 1963.

40. Wylie, C. R., Advanced Engineering Mathematics, 2nd edition, McGraw-Hill Book Company, New York, 1960.

41. Thorpe, T. E., and Rogers, J. W., "On the Relations Between the Viscosity of Liquids and Their Chemical Nature," Journal of Fluid Mechanics, Vol. 2, pp. 443-446, 1957.

VITA

Reginald B. Pollard, som of Sam and Martha (Barber) Pollard, was born in Auburndale, Florida, on October 11, 1939. He was educated in the public schools of Albany, Georgia. He was graduated from Albany High School in May of 1958 and entered Middle Georgia Junior College in September of 1958. Upon completion of a two-year program at Middle Georgia, he entered Auburn University. He received the degree of Bachelor of Mechanical Engineering in December, 1962, and immediately entered graduate school at Auburn. In August of 1965, he received the degree of Master of Science in Mechanical Engineering. In September of 1965 he entered the graduate school of the Georgia Institute of Technology.

Mr. Pollard was married in June, 1961 to the former Joan Ellen Cato, and they have three children, Regina, Jo Ellen, and Reginald Jr.